EPFL

Thèse n° 10190

Selection and Optimal Use of Nanoporous Materials for Adsorption Energy Technologies

Présentée le 2 mai 2023

Faculté des sciences et techniques de l'ingénieur
Groupe SCI STI FM
Programme doctoral en énergie

pour l'obtention du grade de Docteur ès Sciences

par

Emanuele PICCOLI

Acceptée sur proposition du jury

Prof. J. A. Schiffmann, président du jury
Prof. F. Maréchal, Dr S. C. Galmarini, directeurs de thèse
Dr A. Freni, rapporteur
Dr G. Füldner, rapporteur
Prof. M. Mazzotti, rapporteur

École polytechnique fédérale de Lausanne

2023

Each time dawn appears,
the mystery is there in its entirety.
— René Daumal

Acknowledgements

First of all, I would like to thank Sandra Galmarini and François Maréchal for their constant and unfailing guidance.
Sandra, you have been the mainstay in the daily routine and the highlights of this adventure. With your kindness, understanding, interest and curiosity you have been an inspiration and a great help. Without you, this thesis simply would not have been possible, and my experience would not have been the same. Besides my thanks, my best wishes go out to you for the challenges that lie ahead.
Thank you, François, for the many exciting conversations. Your energy and positivity are contagious and truly inspiring. Thank you also for your guidance in the most delicate and important moments.

I feel very honoured that Angelo Freni, Gerrit Füldner and Marco Mazzotti were part of the thesis jury. Not only do they exude an extraordinary level of knowledge and clarity of mind, but I greatly admire and appreciate the passion they demonstrate in every single conversation.

This thesis would not have been possible at all without the help and unwavering cooperation of many colleagues.
From Empa, undoubtedly Romain, Ricardo and Riccardo were among the most important, and I am extremely grateful for the time and energy devoted to our work together. Many others have been of great support, and among them, I would like to mention at least Matthias, Wim, Lukas, Bruno, Robert, Luca, Sara, Danica, Karama, Yael, Arijit, Tanay, Juan, Foteini, Sahana, Tingting and Favio.
From outside Empa, too, the collaborations and support have been abundant and truly invaluable. First and foremost, I remember the precious supervision of Bruno Michel, a true sustainability enthusiast. From Switzerland, the collaboration with Paul, Xavier D., Alexis and Xavier J. was very satisfying. My thanks also go to my colleagues from Messina, especially Andrea, Enza, Giuseppe and Valeria, with the only regret that I could not stay longer with them during the pandemic period.

All this would not have been possible without the benefits derived from personal relationships with so many colleagues and friends in so many different places and times that I would feel great shame in not mentioning at least some of them.

Deepu and Samarth, who complete the list of aspiring doctors. Ana, Natalia, Michal, Sami, Jannis, Shanyu, Zahra, Marek, Steffi, Katja, Juliana, Rawan, Zuza and so many others from the tribe of 312.
Thanks for the friendship and the carefree evenings to Michael, Rani, Spyros, Nico, Erik, Sugu and Ely.
Thanks to Gian, Giulia, Diego and all the friends in Rüschlikon, who welcomed me as one of the family from day one. It was truly a gift to get to know you.
When I came to Zürich, I didn't know I would find a brother: with Frenki I have so many indelible memories that I don't think I will ever be able to shake off his positivity.
During the ups and downs of this experience, there was a group of heroic and adventure-hungry friends who accompanied me: my roomie Kati, Seb, Nacho, Ste and Mathis, keep up the spirit!
It was so nice to meet and discuss with so many wonderful and diverse people, like the whole Hycool family, Giulio, Patrik, Eric, and Eduardo.

For as many people as I have met on my path, there are just as many who have been patient with me and are waiting for me at home.
First and foremost, my family. My sister, my mum and my dad, who have always been there and have seen me through. To my grandmothers, who saw me start this journey, goes a sweet thought.
Pie, Ste and Andre, unwavering under the roar of the years.
Pier, my distant brother who has always kept me close.
My newly acquired family from Turin and the surrounding area, who every time makes me feel at home wherever I am: there are really too many of your names to list here, but please know that you have made my life better.

A thought also goes to the people I lost along the way. Life may have brought us apart, but I will forever carry a piece of view with me.

Of all the surprises that came my way, the most incredible was meeting Ghella. Before meeting her, I was simply unaware it was possible to enjoy life so much. Being able to share a part of my journey with you is a gift for which I will always be grateful.

Zürich, March 17, 2023 Ema

Abstract

Due to the large waste of heat in the power and industrial sectors, our use of energy is inefficient. Moreover, it relies on rapidly depleting and greenhouse-gas-emitting sources such as fossil fuels. While the scarcity of energy resources is a relevant societal concern, the emission of climate-altering gases poses serious threats to global ecosystems and our civilization.
The development and deployment of heat-powered adsorption energy technology tackle all of these issues:

- Adsorption heat pumps and chillers require little electricity, which could save strain on the power grid
- Adsorption energy storage allows long-term management of heat, increasing energy efficiency
- Separation of carbon dioxide by adsorption allows for carbon-neutral and negative-emission technology
- Adsorption energy technology runs on low-grade heat, which improves the system efficiency and enables the use of solar energy.

The deployment of the technology is constrained by:

- Relatively low energy efficiency
- Low power density/ high required volume
- High capital costs

These challenges are sensitive to a better selection and use of the nanoporous adsorbent materials employed.
In this thesis, after identifying the main areas of research necessary to improve the understanding and the performance of adsorption energy transformers, materials' characterization and modelling tools are used to tackle some of them.
In particular, the research focuses on:

- Minimizing the experimental effort necessary to screen a large number of adsorbent materials

- Integrating the selection of the adsorbent and the design of the adsorption energy processes
- Developing a novel modelling method for heat and mass transfer within the material to enable affordable simulations
- Tailoring a sustainable activated carbon for the heating/cooling operation in district heating networks
- Developing and pre-design an adsorption heat exchanger based on the agitated screw-conveyor concept
- Applying the rapid adsorption coatings to the post-combustion capture of carbon dioxide
- Investigating the effects of long-term use and storage of the adsorbent

The results show that characterization and modelling activities dedicated to the adsorbent materials are effective to develop improved adsorption technology.
In particular, better methods of characterization guarantee an accurate selection of the adsorbent material from a wide range of candidates. This process triggers increases in performance, especially when the materials are integrated with the process energy flows.
The proposed modelling method was capable of describing accurately the dynamics of adsorption. This enables less expensive simulations for material and technology development. In fact, the ideal process parameters for the production of activated carbon were identified. Furthermore, the model proved to be compatible with the feasibility study of an agitated heat and mass exchanger, which is a first-of-a-kind. The device provides good material usage and power density.
The application of concepts and methods developed for heat transformers to gas separation delivered promising results. High rates of adsorption were demonstrated and different materials could be ranked. However, some limitations were highlighted and further research is envisaged.
Finally, ageing tests were useful to determine the conditions in which material degradation happens and the effect it has on a selection of adsorbents.

Keywords:
Adsorption, Materials, Characterization, Modelling, Isotherms, Selection, Integration, Heat and Mass Transfer, Ageing, Carbon capture

Sintesi

A causa del grande spreco di calore nei settori energetico e industriale, il nostro uso dell'energia è inefficiente. Inoltre, si basa su fonti in rapido esaurimento e che emettono gas a effetto serra, come i combustibili fossili. Se la scarsità di risorse energetiche è un problema sociale rilevante, l'emissione di gas climalteranti pone serie minacce agli ecosistemi globali e alla nostra civiltà. Lo sviluppo e la diffusione della tecnologia energetica ad adsorbimento alimentata dal calore affronta tutti questi problemi:

- Le pompe di calore e i refrigeratori ad adsorbimento richiedono poca elettricità, il che potrebbe ridurre la pressione sulla rete elettrica
- L'accumulo di energia ad adsorbimento consente una gestione a lungo termine del calore, aumentando l'efficienza energetica
- La separazione dell'anidride carbonica mediante adsorbimento consente di ottenere tecnologie a emissioni zero o negative
- Le tecnologie energetiche ad adsorbimento funzionano con calore di bassa qualità, il che migliora l'efficienza del sistema e consente di utilizzare l'energia solare

La diffusione della tecnologia è limitata da:

- Efficienza energetica relativamente bassa
- Bassa densità di potenza/alto volume richiesto
- Alti costi di capitale

Queste sfide sono sensibili a una migliore selezione e utilizzo dei materiali adsorbenti nanoporosi impiegati.
In questa tesi, dopo aver identificato le principali aree di ricerca necessarie per migliorare la comprensione e le prestazioni dei trasformatori di energia ad adsorbimento, vengono utilizzati strumenti di caratterizzazione e modellazione dei materiali per affrontare alcune di esse.
In particolare, la ricerca si concentra su:

- Ridurre al minimo lo sforzo sperimentale necessario per vagliare un gran numero di materiali adsorbenti.
- Integrare la selezione dell'adsorbente e la progettazione dei processi energetici di adsorbimento.
- Sviluppare un nuovo metodo di modellazione per il trasferimento di calore e massa all'interno del materiale per consentire simulazioni a costi contenuti
- Creare un carbone attivo sostenibile per il riscaldamento/raffreddamento nelle reti di teleriscaldamento.
- Sviluppare e pre-progettare uno scambiatore di calore ad adsorbimento basato sul concetto di coclea agitata.
- Applicare dei rivestimenti ad adsorbimento rapido alla cattura post-combustione del biossido di carbonio
- Indagare sugli effetti dell'uso e dello stoccaggio a lungo termine dell'adsorbente.

I risultati dimostrano che le attività di caratterizzazione e modellazione dedicate ai materiali adsorbenti sono efficaci per sviluppare una migliore tecnologia ad adsorbimento.
In particolare, migliori metodi di caratterizzazione garantiscono una selezione accurata del materiale adsorbente da un'ampia gamma di candidati. Questo processo innesca un aumento delle prestazioni, soprattutto quando i materiali sono integrati con i flussi energetici del processo.
Il metodo di modellazione proposto è stato in grado di descrivere accuratamente la dinamica dell'adsorbimento. Ciò consente simulazioni meno costose per lo sviluppo di materiali e tecnologie. Infatti, sono stati identificati i parametri di processo ideali per la produzione di carbone attivo. Inoltre, il modello si è rivelato compatibile con lo studio di fattibilità di uno scambiatore di calore e massa agitato, che rappresenta una novità assoluta nel suo genere. Il dispositivo offre un buon utilizzo del materiale e una buona densità di potenza.
L'applicazione dei concetti e dei metodi sviluppati per i trasformatori di calore alla separazione dei gas ha dato risultati promettenti. Sono stati dimostrati alti tassi di adsorbimento ed è stato possibile classificare diversi materiali. Tuttavia, sono state evidenziate alcune limitazioni e sono previste ulteriori ricerche.
Infine, i test di invecchiamento sono stati utili per determinare le condizioni in cui avviene il degrado del materiale e l'effetto che ha su una selezione di adsorbenti.

Parole chiave:
Adsorbimento, Materiali, Caratterizzazione, Modellazione, Isoterme, Selezione, Integrazione, Trasferimento di calore e massa, Invecchiamento, Cattura del carbonio

Contents

List of Figures

List of Tables

1 Introduction

1.1 Conducting Energy Research During the Anthropocene

Given the mainstream narrative implicitly supported by the current educational and social systems, the idea of humanity as it has developed in historical times is prevalent. There is a tendency to focus on how it has developed in many fields, from science to philosophy and from art to economics, in the last 6000 years or so. However, considering that the history of humankind (fully developed and de facto unchanged physically, artistically and spiritually) dates back roughly 200 thousand years, the hypothesis that its last 2% is representative of our nature would seem to be worth testing. Obviously, there are extremely relevant lessons to be learned about the nature of humanity within this temporal frame, but the fact that our contemporary society is a mere temporary fashion within the greater human history is largely overlooked. Of course, there is no way back to what humanity was, but the possible features of the *future* humanity are as diverse as the human imagination. What allowed us to thrive in complex natural circumstances is the ability to use and transfer information, our culture, in an ever-evolving way (see Spier, 2015).

Curiously (or rather forcibly), the portion of history that we are most familiar with and that is taught at school coincides with the development of humans during the Holocene. Holocene began roughly ten thousand years ago, with an almost unprecedented stable and warm climate, according to Hogan, 2012. These ideal conditions for life and human development caused the abrupt increment of our population and witnessed the rise and fall of our civilizations, which popularly we perceive as the true and only human societies, even though they are a rather ephemeral manifestation of them. During civilized times, many things have changed: farming, writing, monotheism, industrial revolutions, and globalization. Our perception of ourselves and of nature must have unavoidably changed as well. We started having words in our dictionaries such as environment, wild, resources, services: ideas that are children of this very specific form of society. It is not a big surprise that we developed economic, scientific and technological concepts that are shaped outside nature, with which they interact as a source to extract resources and as a sink to dispose of waste, in a very Descartes-like, mechanistic way.

As part of the development of our civilizations, we influenced the environment (here used as with humans included), to a degree and with a rapidity that no other species that we know of could rival, as reported by Hogan, 2012. This is why the use of another name for the epoch we are living in, the Anthropocene, is often debated. Its temporal limits are controversial (between 70 and 8000 years depending on the definitions, according to Gulledge, 2013; Syvitski et al., 2020), but its concept is widely accepted. The single most significant attribute of the Anthropocene is the human driving of climate change, as reported by IPCC, 2014, one of the most severe threats to human civilizations we are currently facing, as stated by the IEA, 2021. The scientific community has reached an unprecedented consensus around the findings such as the warming of the atmosphere and oceans, the diminishing of ice and snow amounts and the rise of sea levels that we have directly caused with the emissions of greenhouse gas, driven by economic and population growth, as reported by IPCC, 2014. The immediate consequences of these changes include extreme weather and climate events (cold and warm waves, heavy precipitations), and possibly severe, pervasive and irreversible impacts on people and ecosystems. Additionally, according to the reports by IPCC, 2014 the risks brought by climate change are greater for disadvantaged people and communities. The global picture drawn is one of a deep ecological and societal crisis. In fact, really the Holocene is the scene not only of jubilation of life but also of new mass extinction, according to Ceballos et al., 2015; Cowie et al., 2022. To grasp the entity of the problem, during the last 50 years, we lost on average almost 70% of the monitored wildlife, with a peak of 94% in Latin America according to WWF, 2022. The most conservative estimates scientists can provide show a resounding extinction rate of at least 100 times the normality, but it could be more than one order of magnitude higher for some animal classes according to Ceballos et al., 2015.

The implications of our impact on the planet (including on the preservation of our civilization) have been known, at least partially, for nearly half a century by now. However, no progress can be observed in this direction at a global scale. The reason for this paradox is complex and possibly rooted in the nature of our current culture and economic system. Among the key factors, one could list the lobbying of fossil fuel companies and the addiction of our political system to capitalism and GDP growth, according to Hickel, 2021; Raworth, 2017. The main global driver of greenhouse gas emissions (causing climate change) is the use of fossil fuels for energy purposes according to the IEA, 2019. It is therefore evident that any attempt to advert the crisis must include a massive scale-down of fossil fuels and the deployment of renewable energy. Despite the consensus on this aspect, the needed changes in the energy policies are still lagging, as the near-term measures currently implemented are not sufficient to achieve the target (global warming below 1.5 °C), which seems to be more out of reach for each year that goes by (see IEA, 2021). All the scenarios prospected that could bring us within the estimated "safe planetary boundary" of 1.5 °C temperature increase, involve risky and not fully understood factors, such as massive use of bioenergy, upscaled carbon capture and behavioural changes. In other words, the global political systems are basing their inactivity regarding the safeguarding of a diverse and safe ecological and human world on the hope that in the future we will master currently unreliable technologies.

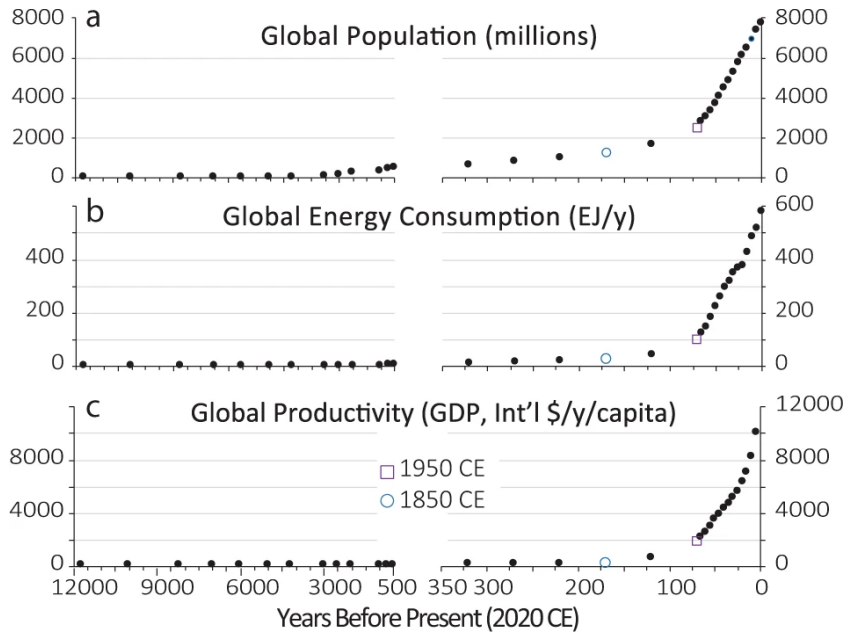

Figure 1.1: From Syvitski et al., 2020. a) Global human population (millions), b) global energy consumption (EJ/y), and c) global productivity ($/y/capita), across the Holocene and proposed Anthropocene epochs (here starting in 1950 CE). All three parameters are highly correlated (Spearman's rank coefficient=1.00). Larger circle=1850 CE; large square=1950 CE.

But would energy technology alone be able to solve such a crisis, that is deeply rooted in our culture? Are we not having a too narrow vision of the problem and of the required solution? I personally believe that any attempt to solve the climate crisis will enhance exponentially its chances of success if it will include an energy technology revolution within a much wider cultural and economic revolution, and I believe that to do so we need to reinvestigate what we take as a given. There are some questions that may be important to answer if we want to shape a different future: What is the human position within any ecosystem? What is the purpose of civilizations? How does the economy connect to the broader world? Only after answering them, we may correctly develop energy technologies that satisfy current needs (providing good living conditions for all, within a finite and destructible world). Luckily, we have all the means necessary to leave in a sustainable way, as we managed to do so for at least the 98% of our history. The matter is now how to use our knowledge to shape a civilization that is also guaranteeing the flourishment of human lives simultaneously.

Along with the other fundamental aspects of society, the type and structure of knowledge deeply changed during the Anthropocene too. In prehistorical hunter-gatherers societies, humanity was relying on an intimate knowledge of the living world around them, as reported by Scarre, 2018: to survive and thrive they had to master and memorize plenty of information on plants, animals and landscapes in their habitat. Not surprisingly, also the first form of spirituality, animism, entailed a strong connection with those elements, as reported by Peoples et al., 2016, emphasizing the inextricable connection between humans and all the rest of the

natural world. This type of spirituality strongly resonates in modern ecological ethics, as in the work by Curry, 2011, economics, as in the work by Daly, 1997 and complex systems science, as in the work by Shalizi, 2006. With the fast rise of civilization, knowledge expanded to different subjects and diversified greatly. However, at the same time, the spiritual world got separated from the rest, especially under empires and transcendental religions (Confucianism, Hinduism, Zoroastrianism, Judaism and Sophism), as reported by Hickel, 2021. In Europe, we have a strong and still proud scientific tradition, relying on fathers like Francis Bacon, which sees the "wild" world as an external, usable resource, to be kept in check and exploited according to our needs. This is still visible not only in the operation methods of economic activities (from farming to mining) but also in new terminology like "ecological services". It is interesting to observe how the scientific community is currently experiencing a sort of scattered awakening: Jungell-Michelsson and Heikkurinen, 2022 observe that a growing number of authors in the fields of ecological economics, political ecology, and ecological philosophy propose the concept of sufficiency, the idea that it is desirable to shift the attention from increasing people's wants to meeting people's needs. These ideas find strong agreement with the ones of Raworth, 2017 and Hickel, 2021, and might be the only pathway towards a sustainable and just future for humanity (see Hickel, 2019; O'Neill et al., 2018). It may be time to rediscover the way we think about science and engineering, looking back at the roots of what is knowledge for, as part of the cultural revolution needed to drive us out of the climatic, ecological and societal crisis we are facing.

We should remember that it is the adaptability of culture the most prominent feature of humanity, and the one we should harness to ride this new tide of change. Humanity adapted its culture from nomadic to agricultural, from tribal to state-based, and from regional to global. Humans' mindset changed from when biological energy was the limiting factor to growth to when virtually infinite power was available through fossil fuels, and from when human interactions were the limits of communication to when computers extended our possibilities.

As mentioned, energy technology plays a pivotal role in shaping a sustainable future. Its importance, though, does not reside uniquely in the emission or capture of greenhouse gas. Energy sources like plants, animals and fuels are effectively shaping human lives and societies. The word *fire* alone is awaking a long series of ancestral feelings. Fire is light, warmth, safety, destruction, and purification, it is the hearth from which every journey starts and to which every journey ends. It was also the main form of energy humans used for most of their history, both during the hunter-gatherer period and the farming period, as reported by Froestad and Shearing, 2017. Around the need for fire, we developed knowledge, activities, social interactions, division of labour, and cooking. Later on, we used biomass fire for the first industrial activities (baking clay, melting metals) and agricultural purposes. Those uses deeply changed society, bringing people to specialize and separate from each other, as highlighted by Froestad and Shearing, 2017.

Then, the use of fossil fuels and the industrial revolution came, hand in hand, to drastically change things. Poverty was greatly reduced, mobility was revolutionized, and electricity was

invented. The energy available to each human being increased exponentially together with the resource use, as reported by Fischer-Kowalski et al., 2014, boosting the world's population, life expectancy and quality. At the same time, fossil fuels powered the Western colonisations, and in general unprecedented divisions among people and inequalities, as reported by Kocka, 2018. Another fundamental aspect is energy security, which motivated many modern wars and is today a major societal risk over the world and in Europe, for example, evident in the words of von der Leyen, 2022. On top of this, the additional (and long-neglected) cost of their use is, as mentioned, the disruption of the Holocene's climatic balance.

We could well expect that the choices on energy technology and sources we make today will greatly affect how our society will look in the future. My hope is that we can design an energy system that is sustainable and fair. A system that is placed within the ecosystems and not out of them. A system that satisfies human needs, accounting for their complexity. A system that distributes the benefits and the costs and that is meant to last.

Reducing energy consumption, energy efficiency and renewable energy are the three pillars that must sustain this new energy system. However, to be realistic, the mitigation of greenhouse gas emissions will be also necessary to try to limit the effects of climate change in this slowly reacting world.

As a researcher working in the field of energy science and technology, the idea of needing such broad and fundamental changes can feel overwhelming. Luckily, nobody has to solve all the problems at once, or rewrite scientific history in one day, but we can rely on the community. In fact, knowledge is mostly cultural progress rather than a personal one. As observed by Nelson and Nelson, 2003, the learning process of the people earning the knowledge is often accompanied by a more or less formal training mechanism, which is a substantially cultural feature as it is based on the experience of previous generations. It is truly encouraging, then, to think about how good we became at making knowledge accessible. It is in this spirit, in the awareness of being a piece of our complex and fallible culture, that this thesis was compiled. In it, some open challenges regarding the investigation and application of nanoporous materials for adsorption energy technology are addressed. As for most efforts, it is not much, just an ephemeral piece of an ever-evolving puzzle, a quick blink of the eye for the human traveller embarked on the journey of discovery and of rediscovery. As an individual, it is a pleasure to contribute to the cumulative knowledge of a field that has the potential to bring us one step closer to a sustainable and fair energy system. In fact, adsorption energy technology touches more than one of the pillars of a new and desirable energy system: it can increase energy efficiency and the use of renewable energy, as well as mitigate greenhouse gas emissions.

In addition to the confidence that the human knowledge culture brings, one must be aware of its intrinsic flaws. While knowledge often simplifies the path to the *know-what* and *know-how*, it certainly implies a strong bias on *what-is* and *how-is*. Even within the very field of adsorption, the theory of Polanyi had a hard time becoming accepted given its historical context, as himself recounted (Polanyi, 1963). A moment in which we face challenges whose relevance is inter-

generational raises a reinforced interest in these cultural patterns. Unfortunately, it is not enough to design the most efficient process or the most powerful equipment to "save the world": it is remembering why we want it in the first place that does. We must remain aware of the complexity, keep challenging the *what* and the *how*, and not close our minds around our own culture and knowledge. As individuals, and especially as scientists, we must be humble and curious. Conducting energy research in these times requires it, maybe even more than in any other field.

1.2 Adsorption Energy Technology: History, Applications, Market and Main Challenges

Let us be started with some definitions of what adsorption is.

Adsorption can be defined as a process in which material (adsorbate) travels from a gas or liquid phase and forms a superficial monomolecular layer on a solid or liquid condensed phase (substrate), Crawford and Quinn, 2017.

Adsorption is the accumulation of concentration at a surface and is the consequence of interactive forces of physical attraction between the surface of porous solids and component molecules being removed from the bulk phase, Thomas and Crittenden, 1998.

What one can notice is that these kinds of definitions are quite general, and do not refer to any specific field of application. Actually, their formulation does not even strictly determine the thermodynamic state of the "travelling" or "concentrating" substance (which we will call adsorbate) and the receiving surface (which we will call adsorbent). One definition is more strict in defining the destination (which has to be a monomolecular layer), while the other is more strict in defining the mechanisms of transfer involved (concentration due to physical attraction). Both definitions agree on the fact that adsorption happens at a molecular level.

The IUPAC definition goes *Increase in the concentration of a substance at the interface of a condensed and a liquid or gaseous layer owing to the operation of surface forces.*

The consequence of this increase in concentration during adsorption will always be some sort of mass transfer (especially diffusive) and accumulation of the adsorbate, as explained by Ruthven, 1984.

Hygrometry belongs to the family of adsorption techniques and has been used since ancient times, as reported by Robens and Jayaweera, 2014, with first experiments documented in the Bible and later on quantitatively measured in the 1st century BC. The modern chemistry developed in the 18th century marked the beginning of surface measurements (Lavoisier, 1789), but it is with the experiments of scientists like Brunauer et al., 1938, McBain and Bakr, 1926 and Langmuir, 1918 that the classical theory of adsorption is founded. The main application of adsorption was to remove contaminants from gases and liquids, in particular,

charcoal in gas masks during World War I, as reported by Thomas and Crittenden, 1998. Other adsorbent materials of this first phase included alumina, bauxite, silica gel, bone char, activated charcoal, magnesia, and activated carbons. Both batch and continuous flow adsorption configurations were used, as reported by Thomas and Crittenden, 1998.

Since then, adsorption was vastly used in chemical engineering for many purposes (oil refinement, decolourization, drying etc.). Modern applications in carbon capture and storage facilities belong to this category. In particular, state-of-the-art physical CO2 adsorption is being studied as a less energy-intensive alternative to absorption processes, as reported by D'Alessandro et al., 2010.

The application for energy conversion and storage belongs to a different family. In this case, the adsorption capacity of the adsorbent is not used to change the composition of the adsorbate, but rather to harness the high bonding energy between adsorbent and adsorbate, as reported by Builes et al., 2013. During adsorption, the adsorbate releases high amounts of energy in form of heat as it changes its thermodynamic state. By providing an equivalent amount of heat, the process can be reversed, enabling the conversion and storage of heat. Current applications include heat pumps, as by reported by Demir et al., 2008, chillers, as reported by D. Wang et al., 2010 and energy storage solutions, as reported by Lefebvre and Tezel, 2017, powered by the heat of combustion, solar or waste heat (see respectively the works of Meunier, 2013; Zhai and Wang, 2009; L. Zhang, 2000).

Heat-powered adsorption cycles for energy conversion and storage have been the topic of extensive research since the 1973 energy crisis, as reported by Meunier, 2013, in particular for the first time with solar-powered systems using natural and 13X zeolites. Since then, numerous combinations of adsorbent and adsorbates (working pairs) have been tested, including activated carbons/methanol, activated carbons/ammonia, silica gel/water, and NaX zeolites/water.

Adsorption energy technology is obviously attractive as an environmentally friendly technology, promising to maximise the usage of solar and waste heat, while at the same time decreasing the stress on the electric power system. However, after fifty years since their first commercial development, it remains a niche technology, with limited market size (several hundreds of units) and therefore high costs of production, according to the report on Renewable Heating and Cooling, 2012.

Commercial manufacturers such as HIJC (USA) and Mayakewa (Japan) exited the market after a 20-years presence. Current manufacturers of adsorption machines include:

- Bry-Air (Asia) Pvt. Ltd., with 10-1000 kW products range, using silica gel/water, India
- Fahrenheit GmbH, with 10-100 kW products range, using silica gel/water and zeolite/water, Germany

Bigger companies such as Viessmann and Vaillant released adsorption heat pumps for a short period of time, as reported by the report on Renewable Heating and Cooling, 2012 and by Jobard et al., 2020. Also, the promising development and commercialization of dedicated adsorbent materials (AQSOA-FAM) (see the work by Kayal et al., 2016) by Mitsubishi Plastics (Japan) was interrupted. Interestingly, adsorption heat pumps have been identified by NASA as suitable for lunar applications, as reported by Lambert and Jones, 2005.

Despite this, the research community remains very active and works at different scales. The most commonly reported bottlenecks to the widespread use of adsorption devices are poor heat and mass transfer, deterioration of the adsorbent, low efficiency, vacuum requirements, large volumes, and weight, too narrow window of operation, as reported by Demir et al., 2008; on Renewable Heating and Cooling, 2012; D. Wang et al., 2010. Those issues can be effectively addressed in different ways, including:

- The selection of the adsorbent/adsorbate working pair (L. Wang et al., 2009)
- The enhancement of adsorption (Huber et al., 2019), heat conduction (L. Wang et al., 1999) and gas diffusion (Ammann, Ruch, et al., 2019) properties of the adsorbents
- The minimization of heat and mass transfer resistances in the adsorber component (Eun et al., 2000), including the material integration on the heat exchangers (Schnabel et al., 2018)
- The design of the adsorption, the evaporator and the condensers heat exchangers (Lanzerath et al., 2016; Schnabel et al., 2018; D. Wang and Zhang, 2009)
- The design of the adsorption equipment, including energy recovery (van Benthem et al., 1995; Wu et al., 2002) and temperature difference optimization (Pan et al., 2022)
- The implementation of advanced control strategy (Bau et al., 2017)
- The integration in energy systems (R. Li et al., 2019), taking advantage of the available or desirable energy flows in combination with the properties of the working pairs.

Moreover, it will be fundamental to break the cost barrier by improving the manufacturing methods, including assembly, coating, nanostructuring, adsorbent materials production, the combination with compressor technology, and the use of ultra-low grade heat. Given that adsorption heat pumps and heat storages are still in the demonstration phase, it is reasonable to expect that there will be tremendous improvements during the commercialization phase if they prove to be affordable and reliable.

In fact, there are some key non-technological factors that are influencing the current situation and that may determine the future commercialization of adsorption energy technology, as reported by the report on Renewable Heating and Cooling, 2012:

- Energy prices
- Heat/electricity energy prices ratio
- Public opinion
- Knowledge and training in planning, installing and operating personnel
- Policies such as subsidies and incentives
- Regulation (affecting the time of delivery)
- Standardization

The application of adsorption technology to Carbon Capture Use and Storage (CCUS) is gaining the spotlight instead (see Abbasi, 2022; Pole, 2022; Wright, 2022; "Xebec Announces MOU for CO2 Capture and Sequestration Equipment with Summit Carbon Solutions", 2022), and is attracting a lot of investments from both public and private investors. As mentioned in the previous section, all the possible paths that could keep us within the global warming planetary boundary of 1.5°C include a massive upscale of carbon capture and storage, in particular from biomass. While solar thermal heat is barely mentioned by the International Energy Agency, CCUS is ubiquitous (see IEA, 2020).

Whichever the reasons for this fact might be, it is interesting that in this case the emphasis given by international agencies is reflected in the hype in the media. However, the overall benefits of the implementations are under debate, given the high energetic costs, the necessary time of development and the use of the captured carbon dioxide for enhanced fossil fuel extraction, which might make the technology not compatible with the Paris Agreement (see Minx and Nemet, 2018; "The reality of carbon capture utilisation technology", 2022; Thorpe, 2021).

The use of thermally-driven adsorption cycles, or Temperature Swing Adsorption (TSA), in post-combustion mode aims at reducing the energetic costs when compared to state-of-the-art solutions such as amine scrubbing, while also the possibility of installation at low cost on existing plants (without modifying the energy production), and running on the abundant waste heat of power plants, as reported by Chao et al., 2021; Jiang et al., 2020.

The power sector (coal, oil and gas power plants, with coal being quickly replaced by biomass) and the cement and chemical industry should massively deploy CCUS (in the order of gigatonnes per year). Direct air capture should also be implemented, but on a smaller scale (in the order of hundreds of megatonnes per year) (see IEA, 2020). Those are impressive numbers considering that today's total capacity is in the order of tens of megatonnes per year. This means an expected average growth rate of the sector between 10% and 20% depending on the scenario. Current numbers reported by Institute, 2021 are strikingly encouraging, but its future strongly depends on the demonstration of the effectiveness of the technology.

TSA could clearly contribute to the success of this strategy, but some challenges should be tackled (as reported by Drage et al., 2012; McDonough et al., 2018; Siegelman et al., 2019):

Object	**Power density [W/kg]**
Stars	2.00E-04
Plants	9.00E-02
Traditional Dutch windmill	1.50E-01
Human body	2.00E+00
Modern German windmill	2.00E+00
Human brain	1.50E+01
Vacuum cleaner	1.80E+02
Adsorption heat pump	0.2-2E+03
Jet engine Boeing 747	2.00E+03
Space shuttle engine	2.12E+06

Table 1.1: Power densities of various objects reported by Spier, 2015, provocatively compared with adsorption heat pumps.

- Developing long-lasting materials that can capture carbon dioxide from real flue gas, which means
  - Low partial pressure of carbon dioxide
  - High partial pressure of oxygen
  - Saturation with water
  - Presence of pollutants
- Reduce the energy and temperature required for the regeneration of the adsorbents
- Increase the mechanical resistance of adsorbents for moving beds
- Reduce the cost of production of the adsorbents
- Reduce the cycle times by material and bed design
- Improve heat recovery

It is possible to notice that the challenges to the success of adsorption energy transformers and adsorption carbon capture technologies are largely overlapping. The development of more adsorbing and faster materials, their scale up and integration in efficient reactor designs are fundamental. For this reason, it is possible to apply similar research methods to the two fields and to transfer knowledge between them. This fact is of great interest to both the research communities of adsorption heat transformers and carbon capture, as their knowledge has been traditionally separated and now there is the chance for fast and effective communication, leading to novel methodologies, improved understanding and effective processes. In this thesis, after addressing some challenges in the field of energy transformation, we will investigate possible pathways to transfer knowledge, methods and results to carbon capture applications.

1.3 The Position of the Thesis within the Literature

1.3.1 Recent Research

As highlighted in Section 1.2, for adsorption technology to come to the aid of the current energy crisis, multiple challenges must be solved. In this section, the ones pertaining to heat transformation by adsorption will be analysed in more detail so that it will be possible to position the present work within the broader research field. Some of the more recent works addressing each specific challenge are used as examples to clarify the type of research currently ongoing, but given the high amount of existing work, this is not meant to be a complete review. More space will be given to those specific aspects of research that are more relevant to the thesis.

Given the relevance of heat-driven carbon capture application, in the thesis, we will build on the knowledge and existing methodologies in the field of heat transformation and attempt to transfer the knowledge in a preliminary way and highlight the open challenges for a more complete transfer. For this reason, a similar brief overview of this second field is omitted here but will be compensated in the relative sections.

Fundamental adsorption theory and experimental characterization

The investigation of the fundamental aspects of the adsorption of gases on solids strongly relies on the theory and experiments developed during the last decades.

There exist many established characterization techniques relevant to adsorbents (e.g. surface area analysis, thermogravimetric analysis, porosimetry, differential scanning calorimetry etc.). However many of these are either indirect (e.g. physisorption of gases for characterizing porosity) or limited in range (e.g. dynamic vapour sorption (DVS)) and thus rely on models for interpretation or extrapolation of data respectively. Many of the models used for the traditional characterization of adsorbent materials (e.g. the Brunauer–Emmett–Teller theory by Brunauer et al., 1938) are subject to fundamental errors that can lead to interpretation errors. Moreover, experimental difficulties and uncertainties, such as the difficulty of the determination of the adsorbent mass for DVS, are not to be underestimated.

Statistical physics (see Roque-Malherbe, 2018; Tovbin, 2018) such as classical adsorption theory and gas-lattice models are being used to improve our understanding and the models used for data interpretation. These methods give new insights into different phenomena including:

- the influence of neighbouring adsorption sites on heterogeneous surfaces
- non-uniform stratification of the adsorbed layers
- the mechanisms of transport of molecules within the porous material

- the derivation of diffusion coefficients explaining experimental observations
- a description of the capillary flow in mesopores
- the behaviour of gas mixtures
- hysteresis and meniscus formation

Materials science progressed rapidly and led to the discovery of a great number of porous adsorbent materials. One can only imagine the benefits that adsorption energy technology could get from exploring all the possible materials, as they greatly impact practical performance in various ways. However, this is a challenge for the classical theoretical model enhanced experimental approach as the extremely large number of possible adsorbent-adsorbate pairs are outside the range of worldwide characterization capacity. In addition, the analytical techniques are constantly updated, integrated and evolving. In particular, the validation of microscopic details of adsorption is a challenging task.

Development, tailoring and integration adsorbent materials

The adsorbent materials are either natural or (mostly) synthetic. Either way, they have to be produced, treated or processed before their application in adsorption energy technology.

In particular, the synthesis of new materials and the production of sorbents integrable into the heat exchangers (e.g. for coatings) are of interest. For example, Khutia et al., 2013 synthetized MIL-101Cr functionalized materials specifically for heat transformation applications. More works on this line are being conducted for MOFs by various authors as Jeremias et al., 2014; Jeremias et al., 2013; Towsif Abtab et al., 2018.

However, not only MOFs are under development. Novel activated carbons were produced from biomass by Pal et al., 2017 and by sol-gel route by Huber, Ruch, Hauert, Saucke, et al., 2016. Furthermore, commercial activated carbons were tested with methanol by Gordeeva and Aristov, 2014 and ethanol by Tierney et al., 2017. Even the well-known silica gels are being investigated, for example, by the creation of microfibers for coatings by Freni et al., 2019.

The adsorbent materials can often be improved, tuned and optimized for certain applications with both physical and chemical methods. In their reviews S. K. Henninger et al., 2017 and Y. Aristov, 2014 both reported many examples of tuning the adsorption behaviour of:

- dealuminiated zeolites,
- functionalized zeolites,
- tailor-made aluminophosphates, silico-aluminophosphates and metal-organic-frameworks,
- composites salts inside porous matrixes.

Moreover, the heat and mass transfer properties can be improved with novel integration methods in the heat and mass exchanger. H. Liu et al., 2013 improved mass transfer with a honeycomb shape, while Ammann, Ruch, et al., 2019 used magnetically aligned porosity. The heat transfer can also be enhanced with metal additives, as done by Rezk et al., 2013b, or with expanded graphite, as done by El-Sharkawy et al., 2016. Freni et al., 2015 instead, focused on the preparation of optimal coatings from a mechanical standpoint.

In general, the research in this field continues on two fronts: the production of more performing materials and strategies to make optimal use of the existing materials. Both are equally relevant and have the potential to level up the device's performance. If new materials show much higher adsorption capacity, it is also true that without their effective and long-lasting integration on heat-exchanging surfaces, they cannot be used satisfactorily.

Selection of the working pair

The selection of the working pair for energy applications is a hot topic, as it determines the achievable performance in a given application. A database of material's properties and adsorption curves can be used in a thermodynamic model to calculate performance indicators, as done for example by Freni et al., 2016. This method can be very effective to identify the most promising pairs for pre-determined working conditions. Similarly, de Lange, van Velzen, et al., 2015; de Lange, Verouden, et al., 2015 analyzed working pairs with MOF sorbents one by one. As highlighted in the overview by Askalany et al., 2013, many more working pairs are possible and could be tested in the future. However, most work reported in the literature focus on expected adsorption per gram at equilibrium and, as Y. Aristov, 2014 correctly comments, other factors should also be included to determine the optimal working pair, such as the shape and the density of the adsorbent and the cycle management.

As Santori and Di Santis, 2017 correctly report, the search for new working pairs often involved many adsorbents combined with few adsorbates by trial and error. However, they present a more thermodynamically sound analysis of the adsorbate's required characteristics that should be included in future investigations in this field.

Computational materials science and materials discovery

The progress of computational material science and artificial intelligence (see for example Mahmoodi et al., 2018) is opening new exciting opportunities and is likely to continue to do so in the future. Quantum chemistry for example has been used to understand the properties of materials and gases (see Mehio et al., 2014; Odoh et al., 2015) and the adsorption energy (see D. Yu et al., 2013), especially for crystalline sorbents.

Based on these techniques, advanced adsorbent material discovery is currently being proposed for various purposes: finding optimal adsorbents among existing materials (see Moghadam et al., 2018), guiding the synthesis of new materials (see Pulido et al., 2017), and finding optimal

adsorbents within a theoretical database (see Banerjee et al., 2016). These approaches are already being applied to many use cases and can be tailored and perfected. These methods rely on good property-performance relationships, either based on theory or on statistical extrapolation (e.g. through machine learning/artificial intelligence). Where based solely on theory and computational materials science, the methods are limited by the accuracy of those methods (especially when applied for high throughput) and where based on experimental results on the accuracy and availability of the training data.

Characterization of heat and mass transfer & Design and characterization of adsorption heat exchangers

These two challenges are conceptually different, as the first directly addresses the phenomena occurring at the material level and the second considers the whole heat exchanger as an object. However, they are so intimately connected that a completely separate analysis is not possible. In fact, the reciprocal influence of materials and heat exchangers' characteristics is prominent, and the methods used for their development overlapping.

Heat and mass transfer in porous media during adsorption is a topic of its own. Due to the entanglement and non-linearity, it is particularly difficult to characterize and many approaches are possible, depending on the scope of the research.

When effective coefficients of a whole heat exchanger within a specific range are needed, they can be experimentally characterized as done by Seol et al., 2020.

In terms of modelling the effective heat exchanger coefficients, approaches with different levels of complexity are possible as well, as summarized in a review by Pesaran et al., 2016. Cheng et al., 2016 report that 3D models including the adsorbate flow within the heat exchanger deliver much more accurate results and are therefore desirable. For this reason, most of the latest models include full-scale CFD techniques to explore different designs, as well depicted in the work reported by M. M. Saleh et al., 2020 for three geometries of MOF-coated heat exchangers.

Within such 3D models, the models for specific mechanisms of heat and mass transfer are included. The choice of the theoretical description of heat conduction and, even more, of mass diffusion is particularly debated (see the review by Pesaran et al., 2016). Teng et al., 2016 reports a similar finding, and highlights how classical heat and mass transfer models fail to describe correctly complex systems and that simple lumped-parameter models are often preferred over more accurate but complex ones in practice.

Among the mechanisms that could be studied one could list heat conduction (see for example Yin et al., 2021), intraparticle mass diffusion (see for example Hong et al., 2014) and interparticle mass diffusion (see for example Ammann, Michel, and Ruch, 2019).

The reason behind the focus on intraparticle mass transfer is that it often limits the rate

of reaction in most granular adsorbent materials, that are microporous. In materials with a different pore structure, this would be different and understanding heat conduction, for example in the case of materials with low thermal conductivity and high gas diffusivity, would become fundamental.

The preference towards simple modelling techniques applies also when coupling the adsorption dynamics with other system components, and lumped-parameter models are effective to save computational time (see Palomba et al., 2021), especially when modelling spatially extensive systems such as heat exchangers. Moreover, accuracy in the characterization of such systems is not always guaranteed, and such grey-box approaches are indeed a reasonable compromise between precision and accuracy, and a more detailed model might be more precise but not more accurate.

On top of describing the heat and mass transfer mechanisms taking place at the material level, the heat exchangers are produced by integrating the adsorbent, characterized and modelled to understand and predict their performance as a whole. For example, Freni et al., 2015 did it with a SAPO-34 coated heat exchanger, and Rezk et al., 2013b with a packed-bed heat exchanger with silica gel. Many more works on this line exist, underlying the relevance of this step of research and development (see the review fromSharafian and Bahrami, 2014).

In general, despite the modelling techniques for describing adsorption heat exchangers being widely available and applied, the debate on its fundamental assumption is still relevant. In particular, grey-box approaches adopted so far deliver accurate results, but leave unsatisfied a part of the research community that sees the application of such a simplified description of the heat and mass transfer as limiting in the sense of extrapolation ability. On the other hand, the more complex 3D approaches exist (sometimes relying on debatable submodels), but are not implemented in practice due to their high computational cost.

Design and characterization of heat-driven adsorption devices

Instead of focusing on the heat exchangers, it is sometimes useful to investigate the whole heat transformer. Given the growing complexity of entire devices, more accurate and material-based approaches start giving place to effective descriptions of the overall performance. There are many approaches to doing so.

Dino et al., 2021 experimentally characterized a hybrid adsorption chiller based on the layout and on driving temperatures. Sapienza et al., 2017 experimentally characterized a 3-bed adsorption chiller, reallocating adsorption and desorption times to improve the performance. Han and Chakraborty, 2020 model an adsorption chiller to investigate the effect on the overall performance of a specific MOF functionalization. San and Tsai, 2014 tested a 4-bed adsorption heat pump to analyse the performance of the different components. Graf et al., 2016 combined heat exchanger tests and dynamic heat transformer models to have an adsorption-focused analysis of the heat transformer performance. Frazzica et al., 2016 designed, realized and

tested a carbon/ethanol chiller which could work in refrigeration (sub-zero $^{\circ}C$) applications. Rezk et al., 2013b used a chiller model to investigate the potential effects of heat and mass transfer improvement techniques applied to the adsorber component. Krzywanski et al., 2017 developed a genetic algorithms/neural network model to optimize adsorption chillers without a heat and mass transfer model.

In this kind of study, given the complexity of the analysis and the many factors at play, most of the design choices are fixed, so that the role of the ones under investigation in the experimental range can be clarified.

Heat and mass recovery and advanced cycles

As the coefficient of performance of an adsorption energy transformer is low when compared to mechanical-compression devices, efficiency measures such as heat and mass recovery become extremely important.

Adding heat and mass recovery steps in the cycles by putting in communication different beds can significantly improve the power and efficiency performance, as reported by Lu and Wang, 2013. Pan et al., 2015 used a computational fluid dynamic model to compare different heat recovery strategies, including circular, serial and passive recoveries. Serial and passive heat recovery (involving only a partial recovery) seems preferable, especially in terms of implementation cost, with serial heat recovery being faster. Most of the heat recovery is dedicated to the heat transfer fluid, and part to the metal, while the adsorbent is not particularly influenced. A similar finding was obtained experimentally by Pan and Wang, 2017 for serial heat recovery. The thermal wave process (see Çağlar, 2016; Qian et al., 2015) aims at heating and cooling gradually the adsorption heat exchanger, creating a gradient of temperature that can be used to maximize heat usage. It is a similar approach to using counter-flow heat exchangers, with the difference that in the thermal wave, a heat transfer fluid circulates between the hot and the cold bodies. The geometrical parameters affect the heat recovery performance, which can be up to 60%. X. Li et al., 2015 instead summarize different works from the literature and conclude that improvements of COP are up to 100% with mass recovery.

Cycle time management is another strategy to improve the cycle (see Y. Aristov et al., 2012; Sapienza et al., 2017), which in some cases is one of the most significant efficiency measures, as reported by Alahmer et al., 2019.

These cycle enhancements have been also experimentally tested by several authors (see Dino et al., 2021; Pan and Wang, 2017; Pan et al., 2016).

Design and integration of adsorption processes

Some works aim to optimally implement adsorption machines into various energy processes. Lombardo et al., 2019 investigated the integration of an organic Rankine cycle with an adsorption chiller for trigeneration by dynamic modelling. Palomba et al., 2018 investigate experimentally and numerically the combination of a solid-oxide fuel cell and an adsorption chiller for multi-generation. Calise et al., 2017 modelled a quite complex polygeneration system based on solar energy (PVT), heat pumps, adsorption chillers and electrical energy storage.

The results obtained in this field are auspicious and show high potential for synergies with different technologies that should be further investigated. For example, in their review, Fernandes et al., 2014 highlighted many existing integrations with solar energy sources and Maraver et al., 2013 show high potential for integration with biomass energy.

In general, this kind of study is often restricted to a quite limited set of technological choices and components. There is a lack of a more complete design and integration framework addressing specifically adsorption heat transformers.

Decreasing costs

While solving the technical challenges listed above would improve the attractivity of adsorption energy transformers, it is certainly possible to aim to decrease their cost also by other means.

One obvious way is to decrease the cost of the adsorbent material itself, as it is a limiting factor to the development of innovative adsorbents. S. K. Henninger et al., 2017 discuss the difference in the production methods of the adsorbers and highlight how some have intrinsically more chances than others to compete in the market.

At the heat exchanger level, radically new approaches include the use of different materials such as plastics (see Sapienza et al., 2021) and manufacturing techniques such as 3D printing (see AL-Hasni and Santori, 2020). As the cost is such an important aspect of the technology attractiveness, this type of activity should continue and be more integrated with other research activity (i.e. in the characterization and design of adsorption heat exchangers and systems), possibly with an explicit quantification of the costs related to the different components.

Demonstration of commercial applications

The success of a new technology often comes by gaining the trust of the market by demonstrating its advantages and feasibility in commercial applications. This is true also for adsorption energy systems, which despite their long history have a short list of successful applications and lack a network of experienced professionals. However, in recent years demonstration activities have been carried out in Europe (see Scotton et al., 2019), showing at least a growing expertise

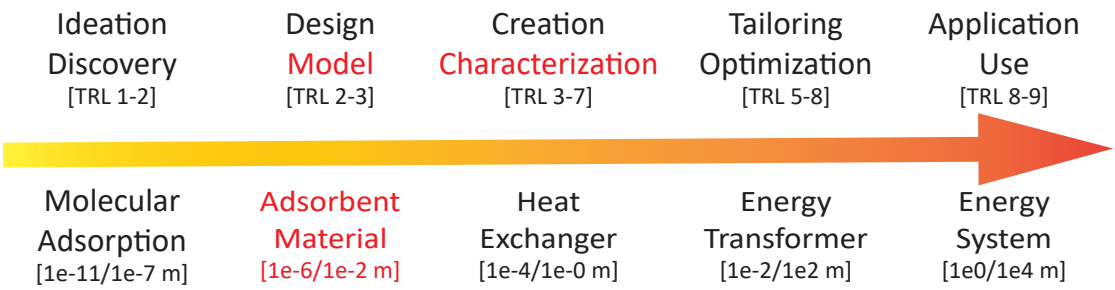

Figure 1.2: Positioning of the thesis with respect to the research field. Top: technological development. Bottom: the spatial scale.

in the engineering sector. From their results, it is surprising how most of the challenges to the application of adsorption technology in energy systems derive from the relation with other technologies: managing the solar heat, satisfying flexible/discontinuous users, monitoring the system, evaluating the performance, gathering trained technicians, standardizing the methodologies etc. In particular, the main difficulties emerge in the application to the building sector (see Frazzica et al., 2020), where the development of heat storage is essential. Another crucial aspect is the ability to share experiences and the lessons learned, thus improving the rate of technology-readiness-level progress. These reports highlight the importance of digitalization tools to penetrate the energy market of the future as well as the development of dedicated financing instruments and design tools.

1.3.2 Positioning and Structure of the Thesis

As evident from the brief categorization of the literature reported above, the research in the field covers a wide range of spatial scales (from molecular phenomena to whole industrial or residential systems) and technology readiness levels (from fundamental scientific questions to commercial operation).

In the thesis, we make use of established as well as novel techniques for characterizing and modelling adsorbent materials for different purposes. This means that the methods applied and the results obtained pertain to a relatively small spatial scale (between the μm and the cm) and relatively early technological development (TRL between 2 and 7). Figure 1.2 reports a graphical representation.

As reported above, many different approaches to materials characterization and modelling are possible, depending on the purpose. Here we try to build two novel bridges between some of the scientific challenges existing in the research field, using as a foundation the knowledge of the adsorbent materials. The application of the findings spans from the creation of improved materials and heat exchangers to the ideation of novel energy transformers and systems.

In Chapter 2, we propose to connect the exploration of adsorbent materials and of system designs more. After discussing different strategies of material characterization, we test the

harmonic selection of the adsorbent materials and the design of the systems depending on the heating and cooling needs. The chapter will reveal that the necessary tools for more tailored system designs already exist and could and should be harvested, delivering improved system efficiency. This chapter contributes to the scientific challenges *Selection of the working pair* and connects it with the *Design and integration of adsorption processes*.

In Chapter 3, we propose a new methodology to model the transient heat and mass transfer within the adsorbent material. The model combines the simplicity of the lumped-parameter approach and the accuracy of local models. In fact, for material and application development, there is a need for both, as the risk is to need unfeasibly many computational resources or to obtain unreliable results. Even if the method still has its limitation, we prove its potential with experimental validation, paving the way to its extension and application to relevant problems. This chapter contributes directly to the scientific challenge *Characterization of heat and mass transfer* and the more indirect impacts will be discussed in some use cases in Chapter 4.

In Chapter 4, we use the modelling approach from Chapter 3 to two relevant cases: the tailoring of adsorbent material to a versatile heat transformation application and the preliminary design of a novel heat exchanger based on agitation and transportation of the adsorbent. Both examples are technologically relevant and show the usefulness of the modelling technique proposed previously. In fact, the computation of the performance is particularly fast, allowing a wide screening of design parameters in the early phases of technology development, and it gives enough insights to effectively tackle the limiting factors. For both cases, the necessary research and development are not over, but we show how many other applications could benefit from the modelling approaches here adopted. This chapter contributes to the scientific challenges *Tailoring and integration of adsorbent materials* and *Design and characterization of adsorption heat exchangers*. Moreover, it includes a reflection about possible ways to contribute to *Design and integration of adsorption processes*.

In Chapter 5, we apply the existing methodology for adsorbent material characterization to the evaluation of adsorbents for post-combustion carbon capture. Similarly to what has been done for water adsorbents for energy transformation, the most important properties are characterized, this time to screen materials from a certain selection. In particular, proposing a rapid thermal swing concept in an analogy with the most competitive adsorption heat pumps, we adapt the development and characterization of fast coatings. Finally, we critically analyse the results and point towards the necessary further steps. Therefore, the chapter addresses the challenges of *Selection* and of *Tailoring and integration of adsorbent materials*, using modified methods for *characterizing heat and mass transfer during adsorption*, as they apply to rapid thermal swing adsorption.

In Chapter 6, we report the effect of long-term use and storage of the water adsorbents. This is a relevant and often neglected issue in the heat transformers research and has an immediate effect on the application under development (also in Chapter 4). In the carbon capture field, and especially for some classes of materials, some tests already exist. However, it is believed

the results can be largely extended to future research in this direction.

Finally, Chapter 7 reports a brief summary of the research exposed in the thesis, the main conclusions that can be drawn from it, as well as a summary of the key outlook.

2 Screening and Pre-Selecting Adsorbent Materials

2.1 Introduction

The thermophysical and structural properties of nanoporous adsorbents contain numerous and relevant information regarding their application potential. The researcher that aims to develop new and improved adsorption materials, devices and systems can draw a great deal of knowledge from the characterization of the adsorbent materials. In fact, if correctly questioned, the material properties can tell what an adsorbent can do if used at its best.

In this chapter, we make extensive use of them to understand, model and select the adsorbent materials for the heat transformation processes. As the materials' properties are so important, the relevance of the methodology used for their characterization cannot be overestimated. The correct characterization of the adsorption equilibrium curves will lead to an accurate estimation of the efficiency of the processes and to an improved understanding of the adsorption process experimentally measured. The correct estimation of the density and of the specific heat capacity will lead to an accurate estimation of the energy requirements of the process and improve designs.

While each material, or at least each material class, is somewhat specific in terms of its requirements for a correct characterization, it is fundamental to develop methodologies that are as accurate, reproducible and effective as possible for a wide range of them. Only with a general methodology do the researchers stand a chance to correctly compare and select the appropriate material for their application or, in turn, to understand what could be improved. This chapter is strongly built on these facts, proposing and applying methodologies for material characterization and selection as generally as possible.

Recently there has also been a push to use what is termed accelerated discovery of materials, involving statistical methods such as machine learning and artificial intelligence to scan the literature and make use of atomistic modelling techniques (see Butler et al., 2018; C. Zhang et al., 2022). While the accelerated discovery of materials is not directly addressed in this thesis, our research approach should aim to be compatible with these new and still evolving

methods. The next steps of research ideally combine the two approaches, further minimizing experimental effort and accelerating targeted materials development.

It is important to mention that an interesting and relevant effort in this direction was undertaken by Engelpracht et al., 2020. The authors created the SorpPropLib open database of adsorption equilibrium curves, accessible from several programming environments.

In this chapter, we investigate the possible improvements of current approaches to the characterization of the adsorption equilibrium curves. While we are only discussing the case of water here, the considerations about the trade-off between accuracy and effort can be extended to other adsorbates.

Furthermore, we propose a methodology to harmonize the pre-selection of the adsorbent materials and process design, based on the equilibrium properties of the material and thermodynamic modelling. By doing so, we demonstrate that this task is not only possible but also highly beneficial. The methodology could be extended and integrated with existing tools for heat integration for more serious design work, given an application of interest. Moreover, it could be further extended to include heat integration and gas separation within one modelling framework.

The chapter is organized as follows.

In Section 2.2, the adsorbent materials used in this chapter are introduced.

In Section 2.3.1, the experimental procedures used to generate the adsorption equilibrium data will be reported, while in Section 2.3.2, the rest of the experimental methods are described.

In Section 2.4 we will discuss methods of characterization of adsorption equilibrium curves. In particular: in Section 2.4.1, an analysis of the literature serves as a basis for discussing the strengths and open challenges of the current methods; in Section 2.4.2 we will propose different characterization methods; in Section 2.4.3 we will analyse the results for each of them; in Section 2.4.4 we will draw some conclusions.

In Section 2.5, we will discuss the harmonic selection of adsorbent material and process pre-design. In particular: in Section 2.5.1 we will analyse the state-of-the-art and highlight the research gaps; in Section 2.5.2 we will provide a methodology to select materials and pre-design systems based on the properties of the materials; in Section 2.5.3 we will provide the results obtained on test cases; in Section 2.5.4 we will draw some conclusions.

Finally, in Section 2.6, we will provide the general conclusions and some key outlooks of the research.

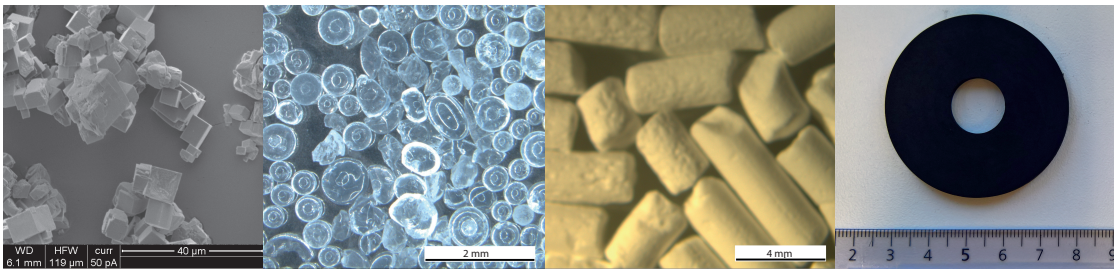

Figure 2.1: Images of some of the characterized materials. From left to right, SEM of SAPO-34 from Fahrenheit, optical microscopy of Siogel from Oker and Aluminum Fumarate from MOF Technologies, picture of the Resorcinol-Melamine-Formaldehyde Activated Carbon from Empa.

2.2 Materials

All the methods detailed in this chapter have been tested on a set of materials considered representative of the main families of adsorbents currently available on the market and compatible with water-based low-temperature heat transformation applications: silica gels, activated carbons, zeolites, Metal-Organic Frameworks (MOFs). Specifically, the seven adsorbents, some of which are shown in Figure 2.1, are:

- Siogel from Oker-Chemie GmbH, beads
- RD Silica Gel from Fuji Davison Chemical Ltd, granules
- RMF Activated Carbon produced in-house at Empa, monolithic
- SAPO-34 from Fahrenheit GmbH, powder
- AQZOA-Z02 from Mitsubishi Plastic, beads
- Aluminium Fumarate from MOF Technologies, pellets
- Aluminium Isophthalate from MOF Technologies, pellets

The RD silica gel from Fuji Davison is irregular granules with an average size of 0.84 mm. The Siogel from Oker is round beads with an average diameter of 1.1 mm. The SAPO-34 powder from Fahrenheit is an irregular powder with an average size of 0.025 mm. The AQSOA-Z02 from Mitsubishi Plastics are round beads with an average diameter of 2 mm. The Aluminium Fumarate and Aluminium Isophthalate from MOF Technologies are elongated, quasi-cylindrical pellets, with average dimensions of 1.9x3.8 mm and 1.5x3.7 mm, respectively. The Resorcinol-Melamine-Formaldehyde activated carbon from Empa is a shapeable monolith with integrated macroporosity.

2.3 Experimental

2.3.1 Water Adsorption Equilibria

Water adsorption isotherms are fundamental to calculate the heat released/absorbed during the adsorption/desorption process and the sensible heat spent during each cycle to heat up and cool down the adsorbed phase. This property is the main indicator for ranking adsorbent materials and the most complex to model, as it will be detailed further below. It was decided to measure the adsorption curves first-hand, as the experiment, as deceivingly simple as it seems, is critical and can easily be misinterpreted. The experimental measurement of the adsorption equilibria was performed primarily with a DVS Endeavour instrument from Surface Measurement System. Prior to the measurement, the adsorbents were dried under nitrogen at temperatures up to 84 °C. Due to the absence of pre-heater elements, the drying temperature was limited, and occasionally below the recommendations deriving from TGA measurement, as described in the deliverable D4.1 of the Horizon 2020 project Hycool by Galmarini et al., 2019. To make sure the drying was complete before the measurement, some additional water isotherms were measured with a VTI-SA+ device from TA Instruments, which allowed for higher drying temperatures. In particular, after drying under nitrogen at 140 °C it was found that the residual water content of the SAPO-34 and the AQSOA-Z02 was 1.2% and 6% in mass respectively. For this reason, all the adsorption equilibria experimental points obtained with the DVS Endeavour instrument were corrected by these amounts before applying fitting and test procedures.

As materials were measured in batches, the experimental points for each are slightly different. The first set, measured under the same conditions, comprises the Siogel, the RMF activated carbon and the SAPO-34. The second set is composed of the RD silica gel only. The third set comprises the AQSOA-Z02 and the two MOFs.

The measurement errors are in the order of 0.01 $[g/g]$. To improve the reproducibility of the measurements, the water isotherms were analysed according to the protocol produced in the framework of the Hycool project, as reported by Galmarini et al., 2019. Each ad/desorption step is fitted to an exponential function ($w = w_{in} + \Delta w_{max} * \left(1 - exp\left(\frac{t-t_{in}}{\tau}\right)\right)$), where w and w_{in} are the current and initial loading, Δw_{max} is the equilibrium uptake for the step, t_{in} and t are the initial and the current time, and τ is the characteristic response time of the system) using the Nelder-Mead method, described by Nelder and Mead, 1965, as implemented in R. If most of the steps were interrupted after reaching 95% of the equilibrium loading change ($t - t_{in} > 3\tau$), the experiment was considered successful and the data accepted. This systematic control leads to a significant improvement in the reproducibility of the adsorption curves, reducing scatter and allowing a more reliable interpretation of the results. For duplicates on 30°C and 50°C isotherms of Oker Siogel, RMF-AC and Fahrenheit SAPO34, the maximum deviation between isotherm points, considered valid within the limit of the a-posteriori validity check mentioned and with the same relative humidity were $\pm 0.02 [g/g]$.

Each adsorbent material was characterized with at least three full isotherms (between 2% and 95% relative humidity) at three different temperatures (between 20 °C and 70 °C). The zeolites were characterized with an additional isotherm at 80°C. Taking into account larger variations due to differences in measurement methodology in different laboratories and variation between sample batches, a good agreement was found with other data published in the literature, as the ones obtained by Brancato and Frazzica, 2018; Chakraborty et al., 2009; Huber, Ruch, Hauert, Saucke, et al., 2016; Kayal et al., 2018; Schlüsener et al., 2019. The complete water adsorption isotherm data are made publicly available on a Zenodo database by Piccoli, 2022.

The thus obtained data were split using a stratification based on the total loading into a training set (80%) and a test set (20%), in order to have a more robust fitting in both areas of high loading and low loading. The random split was performed with the Python library *scikit-learn* by Pedregosa et al., n.d.

2.3.2 Other Thermodynamically Relevant Properties

In order to compute first-law thermodynamic analysis on potential adsorbent materials, some other of their thermophysical and structural properties must be characterized, namely specific heat capacity, the specific heat of adsorption, and tap density.

To calculate the energy the sensible heat spent during each cycle to heat up and cool down the adsorbent, specific heat capacity has been measured on dry samples by differential scanning calorimetry using a Mettler Toledo DSC 1 instrument, available at CNR-ITAE, following the standard method DIN 51007. The accuracy of the method is ±2%. However, it should be noted how, due to the different formats of the studied adsorbent candidates (powders, beads, monoliths; see Figure 2.1), the achieved thermal contact during thermal characterization is not uniform. When comparing the obtained values for specific heat capacity this should be kept in mind. For the same reason, for the specific heat of sorption, the simplified theoretical value, suggested by Brancato and Frazzica, 2018, $H = L(T) + F(T, p)$ was preferred to experimental values $H = H(w)$ (see the Nomenclature at the end of the chapter).

To have realistic information about the volume of adsorption heat transformers, the effective density of the materials must be characterized as well. Tap density, which depends not only on the material structure but also on its format, was measured on a Jolting volumeter JEL STAV II, available at Empa. The dried material is put into a cylinder and weighed. The sample is tapped in multiple rounds until the difference in volume between two consecutive rounds is less than 2%, according to the American Standard ASTM D7481-18. The ratio of the sample mass and filled cylinder volume is the tap density. The size of the measurement cylinder was chosen in function of the particle size of the powder/granules measured, as the particle size (d_{V50}) has to be much smaller than the size of the cylinder to avoid surface effects (d_{V50} [mm] * 125 < cylinder volume [mL]).

2.4 Effective Strategies for Characterizing and Modelling Water Adsorption Equilibrium Curves

2.4.1 Introduction

Space, process and water heating often represent the absolute majority of the energy requirements in Europe, reaching 80% in buildings and 70% in industry, as highlighted in the report *Mapping and analysis of the current and future (2020-2030) heating/cooling fuel deployment (fossil/renewables)*, 2016. Furthermore, the demand for cooling energy is growing increasingly fast in many regions of the world, as reported by Birol, 2018. For these reasons, and in combination with the major concerns regarding the greenhouse gas (GHG) emissions coming from the energy sector highlighted in the report *Greenhouse gas emissions from energy: overview*, 2021, technological solutions able to provide clean and affordable heating and cooling are currently of great interest. Among these, adsorption heat transformers (heat pumps, chillers and thermal storages) could allow using renewable or waste heat instead of electricity, reducing the strain on the power system and reducing GHG emissions, as reported by Meunier, 2001.

The performance of adsorption equipment, however, is strictly related to the adsorbent material used. In fact, the energy efficiency depends on the adsorbent-adsorbate working pair and the power density by the adsorbent material structure and the adsorbed bed design, as reported by Demir et al., 2008. Water, due to its harmless nature and its good heat transfer and adsorption properties, is often identified as adsorbate for air conditioning and heat pumping purposes, as reported by Freni et al., 2016. As a natural consequence, many of the studies analysing the feasibility of adsorption heat transformers for these applications are based on materials research, especially focusing on their water adsorption characteristics, as reported by Demir et al., 2008. When establishing the quality of a porous material as an adsorbent for heating or cooling purposes, the main indicator is often the water adsorption equilibrium characteristic, which is used as a primary classification parameter and term of comparison, as it was done, for example, by Calabrese et al., 2018; S. K. Henninger et al., 2012; Jahan et al., 2022; Rezk et al., 2013a.

The characterization of the water adsorption curves is commonly expressed in terms of isotherm or isobar curves obtained by gravimetric or volumetric methods, as done, for example, by Kohler et al., 2017; K. Ng et al., 2001. For each material, to calculate the mass of water that can be cycled between different adsorption and desorption conditions, the water adsorption data must be described in form of temperature- and/or pressure-dependent equations, derived from the adsorption equilibrium curves in various ways. Depending on the scope of the adsorption characteristic modelling, different approaches are used in the literature.

The typical method used to experimentally characterize water-adsorbing materials is to fix one of temperature and water pressure, and gradually change the other while monitoring the sample weight (gravimetric method), as explained by Glass et al., 2018. This can be done in a relatively fast and accurate way by Dynamic Vapor Sorption (DVS). Because the

balance sensitivity is so high, the required amount of sample is in the orders of the tens of milligrams, and with modern instruments, the measurement is not labour-intensive. However, the characteristic time needed for a given sample to reach equilibrium can be relatively long, as you must ensure complete equilibrium to avoid misinterpretation of the results (e.g. reduced loading, fake hysteresis). Depending on the amount and characteristics of the material under investigation, each measurement point can require from ten minutes to several hours. When screening many potentially interesting materials for a wide range of conditions, the experiment time can therefore quickly become unsustainable. Furthermore, when the adsorption characteristic curve of a material is unknown, often more points than needed are measured, or in the wrong conditions, highlighting a problem in selecting the measurement conditions. This same issue will be present, and at a much wider scale, when screening thousands of theoretically possible materials (see, for example, the databases by Altintas et al., 2018; Ongari et al., 2019) such as Metal-Organic Frameworks (MOFs) and Covalent Organic Frameworks (COFs), through molecular simulations, as done, for example, by Dubbeldam et al., 2016; Düren et al., 2009. Exactly for this reason, when it comes to preliminary screening such a wide range of materials, simple indicators such as the Henry constant can be used for initially ranking them, as done, for example, by Monpezat et al., 2019; X. Yu et al., 2021. One of the problems of applying this approach to water-paired adsorption heat transformers applications is that typically the adsorption curves are often not of the Langmuir type, as will be detailed further below.

In case the purpose of the investigation is to determine the adsorption mechanism typical of a certain material-adsorbate pair, detailed and specific models are developed and applied, as done, for example, by Do and Do, 2000; Hou et al., 2021; McCallum et al., 1999. However, in the community of researchers dedicated to the development of materials for adsorption heat transformers, it is more common to use simpler adsorption models, whose generality and easy implementation is of great advantage. Common examples are the Langmuir model, the Sips model, the Toth model, the UNILAN model, the Dubin-Astakhov model *et cetera*. For an overview of those models, interested readers can read the works by Lima et al., 2015; Llano-Restrepo and Mosquera, 2009. In particular, the latter gained wide popularity due to its ability to describe adsorbents with an S-shaped adsorption characteristic, which happens to be advantageous in heat transformers, as reported by W. Li et al., 2021; Z. Liu et al., 2021. The Dubinin-Astakhov (D-A) model, proposed by Dubinin and Astakhov, 1971, is based on the so-called Dubinin-Polanyi theory. In short, the adsorbed phase is assumed to behave as a liquid, but with a difference in free energy called adsorption potential, including both energy and entropy terms. In the case of non-polar systems this temperature-independent formulation holds, but for polar systems (such as the case of water) this is not to be generally expected, as explained by Ruthven, 1984. Furthermore, a single D-A equation is representative of a uniform pore size distribution around a well-defined diameter, while in many commercial and novel adsorbents, more than one pore type can contribute to the total adsorption, as reported by Chun et al., 2014; H.-J. Wang et al., 2014. The limitations deriving from the use of such a model are sometimes overcome with artefacts such as the segmentation of the

fitting equation, or the limitation of the range of validity of the adsorption curve fitting to one temperature only and/or a limited range of water pressures, as done, for example, by Brancato and Frazzica, 2018. Additionally, the potential hysteresis occurring during desorption is not taken into account in the model, but two different curves are measured (or fitted) and the values obtained for the fixed adsorption and desorption conditions are used, as done, for example, by Frazzica et al., 2014. While these methods can be effective in increasing the accuracy of water adsorption loading predictions in a given temperature and pressure range, they sacrifice the extrapolation capabilities of the model. This implies that the wider the model application range aims to be, to more numerous the data points must be.

It appears that the characterization of the adsorption equilibria is subject to different challenges, depending on the motivation of the characterization itself. In the case of a preliminary screening of materials from a wide set, there is a need for a method to characterize the water adsorption properties for a wide range of conditions with a reduced experimental effort (in the laboratory or *in silico*). In the case of applying a robust and accurate characterization method of promising water adsorbents for heat transformers, there is a need for a general model capable of dealing with the inherent complexity of water adsorption in materials with inhomogeneous pores. Recently, a so-called universal adsorption model was developed with this purpose by K. C. Ng et al., 2017 and applied by Z. Liu et al., 2021 to the NIST/ARPA-E Database of Novel and Emerging Adsorbent Materials, curated by Siderius, 2020, to identify the most promising adsorbent materials. The database contained over two hundred isotherms, but only ten materials were measured at multiple temperatures. Among these, only one activated carbon fibre highlighted a significant difference in adsorption equilibria depending on temperature (see the work by Ohba and Kaneko, 2007). In none of those cases, there was a strategy to minimize the characterization effort. Based on these considerations, the present work presents two different strategies for the characterization of water adsorption equilibria in nanoporous materials and compares them against a benchmark method.

2.4.2 Methods

Benchmark

As was discussed in Section 2.4.1, one of the most common methodologies for characterizing the adsorption equilibrium curve of adsorbent materials for materials and energy transformation applications development is by fitting the simple and robust Dubinin-Astakhov model on a water isotherm curve. For this reason, this method was chosen as the benchmark characterization strategy.

Following Dubinin's theory, described by Dubinin and Astakhov, 1971, which proved to hold for many working pairs according to Stoeckli et al., 1994, the adsorption in microporous adsorbents seems to be a function of the adsorption potential F. This driving force of adsorption was first proposed by Polanyi in 1914 and widely accepted only half a century later, as reported by Polanyi, 1963:

$$F = -\frac{R}{M} \cdot T \cdot ln\left(\frac{p}{p_{sat}}\right) \tag{2.1}$$

The adsorption equilibria would be then following equation 2.2, where the coefficients w_0, C and n are temperature independent:

$$w = w_0 \cdot exp\left(-\left(\frac{F}{C}\right)^n\right) \tag{2.2}$$

In Equation 2.2, w_0 is the total volumetric adsorption capacity of the micropores, C is the characteristic energy of adsorption, and n is the shape coefficient, which expresses the pore size distribution and capillary condensation effects. Given the classical application of this model to traditional zeolites and microporous carbons, these parameters were commonly found to be temperature independent, as by Stoeckli et al., 1994. However, in novel working pairs, this might not hold true, as after all for a polar system this is not necessarily the case, as explained by Ruthven, 1984. Section 2.4.1 discusses this topic in more detail.

The definition of the adsorption equilibrium points to be characterized is arbitrary of course. However, given that the experimental control parameter is often the relative humidity, it is considered that steps of 5 % RH are sufficient to guarantee catching the adsorption peak area and big enough to not excessively waste experimental resources. As discussed, prior knowledge of the material and the application can influence this choice, but here we try to propose a methodology as generally applicable as possible. Such a choice, on the maximum range of relative humidity reasonably obtained experimentally (i.e. 2.5%-97.5%), entails the characterization of 20 points for each experiment. However, it is known from the beginning that the water loading, in first approximation, will not follow the relative humidity, but the adsorption potential. So if 20 points are to be measured on one isotherm curve, they should better be organized on *F-steps* instead of on *RH-steps*. Figure 2.2 gives a visualization of the difference between these two approaches for a 40°C isotherm. Following the "default" RH-steps, a lot of information is wasted in the low adsorption potential area, while relatively big holes are left in the high adsorption potential area. The F-steps ensure the correct capture of the adsorption peak irrespective of the nature of the adsorbent material. To plan such experiments requires $n \in \{1, ..., N\}$ steps which relative humidity is determined by the Equation 2.3:

$$RH(n) \cong exp\left(ln\left(RH(n-1)\right) - \frac{ln\left(RH_{min}\right) - \left(RH_{max}\right)}{N-1}\right) \tag{2.3}$$

In this work, the isotherms were measured with the RH-steps method, as often happens

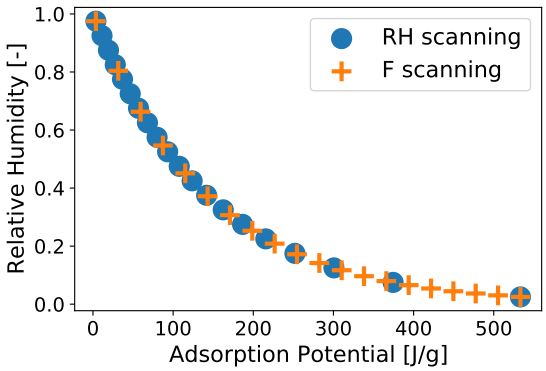

Figure 2.2: An example of characterization conditions for adsorption isotherms. A scan based on values of relative humidity does not cover homogeneously the adsorption space, and should probably be revised.

following intuitively the DVS setting options, to better emphasize the improvements achievable with the effective screening method. The optimal fits of the D-A model were obtained with the R library *nlrob*, described by Andreas Ruckstuhl, 2005, as detailed below for the *Detailed Modelling*.

Detailed Modelling

The hasty and/or unsupervised fit of the D-A model to water adsorption equilibrium data of unknown adsorbent could lead to substantial mistakes when the curves are extrapolated to different conditions. For accurate predictions of the adsorption equilibria, more robust methods such as the one proposed by K. C. Ng et al., 2017; Stoeckli et al., 1994 should be applied instead.

The DA model has been developed for non-polar adsorbates and adsorption materials with a uniform pore size distribution. When water is used as adsorbate, the adsorption equilibrium should in general be expected to be temperature dependent, as explained by Ruthven, 1984. Additionally, many of the studied adsorbent materials are characterized by multiple pore types, ranging from micropores to macropores. This can lead to inaccuracies in the DA modelling approach, as reported by Llano-Restrepo and Mosquera, 2009. Thus, an empirical modification of the DA model, accounting for up to two different pore types and an additional linear dependence of the DA parameters on temperature, is proposed, similarly to what was proposed by Stoeckli, 2002. The aim of the modification was to increase the accuracy of adsorption equilibria prediction under different conditions, keeping at the same time the original generality.

As with the original DA approach, we assume the density of the water to be constant. However, as done by Stoeckli, 2002, we allow for up to two different adsorption sites for every material (see equations 2.4-2.5, where w_{ad} is the equilibrium adsorption water loading, W_0 is the

maximum loading capacities, C is the characteristic energy of adsorption, n is characteristic of the width of the adsorption peak and F is the Polanyi adsorption potential, T the temperature, R the ideal gas constant and p_{sat} the saturation pressure and M the molar weight of the sorbate. The subscript 1 and 2 indicate the two adsorption sites.)

$$w_{ad} = W_{0,1} \cdot exp\left(-(F/C_1)^{n_1}\right) + W_{0,2} \cdot exp\left(-(F/C_2)^{n_2}\right) \tag{2.4}$$

$$F = \frac{R \cdot T}{M} ln(p/p_{sat}) \tag{2.5}$$

In addition to the above, all parameters $P \in (W_0, C, n)$ are considered to be potentially linearly dependent on temperature (equation 2.6). This temperature-dependent description of the parameters allows for a more robust application of the model to materials for which the researcher does not know *a priori* the isotherm shape.

$$P = a_P \cdot T + b_P \tag{2.6}$$

To calculate the saturation pressure of water, we used the approximation reported by Wagner and Pruß, 2002 (eq. 2.7-2.8, where T_c and p_c are the temperature and pressure of the critical point of water respectively).

$$\begin{aligned} p_{sat} = p_c \cdot exp\Big(\frac{T_c}{T} \cdot \big(&-7.860 \cdot \nu + 1.844 \cdot \nu^{1.5} - 11.79 \cdot \nu^3 + \\ &22.68 \cdot \nu^{3.5} - 15.96 \cdot \nu^4 + 1.801 \cdot \nu^{7.5}\big)\Big) \end{aligned} \tag{2.7}$$

$$\nu = 1 - T/T_c \tag{2.8}$$

Adsorption and desorption isotherms are in general different, and the difference between them is known as hysteresis. The hysteresis will significantly affect the amount of cyclable water under any conditions that do not encompass both the full adsorption as well as the full desorption peak. Geometrical and chemical features of the pores may determine the need for additional energy to desorb from certain sites (overcoming a bottleneck for example), as reported by Ruthven, 1984; Velasco et al., 2016. As a consequence of such "delayed" desorption,

the latter can be concentrated in a smaller range than during adsorption, leading to a higher desorption characteristic energy C and a modified shape n, as reported by Kutarov et al., 2011. Depending on the material and the reason for the hysteresis, some physical model can be used to describe them. As in this work we do not focus on any specific type of hysteresis, instead of following the approach proposed in the literature by Kutarov et al., 2011, it is preferred a general solution based on the curve fitting results. This can be expressed according to equation 2.9, where ΔC and Δn take into account the difference between ad- and desorption described above. The two terms describing hysteresis are also considered to be potentially linearly dependent on temperature (eq. 2.6).

$$w_{de} = W_{0,1} \cdot exp\left(-\left(\frac{F}{C_1 + \Delta C_1}\right)^{n_1+\Delta n_1}\right) + W_{0,2} \cdot exp\left(-\left(\frac{F}{C_2 + \Delta C_2}\right)^{n_2+\Delta n_2}\right) \tag{2.9}$$

To ensure a good quality of the parameters describing the adsorption equilibria, and at the same time avoid over-fitting, a rigorous curve-fitting procedure has been followed.

The obtained data was split using a stratification based on the total loading into a training set (80%) and a test set (20%), to have a more robust fitting in both areas of high loading and low loading. The random split was performed with the Python library *scikit-learn*, curated by Pedregosa et al., n.d.

The adsorption branch data were then fitted with both the original DA and the adapted model (eq. 2.4 and 2.6). The optimal fit was obtained with the R library *nlrob*, created by Andreas Ruckstuhl, 2005. Subsequently, the parameters ΔC and Δn (eq. 2.9) were fitted on the desorption branches, using the same procedure. To ensure that for each material only the significant parameters are included in the final equation when fitting the model parameters we followed the procedure below:

1. all the model parameters are included in the curve fitting;
2. the least significant of the parameters with a *p-value* > 0.05 is excluded;
3. if the overall quality of the model worsens, the parameter is restored and the second least significant is excluded;
4. The parameters are excluded until only the minimum number remains (either significant or necessary for the adsorption site to exist);
5. if two out of three parameters for each adsorption site distribution are significant, the distribution is kept, otherwise, it is excluded.

This routine can ensure that only the most significant parameters are included in the fit.

However, given the limited number of materials, it was performed manually and it should be automated before its application to a wide database.

Effective Screening

As discussed in Section 2.4.1, there is a growing need for the effective characterization of adsorbent materials during preliminary screenings. To this aim, we propose here a methodology to decrease the characterization effort without jeopardizing the prediction accuracy compared to benchmark methods. As highlighted above, without prior knowledge of the adsorbent material, there is a risk of wasting time on data points that do not bring much added value. It is considered that the added value of adsorption equilibrium data points derives primarily from two factors:

1. determining how much water is adsorbed in a particular condition;
2. making sure the fitted model coefficients are valid for the interesting application range.

If in first approximation, as shown valid, the adsorption is driven by the adsorption potential, which means:

1. characterizing appropriately the adsorption peak area;
2. characterizing conditions at different adsorption potentials.

Our methodology involves the determination of the location of the minimum set of conditions that must be characterized to successfully fit the adsorption equilibrium model. The determination methodology is formulated for a *known* application range and an *unknown* adsorbent material. The starting point would be the characterization of three points, at minimum, average and maximum adsorption potential, F_1, F_2 and F_3 respectively. These points, characterized by the loadings w_1, w_2 and w_3, define the mapping indicators A_1 and A_2:

$$A_1 = (w_1 - w_2) \cdot (F_2 - F_1) \tag{2.10}$$

$$A_2 = (w_2 - w_3) \cdot (F_3 - F_2) \tag{2.11}$$

The indicators represent the areas on the $F - w$ plot of Figure 2.3 and express the added value embodied in the characterization space between the characterized equilibria. The successive characterization point will be characterized by an intermediate adsorption potential between the two points that provided the biggest added-value mapping indicator. Each data point

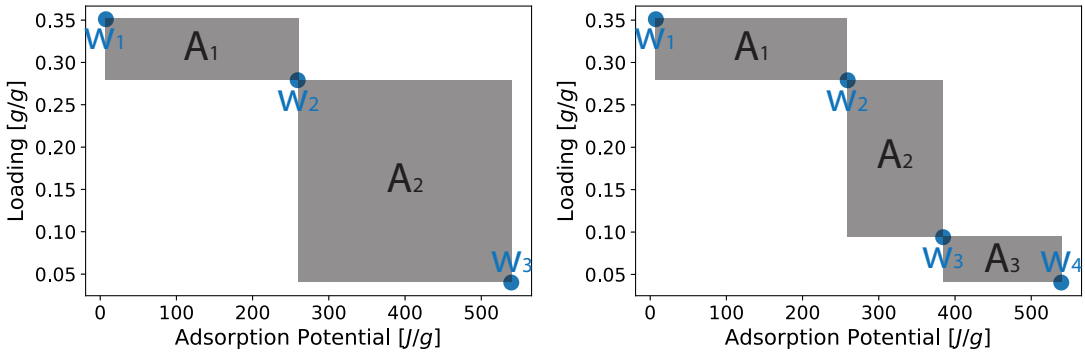

Figure 2.3: Example of determination of the adsorption equilibrium characterization conditions based on the mapping added-value indicators. Left: the initial three adsorption equilibria determine the indicators A_1 and A_2. Right: the new point w_3, characterized at an intermediate adsorption potential between w_2 and the old w_3, provides the most added value and the operation can continue with minimum effort.

$i \in \{1,...,n\}$, where n is the total number of adsorption equilibria characterized, will be denoted with a number ordered according to growing adsorption potential:

$$F_i > F_{i-1} \tag{2.12}$$

Equation 2.12 is used to relabel the characterized points before the definition of the next best point to characterize i^*, which will be defined by the adsorption potential:

$$F_{i^*} = \frac{F_i + F_{i+1}}{2} : A_i = max\,(A \in \{(w_i - w_{i+1}) \cdot (F_{i+1} - F_i) : i \in \{1,...,n-1\}) \tag{2.13}$$

New points can be determined until an arbitrary criterion is met, for example, the maximum mapping indicator size to be allowed.

$$max(A) < A_{max} \tag{2.14}$$

Based on the data gathered with this method, it is possible to fit traditional models, such as the benchmark D-A model. However, if Polanyi's theory holds true for the characterized points, the characteristic curve of adsorption will be a monotonically decreasing function of the adsorption potential. Thus, independently from the shape and type of the isotherm, it is in principle possible to interpolate the data without breaking Polanyi's theory. The

only requirements for physical consistency and for implementation in simulations are that the interpolant must be monotonic and its derivative must be continuous. Widely used algorithms such as the Piecewise Cubic Hermite Interpolating Polynomial (PCHIP) satisfy these requirements, as described by Fritsch and Butland, 1984. This approach puts any physical understanding out of the question, but it can work completely unsupervised and will fit the behaviour of any number and type of different adsorption sites. The interpolation was performed with the *PchipInterpolator* SciPy library in Python, as developed by the Scipy community, n.d.

As found by Stoeckli et al., 1994, the presence of multiple adsorption sites is the most common trait of complex adsorption curves, so at least for those cases it would be well suited. For materials that do show the effects of the temperature on their adsorption curves, additional care should be taken. It is therefore advisable to apply this method only for a first screening, while for more accurate analysis, more detailed models should be applied.

However, one cannot rule out that during the preliminary screening of adsorbent materials, some of the points characterized might break Polanyi's theory (i.e. a point characterized at higher adsorption potential F_i produces a higher loading w_i than a point characterized at lower adsorption potential F_j). To solve the issue, it is proposed to substitute the two conflicting points i and j with one artificial point i^* with their average:

$$w_i^* = \frac{w_i + w_j}{2} \tag{2.15}$$

$$F_i^* = \frac{F_i + F_j}{2} \tag{2.16}$$

2.4.3 Results

The characterization methods are initially applied to adsorption branches for brevity, but they can be equally applied to desorption branches with the given modifications to account for hysteresis, as for example proposed by Kutarov et al., 2011 and in this section further below. In light of these results, we will discuss how the different approaches compare.

To evaluate the quality of the different characterization approaches, the Root Mean Square Error ($RMSE$) on the predictions of the test set is obtained by dividing the squared root of the sum of the squared residuals by the total number of test points N_{test}:

$$RMSE = \sqrt{\frac{\sum \epsilon_i^2}{N_{test}}} \tag{2.17}$$

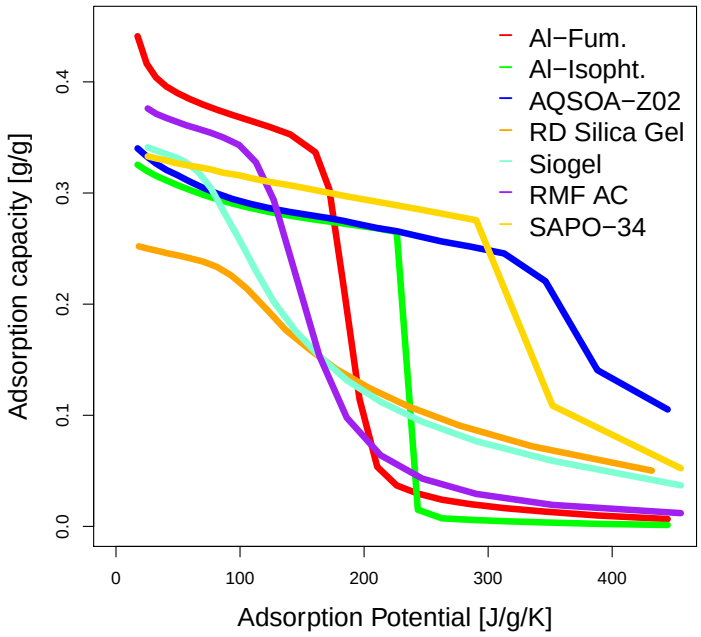

Figure 2.4: Adsorption isotherms of Aluminium Fumarate, Aluminium Isophthalate, AQSOA-Z02 and RD Silica Gel at 40°C and of Siogel, RMF Activated Carbon and SAPO-34 at 50°C, between 5-95% relative humidity. It is worth noting how AQSOA-Z02, is a SAPO-34 material, but slightly differs from the SAPO-34 powder produced in excess during the direct crystallization production process by Fahrenheit.

Further below, both adsorption and desorption branches of the Benchmark and Detailed Modelling methods will be analysed, comparing both curve fitting and prediction errors, and discussing the advantages and disadvantages of the proposed general detailed model.

To clarify the main difference among the characterized adsorbent materials, a single adsorption isotherm at intermediate temperature for each of them is reported in Figure 2.4.

Benchmark

The prediction results obtained by fitting the Dubinin-Astakhov model on one isotherm measured at intermediate temperature are represented in Figure 2.5 and summarized in Table 2.1. Analysing the results, one can appreciate how the D-A model, even though fits on a quite complete data set, does not always deliver accurate predictions.

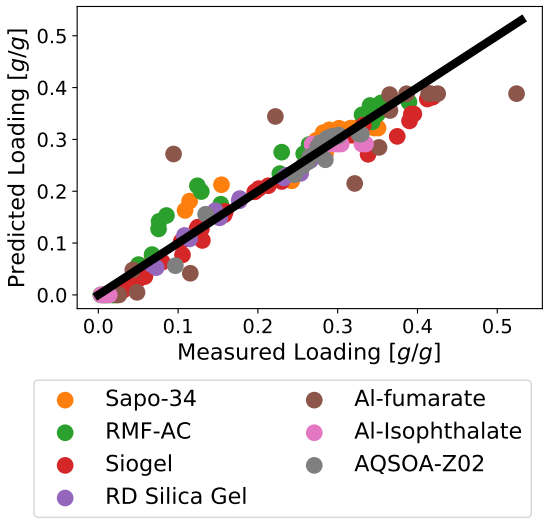

Figure 2.5: Adsorption equilibria prediction based on the*Benchmark* characterization method against the test data set.

Material	**N° Points**	*RMSE*
Sapo-34	19	2.5%
RMF-AC	19	3.1%
Siogel	19	2.8%
RD Silica Gel	19	1.1%
Al-fumarate	25	7.6%
Al-Isophthalate	25	1.9%
AQSOA-Z02	25	1.6%

Table 2.1: *RMSE* prediction errors for adsorption equilibrium obtained with the *Benchmark* characterization method, and the number of points used to train the model.

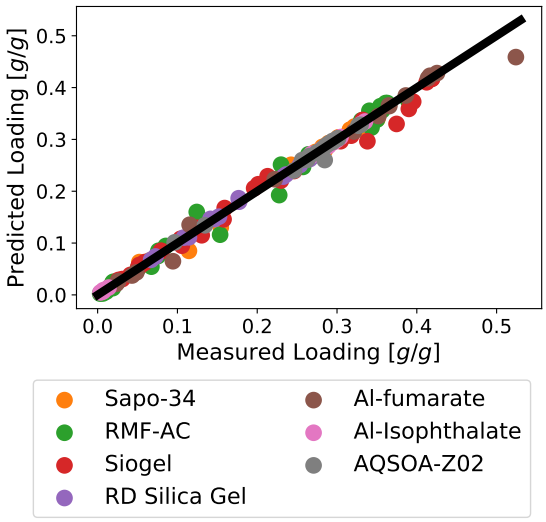

Figure 2.6: Adsorption equilibria prediction based on the*Detailed Modelling* characterization method against the test data set.

Material	**N° Points**	*RMSE*
Sapo-34	104	0.9%
RMF-AC	132	1.4%
Siogel	127	1.5%
RD Silica Gel	51	0.4%
Al-fumarate	63	1.9%
Al-Isophthalate	63	0.1%
AQSOA-Z02	69	0.6%

Table 2.2: *RMSE* prediction errors for adsorption equilibrium obtained with the *Detailed Modelling* characterization method, and the number of points used to train the model.

Detailed Modelling

The prediction results obtained by fitting the modified Dubinin-Astakhov model on multiple isotherms are represented in Figure 2.6 and summarized in Table 2.2.

Comparing the results with the ones obtained for the benchmark method, one can appreciate that the quality of the predictions is consistently improved by a factor of 1.8-20, depending on the material. This is particularly important for the elimination of the out-layers that can cause problems during unsupervised simulations. As discussed in detail further below, the reason is to be attributed to second-order effects, and an increase of the data points in the training set, including different temperatures, does not improve the results for the Benchmark method.

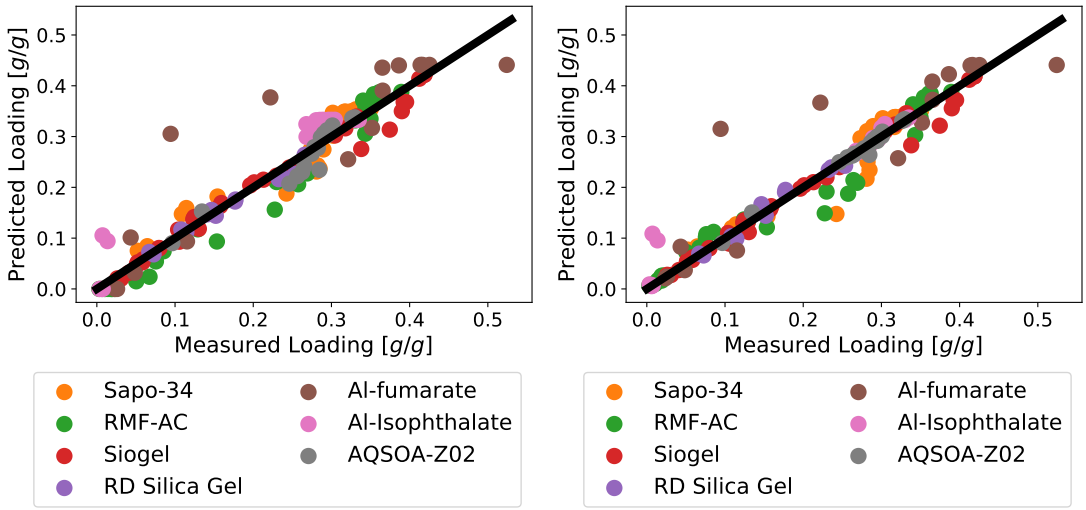

Figure 2.7: Adsorption equilibria prediction based on the*Effective Screening* characterization method against the test data set. Left: Fit of Dubinin-Astakhov model (D-A). Right: Interpolation with Piecewise Cubic Hermite Interpolating Polynomial (PCHIP).

Material	**N° Points**	$RMSE$ **of D-A**	$RMSE$ **of PCHIP**
Sapo-34	6	2.9%	3.0%
RMF-AC	5	2.8%	2.8%
Siogel	5	1.9%	1.7%
RD Silica Gel	5	1.1%	1.1%
Al-fumarate	5	7.8%	7.5%
Al-Isophthalate	5	4.5%	3.3%
AQSOA-Z02	6	2.2%	0.7%

Table 2.3: $RMSE$ prediction errors for adsorption equilibrium obtained with the *Effective Screening* characterization method, and the number of points used to train the model. The fit of Dubinin-Astakhov model (D-A) and the Interpolation with Piecewise Cubic Hermite Interpolating Polynomial (PCHIP) deliver similar results.

Effective Screening

The prediction results obtained by fitting the Dubinin-Astakhov model and by interpolating with the PCHIP method are represented in Figure 2.7 and summarized in Table 2.3. The criterion used for stopping the process of data creation was:

$$max(A_{i,j}) < 0.1 \cdot (w_{max} - w_{min}) \cdot (F_{max} - F_{min}) \tag{2.18}$$

The effective screening method allowed reducing the characterization effort by a factor of 3-5 when compared to traditional isotherms. However, when comparing the $RMSE$ with the effort of the benchmark method, one can notice that is changed by a factor of 0.6-2.4 only. This means that this method is way more effective for quick materials screening, and only for

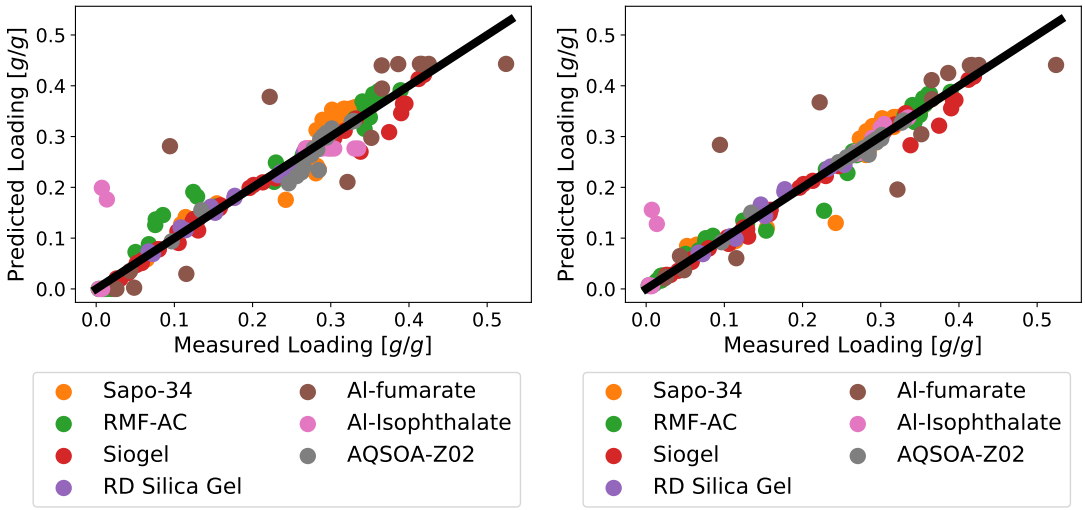

Figure 2.8: Adsorption equilibria prediction based on the*Effective Screening* characterization method with an increased amount of training points against the test data set. Left: Fit of Dubinin-Astakhov model (D-A). Right: Interpolation with Piecewise Cubic Hermite Interpolating Polynomial (PCHIP). The results are similar to the ones obtained with fewer training points.

some materials, the prediction quality is worsened.

If instead of fitting the D-A model, the minimized training data set is interpolated using the PCHIP algorithm, the results are similar or better (the RMSEs decrease by a factor of 0.9-3). This means that the prediction quality is maintained and even improved for materials with high second-order effects (such as AQSOA-Z02). On the other hand, the PCHIP equations should never be extrapolated outside the characterization range, while for the D-A model at least the behaviour will be surely physical (even if possibly wrong).

Reducing by half the maximum allowed added-value mapping indicator size, the accuracy of the results is not much improved, as shown in Figure 2.8 and in Table 2.4. Compared to the case just discussed, the characterization effort increased by 20%-40%, but the errors improved by factors of 0.6-1.3 and 0.7-1.5 for the D-A model and the PCHIP interpolation respectively. This means that there is no advantage in increasing the adsorption potential resolution with this approach. The worsening of the indicators with more characterization points is due to the different relevance of the adsorption peak area in the training set of data (here selected according to the mapping indicator added-value) and the test set of data (more homogeneous), which results in over-fitting of the peak region at the expenses of the other regions.

Effectiveness of the Strategies

Given the results obtained for the different strategies, it is possible to notice how both the *Detailed Modelling* and the *Effective Screening* bring some advantage with respect to the

Material	**N° Points**	$RMSE$ **of D-A**	$RMSE$ **of PCHIP**
Sapo-34	8	3.1%	2.9%
RMF-AC	7	2.8%	1.9%
Siogel	7	2.0%	1.7%
RD Silica Gel	7	0.9%	1.1%
Al-fumarate	6	8.0%	7.5%
Al-isophthalate	6*	6.7%	4.7%
AQSOA-Z02	8	2.1%	0.7%

Table 2.4: $RMSE$ prediction errors for adsorption equilibrium obtained with the *Effective Screening* characterization method with an increased number of training points, and the number of points used to train the model. For the Al-isophthalate, * means that two conflicting data points were substituted by their average according to Equations 2.15 and 2.16. The fit of Dubinin-Astakhov model (D-A) delivers slightly worse results than the Interpolation with Piecewise Cubic Hermite Interpolating Polynomial (PCHIP).

conventional *Benchmark* strategy. In particular, it is demonstrated that only through the combination of an increased effort in the characterization and in the modelling of the adsorption curves it is possible to improve the accuracy of the prediction of the adsorption equilibria. This is considered to be relevant in various stages of the design of adsorption equipment when the prediction of the amount of water adsorbent is relevant to decision-making.

Moreover, it is demonstrated that the appropriate choice of characterization points can decrease drastically the experimental or computational effort. This is considered to be relevant during adsorbent material screening phases. This methodology could be simply and effectively implemented in material discovery simulations, even when the nature of the adsorption sites is not known *a priori*. Furthermore, it could be implemented in DVS control software to decrease the experimental time for material developers.

Based on the experimental results on seven different water adsorbents of industrial interest obtained in this work, one can estimate the likely relative effectiveness of the three methods in obtaining accurate water adsorption curves. Quantifying the characterization effort in terms of the number of points to be measured, this is three times higher for the detailed modelling and four times lower for the effective screening when compared to the benchmark (≈ 20). Quantifying the method accuracy in terms of $RMSE$, this is three times higher for the detailed modelling and equal for the effective screening when compared to the benchmark ($\approx 3\%$).

One could define a prediction efficiency for the three methods:

$$\eta_{prediction} = \frac{1}{N° points \cdot RMSE} \tag{2.19}$$

Using the average of the experimental results obtained in this work for the two factors in

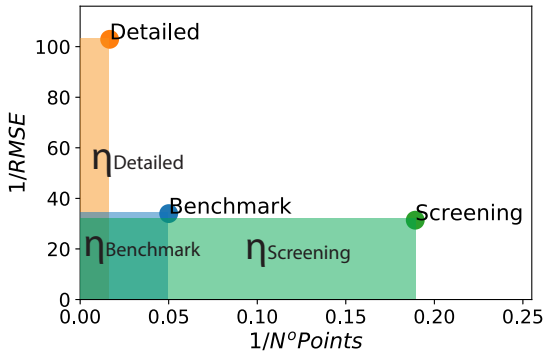

Figure 2.9: Visualization of the prediction efficiency of the three methods tested. The *Benchmark* method performs an easy job with low efficiency. The *Detailed Modelling* method performs a difficult job with low efficiency. The *Effective Screening* method performs an easy job with high efficiency.

Equation 2.19, we obtain the values $\eta_{prediction}$ of 1.7 for both the benchmark and the detailed modelling and 5.9 for the effective screening. A graphical representation of the prediction efficiency is depicted in Figure 2.9.

Benchmark vs Detailed Modelling: a Deeper Analysis

In addition to the evaluation of the RMSE used to quantify the accuracy of the predictions, the quality of the models in terms of curve fitting accuracy has been evaluated according to the residual standard error RSE. It is the square root of the ratio between the sum of the squared residuals ϵ_i^2, and the degrees of freedom calculated from the number of observations/measured updates N_{train} and the number of parameters of the model N_{param} (see Equation 2.20), and represents an indication of the trade-off between accuracy and overfitting.

$$RSE = \sqrt{\frac{\sum \left(\epsilon_i^{train}\right)^2}{N_{train} - N_{param} - 2}} \tag{2.20}$$

The results of training set fitting and test set predictions of adsorption equilibria for the Dubinin-Astakhov (DA) model are shown in Figure 2.10, while the same results for the proposed model are shown in Figure 2.11. The fitted parameters of the proposed model for the adsorption branch are gathered in Table 2.5. The results of the proposed model for the desorption branches are shown in Figure 2.12. The fitted parameters for the desorption branch are gathered in Table 2.6. The result metrics for both models and both adsorption and desorption are summarized in Table 2.7.

Looking at the differences between fitted and measured water uptake for the DA model (Figure

Code	$W_0 1$ $[g_w/g]$	$C1$ $[J/g]$	$n1$ $[-]$	$W_0 2$ $[g_w/g]$	$C2$ $[J/g]$	$n2$ $[-]$	N_{param} $[-]$
RD Silica Gel	$0.2-0.00032\cdot T$	$260-0.32\cdot T$	$0.01\cdot T$	0.16	$710-0.92\cdot T$	1.7	9
Siogel	$0.62-0.00086\cdot T$	200	0.94	0.077	150	3.8	7
SAPO-34	0.15	500	1.4	$0.39-0.00067\cdot T$	$910-1.8\cdot T$	20	8
AQSOA-Z02	$0.088+0.00014\cdot T$	$720-1.1\cdot T$	$40-0.247\cdot T$	0.26	620	0.4	9
Al-fumarate	$0.54-0.00073\cdot T$	$490-0.96\cdot T$	14	$0.001\cdot T$	23	0.36	8
Al-isophthalate	0.087	110	$3.6-0.0085\cdot T$	$0.3-0.00015\cdot T$	$630-1.3\cdot T$	$0.28\cdot T$	9
RMF-AC	0.25	150	6.2	0.12	210	1.5	6

Table 2.5: Proposed water adsorption *Detailed Model* fitted parameters.

Code	$\Delta C1$ $[J/g]$	$\Delta n1$ $[-]$	$\Delta C2$ $[J/g]$	$\Delta n2$ $[-]$	N_{param} $[-]$
RD Silica Gel	13	$0.0092\cdot T$	–	–	2
Siogel	$0.04\cdot T$	0.11	$0.016\cdot T$	32	4
SAPO-34	45	$0.0011\cdot T$	$280-0.63\cdot T$	$-0.017\cdot T$	5
AQSOA-Z02	$169-0.32\cdot T$	$92-0.25\cdot T$	170	$0.29-0.00087\cdot T$	7
Al-fumarate	$0.027\cdot T$	$0.014\cdot T$	$75-0.2\cdot T$	0.044	5
Al-isophthalate	$0.028\cdot T$	–	$170-0.5\cdot T$	–	3
RMF-AC	–	1.4	21	$6.6-0.02\cdot T$	4

Table 2.6: Proposed water desorption *Detailed Model* fitted parameters.

Code	**DA Ads. RSE**	**DA Ads. RMSE**	**Det. Ads. RSE**	**Det. Ads. RMSE**	**Det. Des. RSE**	**Det. Des. RMSE**
RD Silica Gel	1.1%	1.0%	0.4%	0.4%	0.6%	1.2%
Siogel	1.2%	1.8%	1.2%	1.4%	0.8%	2.1%
SAPO-34	2.1%	2.2%	0.3%	0.9%	0.9%	1.3%
AQSOA-Z02	1.4%	1.5%	0.2%	0.6%	0.2%	0.4%
Al-fum.	2.7%	7.2%	0.4%	1.9%	0.7%	1.5%
Al-iso.	1.5%	7.5%	0.2%	0.1%	0.2%	2.0%
RMF-AC	2.2%	2.2%	0.7%	1.4%	0.9%	1.0%

Table 2.7: Detailed comparison of the *Benchmark* and *Detailed Modelling* adsorption and desorption equilibria modelling results. RSEs are calculated over the training data sets, while RMSEs are calculated over the test data sets. Both the quality of the model and the prediction accuracy are improved with *Detailed Modelling* (Det.) with respect to the *Benchmark* (DA). Also desorption branches are modelled and predicted satisfactorily.

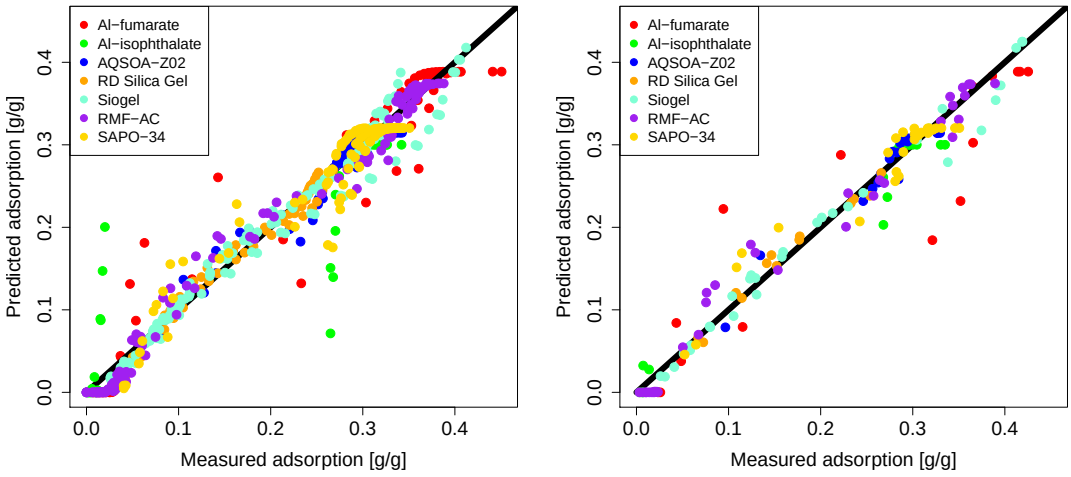

Figure 2.10: Adsorption equilibria modelling results of the *Benchmark* method for both the training data set (left) and for the test data set (right).

2.10), one can see systematic deviation between fits and measurements. In addition with differences > 0.1 $[g/g]$, the scatter of the residuals is larger than the observed differences between duplicate measurements ($\leq 0.02[g/g]$). This indicates that water uptake predictions can be improved with a more adapted model.

With the adapted model chosen here (Eq. 2.4), the three parameters of the DA model are replaced by minimum 6 and maximum 9 parameters (see Table 2.5). When comparing the standard DA model with the proposed empirical modification, the latter seems to provide a better representation of the equilibrium adsorption loadings, both with respect to accuracy and significance. The relative improvement achieved in model quality (residual standard error Eq. 2.20) is normally between 60% and 87%. The only exception is Oker Siogel, which goes from the lowest residual standard error (1.2 %) for the DA model to the highest (1.2 %) for the new approach, thus showing no model quality improvement.

This general model improvement is reflected in better predictions, with an enhancement of the mean square error of 60% to more than 97%, the latter in the case of Al Isophthalate, which presents an almost perfect step-like isotherm (see Figure 2.12). Interestingly, also for Oker Siogel, the predictions are greatly improved, highlighting an improved predictive capability of the new approach compared to the DA model, justifying the additional parameters. Constraining the desorption branch equation to have the same maximum loading capacities as the adsorption branch is, from the model fitting point of view, an additional constraint, resulting in a slightly higher mean squared error (average mean squared error of 1.4% compared to 0.5% for the adsorption branch). Nonetheless, the results of both the model fit and the predictions remain comparable to the reproducibility of the measurements, indicating a good fit.

Taking a closer look at the fitting results, one can notice how not all the materials have the same

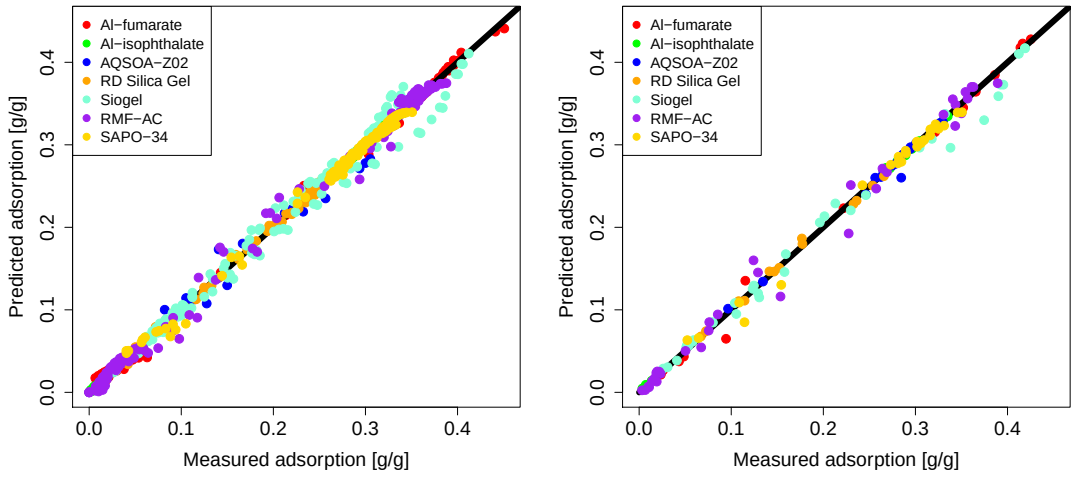

Figure 2.11: Adsorption equilibria modelling results of the *Detailed Modelling* method for both the training data set (left) and for the test data set (right).

dependence on temperature. The Empa RMF activated carbon has an almost temperature-independent adsorption behaviour, which makes its characterization less vulnerable to misinterpretation (i.e. extrapolation of the curve to temperatures outside the characterization range). Other materials, such as Fuji RD Silica Gel and Al-Isophthalate, have a stronger temperature dependence.

During the fitting procedure, on one hand, it was observed that only the inclusion of the temperature dependence of the model parameters could explain the differences observed between isotherms measured at different temperatures. On the other hand, it was observed that the most significant contribution to the improvement of the model predictions over the wide range of relative humidity here reported was due to the presence of an additional adsorption site (the second term of Equation 2.4). This means that if the experimental resources are scarce (e.g. the time available for the characterization of the adsorption curves, or the temperature range available), it would still be possible to improve the D-A model even if the temperature effects are not detected in the measurement range. This approach, which coincides with the extension of Stoeckli, 2002 to include the desorption branches, would be suited for a quicker scan of the adsorbent materials available, but at the risk of introducing errors. Those could be potentially extremely significant for materials characterized by step-like adsorption characteristics. In fact, the effects of temperature might shift the desorption peak towards different adsorption potentials. In Figure 2.12 (right), the adsorption peak shift for Al-isophthalate can be easily observed.

Given that the *detailed modelling* approach delivers the minimum prediction errors, the method is selected to screen materials in Section 2.5, to avoid a misinterpretation of the equilibrium curves.

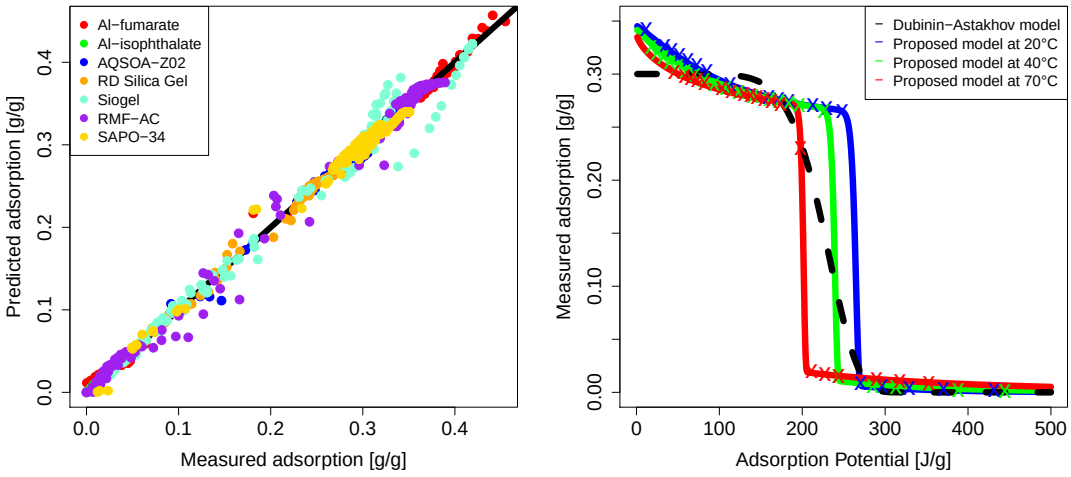

Figure 2.12: Left: desorption equilibria results of the *Detailed Modelling* method for the training data set. Right: the difference between the *Benchmark* and the *Detailed Modelling* methods visualized for the MOF Technologies Al-Isophthalate adsorption curve.

2.4.4 Conclusions

After comparing different strategies for characterizing and modelling the water adsorption equilibrium curves of a diverse set of relevant materials, some key insights have been highlighted:

1. When simple models are used to describe the adsorption equilibria, the inclusion of multiple isotherms in the fitting procedure does not bring any advantage,
2. Only measuring adsorption equilibria at multiple temperatures (e.g. with multiple isotherms) and the application of a detailed model can significantly enhance the capability of producing accurate prediction of water adsorption. The proposed modification of the Dubinin-Astakhov model proved to be a valid option to do so.
3. The appropriate selection of a limited number of characterization conditions allows for a minimization of the required effort without compromising the quality of the results.
4. The application of appropriate interpolation algorithms (such as PCHIP) instead of model fitting seems to be particularly efficient in capturing the most significant characteristic of a material's adsorption curve without any prior knowledge of it.

These findings can enable more effective research on the identification of suitable water-adsorbing materials in a robust and general fashion. The characterization times can be reduced on-demand depending on the needs (by 50-75% respect to conventional isotherms) and even combined with purely mathematical interpolation methods, paving the way for

effective material discovery methods. Furthermore, the subsequent detailed characterization of the most promising materials can be performed in a robust and general fashion including second-order effects with the proposed modification of the D-A model. The equilibrium adsorption data use was improved by the fitting of the novel empirical modification of the Dubinin-Astakhov model, which shows increased significance and accuracy with respect to the original. The effects of temperature and, especially, of multiple adsorption sites explain in an effective and general way the observed water adsorption behaviour.

2.5 Harmonic Adsorbent Materials Selection and Process Design

2.5.1 Introduction

Adsorption energy technologies can play an important role in making energy systems more sustainable, as highlighted by Ntiamoah et al., 2016; Sonar et al., 2014. Cooling, heating, and energy storage systems can be more efficient using the full potential of adsorbent materials, which allows for providing those services requiring little electricity (i.e. only auxiliary systems like valves and pumps). Nonetheless, several factors are limiting their widespread application, including low thermal efficiencies and large volumes when compared to competing solutions, as reported by Demir et al., 2008.

The performance of adsorption equipment strongly depends on the adsorbent-adsorbate working pair, and because of that, it is highly sensitive to the operational conditions (i.e. temperature, pressure), as reported by Younes et al., 2017. The pre-selection of the appropriate working pairs in the early stage of the design - before prototyping, testing and optimizing the equipment - can therefore enable competitive applications, as highlighted by Y. I. Aristov, 2007, at minimum time and costs for R&D. This can be achieved by characterizing the equilibrium thermophysical properties of the materials. These measurements demand only small amounts of material and allow the estimation of the maximum achievable thermal energy performance, identifying the most suitable adsorbents, as for example performed by Brancato and Frazzica, 2018. While these quantities do not take into account the kinetics of the adsorption process, no good performance can be reached without suitable equilibrium properties. Additionally, the kinetics depend heavily on the heat exchanger design and will need either measurement on prototypes or advanced modelling. The adsorbent-adsorbate working pair is not the only driver of the adsorption heat transformer performance, but it is considered a preliminary requirement. In fact, other aspects such as material integration, heat exchanger design and control are similarly relevant. However, their optimization is not so dependent on the working pair obtained and can be included in later stages of the system design.

Being such an important step in the development of adsorption heat transformers, several approaches for material selection were already developed. Specifically, Aristov and colleagues played a central role in developing the field. Y. I. Aristov, 2009 considered the dynamic characterization and optimization of materials as the key indicator of performance. Y. I. Aristov, 2012

recognized the importance of adsorbent databases as the foundation for comprehensive and quantitative evaluation of the existing water adsorbents. Nowadays, with the computational power growing unprecedentedly also within the scientific community, such databases are becoming even more important and are currently being maintained, for example by Siderius, 2020. Y. I. Aristov, 2013 reviewed the most promising classes of materials being developed and systematically exposed their pros and cons. More recently, Gordeeva and Aristov, 2019 highlighted how adsorption cycles and materials should be developed harmoniously to maximize the thermodynamic synergy among them in both first-law and second-law terms.

Moreover, more authors have been contributing to the development of the field. Frazzica et al., 2021 simulated several working pairs for different working conditions, providing insights on how to achieve maximum performance improving the cycles with heat recovery. Frazzica and Freni, 2017 evaluated and compared several working pairs for different types of heat storage applications. Freni et al., 2016 used modelling and simulations of several working pairs as a method to design systems considering both thermodynamic and dynamic aspects. S. Henninger et al., 2010 used a fingerprint method to evaluate a given material with two different driving temperatures as representative of different classes of applications. Z. Liu et al., 2021 used the adsorption isotherms extracted from a database to calculate the theoretical coefficient of performance for a cooling and a heating cycle. Boman et al., 2017 computed a screening over a large number adsorbent-adsorbate of working pairs for heating and cooling applications, with fixed evaporator and adsorption temperatures but with free desorption temperature. In their work, both thermodynamic and heat transfer considerations are used as selection criteria.

In the field of pressure swing adsorption (PSA) systems for gas separation, optimization methods have already been used to optimize design decisions. Those included the system design and operation, as done, for example, by Fu et al., 2018; Jiang et al., 2004; Smith and Westerberg, 1991; Sung et al., 1979. In the field of adsorption heat transformers, the optimization often consisted of parameter sweeps, as done, for example, by Lanzerath et al., 2015 where a dynamic model is used to optimize the design and the control of an adsorption chiller with two different adsorbent materials.

Analysing the state-of-the-art research some considerations can be taken:

- Experimental data on adsorbent material properties are needed to estimate the performance of AHT;
- Automated screening from a database of materials is possible and enables novel solutions;
- The description of adsorption characteristics in a general way is necessary to analyse generally unknown materials;
- Equilibrium properties can be sufficient to narrow down the selection of the materials to the feasible candidates (and dynamic considerations are necessary afterwards);

- The feasibility of a complex adsorption system can be studied with optimization algorithms.

In this chapter, we intend to fill some of the gaps necessary to estimate the feasibility of complex water-based adsorption heat transformers systems in a preliminary stage. In fact, by selecting at the same time materials and system design, the maximum benefits can be obtained. In a preliminary phase of the design, it is not worth measuring the kinetic performance of tens (and even less of hundreds or thousands) of adsorbents under many different conditions, so one must rely on as little data as possible. Here a simple formulation for the maximum equilibrium performance is used to estimate the achievable energy and exergy efficiency and the minimum volume necessary. This estimation relies heavily on the water adsorption characteristic, therefore we propose to use the *Detailed Modelling* characterization approach to minimize the errors deriving from the extrapolation of those characteristics. Having such a simple description of the performance of the system, a simple optimization algorithm based on algebraic equations will be sufficient to demonstrate the feasibility of the approach, leaving a more detailed application of the methodology for later stages of design (including dynamic considerations and more representative process functions).

A similar effort was undertaken by Boman et al., 2017. However, some important differences between their approach and the one here proposed can be found. Those differences concern the use of a more general and detailed adsorption model, and the simultaneous choice of material and system design.

Therefore, a new methodology for screening adsorbents for water as refrigerant fluid is reported, taking into account both the characterisation and selection criteria. The aims include:

- a more accurate estimation of the maximum thermal performance;
- a robust method to identify the best adsorbent material depending on the temperature boundaries;
- a methodology that applies to a wide range of materials with very different characteristics;
- a methodology that could be expanded and automated to find optimal designs when connected to a database of materials properties.

This will be achieved by:

- applying the *Detailed Modelling* approach to describe the equilibrium adsorption characteristics;
- applying Mixed Integer Linear Programming (MILP) techniques as a tool for material selection;

- testing the methodology by estimating the maximum energy performance of a range of adsorber materials of different types, shapes and formats (state-of-the-art silica gels, zeo-types, Metal-Organic Frameworks (MOFs) and activated carbons (ACs)) for different heating and cooling scenarios.

2.5.2 Methods

Maximum Theoretical Performance Estimation

While a precise analysis of the performance and the cost of adsorption heat exchangers can only be obtained through dynamic analysis, as the ones proposed by Ammann, Michel, and Ruch, 2019; Y. I. Aristov et al., 2012; Bau et al., 2017; Graf et al., 2016, for the first screening in the early stage of the design, the effort of constructing the lab-scale prototype necessary for such an analysis is excessive. From the measured equilibrium data, it is possible to calculate the maximum achievable energy performance of cooling cycles under well-defined working conditions, as proposed by Brancato and Frazzica, 2018. While these values do not take into account any kinetic effects, a reasonable performance in terms of equilibrium properties is needed for a cycle to be efficient. Therefore, the maximum achievable energy performance is a good criterion for fast pre-selection of promising adsorption materials. For cooling applications the maximum theoretical thermal coefficient of performance (COP) - evaluating the ratio between delivered energy and thermal energy needed to drive the thermodynamic cycle - can be calculated as a function of the evaporator temperature T_{eva}, the adsorption temperature T_{con}, and the hot source temperature T_{hot} (eq. 2.21, where L is the latent heat of vaporization of water). For an ideal cooling cycle, the transformations are either isosteric or isobaric, as described by Younes et al., 2017.

$$\begin{aligned} COP =& L(T_{eva}) \cdot \Delta w \cdot \left(\int_{T_{con}}^{T_{switch}} \left[cp_s(T) + cp_w(T) \cdot w(p_{eva}, T_{con}) \right] dT + \right. \\ & \left. \int_{T_{switch}}^{T_{hot}} \left[cp_s(T) + cp_w(T) \cdot w(p_{con}, T) - H_{de}(T) \cdot \frac{dw(p_{con}, T)}{dT} \right] dT \right)^{-1} \end{aligned} \tag{2.21}$$

The temperature T_{switch}, at which the ideal desorption process switches from isosteric to isobaric is a function of the condensation (T_{con}) and evaporation (T_{eva}) temperatures, as explained by Y. I. Aristov, 2007 (eq. 2.22).

$$T_{switch} = \frac{T_{con}^2}{T_{eva}} \tag{2.22}$$

The energy (EN) and exergy (EX) use of the cycles can be respectively approximated as eq.

2.23 and 2.24.

$$EN = \frac{1}{COP} \tag{2.23}$$

$$EX = \frac{1}{COP} \cdot \left(1 - \frac{T_{env}}{T_{hot}}\right) \tag{2.24}$$

As a first indicator of reactor volume, at least in relative terms, the energy-specific adsorbent volume (in cm^3/J, eq. 2.25) can be used. This is useful as it is a material property, such that does not depend on integration and kinetics, coherently with the maximum theoretical COP.

$$EV = \frac{1}{L(T_{eva}) \cdot \Delta w \cdot \rho_{tap}} \tag{2.25}$$

Formulation of the Optimization Problem

Finding the most advantageous solution to satisfy the heating and cooling loads of a specific energy system can be formulated as an optimization problem, as done, for example, by Samsatli and Samsatli, 2018. To this end, an objective function is defined and optimization is used to find the best values of the decision variables, within the limits of some constraints. This is also true for the number and type of adsorption materials used. Even though only equilibrium properties were considered within the current work, such optimization will allow a better understanding of how the decision variables (the type and the number of adsorber materials used) influence the objectives set (exergy, energy, volume) and should allow for a good pre-selection of materials.

To explore the possibilities of this approach, almost 700 feasible scenarios have been simulated. The scenarios have been created with cooling needs (goods and room cooling) during summer in Europe in mind (environmental temperature $T_{env} = 30°C$), using a solar thermal heat source. The cooling needs can be complemented by a heating need, either within industrial processes or for domestic hot water. Consequently each scenario has $1 \leq N_{cooling} \leq 5$ cooling demands $Q^{T_l}_{cooling}$ at temperatures $T_l \in \{5, 10, 15, 20, 25°C\}$ and can additionally have $N_{heating} \leq 5$ heating demands $Q^{T_m}_{heating}$ at a temperature $T_m \in \{35, 40, 45, 55°C\}$. The energy demands are normalized by an energy unit Δu (i.e. $Q^{T_m}_{heating} = Q^{'T_m}_{heating}/\Delta u$) and can only have discreet sizes of 1 or 2.

The number of adsorption heat transformers N_{AHT} used to meet the energy needs is part

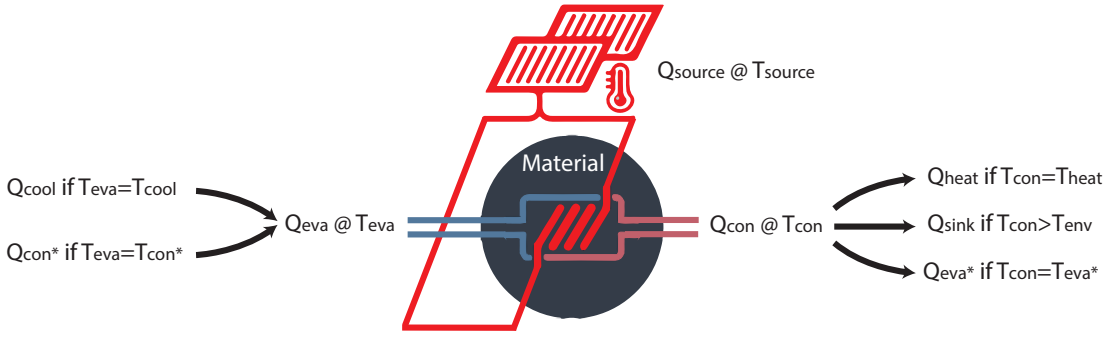

Figure 2.13: Possible connections of each adsorption heat transformer (AHT) depending on the temperature levels of its evaporator eva and condenser con. * indicates a different adsorption heat transformer. The cooling needs are at temperature T_{cool}. The heating needs are at temperature T_{heat}. The heat sources are at temperature T_{source}. Each AHT receives heat from a cold source (the condenser of another AHT or a cooling need) and a hot source (some kind of generator), and rejects heat to an intermediate sink (to the environment or towards the evaporator of another AHT).

of the optimization. The ideal adsorption cycle of each adsorption heat transformer i is represented by three temperature levels ($T^i_{eva} < T^i_{con} < T^i_{hot}$, i.e evaporation, condensation and hot/desorption temperatures respectively). The temperature levels were restricted to the following ranges: evaporator between 5°C and 25°C; condenser between 15 and 55°C; hot source between 25°C and 95°C, for simplification with discrete levels every 5 °C. Furthermore, each heat transformer is characterized by size (s_i) and three energy streams associated with the three temperature levels ($Q_i^{T_k}$). Again the energy streams are normalized by an energy unit Δu ($Q_i^{T_k} = Q_i'^{T_k}/\Delta u$) such that for each adsorption heat transformer the evaporator stream is a unitary stream $Q_i^{T_{eva}} = 1$. The hot source stream is $Q_i^{T_{hot}} = -Q_i^{T_{eva}}/COP = -1/COP$, and the condenser stream is $Q_i^{T_{con}} = Q_i^{T_{eva}} \cdot (1 + 1/COP) = 1 + 1/COP$. The sign convention used is positive for energy streams entering the system (evaporators and hot sources), and negative streams for energy streams leaving the system (condensers). For each adsorption heat transformer, a different adsorber material can be chosen. The hot energy demands of the heat transformers $s_i \cdot Q_i^{T_{hot}}$ are met by external sources $Q_{source}^{T_{hot}}$ and energy exiting the system at temperatures above T_{env} can be ejected to environmental sinks $Q_{sink}^{T_{con}}$. A schematic representation of the possible configurations is given in Figure 2.13.

The systems thus defined is composed of a certain number of temperature levels $\{T_l\} = \bigcup_{i,k} T_k^i$, where $k \in \{cool, heat, sink, source\}$. For each temperature level T_l, an energy balance, defined in eq. 2.26 using the Dirac delta function δ, has to be satisfied.

$$\sum_{i,k} \delta(T_k^i - T_l) \cdot s_i \cdot Q_i^{T_k} = \\ \sum_{cool} \delta(T_{cool} - T_l) \cdot Q_{cool}^{T_{cool}} - \sum_{heat} \delta(T_{heat} - T_l) \cdot Q_{heat}^{T_{heat}} \\ + \sum_{sink} \delta(T_{sink} - T_l) \cdot Q_{sink}^{T_{sink}} - \sum_{source} \delta(T_{source} - T_l) \cdot Q_{source}^{T_{source}} \tag{2.26}$$

Namely this energy balance implies, that the cooling and heating demands have to be met (eq. 2.27-2.28).

$$\sum_{i,k} \delta(T_k^i - T_{cool}) \cdot s_i \cdot Q_i^{T_k} = -Q_{cool}^{T_{cool}} \tag{2.27}$$

$$\sum_{i,k} \delta(T_k^i - T_{heat}) \cdot s_i \cdot Q_i^{T_k} <= -Q_{heat}^{T_{heat}} \tag{2.28}$$

The objective function to minimize can be formulated in a similar way for both energy and exergy consumption, summing over energy/exergy of the heating/cooling cycle (according to Eqs 2.23 and 2.24 respectively), counting only hot temperatures/heat sources above the environment temperature $T_{env} = 30°C$.

$$OBJ_{EN} = \sum_{i \in \{i | T_{hot}^i > T_{env}\}} s_i \cdot EN_i \tag{2.29}$$

$$OBJ_{EX} = \sum_{i \in \{i | T_{hot}^i > T_{env}\}} s_i \cdot EX_i \tag{2.30}$$

In the case of minimum required volume, the objective function is summed over the volume of all adsorption heating/cooling cycles (eq. 2.31).

$$OBJ_{EV} = \sum_i s_i \cdot EV_i \tag{2.31}$$

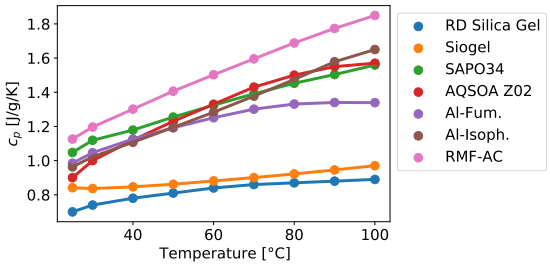

Figure 2.14: Measured specific heat capacity of the adsorbent materials.

Material	**Specific Heat Capacity** $[J/g/K]$	**Tap density** $[g/cm^3]$
Fuji Davison RD Silica Gel	$0.7 + 0.0019 \cdot (T - 273.15)$	0.87
Oker Chemie Siogel	$0.79 + 0.0016 \cdot (T - 273.15)$	0.77
Fahrenheit SAPO-34	$0.93 + 0.0063 \cdot (T - 273.15)$	0.85
Mitshubishi AQSOA-Z02	$0.84 + 0.0071 \cdot (T - 273.15)$	0.60
MOF Tech. Al-Fumarate	$0.97 + 0.0034 \cdot (T - 273.15)$	0.51
MOF Tech. Al-Isophthalate	$0.77 + 0.0086 \cdot (T - 273.15)$	0.33
Empa RMF Activated Carbon	$0.93 + 0.0063 \cdot (T - 273.15)$	0.43

Table 2.8: Measured specific heat capacity and tap density of the adsorbent materials. Specific heat capacity is valid between 298 and 393 K.

The Python library *mip*, developed by Santos and Toffolo, 2020, was used to optimize the choice and the connection of materials and boundary temperatures to deliver the cooling and heating needs of the system, according to the defined objective function. To speed up the optimization, the COPs of all materials and temperature levels T_k^i were pre-calculated.

2.5.3 Results

Heat Capacity and Density

The experimental specific heat capacity and tap densities are shown in Figure 2.14 and summarized in Table 2.8, showing a good agreement with the data available in the literature, as the ones by Ammann, Michel, and Ruch, 2019; Chakraborty et al., 2009; Jahan et al., 2020; Nienborg et al., 2018; Uddin, 2018, except for Empa RMF activated carbon that shows a higher specific heat capacity than typical commercial activated carbons. The specific heat capacity of water has been assumed to be $cp_w = 1.271e-5 \cdot T^2 - 8.170e-3 \cdot T + 5.493$, extracted from Toolbox, 2004.

Materials Selection and Process Pre-Design

The maximum calculated cooling COP of the 212 possible, single, ideal cycles with temperature boundaries as described in the methods section ranged between 0.05 and 0.95, with most of the cycles between 0.75 and 0.85, in agreement with values found in the literature, as in the works by Brancato and Frazzica, 2018; Restuccia et al., 2004. The cycles' performance has been pre-calculated to avoid calling the performance model from within the optimization algorithm, therefore lightening the computational effort required during the system design.

To show the applicability of the methodology to complex energy needs and to screen among materials to see which ones are more recurrently selected, the energy use, the exergy use, and the reactor volume objective functions were minimized for almost 700 scenarios, as described in Section 2.5.2. As shown in Figure 2.15, it was possible to achieve good system efficiencies for most of the scenarios. For analysing the results, the optimal solutions have been plotted against the averaged temperature lift (ATL) with respect to the environmental temperature T_{env}=30 °C (eq 2.32).

$$ATL = \frac{\sum_l Q_{need}^{T_{need}} * T_{need}}{\sum_{T_{need}} Q_{need}^{T_{need}}} - T_{env} \tag{2.32}$$

To compare scenarios with different amounts of energy needs, the normalized energy and exergy use (NU, eq. 2.33) are plotted.

$$NU = \frac{OBJ}{\sum_{T_{need}} Q_{need}^{T_{need}}} \tag{2.33}$$

As is expected, higher ATLs allow for better thermodynamic performance, including the ones that are generated as a combination of energy needs at different temperatures. Only in a few cases, the NU of energy was above 1.1 (for ATL < -15 °C) and the NU of exergy was above 3. Interestingly, the synergies among multiple heat transformers deliver NU of energy below one for ATLs below zero (ATL > -15°C), showing the potential of harmonic material choice and system design.

It can also be noted how, for some scenarios of mixed heating and cooling (ATL between -5 and 10), extremely compact designs are achievable (theoretical minimum energy-specific volumes below 1 mm^3/J, see figure 2.16). This is the case when one adsorption heat transformer can provide cooling and heating at the same time, which means that the temperature levels are not far from each other (e.g. cooling at 15°C and heating at 35°C, with ATL of -1.7 °C). However, these scenarios are less likely to exist in the industry. The less compact outlayers at high ATL

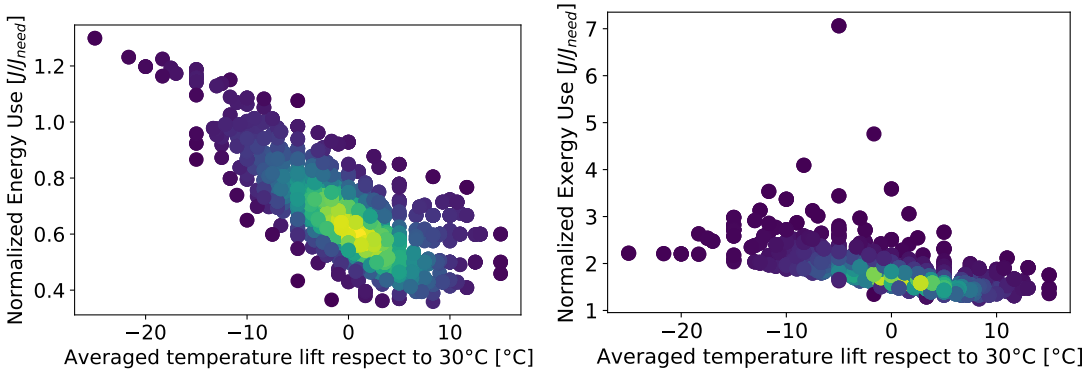

Figure 2.15: Minimum normalized energy use (left) and exergy use (right) of the adsorption systems as a function of the averaged temperature lift. The colour of the points is scaled on the point density as a qualitative guide to the eye.

are due to the upper limit of 90°C imposed on the regeneration temperature.

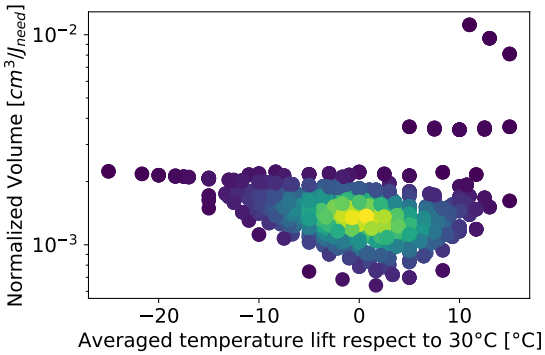

Figure 2.16: Minimum normalized volume of the adsorption systems as a function of the averaged temperature lift. The colour of the points is scaled on the point density as a qualitative guide to the eye.

Looking at the composition of the optimal solutions, as in Figure 2.17, it is possible to notice that most of the optimal solutions are composed of 3 to 5 adsorption heat transformers. Cascade configurations (where the condenser of one cycle feed the evaporator of another cycle) are beneficial when the energy needs happen at very different temperature (e.g. when cooling at 5°C and heating at 55°C are required, as in Figure 2.19). While this highlights the options offered by combining AHTs, it also shows that the inclusion of cost functions in the optimization algorithm is necessary to avoid an over-population of AHTs, as it is known that manufacturing and equipment costs are an important share of the total costs, as highlighted by AL-Hasni et al., 2022.

When the energy consumption is being minimized, the majority of the adsorption heat transformers use Fahrenheit SAPO34 (for low adsorbate partial pressure cycles) and Al-fumarate (for intermediate adsorbate partial pressure cycles), proving that they are the most promising

materials for the here studied scenarios. On average, Fahrenheit SAPO34 is used for temperature lifts ($\Delta T_{lift} = T_{con} - T_{eva}$) of 30°C with a COP of 0.73 but requires a regeneration temperature lift ($\Delta T_{reg} = T_{hot} - T_{con}$) of 46°C. On average, the MOF Tech. Al-fumarate is used for ΔT_{lift} of 20°C and needs ΔT_{reg} of 32°C, delivering a COP of 0.87. Most of the remaining cycles needed to balance the energy needs are using Mitsubishi AQSOA Z02 beads, specifically on average for ΔT_{lift} of 11°C and needing ΔT_{reg} of 33°C, delivering a COP of 0.43.

Similarly, when exergy use is being minimized, Fahrenheit SAPO34 and MOF Tech. Al-fumarate is chosen the most. However, given the different objectives, their average regeneration temperature lifts are reduced to 40°C and 31°C, respectively. The reported exergetic COP for these two materials and Mitsubishi AQSOA Z02 are 0.61, 0.80 and 0.31, respectively. In this case, the extremely narrow shape of the adsorption curve (without hysteresis and temperature effects) of the Empa RMF Activated Carbon combined with its high adsorption capacity seem beneficial for exergetic performance, and this adsorbent is used when small temperature lifts are required (ΔT_{lift} of 10°C and ΔT_{reg} of 27°C), with an average exergetic COP of 0.83.

While these first two indicators are informative about the operational expenditure, having low running costs is often not enough, especially when competing with conventional heat pumps. In the scenarios minimizing the reactor volume, the figure for cycles at intermediate relative pressures change completely: the low density of the MOFs is penalizing, and almost only the denser zeo-types are used. This emphasizes how a screening only based on the adsorption isotherms is not the most efficient, and some parameters representing the integration on the heat exchangers must be included. Using V_{EN} is a good first approximation, but it is important to keep in mind that different material formats (powders, granules, monoliths) provide different packing densities according to their shape and size distribution. More advanced stages of design would require the characterization of the materials as integrated into the heat exchanger and more complete thermodynamic and kinetic considerations, that can deeply change the results in favour of faster and more practical-to-handle materials. As stated in Section 2.5.1, those elements have to be ideally integrated into the harmonic design of adsorption energy systems, however, they cannot be included when analysing materials as coming from the production factories and laboratories. For minimizing the energy-specific volume of the system, the most frequently selected material is Fahrenheit SAPO34, with an average ΔT_{lift} of 21°C, ΔT_{reg} of 53°C and an energy density of 350 J/cm^3. Mitsubishi AQSOA Z02 is again mostly used to balance the energy needs, with average ΔT_{lift} of 23°C, ΔT_{reg} of 39°C and an energy density of 35 J/cm^3.

As a general consideration of the material selection methodology applied to simplified energy systems, it appears that the combination of "heavy-duty" materials such as zeo-types and "light-duty" materials such as MOFs and ACs is beneficial depending on the needs. The average working conditions chosen for the best materials are summarized in Figure 2.18. Fahrenheit SAPO34 seems to be able to work in conditions that are more challenging for adsorption processes, such as high-temperature lifts and limited regeneration temperatures. Despite its very interesting adsorption characteristic, the MOF Tech. Al-isophthalate cannot

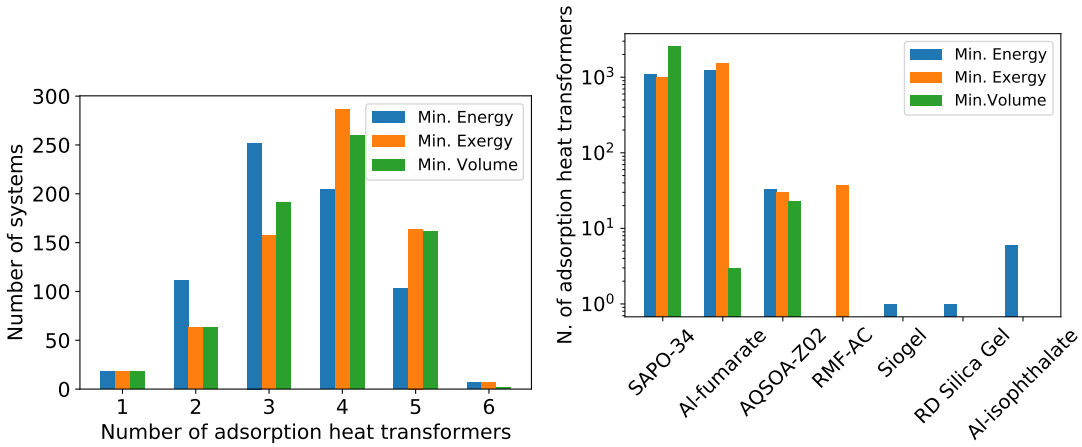

Figure 2.17: Left: the distribution of the number of adsorption heat transformers per system. Right: the adsorbent material candidates use (right) for energy and exergy consumption, and volume minimization. Most optimal solutions required from 3 to 5 AHT, and rarely implemented silica gels or Al-Isophthalate.

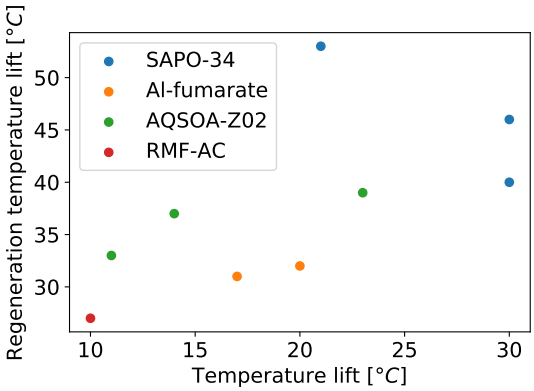

Figure 2.18: Average use conditions (temperature lift TL provided during adsorption and regeneration temperature lift RTL necessary during desorption) of the most selected materials in the optimal solutions. SAPO-34 from Fahrenheit works with high TL and high RTL. Al-fumarate from MOF Technologies works with intermediate TL and low RTL. AQSOA-Z02 from Mitsubishiworks with intermediate TL and intermediate RTL. RMF-AC from Empa works with low TL and low RTL.

compete with the high water capacity of Al-fumarate. It is also interesting to notice how the silica gels, despite their good adsorption capacity, are rarely a good choice because of the adsorption hysteresis and the broad adsorption peak, both limiting the actual cycled water.

Looking at specific scenarios is the goal of a screening performed by the system designer/developer interested in a specific application. In general, simple energy needs lead to simple solutions. For example, refrigeration at 5°C is most energy-efficiently provided by a single adsorption cycle using Fahrenheit SAPO34 fed by a hot stream at 85°C and discharging energy

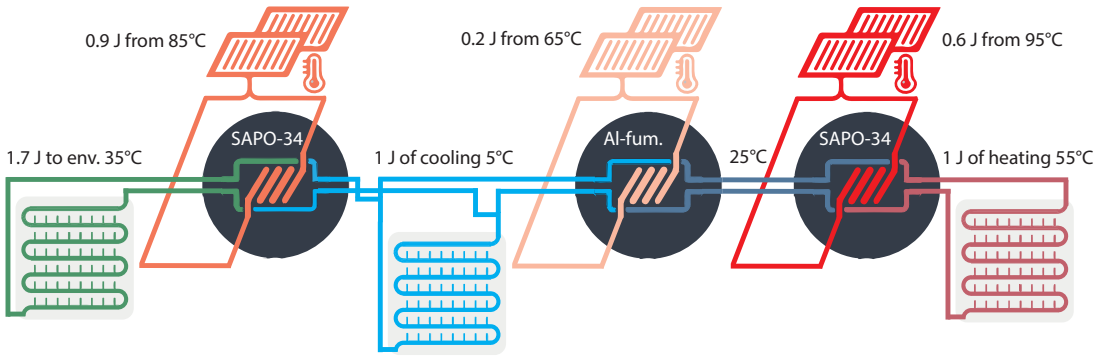

Figure 2.19: Example of cascade configuration for for a system with mixed energy needs (cooling at 5°C and heating at 55°C, with minimum energy use). Part of the cooling needs are satisfied with a less efficient cycle using Al-fumarate, but gaining overall efficiency thanks to its synergy with the heating cycle.

to a 35°C condenser. This thermodynamically challenging solution has an ATL of -25 °C and an overall NU of energy of 1.3. The exergy minimization brings the same choice, as the COP loss using lower-temperature hot streams is in this case too big. If the reactor must have the minimum possible volume, a hot stream temperature of 95°C is preferred.

If the energy needs are more diverse, such as in the case depicted in Figure 2.19, having multiple reactors is more convenient. If the amount of cooling energy needed does not surpass the need for heating, the minimum number of adsorption heat transformers is equal to the number of temperature levels of the energy needs. From the illustration, one can appreciate how the NU of energy is minimized thanks to the double use of the Al-Fumarate adsorption cycle. This combined heating and cooling scenario is characterized by an ATL of 0 °C and a NU of energy of 0.85.

The use of energy sources at different temperatures, often recurring in scenarios characterized by complex energy needs, adds some complexity to the system, for example spilling some of the hot streams from one reactor to another or having multiple heat generators. Anyway, it brings efficiency improvements also on the generator side (e.g. minimizing the fraction of solar collectors running at high temperatures).

2.5.4 Conclusions

Based on the equilibrium adsorption data, a reliable and robust methodology to screen and pre-select adsorbent materials for adsorption heat transformer systems was presented. The characterization of tap density, specific heat capacity and equilibrium water vapour adsorption and desorption at different temperatures provided enough information to evaluate the maximum achievable performances of heating and cooling cycles for energy use, exergy use and volume required. In particular, measuring the adsorption curves over wide ranges of relative humidity and temperature is fundamental for extrapolating the results for simulation

purposes.

Ideal adsorption cycles have been evaluated as a function of adsorbent temperature-dependent properties and target system temperatures only. This enables the evaluation of the suitability of adsorbent materials as coming from the manufacturer for given adsorption energy transformation applications. The simulation and optimization of different application scenarios allow for determining the most suitable adsorbent materials and system designs at the same time, potentially enabling high-performance solutions. In particular, the combination of zeolites for high-temperature lifts and MOFs or ACs for smaller-temperature lifts provided promising results.

In conclusion, the method presented here proved to be a powerful tool to help material, equipment and system developers to estimate the achievable performances, and to focus the R&D efforts only on the most attractive adsorbent materials. While contributing to the foundation of exhaustive adsorption energy systems design tools, this methodology should be further expanded to integrate a more appropriate performance evaluation, specifically including kinetics, material integration on the heat exchangers, cost functions, and realistic applications. Moreover, for the further extension of this modelling approach to a vast library of adsorbent materials, the application of the *Effective screening* characterization approach could be implemented.

2.6 Conclusions and Outlook

In this chapter, we filled some gaps in the research using the equilibrium properties of adsorbent materials to conceive promising adsorption heat transformation processes. In particular, we lingered on the effectiveness of the strategies for material characterization depending on the need. A method for quick pre-screening of the adsorption equilibria and one for more detailed predictions are proposed. They offer new trade-offs between generality, accuracy and resource use.

Subsequently, the equilibrium properties are used to calculate the maximum theoretical performance of the adsorbents and implemented into an optimization algorithm for their selection and pre-sizing. The results show that the use of such a methodology can be highly beneficial for designing efficient systems.

The methodology could be extended to integrate material discovery and a more realistic model of the adsorption system.

2.7 Acknowledgments

This section was elaborated in collaboration with Vincenza Brancato and Andrea Frazzica from CNR-ITAE, Italy, and with the support of the project *HyCool: Industrial Cooling through*

Hybrid system based on Solar Heat, funded by the European Commission H2020 Programme under Grant Agreement No. 792073. Part of the content was published by Piccoli, Brancato, et al., 2022.

Nomenclature

Acronyms		**Symbols**	
$Al-fum.$	Aluminium Fumarate from MOF Technologies	C	Characteristic energy of adsorption $[J/g_w]$
$Al-iso.$	Aluminium Isophthalate from MOF Technologies	cp	Specific heat capacity $[J/g/K]$
AC	Activated Carbon	F	Specific work of adsorption $[J/g_w]$
$AQSOA-Z02$	AQSOA-Z02 from Mitsubishi Plastics	f	degrees of freedom of the model
ATL	Averaged Temperature Lift	H	Specific heat of adsorption $[J/g_w]$
COP	Coefficient Of Performance	k	Total number of points predicted
DA	Dubinin-Astakhov	M	Molar weight of water $[g/mol]$
EN	Energy use	n	Adsorption exponential shape factor $[-]$
EX	Exergy use	L	Latent heat of evaporation of water $[J/g_w]$
EV	Energy-specific Volume	p	Pressure $[mbar]$
$MILP$	Mixed Integer Linear Programming	R	Ideal gas constant $[J/mol/K]$
MOF	Metal-Organic Framework	s	Size of the unit $[-]$
MSE	Mean Square Error	T	Temperature $[K]$
NU	Normalized use (of energy/exergy)	t	time $[s]$
OBJ	Objective function	Q	Energy stream $[J]$
$RD\ Silica\ Gel$	RD Silica Gel from Fuji Davison	w	Specific adsorbed water loading $[g_w/g_s]$
$RMF-AC$	Resorcinol-Melamine-Formaldehyde AC from Empa	W_0	Specific adsorbed water at saturation $[g_w/g_s]$
RSE	Residual Standard Error	ϵ^2	Squared residuals
$SAPO-34$	SAPO-34 from Fahrenheit	ρ	Density $[g/cm3]$
$Siogel$	Siogel from Oker Chemie	τ	Characteristic time $[s]$
SEM	Scanning Electron Microscopy	δ	Dirac delta function
AHT	Adsorption Heat Transformer	N	Number of elements
$R\&D$	Research and Development	d	Particle size $[mm]$
PSA	Pressure Swing Adsorption	Δ	Difference
Sub- and super-scripts			
ad	Adsorption	i,k	Elements of the sums
c	Critical point of water	in	initial
con	Condenser	max	Maximum
de	Desorption	$need$	Energy need/requirement of the system
env	Environment	s	Solid adsorbent
eva	Evaporator	sat	Saturation
fi	Final	T	Temperature level
hot	Hot source of the cycle	w	Water
$train$	Training data	$param$	Model parameter
$cool$	System's cooling demand (also level)	$heat$	System's heating demand (also level)
$sink$	System's heat sink (also level)	$source$	System's heat source (also level)
$V50$	Volumetric median	$switch$	Switching point between isosteric and isobaric adsorption
tap	tap (density)	l	level
$test$	Test data	$lift$	temperature lift from evaporator to condenser
		reg	regeneration temperature lift from condenser to hot source

3 A Scalable Approach to Modelling Adsorption Dynamics

3.1 Introduction

The understanding and the prediction of the performance of adsorption cycles for energy transformation have been interesting to the research community for several decades. Together with experimental observations, modelling and simulation were used to a great extent for this purpose. Already in a review paper by Yong and Sumathy, 2002, different classes of models were identified according to the type of analysis used: thermodynamic, lumped-parameter, and heat and mass transfer models. This classification is still valid today, as reported by Pesaran et al., 2016; Sah et al., 2017, and will also be used in this chapter.

The (simple) thermodynamic models involve first-law and second-law analysis based on the adsorption equilibrium characteristics. They are useful to estimate the maximum energy efficiency of a system and require little information, but they cannot give any insight regarding key performance indicators such as power density.

Lumped-parameter models, instead, aim to describe the dynamic behaviour of the processes with heat and mass balance equations, using ordinary differential equations and some degree of uniformity within the materials involved. For this reason, they are also referred to as global models. Already in the 90s, Sami and Tribes, 1996 used a lumped parameter model to describe the dynamic performance of an adsorption system, using global parameters for the overall heat transfer coefficient. Schreiber et al., 2015 used a lumped-parameter model, calibrated with experimental measurements on a prototype, to study the system performance of heat storage when integrated with a cogenerator. Lumped-parameter models were also used to describe the heat and mass transfer properties of the adsorption materials for numerical simulations of heat pumps by Graf et al., 2017; Velte et al., 2017. Seol et al., 2020 used experiments to determine the heat and mass transfer lumped coefficients of an adsorption heat pump. They used the widespread concept of *linear driving force* to model the mass diffusion kinetics. This model implies that the driving force is, as the name suggests, linearly proportional to the difference between the adsorbate loading and the adsorbate loading that would exist in equilibrium conditions. This linear coefficient has to be calibrated on experiments at

various scales. This calibration has the advantage of saving time in the characterization of the mass diffusion properties of the adsorbent, which is notoriously difficult but does not include the effect of the thermodynamic state on the diffusion phenomenon. Y. I. Aristov, 2020 reports that in general, the linear driving force leads to underestimating the adsorption rate in the first phase and to overestimating it in the second phase. Seol et al., 2020. find that the linear driving force seems to be temperature-dependent. Palomba et al., 2021. used lumped-parameter adsorbent elements in a discretised adsorption system model, fitting some effective material properties to run parametric analysis on design and operational parameters. In conclusion, lumped-parameter models are versatile and scalable tools for evaluating both energy efficiency and power performance, but it is often challenging to extrapolate the results as generally the global effective properties of the system are not valid outside the validation range, given the non-linearity of adsorption systems.

Heat and mass transfer models are detailed in nature, as they aim to describe the evolution in both the time and space of the thermodynamic states. For this reason, they are also referred to as local models. Depending on the model assumptions, their dimensionality can change, but in any case, they involve the momentum equation and state variables are solved in the form of partial derivatives. Given the strong non-linearity and complexity of these models, the numerical method used for their solution is highly relevant. As the underlying assumptions and solving methods vary greatly, transfer models of different complexity exist. Being based on the properties of the materials, heat and mass transfer simulations are highly accurate under different boundary conditions. However, due to their geometrical complexity and the computational effort required, they are not suitable for system optimization on many parameters.

Consequently, the use of these models in the literature is not widespread. Marletta et al., 2002 and Restuccia et al., 2002 developed a lean, numerical heat and mass transfer model with radial symmetry using it in full-factorial analysis to determine the most important parameters influencing the specific cooling. Maggio et al., 2006 used a two-dimensional model to evaluate the benefits of heat recovery between two adsorbent beds, and the sensitivity of power and efficiency performance on some parameters. Radu, 2017 used a fully three-dimensional numerical heat and mass transfer model of the adsorbent material to evaluate the effect of geometrical parameters on the rate of adsorption and the relative importance of heat and mass transfer mechanisms. Finally, Yaïci and Entchev, 2019 used a heat and mass transfer model coupled with computational fluid dynamics to determine the effect of some geometrical parameters on the performance of a solar cooling system.

Mohammed et al., 2019 found that a heat and mass transfer model of an adsorption heat and mass exchanger must include the evaporator dynamics, otherwise it will provide too optimistic power performance for short cycle times. The calibration of a lumped parameter model with the heat and mass transfer model and experiments provided good performance predictions. This confirms the impression that lumped-parameter models must be well-tuned. Dias and Costa, 2019 compared lumped-parameter and heat and mass transfer models and

found that the latter type is more accurate, especially for power prediction. Additionally, they found that increasing the spatial resolution excessively brings limited improvements and a high computational cost. Consequently, the adsorbent material should be evaluated in the tens-of-micrometre range and the heat exchanger in the centimetre range for accurate predictions.

As highlighted by Pesaran et al., 2016, the simultaneous optimization of adsorber material and adsorption equipment design and operation is lacking. The problem is that heat and mass transfer models, well-suited for design as they provide accurate results, are too costly to produce and simulate for many options as this challenge implies.

As done by Palomba et al., 2021, the dynamics of adsorption at the material level can be used for modelling system dynamics as well. However, how to correctly describe and characterize those is not a solved challenge. Several methods to investigate the nature of the adsorption coupled heat and mass transfer are possible, for example, as reported by Y. I. Aristov, 2017; Sapienza et al., 2018. Some approaches characterize the adsorbent effective characteristics (see Ammann et al., 2018; Santamaria et al., 2014; Solovyeva et al., 2017) and some rather the material's properties (see Laurenz, 2021; Velte et al., 2017). Despite the different reasons reported by different authors, the general consensus is, that the linear driving force model of mass transfer usually adopted in system modelling should be modified or discarded, as reported by Y. I. Aristov, 2017, 2020; El-Sharkawy, 2011; Laurenz, 2021. In fact, both adsorbate loading and the locality of adsorption and thermal effects are influencing kinetics in various ways. On top of this, it was proven by Glaznev et al., 2010 that the presence of air in the system affects the adsorption dynamics. However, when characterizing fixed geometries and/or operational conditions, it is possible to determine some parameters such as diffusion coefficients in "grain size insensitive regimes", as reported by Santamaria et al., 2014; Solovyeva et al., 2017, or heat and mass transfer impedances, as reported by Ammann et al., 2018.

To solve the issue reported by Pesaran et al., 2016 (i.e. the simultaneous optimization of adsorbent material and adsorption equipment), we propose a lumped-parameter heat and mass transfer model, that can be integrated easily into many adsorbent bed designs and is fast to simulate, on the line of what was done by Palomba et al., 2021. Each lumped-parameter element is a section of material, similar to previous work by Graf et al., 2017; Palomba et al., 2021; Velte et al., 2017. However, one key difference between the works in literature and this work is that we provide an explanation and a modelling strategy to describe the time evolution of the lumped coefficients regulating heat and mass transfer based on the material properties, therefore integrating their local characteristic rather than fitting average values, as done by El-Sharkawy, 2011; Laurenz, 2021. With respect to the work of Laurenz, 2021, we propose a different description of the transient phenomenon and validate the approach with a dynamic model compared with large temperature jump experiments. Our approach has some limitations in terms of isolating the least important contributions and therefore calibrating the model, but it has the advantage of showing the effect of coupled heat and mass transfer. In fact, we do not try to express the dynamics of heat or mass transfer alone, but their combined effect.

To do so, we use a lumped-parameter approach based on the adimensional time, similar to the one proposed by El-Sharkawy, 2011. The mathematical reasoning is the same, but our application to more generally defined heat and mass transfer resistances should guarantee a more robust definition. In fact, due to the presence of sorption, we propose a modification of the adimensional times with respect to the classic theory described by Carslaw and Jaeger, 1959; Ruthven, 1984.

By combining the lumped-parameter model features with the local transient accuracy of heat and mass transfer models, we aim to achieve a new trade-off between simplicity, accuracy and physical consistency. Instead of using numerical methods to determine the transient behaviour in the microscale of the adsorbent material (which is relevant, as reported by Dias and Costa, 2019; Radu, 2017), we use a semi-analytical derivation, so that it can be calculated for some relevant geometries.

Following the research line of some of the authors in the field, as Graf et al., 2017; Palomba et al., 2021; Schreiber et al., 2015, we developed the model in Modelica for easy integration and application to system models in the future. The proposed model is fully open-source and does not rely on any proprietary software or library.

To prove the validity of the approach in capturing with sufficient detail the locality of the adsorption process, we compare the results of the simulations with heat and mass transfer simulations by Radu, 2017 and experiments.

The proposed modelling approach could be useful at the intermediate stages of the design of the adsorption heat transformer. In fact, it requires less characterization and modelling effort compared to other methods, but it cannot guarantee accurate results for the whole system as it is focused on the material and does not include fundamental aspects of design such as the heat exchangers (adsorption, evaporator, condenser) and the momentum equations. The model is meant for the versatile simulation of complex systems and possibly to address full-scale material and system optimization.

The specific goals of this work include:

- the development of a lumped-parameter model of adsorbent materials that take into account the locality of adsorption
- the application of such an approach to relevant adsorbent materials
- the validation of the model against literature and own results
- the implementation of the model in Modelica for simulation purposes

In Section 3.2, experimental procedures used to generate the observations and the origin of the reference data are discussed. In Section 3.3, the model concept is explained and derivations for the relevant geometries of spheroidal adsorbents and slabs/coatings are presented. In

Section 3.4, we will compare the results of the model with experiments and results of full-scale simulations from the literature. The results will be analysed thoroughly. Finally, in Section 3.5 the key findings are summarized, analysing the advantages and limitations of the current model and deriving an outlook of possible future developments.

3.2 Experimental

To validate modelling approaches that can be useful in predicting the adsorbent material's performance in operational conditions, conceptual validity is not sufficient and experimental validation is necessary. In this work, we aim firstly to demonstrate that lumped parameter models are capable of describing the adsorption dynamics with similar accuracy as more complex heat and mass transfer models. To this aim, we chose to refer to the widely studied case of a monolayer of RD Silica Gel beads subject to large thermal swings (see Ammann et al., 2018; Y. I. Aristov et al., 2012; Glaznev et al., 2010; Radu, 2017). Monolayers are technologically relevant as they deliver higher adsorption rates when compared to more conventional fixed-bed/multi-layer configurations. Among the numerous conclusions available in the literature on the experimental and computational characterization of this case study, we note the following:

- According to Glaznev et al., 2010 heat transfer is the limiting mechanism for bead diameters below 0.55 mm, while diffusion limits the adsorption rate for bigger beads;
- According to Y. I. Aristov et al., 2012 for small beads (<0.5-0.8 mm) the adsorption rate is limited by the heat transfer for up to 8 layers, otherwise mass transfer influences the rate of adsorption;
- According to Radu, 2017 heat transfer through the thermal contacts is found to be critical for small beads, while diffusion can limit the rate of adsorption for large beads or for low values of the diffusion coefficients;
- Ammann et al., 2018 found that for small beads (between 1.2 and 2 mm), where the heat transfer is always the limiting mechanism, the adsorption rate can be enhanced by enhancing the thermal contact.

Consequently, to test our model, we will be considering beads of 0.4 and 0.8 mm in diameter. Thus, the smaller beads should be clearly limited by heat transfer and the bigger ones should be more balanced or limited by mass transfer. The adsorption process for the monolayer configuration was experimentally tested by Glaznev et al., 2010 and modelled in Comsol by Radu, 2017. The data from the references are discussed in Section 3.3 for developing the model and directly used in Section 3.4 for the model validation. For more information on the data used, we refer the interested researcher directly to those two works.

To show the application of our method to different geometries and materials, the case of a glued monolith of activated carbon, which is characterized by a slab-type geometry and a different set of properties, as described by Civioc et al., 2020; Huber, Ruch, Hauert, Saucke, et al., 2016, was also studied. To experimentally characterize the activated carbon, we followed the methodology presented by Ammann, Michel, and Ruch, 2019. However, due to the re-purposing of the setup to gas separation research (see Piccoli, Gantenbein, et al., 2022 and Chapter 5), the volume of the chamber was reduced from 2.615 to 1.93 dm^3. Therefore, the pressure variations during a given cycle are significant even with a small sample size, with consequences on the sample preparation and the modelling methods as detailed below.

The Resorcinol-Melamine-Formaldehyde activated carbon monolith, prepared as previously reported by Civioc et al., 2020; Huber, Ruch, Hauert, Saucke, et al., 2016, was thinned by sand-paper abrasion from the original 3.1 mm to 0.81±0.1 mm. Its structural and thermophysical properties are reported in Table 3.2 and have been obtained following the methods reported by Civioc et al., 2020; Galmarini et al., 2019; Piccoli, Brancato, et al., 2022 (partly reported in Chapter 2). An area of 0.98 cm^2 of the monolith was glued to the Al substrate by application of a thermal glue (EC360 GLUE, Jaden Technologies GmbH, Germany) with thermal conductivity of 2 $W/m/K$.

The experimental procedure also resembles the one detailed by Ammann, Michel, and Ruch, 2019, with the difference that the fast swings at the end of the experiment, which account for dynamic starting conditions during real operations, are not used for the validation of this work. Instead, single swings similar to the ones performed by Glaznev et al., 2010 on silica gel are used. The infrared camera is initially calibrated using the equilibrium states of the material and successively used to record the surface temperature of the sample. The loading of the adsorbate on the sample is indirectly determined by the measurement of pressure thanks to the mass and volume conservation equations. The characteristic adsorption equilibrium curve can be characterized in various ways (see Chapter 2), but an *in-situ* characterization was preferred to eliminate some of the experimental uncertainties, similar to the method reported by Ammann, Michel, and Ruch, 2019. Due to the small volume of the measurement chamber and the S-shaped adsorption characteristic of the activated carbon, the experiments were performed at around 10 $mbar$ and between 25 and 45 $^\circ C$. The equilibrium curve was characterized with 2 $^\circ C$ steps. Following the Dubinin-Astakhov approximation, the equilibrium loading w was modelled as a function of the adsorption energy potential $\Gamma = -R/M \cdot T \cdot ln\left(p/p_{sat}\right)$, for values of Γ between 150 and 320 J/g as reported in Equation 3.1 and represented in Figure 3.7.

$$w = W \cdot exp\left(-\left(\frac{\Gamma}{C}\right)^N\right) \tag{3.1}$$

More details about the processing of the experimental data can be found in the report by

Piccoli et al., 2023.

3.3 Methods

As discussed in Section 3.1, it is important to develop accurate methods for predicting and optimizing the dynamic performance of adsorption energy transformers at a reasonable cost. To have a modular modelling technique, the adsorbent materials must be represented as lumped objects, but there is the risk of jeopardizing the modelling accuracy. Therefore, we propose to describe the adsorbent materials as lumped objects, discretized arbitrarily according to the need (e.g. uniformity of temperature, pressure and adsorbate loading, geometric complexity, and size of the system). The lumped materials objects are characterized by uniform thermodynamic state (temperature T and gas concentration within the pore space γ) and a simple geometry (spherical, slab/layer). The thermodynamic state will determine the material's properties (heat capacity c of the solid, adsorbed and gaseous adsorbate, thermal conductivity k, gas diffusion coefficient D) and the water loading w.

We propose to apply the approach described in this work to the *material scale*. By this, we mean such a scale at which macroscopic effects like pressure drops and gradients in temperature in the heat exchanger are negligible compared to the ones observed within the lumped object (e.g. 0.1-10 mm range depending on the case). In other words, the lumped material object is considered to face uniform temperature/pressure boundary conditions. To take into account any temperature and pressure variations at a larger scale, these would have to be added separately, where adsorption at different positions e.g. within a heat and mass exchanger can be described with separate lumped material objects facing different boundary conditions. However, such a solution is outside the scope of the present work and will not be detailed further.

The heat and mass transfer resistances will be described using semi-analytical solutions for the simple geometries considered, assuming a step-like perturbation of the system leading to a difference $\Delta U = U_{ext} - U$ between the internal state variables $U \in (\gamma, T)$ and that of the boundary U_{ext} at time t_0.

In summary, a lumped material object will be represented by an effective temperature and adsorbate vapour concentration - leading to a specific adsorbate loading and materials properties - as well as a simple geometry. As one can observe from the schematic representation in Figure 3.1, the effective material object is connected to the boundary conditions, specifying the external temperature and vapour concentration, through the material, geometry and time-dependent resistances, which determine the response to the difference between effective adsorbent material and external temperature and vapour concentration.

In the following subsections, we will first detail the general model concept. Then outline the derivation of the equations used to model a monolayer of silica gel spheres subject to a large temperature jump in isobaric conditions. With the derived model, we reproduce the

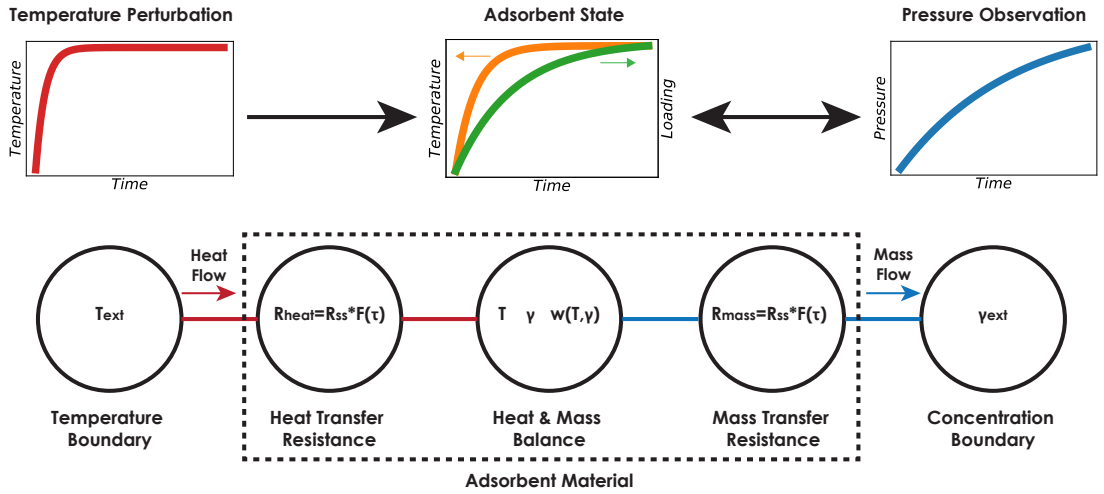

Figure 3.1: Schematic representation of the lumped-parameter modelling approach for thermally-driven adsorption. A temperature perturbation drives an ad/desorption process, that can be observed with the variations in the temperature of the sample, the weight of the sample and/or the pressure around the sample, depending on the boundary conditions.

computational work of Radu, 2017, to prove the validity of the concept as an alternative to heat and mass transfer models. Finally, we will present the extension of the model to the geometry of a slab undergoing temperature swings under isochoric conditions, which is valid for coated and monolithic adsorbents. While these two cases are considered to bring proof of the validity of the approach, more cases of operational relevance can be developed using the same approach described here.

3.3.1 The Heat and Mass Balances

The control volume of the adsorbent material object includes its pore space. All the phases contained in that volume (i.e. the solid adsorbent, the adsorbed adsorbate and the adsorbate vapour) are considered in thermal equilibrium. Consequently, the change of state of vapour passing the boundary of the lumped material object needs to be accounted for in the heat balance. The internal energy change due to the amount of adsorbed phase is considered accounted for within the adsorption term. Otherwise, the heat balance is composed of the typical first-order terms, that account for both the sensible and the adsorption heat. The heat balance of Equation 3.2, comprises the heat flow exchanged with the adsorption heat exchanger surface Q_{cond}, the enthalpy flow rate due to the change in internal energy of the vapour entering the pore volume Q_{mf}, the change of internal energy in the solid adsorbent Q_{sol}, the change of internal energy in the adsorbed phase Q_{ads}, and the change of internal energy in the vapour phase Q_{vap}.

$$Q_{cond} + Q_{mf} = Q_{sol} + Q_{ads} + Q_{vap} \tag{3.2}$$

$$Q_{cond} = \frac{T_{ext} - T}{R_{heat}} \tag{3.3}$$

$$Q_{mf} = \dot{m} \cdot (h_{ext} - h) \tag{3.4}$$

$$Q_{sol} = m_{sol} \cdot c_{sol} \cdot \frac{dT}{dt} \tag{3.5}$$

$$Q_{ads} = m_{ads} \cdot c_{ads} \cdot \frac{dT}{dt} - H_{ads} \cdot \frac{dm_{ads}}{dt} \tag{3.6}$$

$$Q_{vapor} = m_{vapor} \cdot \frac{dh_{vapor}}{dt} \tag{3.7}$$

Similarly, the mass balance in Equation 3.8 comprises the mass flow rate of vapour entering the pore volume $\dot{m}$, the mass change of the adsorbed phase $\dot{m}_{ads}$, and the mass change of the vapour phase $\dot{m}_{vap}$.

$$\dot{m} = \dot{m}_{ads} + \dot{m}_{vap} \tag{3.8}$$

$$\dot{m} = \frac{\gamma_{ext} - \gamma}{R_{mass}} \tag{3.9}$$

$$\dot{m}_{ads} = V_{env} \cdot \rho_{env} \cdot \frac{dw}{dt} \tag{3.10}$$

$$\dot{m}_{vap} = \gamma \cdot \frac{dV_p}{dt} + V_p \cdot \frac{d\gamma}{dt} \tag{3.11}$$

$$V_p = V_{env} \cdot \left(\epsilon - \frac{\rho_{env}}{\rho_{ads}} \cdot w \right) \tag{3.12}$$

Since we model the gas diffusion as a process driven by a mass concentration gradient of the vapour (see Ruthven, 1984), we relate the temperature and pressure of the vapour boundary condition (often used in engineering contexts) to the gas concentration considering an ideal-gas behaviour in the typical range of operation:

$$\gamma = \frac{M \cdot p}{R \cdot T} \tag{3.13}$$

3.3.2 The Heat and Mass Transfer

As the heat and mass balances are including the capacitive effects of adsorption, the heat and mass transfer resistances objects are including resistive effects only.

As reported in the literature, lumped parameter models fall short in determining the rate of adsorption for conditions outside the calibration range (e.g. shorter or longer cycles, different temperatures, different geometry). For this reason, we propose the derivation of transient heat and mass transfer resistances that depend on the material's properties only.

As reported in Equations 3.3 and 3.9, in lumped-parameter models we can generally define a transfer resistance as the ratio between the difference in potential and a flow rate:

$$R = \frac{\Delta U}{\Phi} \tag{3.14}$$

In the case of heat transfer, ΔU will be the temperature difference between the adsorbent and the heat exchanger surface ($T_{ext} - T$), while Φ will be the heat flow rate of conduction (Q_{cond}). In the case of mass transfer, ΔU will be the mass concentration difference between the adsorbate inside the pores and outside the pores ($\gamma_{ext} - \gamma$), while Φ will be the mass flow rate of diffusion ($\dot{m}$).

For simple geometries, such as spheres and layers/monoliths, and a single perturbation ΔU at t_0, it is possible to describe the evolution of the lumped state variable U as a geometry-

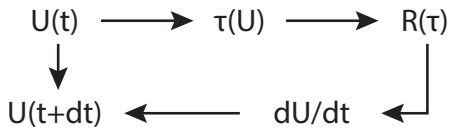

Figure 3.2: Schematic representation of the transient heat and mass transfer modelling approach. U is the state variable (temperature of vapour concentration), t is the time, τ is the adimensional time of the reaction, R is the transfer resistance (to heat or mass). The state variable is used to determine the flow rate by the determination of an adimensional adsorption time and the relative resistance.

dependent function of an *adimensional time* τ. The adimensional time depends on the geometry, the properties of the material and time:

$$U = U(\tau) \tag{3.15}$$

Moreover, it is possible to characterize the transfer resistance as the product of a steady-state resistance R_{ss} and a reduction factor that is a function of the adimensional time $F(\tau)$ (see Carslaw and Jaeger, 1959):

$$R = R_{ss} \cdot F(\tau) \tag{3.16}$$

The reduction factor is a *transient* factor, as it takes into account the locality of the transfer. When the gradient of the potential is concentrated in space and is not distributed over the whole lumped object, the actual characteristic transfer distance is shorter than the characteristic length of the adsorbent. Again the transient factor is a geometry-dependent function of the adimensional time.

In the case of constant properties, the adimensional time is linearly dependent on the time with a pre-determined factor. In the case of varying properties in time, the adimensional time can be expressed as an integral in time over the properties of the material. However, as the Equations 3.15 and 3.16 are linearly independent, it is possible to calculate the adimensional time with Equation 3.15 based on the lumped state of the adsorbent, and use it in Equation 3.16 to calculate the resistance, which will, in turn, be used to determine the flow rate in Equation 3.14. The method is represented in a schematic way in Figure 3.2.

The above equations do not explicitly take into account the source/sink terms due to adsorption. However, these processes will have the effect of additional resistance, slowing down the

evolution of the internal state U. For the rate-limiting transfer mechanism, this is mathematically correct in the case of linear adsorption over an extended range (see Carslaw and Jaeger, 1959). However, the more narrow the adsorption range, the more our approach will become approximate. Indeed, in the case of a step-like adsorption isotherm, the approach will lead to step-like adsorption of the lumped material object, whereas in reality, adsorption will be more gradual. Corrections for the case of a step-like adsorption peak are envisaged in the future but are not part of the current model/validation.

For the transfer mechanism which is not rate limiting, the transient factor has a negligible effect and thus the derived equations should only lead to small errors. Caution has to be taken in situations where mass and heat transfer are balanced. In none of the cases discussed below it was possible to demonstrate an absolute balance and therefore the estimation of the accuracy of our method for such cases should be considered outside the scope of the current work.

3.3.3 Silica Gel Spheres

Within this work, we considered two application cases that can prove the validity of the concept and provide insights for relevant applications. The first case is a monolayer of silica gel beads. This material was tested extensively in the literature, both in experiments at different scales by Ammann et al., 2018; Glaznev et al., 2010; Santamaria et al., 2014 and in models by El-Sharkawy, 2011; Radu, 2017. In particular, our aim is to achieve a similar accuracy of dynamic performance prediction as heat and mass transfer models. For this reason, we selected the same test case that was studied by Radu, 2017 by finite-element modelling. The original experimental data are derived from the works of Y. I. Aristov et al., 2012; Glaznev et al., 2010. The material properties used for the simulation are the same as reported by Radu, 2017. About these properties, it is important to make a few remarks:

- the adsorbent thermal conductivity was assumed to be equal to the one indirectly derived from a packed bed experiment with a similar material;
- the specific heat capacity and heat of adsorption are assumed to be constant, but Santori et al., 2013 report this is often not the case;
- to calculate the effective thermal conductivity of the humid material, one of the many correlations available in literature was used;
- for many properties, the variation of the values reported in the literature is quite large, according to the source.

Among the available cases for the proof of concept, we decided to focus on a single layer of beads, which is particularly relevant for high-power adsorption equipment. Given the experimental setup characteristics, the thermal boundary condition is modelled as a perfect heat

source/sink in thermal contact with the adsorbent beads. No other heat transfer mechanism is included as they are considered negligible under the typical operating conditions for such configuration (see Radu, 2017), except for the transport of energy through the adsorbent control surface as the vapour enters and leaves the pores. The mass transfer boundary condition is modelled as perfect isobaric conditions, as the pressure variation within the setup is rather small.

The thermal contact can be geometrically described by the ratio between the thermal contact radius and the particle radius $\psi = \frac{r_c}{r_b} < 0.1$, as proposed by Siu and Lee, 2000. This parameter cannot be experimentally determined in our case, and it represents a fitting parameter similar to the overlapping coefficient in the reference work of Radu, 2017. Moreover, the exact experimental time lags observed when starting the experiments and the radius of the particle are also to be fitted, as there are some experimental inaccuracies to take into account. More details will follow in Section 3.4.

In 3.8 and 3.9, we derive the equations used for the calculation of the effective adimensional time and resistance for the mass and heat transfer, respectively. They are summarized here as implemented in Modelica, with the exception of τ_{heat} for brevity (see Equations 3.60-3.64 instead):

$$\frac{\gamma - \gamma_{ext}}{\gamma_i - \gamma_{ext}} = \frac{6}{\pi^2} \cdot \left(1.36 \cdot \mathrm{e}^{-15.74 \cdot \tau_{mass}} + 0.2393 \cdot \mathrm{e}^{-575.3 \cdot \tau_{mass}}\right) \tag{3.17}$$

$$R_{mass_{ss}} = \frac{3}{4 \cdot \pi^3 \cdot r_b \cdot D \cdot V_p} \tag{3.18}$$

$$F_{mass} = 1 - 0.1735 \cdot \mathrm{e}^{-938.9 \cdot \tau_{mass}} - 0.7836 \cdot \mathrm{e}^{-39.67 \cdot \tau_{mass}} \tag{3.19}$$

$$\tau_{heat} = \tau_{heat}\left(T, T_i, T_{ext}, \psi\right) \tag{3.20}$$

$$R_{heat_{ss}} = \frac{0.5759}{k \cdot r_b} \cdot \left(\frac{1}{\psi} - \frac{1.093e-3}{\psi^2} + \frac{3.019e-5}{\psi^3} - \frac{1.202e-7}{\psi^4}\right) \tag{3.21}$$

$$F_{heat} = \left(1 + \frac{1}{3 \cdot \tau_{heat}^{1/2}} + \frac{1}{50 \cdot \tau_{heat}} - \frac{1}{400 \cdot \tau_{heat}^{3/2}}\right)^{-1} \tag{3.22}$$

3.3.4 Activated Carbon Monolith

As discussed in Section 3.2, it was decided to investigate the case of a monolith of RMF activated carbon subject to a temperature swing in isochoric conditions, where the pressure variation is not negligible.

In such a case, as well as for coated materials, the geometry can be described by a one-dimensional heat and mass transfer model, as the monolith thickness is one order of magnitude smaller than the other dimensions. For this reason, the analytical solution for a step-like change in temperature on one side of an infinite slab was considered. In Section 3.10 the derivation of the solution for the heat transfer is reported. Given the high thermal conductivity and the small thickness of the thermal glue, the thermal contact resistance is likely to account for a small percentage of the heat transfer resistance, and it is therefore neglected. The final equations as implemented in Modelica are reported here.

$$\frac{T - T_{ext}}{T_i - T_{ext}} = 0.8224 \cdot \mathrm{e}^{-\frac{\tau^*_{heat}}{0.1002}} + 0.1776 \cdot \mathrm{e}^{-\frac{\tau^*_{heat}}{0.004651}} \tag{3.23}$$

$$R_{heat} = R_{heat_{ss}} \cdot F_{heat} \tag{3.24}$$

$$R_{heat_{ss}} = \frac{4 \cdot L}{A \cdot k \cdot \pi^2} \tag{3.25}$$

$$F_{heat} = 1 - 0.6971 \cdot \mathrm{e}^{-\frac{\tau^*_{heat}}{0.01336}} - 0.3029 \cdot \mathrm{e}^{-\frac{\tau^*_{heat}}{0.0008868}} \tag{3.26}$$

While the relevant properties for heat transfer can be directly determined during the material characterization, the effective mass diffusion coefficients cannot be directly determined for small sample quantities. While in the case of silica gel, we followed the assumption of the reference case that mass transfer was happening within the beads only through surface diffusion, given the narrow size of the pores of the silica gel itself, for the activated carbon

this does not hold true (see Table 3.2). Therefore, it is necessary to calculate an effective mass transfer resistance taking into account both the macroscopic diffusion through the monolith and the microscopic diffusion in the solid backbone.

As the Knudsen number for water vapour in the activated carbon macropores in the temperature range of 20-50 $°C$ and in the pressure range 5-15 $mbar$ will be in the range of 1.7-29 (as can be easily computed with the geometrical information reported in Table 3.2, as explained by Ruthven, 1984), we must consider that the collisions between the vapour and the solid backbone slow down the mass transfer process in the macropores. The effective macropores' diffusion coefficient can be calculated with the free gas diffusion coefficient D_{gas} and the Knudsen number K (see Ruthven, 1984):

$$D_{macro} = \frac{D_{gas}}{K} \tag{3.27}$$

The macroscopic mass transfer resistance through a slab in steady-state can be easily calculated as:

$$R_{macro_{ss}} = \frac{4 \cdot L^2}{\pi^2 \cdot V_p \cdot D_{macro}} \tag{3.28}$$

Given the extremely narrow size of the micropores (i.e. in the same order of magnitude as the water molecule), it is assumed that the only possible mass transfer mechanism within the solid backbone of the monolith is the so-called "surface diffusion", whose coefficient can be expressed as a function of temperature:

$$D_{micro} = D_0 \cdot \mathrm{e}^{\frac{E_a}{T}} \tag{3.29}$$

In this case, the pre-exponential diffusion coefficient D_0 and the activation energy E_a are characteristic of the material and should be determined experimentally (e.g. as fitting parameters). However, given the qualitative analysis shown in Section 3.4 (e.g. Figure 3.7), it is evident that the characterization of those coefficients would be extremely uncertain, given the low overall relevance of mass transfer. Therefore, it was decided to assume the same values reported for amorphous silica by Radu, 2017 as a starting point.

As the sample is represented by a lumped object and the macroscopic diffusion front is the driver of the microscopic diffusion, we are forced to assume something regarding the transient nature of the microscopic diffusion. Ideally, it would follow the Fickian diffusion model, but as

there is no time constant available for the whole object, it is found convenient to express the microscopic mass transfer resistance as if it was happening in steady-state:

$$R_{micro} = \frac{r_{\mu}}{D_{micro} \cdot A \cdot a_{\mu} \cdot L \cdot \rho_{env}} \tag{3.30}$$

For the macroscopic mass transfer resistance, instead, it is in principle possible to determine the transient factor as it was done for the silica gel, starting from an analytical analysis of the case study. However, the description of the boundary condition is not known *a priori*, as the adsorption process drives a variation in vapour mass concentration both within the monolith and in the measurement chamber. This scenario could be solved with a series of perturbations, each of which is caused by an incremental change in temperature and a consequent incremental change in vapour concentration. However, given the fact that we know from the beginning that the reaction is limited by heat transfer, we can simplify the analysis. As the heat conduction front advances slower than the mass diffusion reacts to it, it is at first approximation reasonable to assume a steady-state resistance (as the boundary condition changes very slowly the transfer is global and not local):

$$F_{mass} = 1 \tag{3.31}$$

As the adsorption is considered to take place only within the micropore volume, the overall mass transfer resistance will be the sum of the two:

$$R_{mass} = R_{macro_{ss}} \cdot F_{mass} + R_{micro} \tag{3.32}$$

Considering the assumptions made so far, the overall mass transfer resistance is likely to be slightly overestimated, as both the macroscopic and microscopic diffusion should be slightly faster due to unaccounted transient effects.

As for the remaining material's properties, the effective specific heat capacity and thermal conductivity of the humid adsorbent were modelled as by Radu, 2017, while the specific heat of adsorption was modelled as by Ammann, Michel, and Ruch, 2019.

3.4 Results and Discussion

3.4.1 Silica Gel Spheres

To test the proposed lumped parameter model approach, the adsorption process experimentally tested by Glaznev et al., 2010 and modelled in Comsol by Radu, 2017 was reproduced. In that experiment, a monolayer of silica gel beads was subject to a sudden change in temperature, so an ad/desorption process was initiated. The beads, sieved in either small size (diameter between 0.4 and 0.5 mm) or in big size (diameter between 0.8 and 0.9 mm), are approximated as perfect spheres. This would in theory result in infinitely small contact with the heat exchanger surface: Radu, 2017 corrects this by allowing and tuning the degree of overlap between spheres and heat exchanger, while in our approach the contact is described by the thermal contact parameter ψ (see Equation 3.21). Furthermore, in both works, the temperature jump is approximated as a step-like function with a small time delay (in the order of seconds). The exact time of delay is also chosen to best fit the experimental results, as in the reference work. We used all other assumptions, properties and boundary conditions as specified by Radu, 2017, so as to emphasize the role of the heat and mass transfer model alone.

The goal of the comparison between experiments and both CFD and lumped-parameters models is to determine whether the use of the simpler lumped-parameter approach would cause a loss in accuracy. To this aim, besides the visualization of the results, an indicator of the accuracy is introduced. The chosen indicator (the weighted root mean square error $WRMSE$) is not intended as a definitive evaluation of the adsorption performance accuracy, but it will highlight differences in the order of magnitude of the model errors. The $WRMSE$ includes the squared residuals over the n experimental values of the loading w and their relative weighing factor ω:

$$WRMSE = \frac{\sqrt{\sum_{i=1}^{n} \left(w_i - w_i^*\right)^2 \cdot \omega_i}}{n} \tag{3.33}$$

$$\omega = \frac{dw}{dt} \tag{3.34}$$

To give more importance to the accuracy obtained in high-rate regimes, the weighting factors are chosen according to the rate of ad/desorption (Equation 3.34). As the available frequency of the CFD results from Radu, 2017 was low (one point every five seconds), linear interpolation among the points was used. A manual optimization of the three tuning parameters (time lag, particle radius, thermal contact ratio, see Table 3.1), leads to the results shown in Figure 3.3.

Analysing the obtained results, it can be concluded that for all the cases the accuracy of the

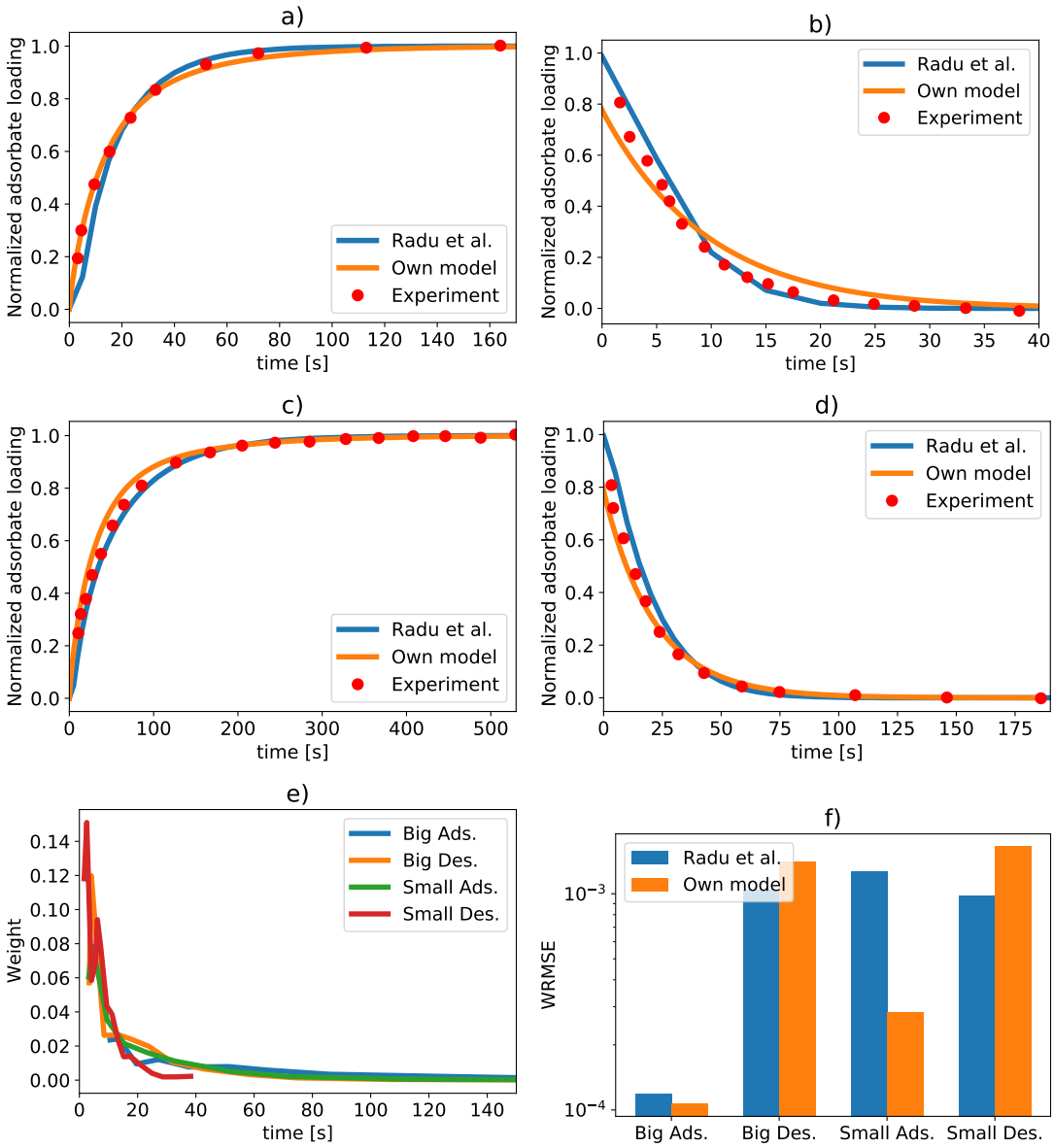

Figure 3.3: Results of the model validation on silica gel beads. a) Adsorption on small beads. b) Desorption on small beads. c) Adsorption in big beads. d) Desorption on big beads. e) Value of the weighing factor over time for the four cases studied. f) Value of the accuracy metric for the cases studied. Overall, the proposed model explains with sufficient accuracy (at the limit of experimental uncertainties) the adsorption rate over time.

Size of beads	**Parameter in Own Model**	**Value**	**Parameter by Radu, 2017**	**Value**
Big	Time Lag ads. - des.	$10s-14s$	Time Lag ads. - des.	$10s-10s$
Big	Particle Radius	$0.4mm$	Particle Radius	$0.425mm$
Big	Thermal Contact Ratio	0.12	Beads Overlap	$\pm 10\%$
Small	Time Lag ads. - des.	$10s-12s$	Time Lag ads. - des.	$10s-10s$
Small	Particle Radius	$0.2mm$	Particle Radius	$0.225mm$
Small	Thermal Contact Ratio	0.07	Beads Overlap	$\pm 10\%$

Table 3.1: Tuning parameters implemented for the simulation of the proposed Own Model compared to the one proposed in the reference model for the validation cases of the silica gel beds. The variations seem to be well within the experimental uncertainties.

lumped-parameter model is of the same order of magnitude as the CFD model. The weak point of both models is the reliance on relatively strong assumptions regarding sensitive aspects of the adsorption process, whose effects can be analysed through a sensitivity analysis as reported in Figure 3.4. In any case, it seems like the development of more detailed models is limited by the difficulty of characterizing the material properties and the adsorption kinetics with sufficient detail and accuracy to evaluate and distinguish between fundamental aspects of adsorption dynamics, as the dominant mechanisms tend to hide the others.

It should be noted that the thermal contact radius ratio ψ used for the beads of $0.8mm$ in diameter is slightly above the originally reported limit of applicability of the implemented model for constrained thermal conduction through spheres (see Siu and Lee, 2000). This highlights a potential problem, which might come either from the model assumptions and simplifications or from the uncertainties deriving from the material properties and from experimental results. However, using $\psi = 0.1$ (within the applicability limit), the $WRMSE$ results worsen by 15% only, due to a worsening in desorption (75%) that is only partly compensated by an improvement in adsorption (60%). In this case, the time lags change to $2-6s$ and overall the accuracy remains in the same order of magnitude, which is reassuring.

In Figure 3.4 the sensitivity of the WRMSE of the optimal solution for adsorption in big beads to a variation of $\pm 10\%$ of the material's properties is shown, calculated as the average variation of the metric in absolute value. It can be noted how the particle radius r_p, the envelope density ρ, and the heat of adsorption H_s have a high impact on the simulations. Other important properties include the thermal conductivity of the dry adsorbent k_s, the surface diffusion activation energy E_a, and the thermal contact ratio ψ. For all these parameters, a deviation of 10% from the experimental value is not excessive given the experimental accuracy. Therefore, we consider a $WRMSE$ below 5e-4 at the limit of the experimental resolution. Thus, while assumptions such as the constant value of the heat of adsorption and the constant gas pressure in the interparticle space will limit the model's accuracy, these limitations are acceptable given the accuracy of the experimental methods.

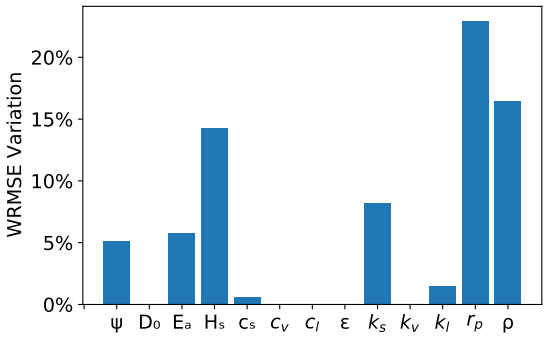

Figure 3.4: Average variations of the WRMSE metric to ±10% variations of the properties of the material for the case of a monolayer of silica gel beads. The analysis show that the results are very sensitive to the bead size and density, as well as to the heat of adsorption.

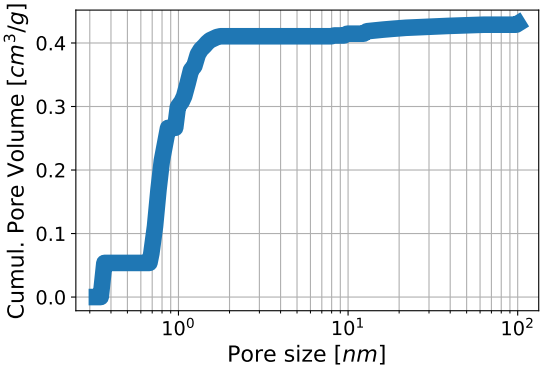

Figure 3.5: Pore size distribution of RMF Activated Carbon from physisorption measurements. Most of the small-scale porosity is below 2 nm.

3.4.2 Characterization of the RMF Activated Carbon

The structural and thermophysical properties were characterized as reported by Galmarini et al., 2019; Piccoli, Brancato, et al., 2022 and are gathered in Table 3.2. Among the available methods for measuring thermal conductivity, we chose the guarded hot plate method as by Civioc et al., 2020. Both pore volume and surface area were evaluated by combining the carbon dioxide and nitrogen isotherms and powder displacement experiments following the protocol from Civioc et al., 2020. Thanks to their combination and complementing with Scanning Electron Microscopy (see Figures 3.5 and 3.6) it was possible to distinguish quantitatively between microporosity ($d_p < 2nm$), mesoporosity ($2nm < d_p < 50nm$) and macroporosity ($d_p > 50nm$). From the SEM images, it was possible to gather geometrical information regarding the nature of the colloidal network forming the porous structure. It is possible to appreciate how the RMF carbon monolith is characterized by a highly interconnected macroporosity existing around a network of spheroids formed in the sol-gel process, in line with our diffusion model (see Section 3.3.4).

Material Property	**Value**
Envelope Density	0.43 $[g/cm^3]$
Skeletal Density	2.0 $[g/cm^3]$
Specific Micropore Volume	0.411 $[cm^3/g]$
Specific Mesopore Volume	0.01 $[cm^3/g]$
Specific Macropore Volume	1.405 $[cm^3/g]$
Specific Micropore Surface Area	1088 $[m^2/g]$
Specific Mesopore Surface Area	1.0 $[m^2/g]$
Characteristic Micropore Diameter*	0.38 $[nm]$
Characteristic Mesopore Diameter*	10 $[nm]$
Characteristic Macropore Diameter	1-5 $[\mu m]$
Characteristic Backbone Diameter	1-3 $[\mu m]$
Thermal Conductivity	0.1005 $[W/m/K]$
Specific Heat Capacity	$930 + 0.63 \cdot (T - 273.15)$ $[J/kg/K]$

Table 3.2: Properties of the RMF activated carbon. Specific heat capacity is valid between 298 and 393 K. The symbol * indicates data obtained by dividing the specific pore volume by the specific surface area.

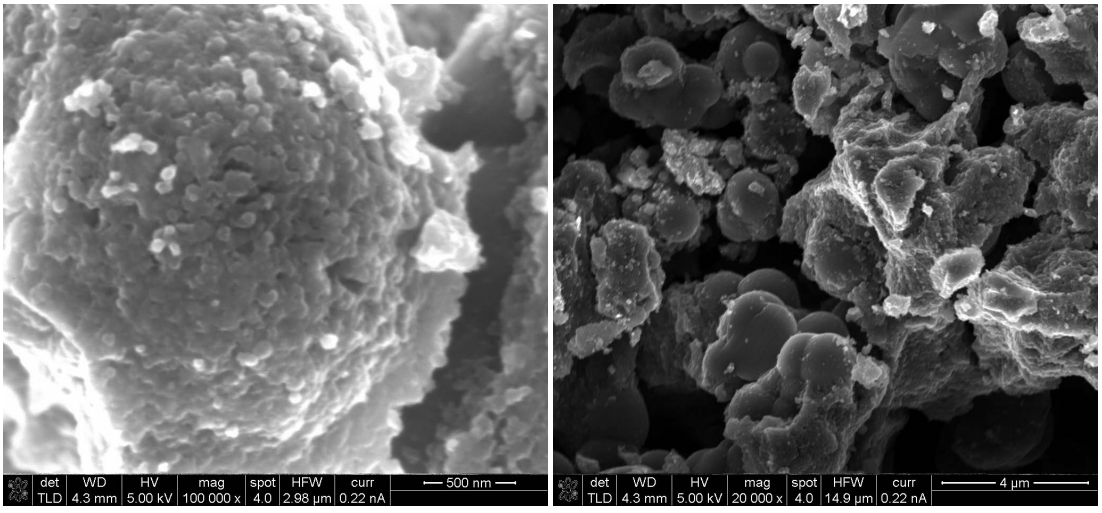

Figure 3.6: SEM images of the RMF Activated Carbon. The solid skeleton is composed by interconnected network of spheroids, typical of the sol-gel synthesis process.

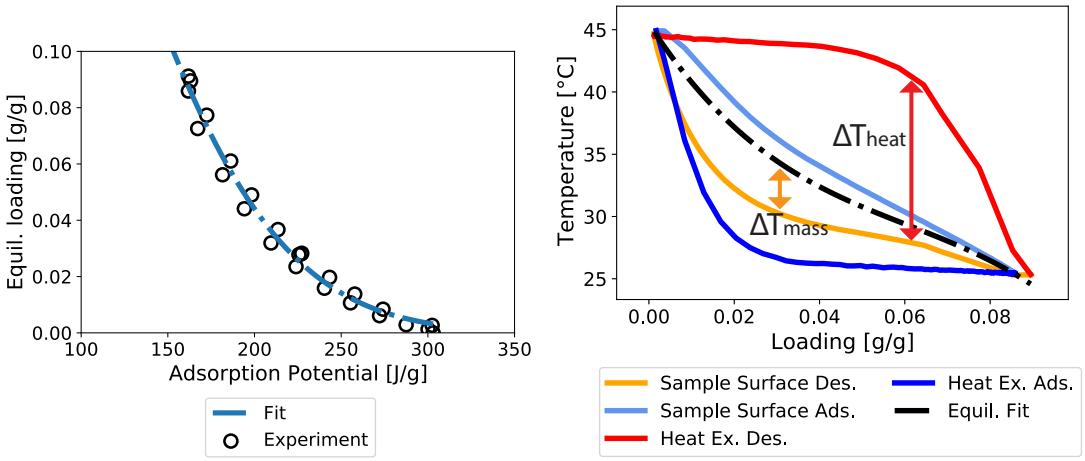

Figure 3.7: Left: the equilibrium curve characterized in-situ shown an offset between adsorption and desorption that could derive from experimental uncertainty. The adsorption condition is in the vicinity of the adsorption peak area. Right: dynamic experimental results of the RMF activated carbon represented in terms of impedance analysis (see Ammann et al., 2018). The results show a very high heat transfer resistance, which requires some additional care.

The *in-situ* characterization of the adsorption equilibrium resulted in the Equation 3.35 (where Γ is the Polanyi's adsorption potential $-R \cdot T \cdot ln\left(p/p_{sat}\right)/M$), which is displayed in Figure 3.7 against the experimental measurements.

$$w = 0.30 \cdot \mathrm{e}^{-\left((\Gamma/145.7)^{2.073}\right)} \pm 0.02 \tag{3.35}$$

We would like to point out that the adsorption condition (10 $mbar$ and 25 $^{\circ}C$) is in the adsorption peak area. Thus, those points are quite sensitive to the measured (and modelled) thermodynamic state. On the other hand, characterizing the sample at lower adsorption potential might cause condensation within the chamber, which would be highly detrimental to the measurement accuracy.

Based on the experiments on the activated carbon monolith, it is possible to perform the impedance analysis, as described by Ammann, Michel, and Ruch, 2019. For the sake of clarity, the basics of this analysis are summarized here and partly depicted in Figure 3.7:

1. From the dynamic measurement, it is possible to plot the heat exchanger temperature T_{HEx} (directly or indirectly determined), the sample temperature T_s (measured with the IR camera) and the equilibrium temperature T_{eq} (obtained with the adsorption equilibrium curve of Equation 3.35) against the adsorbate loading w (determined by the pressure variation);

2. For each loading the heat and mass transfer temperature differences can be determined as $\Delta T_{heat} = T_{HEx} - T_s$ and $\Delta T_{mass} = T_s - T_{eq}$, respectively;
3. For each loading point, the heat flow rate Q_{cond} can be calculated from the heat balance;
4. The impedance to heat and mass transfer can be calculated as $Z_{heat} = \frac{\Delta T_{heat}}{Q}$ and $Z_{mass} = \frac{\Delta T_{mass}}{Q}$ respectively.

By applying the impedance analysis principles to the experimental results as they are (which is without any model of heat and mass transfer), it is possible to qualitatively evaluate the transfer mechanism that is most relevant in determining the rate of adsorption. From Figure 3.7, which reports the dynamic results of the experiments, it is possible to appreciate several facts:

- the equilibrium curve is not linear in the experimental domain;
- the non-linearity of the equilibrium curve is somewhat reflected in the temperature profiles, with a faster development where there is less adsorption;
- the apparent heat transfer impedance is so high that the surface temperature measurement un-physically crosses the equilibrium curve;
- the apparent mass transfer impedance must be un-physically negative to fulfil the impedance analysis.

These experimental findings highlight how heat transfer must be the dominant mechanism determining the adsorption rate, but also (and probably for this very reason) that the sample surface temperature cannot be representative of the adsorption temperature.

3.4.3 Activated Carbon Monolith

After showing that the lumped-parameter approach delivers a similar level of accuracy as heat and mass transfer models for monolayers of silica spheres, we show in this section how it can be used to understand dynamic experiments for monolithic carbon up to the limits of experimental uncertainties. The extension of its validity to different geometries and boundary conditions requires some tailored adjustments, as shown in Section 3.3 for the case of activated carbon monoliths subject to temperature swings in isochoric conditions. The results of the validation are gathered in Figure 3.8. They show a remarkably good determination of the adsorption dynamics, with a credible representation of the effective adsorption temperature. Firstly, it can be observed that the desorption rate is roughly double the adsorption rate. Secondly, it is possible to notice how the effective adsorption temperature is different from both the surface temperature (as expected) and the average between the latter and the heat exchanger temperature (as proposed by Ammann, Michel, and Ruch, 2019).

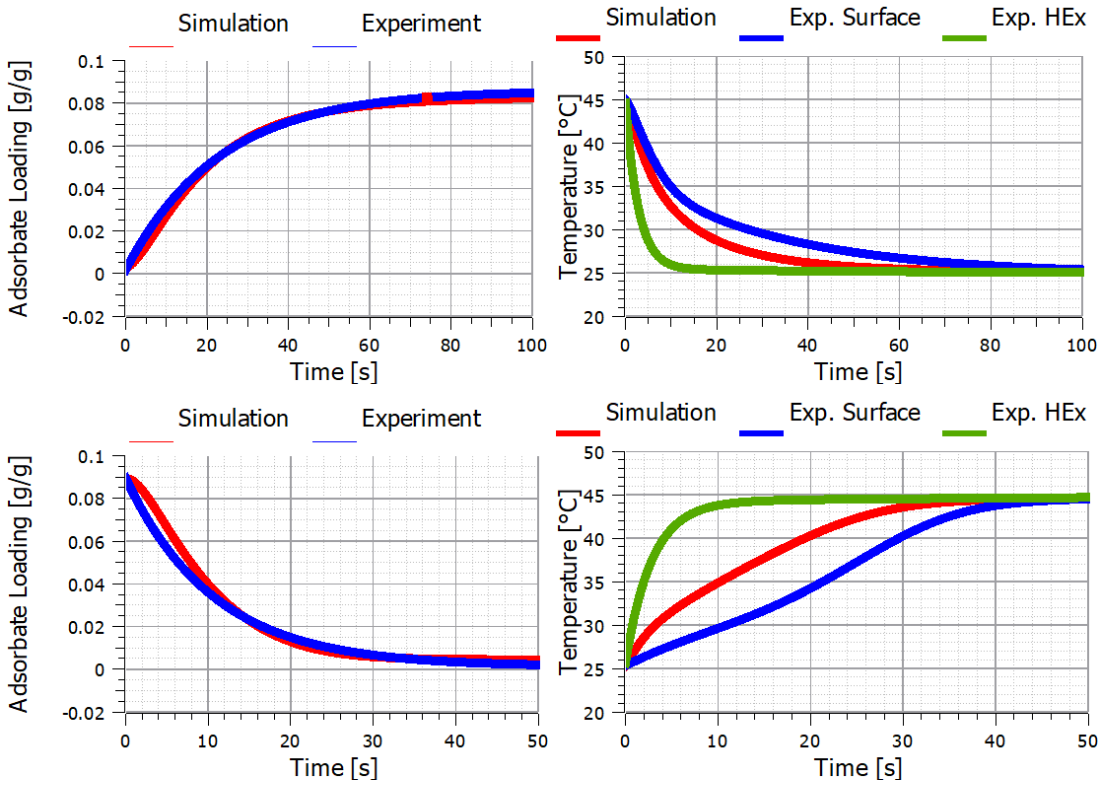

Figure 3.8: Results of the model validation on an activated carbon monolith. Top left: adsorbate loading during adsorption. Top right: temperatures during adsorption. Bottom left: adsorbate loading during desorption. Bottom right: temperatures during desorption. The simulation represents well the experimental loading profile and delivers a credible representation of the effective material temperature.

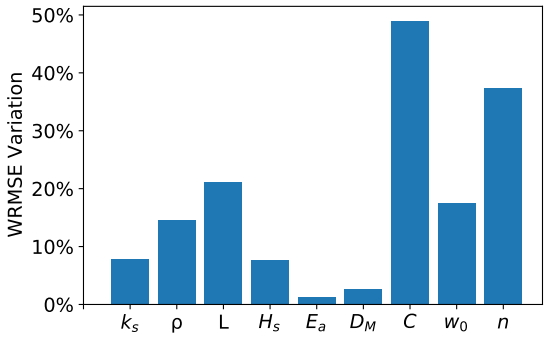

Figure 3.9: Average variations of the WRMSE metric to ±10% variations of the properties of the material for the case of a monolith of RMF activated carbon. The analysis show a great influence of the adsorption curve parameters, the thickness and the density.

The sensitivity analysis (analogous to the one performed for silica gel) performed for the desorption case, reported in Figure 3.9, shows very important findings. On the one hand, it is confirmed that the experimental characterization of the sample, especially in terms of thickness, density, the heat of adsorption and thermal conductivity, is crucial. However, in this case, the determination of the correct macroscopic diffusion coefficient is relatively more important than the activation energy for surface diffusion but overall less important than for the silica gel beads. Moreover, the determination of the heat of adsorption (in this case not assumed constant, but modelled as by Ammann, Michel, and Ruch, 2019) is less important than in the case of silica gel. On the other hand, analyzing the adsorption equilibrium curve, it is found that all its parameters (the characteristic energy of adsorption C, the shape factor N, and the adsorbate capacity W) are crucial to the simulations. This is due to the fact that the adsorption condition is in the vicinity of the adsorption peak, and supports the argumentation reported in Chapter 2 for a very careful characterization of the adsorption curves for simulation purposes, as it may lead to substantial errors if unchecked.

A detailed analysis of the results of the simulation of the adsorption case, reported in Figure 3.10, delivers interesting insights. Regarding the heat balance composition, it can be concluded that the contributions related to sensible heat to the adsorbed phase and of the intraparticle vapour phase can be neglected for simplification. The same applies to the contribution of the intraparticle vapour phase to the mass balance. Furthermore, the microscopic diffusion mechanism is one order of magnitude faster than the macroscopic diffusion, therefore it could be excluded in a simplified analysis, as it seems to contribute too little to the adsorption kinetics to be correctly characterized with these experiments. Regarding the adimensional time of heat transfer, it is interesting to notice that not only it is ten times lower than the Fourier number (its counterpart in absence of adsorption), but it also seems to be a little distorted as well. This is confirmed slightly more evidently by the difference between the measured surface temperature and the one expected by Equation 3.71. This indicates that the starting hypothesis, which is that the shape of the temperature profile is independent of the phenomenon of adsorption, is not entirely correct. However, the difference seems

to reflect only in the surface temperature: this could mean that the temperature gradient can be more or less steep where the heat conduction front is located according to the non-linearity of the equilibrium curve of adsorption of the adsorbent material, even if this does not influence greatly the average internal energy. In fact, it is possible to appreciate that the effective adsorption temperature is now delivering a physical meaning to the impedance analysis. The minor differences between the experimental temperatures in the temperature vs loading plots of Figures 3.7 and 3.10 are due to the shift between measured and modelled loading in the x-axis.

Using the result of the simulations to perform the impedance analysis proposed by Ammann, Michel, and Ruch, 2019, it is confirmed that during the time interval required to reach 80% of the equilibrium change in loading, the heat transfer is limiting the rate of adsorption, as shown in Figure 3.11. In particular, the mass transfer impedance is particularly low for a thickness of 0.8 mm. When compared to high-power zeolite coatings prepared by Ammann, Ruch, et al., 2019, the activated carbon shows the same mass transfer impedance and a heat transfer impedance only three times higher, even if the coating is almost three times thinner. The total adsorption heat and mass transfer coefficient $U = 1/(Z_{heat} + Z_{mass})$ is calculated to be around 370 $W/m^2/K$, which is almost half of the one of the 0.3 mm high-power coating.

The impedance during desorption during the first 5-10 s is much lower than during adsorption, and this is the reason why the initial rate of desorption is much higher than for adsorption. However, during the desorption, the second part of the process is slower, due to the presence of more adsorbate, and starts much earlier. This explains the similar average overall heat transfer coefficient even though the time interval required to reach 80% of the equilibrium change in loading is very different. It is important to notice how the total heat and mass transfer coefficient includes the adsorbent material only. In fact, the temperature of the heat exchanger is greatly influenced by the adsorption process. While the heat exchanger in contact with a naked Al substrate has a characteristic time of 1-2 s, in presence of sorption this increases to 5-6 s. Considering that the sample thermal characteristic time is in the order of 22-23 s, this influence is not negligible. This means that given the ratio of active mass/substrate mass, the adsorption influences the thermal response of the heat exchanger.

It is considered that the RMF activated carbon under investigation is of interest for heat transformation applications as in principle capable of delivering very high adsorption rates and cycled masses of water. However, its tailoring would need an improvement of the heat transfer and the shift of the adsorption peak towards lower adsorption potentials. These two objectives could be reached by decreasing the amount of macroporosity (even if at the expense of the mass transfer, which currently is not limiting the adsorption rate) and by increasing the amount of hydrophilic functional groups on its surface.

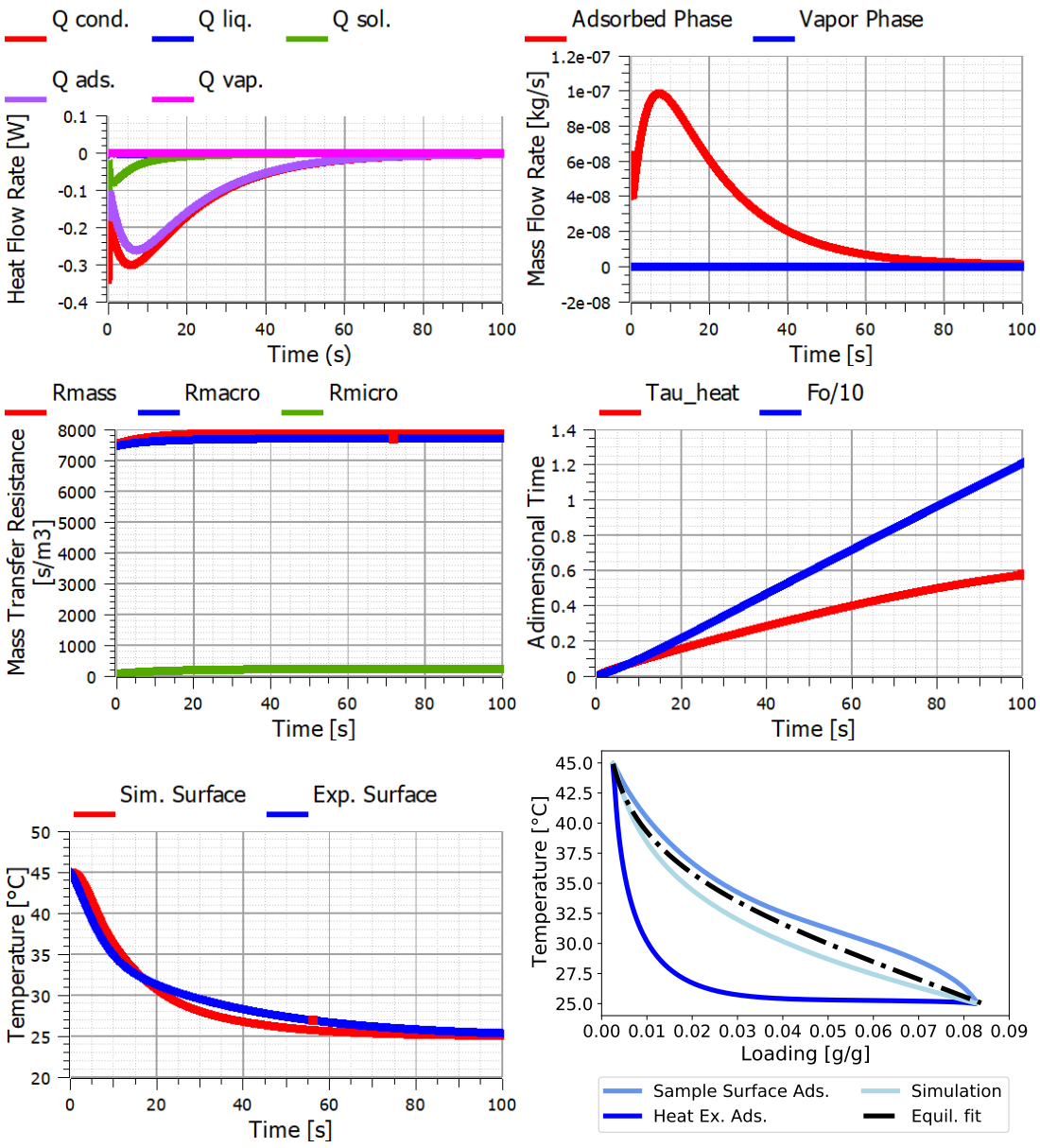

Figure 3.10: Details of the results of the model validation on an activated carbon monolith during adsorption. From left to right and from top to bottom: composition of the heat balance during adsorption; composition of the mass balance during adsorption; mass transfer resistances during adsorption; development of the adimensional time and of the Fourier number during adsorption; expected and measured surface temperature; temperature vs loading profiles during adsorption. The contribution of the vapour phase to the heat and mass balance are negligible. The macroscopic mass diffusion is the dominating mass transfer mechanism. The adimensional time in presence of adsorption is ten times lower than its absence and distorted. The predicted surface temperature is slightly different respect to the one experimentally measured. The model explains credibly the experimental results in terms of impedance analysis.

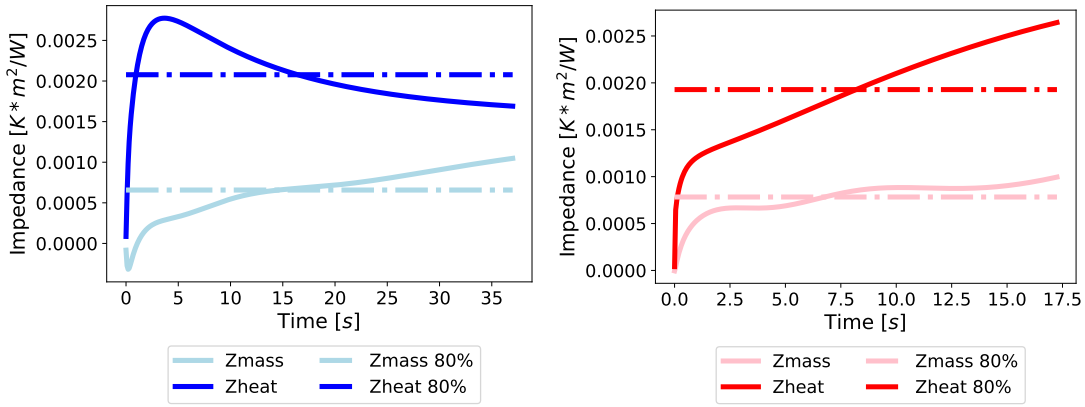

Figure 3.11: Heat and mass transfer impedance in the material obtained by the simulationsv. Left: heat and mass transfer impedances during adsorption. Right: heat and mass transfer impedances during desorption. Even though their evolution is very different (during desorption the heat impedance is much lower than during adsorption), their average value over the time required to reach 80% of the maximum cycled mass is similar.

3.5 Conclusions

In this work, we proposed a new modelling approach to describe the water adsorption dynamics at the adsorbent material scale for heat transformers, based on a localized lumped parameters approach. This approach is based on empirical and theoretical considerations of the nature of adsorption processes and experiments. It entails the application of lumped-parameter heat and mass balances and the derivation of transient heat and mass transfer resistances defined for specific cases, including transient and local effects, and dependent solely on the material's properties and geometry.

The definition of effective heat and mass transfer resistances depends on the analogy to other known - and simpler - heat and mass transfer problems. Here, they have been derived for two industrially relevant cases, that also served for the model validation.

The first case was the one of a monolayer of silica gel beads subject to isobaric temperature swings. The results show good agreement with experimental data with an accuracy comparable to more sophisticated heat and mass transfer models.

The second case was the one of a monolith of activated carbon subject to isochoric temperature swings. The activated carbon was experimentally characterized with both equilibrium and dynamic experiments. The results show a good agreement with those experiments and provide important insights into the nature of the heat and mass transfer processes. In particular, it was found that heat conduction determines the rate of sorption, with the main part of the heat divided between the ad/desorption of the adsorbate and the temperature change of the solid adsorbent. Thanks to the abundant and interconnected macroporous structure, mass transfer plays only a marginal role in determining the rate of sorption. Given the structural properties

of the material, it seems likely that the microscopic diffusion resistance is negligible. Moreover, the model is able to explain the experimental results also in terms of impedance analysis. This analysis returns an overall adsorption heat and mass transfer coefficient of approximately $370 W/m^2/K$ for swings between 25 $°C$ and 45 $°C$ at approximately 10 $mbar$. The monolithic Resorcinol-Melamine-Formaldehyde activated carbon shows interesting properties for heat transformation and could be further tailored to improve its thermal conductivity.

In both cases, a sensitivity analysis of the material properties determined that the uncertainties regarding the characterization of the material are the limiting factor in the understanding of the adsorption dynamics. Adsorption, geometrical, structural and thermophysical properties all play an important role in determining the adsorption rate under different conditions. Therefore, the careful characterization of the material should be an integral part of the analysis/estimation of its performance for heat transformation purposes. It is also important to verify, that the integrated material retains the same properties as the material characterized previously. The dominance of one of the transport mechanisms (heat/mass) over the other made it difficult to clearly analyse the other. This can pose a problem when applying the model to different set-ups where the rate-limiting factor might change. A different experimental approach would be needed to be able to assess the non-dominant diffusion mechanism as well.

It is believed that this modelling approach is potentially relevant for both material and process development. In fact, its simplicity makes it suitable for intensive simulations (e.g. in parameter sweeps and optimization algorithms) at a reduced computational cost. At the same time, it provides information regarding the limiting factors with sufficient accuracy, so that design decisions on the material and the process can be made. For this reason, the model was implemented in Modelica for an agile integration in existing simulation environments for energy technologies.

Future research should investigate the effects of more complex boundary conditions that go beyond the single temperature swings in the determination of the lumped heat and mass transfer resistances. Moreover, it is in principle possible to apply the same methodology with multiple different adsorbates, paving the way to its application in other fields of research (e.g. gas separation).

3.6 Acknowledgments

This chapter has been realised in collaboration with Riccardo Torreggiani and Romain Civioc from Empa, Switzerland. Moreover, the author acknowledges IBM Research Zürich, Switzerland, and in particular Bruno Michel and Patrick Ruch for granting access to the experimental setup and sharing their previously developed know-how on the experimental methods. Finally, this chapter was elaborated with the support of the project *HyCool: Industrial Cooling through Hybrid system based on Solar Heat*, funded by the European Commission H2020 Programme under Grant Agreement No. 792073.

3.7 Nomenclature

Letter	Meaning	Units
A	Area	m^2
a	specific surface area	m^2/g
C	Characteristic energy of adsorption	J/g
c	Specific heat capacity	$J/kg/K$
d	Diameter	m
Ea	Activation energy	J/mol
F	Transient factor	
H	Specific energy of adsorption	J/kg
h	Enthalpy	J/kg
k	Thermal conductivity	$W/m/K$
K	Knudsen number	
L	Thickness	m
m	Mass flow rate	kg
M	Molecular weight of water	g/mol
$\dot{m}$	Mass flow rate	kg/s
N	Shape factor of the adsorption curve	
p	Pressure	Pa
Q	Heat flow rate	W
R	Resistance	K/W or s/m^3
R	Gas constant	$J/mol/K$
r	Radius	m
T	Temperature	K
t	Time	s
V	Volume	m^3
w	Adsorbate loading	g/g
W	Adsorbate total capacity	g/g
Z	Thermal (or thermal-equivalent) impedance	K/W

Greek Letter	Meaning	Units
ϵ	Porosity	
Γ	Adsorption potential	J/g
γ	Gas concentration	kg/m^3
μ	Microscopic	
ω	Weighing factor	
ψ	Thermal contact ratio	
ρ	Density	kg/m^3
τ	Adimensional time	

Acronym	Meaning
AC	Activated Carbon
RMF	Resorcinol-Melamine-Formaldehyde
SEM	Scanning Electron Microscopy
WRMSE	Weighted Root Mean Square Error

Subscript	Meaning
0	Pre-exponential coefficient
ads	Adsorbed phase
b	Beads
c	Contact
cond	Heat conduction
env	Envelope (solid backbone+porosity)
eq	Equilibrium
ext	External (i.e. of the boundary condition)
gas	Free gas
heat	Characteristic of the heat transfer
HEx	Heat Exchanger
macro	Macropores
mass	Characteristic of the mass transfer
mf	Mass flow
micro	Micropores
p	Pores
s	Sample surface
sol	Solid adsorbent
ss	Steady state
vap	Vapour phase

3.8 Derivation of the adimensional time and of the effective resistance to mass transfer for spheres subject to a sudden change of mass concentration difference

We are assuming a constant vapour pressure at the boundary of the particle. This implies either that the interparticle mass transfer resistance is negligible (which generally is the case for optimally designed systems) or that it is taken into account with a separate resistance. The intraparticle diffusion is described as happening through a continuous medium characterized by a diffusion resistance $R_{mass}\left[\frac{s}{m^3}\right]$. As described in the introduction, we will first consider the case of mass diffusion in the absence of adsorption.

$$\frac{d\left(V_{pores}\cdot\gamma\right)}{dt} = V_{pores}\cdot\frac{d\gamma}{dt} = \frac{\gamma_{ext}-\gamma}{R_{mass}} \tag{3.36}$$

The analytical solution of mass diffusion through a homogeneous sphere with constant diffusivity D subject to a sudden change of concentration is known to be a function of the concentration step $\gamma_i - \gamma_{ext}$ and of the adimensional time $\tau_{mass} = t\cdot\frac{D}{r_p^2}$ (see Ruthven, 1984):

$$\frac{\gamma-\gamma_{ext}}{\gamma_i-\gamma_{ext}} = \frac{6}{\pi^2}\cdot\sum_{n=1}^{\infty}\frac{\mathrm{e}^{-n^2\cdot\pi^2\cdot t\cdot\frac{D}{r_p^2}}}{n^2} \tag{3.37}$$

$$\frac{d\gamma}{dt} = \left(\gamma_{ext} - \gamma_i\right) \frac{6 \cdot D}{r_p^2} \sum_{n=1}^{\infty} \mathrm{e}^{-n^2 \cdot \pi^2 \cdot \tau_{mass}} \tag{3.38}$$

Reorganizing Equation 3.36 and substituting with Equations 3.37 and 3.38, for a sphere we obtain:

$$R_{mass} = \frac{3}{4 \cdot \pi^3 \cdot r_p \cdot D \cdot V_{pores}} \cdot \frac{\sum_{n=1}^{\infty} \frac{\mathrm{e}^{-n^2 \cdot \pi^2 \cdot \tau_{mass}}}{n^2}}{\sum_{n=1}^{\infty} \mathrm{e}^{-n^2 \cdot \pi^2 \cdot \tau_{mass}}} \tag{3.39}$$

$$R_{mass} = R_{mass_{ss}} \cdot F_{mass}\left(\tau_{mass}\right) \tag{3.40}$$

Where $R_{mass_{ss}} = \frac{3}{4\pi^3 \cdot r_p \cdot D \cdot V_{pores}}$ is the steady state resistance remaining constant through time and $F_{mass} = \frac{\sum_{n=1}^{\infty} \frac{\mathrm{e}^{-n^2 \cdot \pi^2 \cdot \tau_{mass}}}{n^2}}{\sum_{n=1}^{\infty} \mathrm{e}^{-n^2 \cdot \pi^2 \cdot \tau_{mass}}}$ is the time-dependent transient factor which approaches 1 asymptotically at large τ_{mass}. F_{mass} can be approximated numerically by:

$$F_{mass} \approx 1 - 0.1735 \cdot \mathrm{e}^{-938.9 \cdot \tau_{mass}} - 0.7836 \cdot \mathrm{e}^{-39.67 \cdot \tau_{mass}} \tag{3.41}$$

The derived equations can be extended to the case of a diffusion coefficient varying in time. In this case the adimensional time can be defined as $\tau_{mass} = \int \frac{D(t)}{r_p^2} \, dt$. Let us now consider the case of a material with linear isothermal adsorption profile $w = cst \cdot \gamma + w_{init}$ in the concentration range γ_i to γ_{ext}. Let us further assume that the mass transfer is rate limiting and temperature differences within the particle are negligible. Under these assumptions, the adsorption within the particle acts as an additional resistance for mass transfer leading to a higher effective diffusion coefficient $D^*(t)$ (see Carslaw and Jaeger, 1959). In this case, the relationship $\tau_{mass} = \int \frac{D^*(t)}{r_p^2} \, dt$ is still valid, but as D^* is not known *a priori* it cannot be used to determined τ directly. However, it can be implicitly derived from the state of the material (Equation 3.37) as the average concentration γ of the particle is only dependent on the adimensional time. For our implementation in Modelica, a numerical approximation to equation 3.37 was used to determine the effective adimensional time τ_{mass} based on the progress of the vapour mass concentration evolution:

$$\frac{\gamma-\gamma_{ext}}{\gamma_i-\gamma_{ext}} \approx \frac{6}{\pi^2}\cdot\left(1.36\cdot e^{-15.74\cdot\tau_{mass}}+0.2393\cdot e^{-575.3\cdot\tau_{mass}}\right) \tag{3.42}$$

3.9 Derivation of the adimensional time and of the effective resistance to heat transfer for spheres subject to a sudden change of thermal contact point temperature

The heat transfer between a (metallic) flat surface and an adsorbent bead is mostly governed by the thermal contact bottleneck (see Radu, 2017). Thus the heat transfer resistance depends on the ratio between the thermal contact radius and the particle radius $\psi = \frac{r_c}{r_p} < 0.1$ (see Siu and Lee, 2000). If the temperature of the thermal contact is subject to a step-like change, the heat transfer is initially largely affected by the locality of the heat transfer, which is not captured by traditional lumped-parameters models. Just as for the mass transfer resistance derived in the previous section, the effective thermal resistance can be described as the product of the steady state heat transfer resistance $R_{heat\,s}s$ and a transient factor F_{heat} depending on the adimensional time τ_{heat}:

$$R_{heat} = R_{heat_{ss}}\cdot F_{heat}(\tau_{heat}) \tag{3.43}$$

Contrary to the mass transfer resistance, the heat transfer resistance of a sphere in contact with a flat surface does not have an analytical solution. However, Siu and Lee, 2000 derived a numerical solution (Equations 3.45 and 3.46) for two spheres at two different average (and initially homogeneous) temperatures $T_{sphere1}$ and $T_{sphere2}$, where $\tau_{heat} = \frac{t\cdot\alpha}{r_p^2}$.

$$Q_{sphere1-sphere2} = \frac{T_{sphere1}-T_{sphere2}}{R_{heat,sphere-sphere}} \tag{3.44}$$

$$R_{heat_{ss,sphere-sphere}} = \frac{0.5759}{k\cdot r_p}\cdot\left(\frac{1}{\psi}-\frac{1.093e-3}{\psi^2}+\frac{3.019e-5}{\psi^3}-\frac{1.202e-7}{\psi^4}\right) \tag{3.45}$$

$$F_{heat} = \left(1+\frac{1}{3\cdot\tau_{heat}^{1/2}}+\frac{1}{50\cdot\tau_{heat}}-\frac{1}{400\cdot\tau_{heat}^{3/2}}\right)^{-1} \tag{3.46}$$

We note that Equation 3.46 is only valid for $\tau_{heat} > 0.0103$. Indeed while the transient factor should be continuously increasing with decreasing time, equation 3.46 has a maximum at $\tau_{heat} = 0.0103$ and even becomes negative for $\tau_{heat} < 0.0035$.

In the case above, due to symmetry, the contact temperature at the contact is constant and equal to the average of the temperatures of the individual spheres throughout the heat exchange. Consequently, we can extend the solution above to situations of a sphere in contact with a flat substrate with constant temperature T_{ext}:

$$Q_{heat} = Q_{sphere1-sphere2} = \frac{T_{ext} - T}{R_{heat}} = \frac{0.5 \cdot (T_{sphere1} - T_{sphere2})}{R_{heat}} \tag{3.47}$$

$$R_{heat} = 0.5 \cdot R_{heat,sphere-sphere} \tag{3.48}$$

$$R_{heat\,ss} \doteq 0.5 \cdot R_{heat\,ss,sphere-sphere} \tag{3.49}$$

As in the case of the mass transfer, the equation given for the adimensional time is only valid for constant diffusivities α. However, the remaining equations remain valid for varying diffusivities using an integral formulation for the adimensional time. They can even be extended to the case of an unknown additional resistance caused by linear adsorption, however in that case the adimensional time needs to be inferred from the average temperature. To be able to address this case then, we first derive the evolution of the average temperature in the absence of varying materials properties and adsorption and then use that relationship to infer the adimensional time, analogously to the approach described above. In the case of constant heat capacity, thermal diffusivity and without adsorption we can write the following:

$$Q = \frac{4 \cdot \pi \cdot r_p^3}{3} \cdot \rho_{env} \cdot c_p \cdot \frac{dT}{dt} \tag{3.50}$$

$$\frac{dT}{dt} = \frac{2 \cdot (T_{ext} - T) \cdot \alpha}{r_p^2 \cdot \beta(\psi)} \cdot \left(1 + \frac{1}{3 \cdot \tau_{heat}^{1/2}} + \frac{1}{50 \cdot \tau_{heat}} - \frac{1}{400 \cdot \tau_{heat}^{3/2}}\right) \tag{3.51}$$

$$\beta = R_{heat_{ss}} \cdot \frac{4 \cdot \pi \cdot k \cdot r_p}{3} \tag{3.52}$$

Replacing T by $\theta = T - T_{ext}$ and assuming $\theta = \mathrm{e}^{f(t)}$ such that we have $\frac{d\theta}{dt} = \theta \cdot \frac{df(t)}{dt}$:

$$\theta \cdot \frac{df(t)}{dt} = -\frac{2 \cdot \theta \cdot \alpha}{r_p^2 \cdot \beta(\psi)} \cdot \left(1 + \frac{1}{3 \cdot \tau_{heat}^{1/2}} + \frac{1}{50 \cdot \tau_{heat}} - \frac{1}{400 \cdot \tau_{heat}^{3/2}}\right) \tag{3.53}$$

$$\frac{df(t)}{dt} = -\frac{2 \cdot \alpha}{r_p^2 \cdot \beta(\psi)} \cdot \left(1 + \frac{1}{3 \cdot \tau_{heat}^{1/2}} + \frac{1}{50 \cdot \tau_{heat}} - \frac{1}{400 \cdot \tau_{heat}^{3/2}}\right) \tag{3.54}$$

$$\frac{df(\tau_{heat})}{d\tau_{heat}} = -\frac{2}{\beta(\psi)} \cdot \left(1 + \frac{1}{3 \cdot \tau_{heat}^{1/2}} + \frac{1}{50 \cdot \tau_{heat}} - \frac{1}{400 \cdot \tau_{heat}^{3/2}}\right) \tag{3.55}$$

$$f(\tau_{heat}) = -\frac{2}{\beta(\psi)} \cdot \left(\tau_{heat} + \frac{2 \cdot \tau_{heat}^{1/2}}{3} + \frac{ln(\tau_{heat})}{50} + \frac{\tau_{heat}^{-1/2}}{200}\right) + C \tag{3.56}$$

$$\theta = \mathrm{e}^{-\frac{2}{\beta(\psi)} \cdot \left(\tau_{heat} + \frac{2 \cdot \tau_{heat}^{1/2}}{3} + \frac{ln(\tau_{heat})}{50} + \frac{\tau_{heat}^{-1/2}}{200}\right) + C} \tag{3.57}$$

$$T - T_{ext} = B \cdot \mathrm{e}^{-\frac{2}{\beta(\psi)} \cdot \left(\tau_{heat} + \frac{2 \cdot \tau_{heat}^{1/2}}{3} + \frac{ln(\tau_{heat})}{50} + \frac{\tau_{heat}^{-1/2}}{200}\right)} \tag{3.58}$$

As at $\tau_{heat} = 0$, $T = T_i$ and at $\tau_{heat} = \infty$, $T = T_{ext}$, we can set $B = T_i - T_{ext}$ (the larger ψ is, the closer to 1 gets the solution of the exponential for the minimum valid adimensional time $\tau_{heat} = 0.0103$). Similarly to what was done for the adimensional time of the mass transfer, the effective adimensional time of heat transfer τ_{heat}^* can be derived implicitly from:

$$-0.5 \cdot \beta(\psi) \cdot ln\left(\frac{T - T_{ext}}{T_i - T_{ext}}\right) = \tau^*_{heat} + \frac{2 \cdot {\tau^*_{heat}}^{1/2}}{3} + \frac{ln(\tau^*_{heat})}{50} + \frac{{\tau^*_{heat}}^{-1/2}}{200} \tag{3.59}$$

However, the so-derived Equation 3.59 can lead to numerical problems. Therefore, an piece-wise-polynomial approximated effective adimensional time of the heat transfer τ^{**}_{heat} is used instead:

$$\frac{T - T_{ext}}{T_i - T_{ext}} = \mathrm{e}^{-\frac{2}{\beta(\psi)} \cdot \tilde{\tau_{heat}}} \tag{3.60}$$

$$\tilde{\tau_{heat}} < 0.03571 \rightarrow \tau^{**}_{heat} = 0.0103 \tag{3.61}$$

$$0.03571 \leq \tilde{\tau_{heat}} < 1.672 \rightarrow \tilde{\tau_{heat}} = 2.908 \cdot \tau^{**}_{heat} - 2.684 \cdot {\tau^{**}_{heat}}^2 + 1.499 \cdot {\tau^{**}_{heat}}^3 \tag{3.62}$$

$$1.672 \leq \tilde{\tau_{heat}} < 12.16 \rightarrow \tilde{\tau_{heat}} = 1.479 \cdot \tau^{**}_{heat} - 0.02937 \cdot {\tau^{**}_{heat}}^2 \tag{3.63}$$

$$12.16 \leq \tilde{\tau_{heat}} < 106.8 \rightarrow \tau^{**}_{heat} = \frac{\tilde{\tau_{heat}}}{1.088} \tag{3.64}$$

$$106.8 \leq \tilde{\tau_{heat}} \rightarrow \tau^{**}_{heat} = \frac{\tilde{\tau_{heat}}}{1.009} \tag{3.65}$$

$$R_{heat} = R_{heat_{ss}} \cdot F_{heat}(\tau^{**}_{heat}) \tag{3.66}$$

3.10 Derivation of the adimensional time and of the effective resistance to heat transfer for slabs subject to a sudden change of thermal contact point temperature

As mentioned, the derivation of the model above was performed for spheres in contact with an infinite surface, as relevant for the silica gel beads extensively studied in the literature. Another type of important material integration is the coating. Coated heat exchangers present, at the material level, an almost mono-dimensional transfer process (radially for tubes, linearly for flat fins). Flat-fin coating and monoliths glued to fins are quite similar in geometry, even if with different thicknesses (monoliths are normally several times thicker than coatings). To this mono-dimensional geometry, the same modelling concept can e applied as well, with the respective differences in the definition of the heat and mass transfer resistances.

For the heat transfer, the analytical solution of the temperature of a slab of thickness L subject to a large temperature jump on one side is for symmetry identical to the well-known solution of a slab of thickness $2 * L$ subject to a temperature jump on both sides (see Tomarelli, 2019):

$$T(x,t) = T_{ext} - \frac{4 \cdot (T_{ext} - T_i)}{\pi} \cdot \sum_{n=1,3,5...}^{\infty} \frac{sin\left(n \cdot \pi \cdot \frac{x}{2 \cdot L}\right) \cdot e^{-n^2 \cdot \pi^2 \cdot \frac{\alpha \cdot t}{4 \cdot L^2}}}{n} \tag{3.67}$$

This brings us to the solution for the average and surface temperatures, respectively in Equations 3.68 and 3.69:

$$T = T_{ext} - \frac{8 \cdot (T_{ext} - T_i)}{\pi^2} \cdot \sum_{n=1,3,5...}^{\infty} \frac{e^{-n^2 \cdot \pi^2 \cdot \frac{\alpha \cdot t}{4 \cdot L^2}}}{n^2} \tag{3.68}$$

$$T_s = T_{ext} - \frac{4 \cdot (T_{ext} - T_i)}{\pi} \cdot \sum_{n=1,3,5...}^{\infty} \frac{sin\left(n \cdot \frac{\pi}{2}\right) e^{-n^2 \cdot \pi^2 \cdot \frac{\alpha \cdot t}{4 \cdot L^2}}}{n} \tag{3.69}$$

In the case of pure conduction (i.e. in absence of adsorption), the adimensional time of the heat transfer would be $\tau_{heat} = \frac{\alpha}{4 \cdot L^2} \cdot t$. However, assuming as above that the shape of the temperature profile is not modified for a certain adimensional time, its effective value in presence of adsorption can be obtained implicitly from either of the Equations 3.70 or 3.71, obtained as numerical approximations of Equations 3.68 and 3.69:

$$\frac{T - T_{ext}}{T_i - Text} = 0.8224 \cdot e^{-\frac{\tau^*_{heat}}{0.1002}} + 0.1776 \cdot e^{-\frac{\tau^*_{heat}}{0.004651}} \tag{3.70}$$

$$\frac{T_s - T_{ext}}{T_i - T_{ext}} = 0.3602 \cdot e^{-\left(\frac{\tau^*_{heat}}{0.2209}\right)^{1.686}} + 0.2207 \cdot e^{-\left(\frac{\tau^*_{heat}}{0.05419}\right)^{2.534}} + 0.4191 \cdot e^{-\left(\frac{\tau^*_{heat}}{0.1149}\right)^{2.004}} \tag{3.71}$$

As we aim to capture the effective adimensional time characterizing the average adsorption, we considered that the average temperature was more representative and Equation 3.70 was chosen for the implementation in Modelica.

From the heat balance of Equation 3.2, in absence of adsorption we have:

$$R_{heat} = \frac{T_{ext} - T}{V_{env} \cdot \rho_{env} \cdot c_p \cdot \frac{dT}{dt}} \tag{3.72}$$

$$R_{heat} = \frac{8/\pi^2}{A \cdot L \cdot \rho_{env} \cdot c_p \cdot 2 \cdot \alpha / L^2} \cdot \frac{\sum_{n=1,3,5...}^{\infty} \frac{e^{-n^2 \cdot \pi^2 \cdot \frac{\alpha \cdot t}{4 \cdot L^2}}}{n^2}}{\sum_{n=1,3,5...}^{\infty} e^{-n^2 \cdot \pi^2 \cdot \frac{\alpha \cdot t}{4 \cdot L^2}}} \tag{3.73}$$

$$R_{heat} = R_{heat_{ss}} \cdot F_{heat} \tag{3.74}$$

$$R_{heat_{ss}} = \frac{4L}{A \cdot k \cdot \pi^2} \tag{3.75}$$

$$F_{heat} \approx 1 - 0.6971 \cdot e^{-\frac{\tau^*_{heat}}{0.01336}} - 0.3029 \cdot e^{-\frac{\tau^*_{heat}}{0.0008868}} \tag{3.76}$$

4 Developing Improved Adsorption Materials, Devices and Processes

4.1 Introduction

In this chapter, we will use the modelling technique proposed in Chapter 3 to develop improved materials, devices and processes for adsorption heat transformers. In particular, we address two scientific questions:

- Is it possible to tailor an activated carbon to fit the needs of modern district heating network substations, providing both heating and cooling?

- Would it be convenient to explore concepts of agitated reactors for adsorption heat exchangers?

To answer both questions, the modelling approach proposed in Chapter 3 fits perfectly, as it gives insight into the limitations to the heat and mass transfer during the process and does not entail excessive effort for simulating different scenarios.

In Section 4.2 we will combine the analysis of the system needs, the development and the characterization of the materials, the modelling approach and prototype tests.

In Section 4.3 we will propose the screw-conveyor concept for adsorption heat transformers, and evaluate its potential with a dedicated model for preliminary exploration.

In Section 4.4 we briefly discuss possible pathways to use dynamic modelling to support the design of adsorption energy processes, building on the methods exposed in Chapter 2.

4.2 Tailoring Activated Carbons in Reversible Heat Pumps for District Heating and Cooling Networks

4.2.1 Introduction

Due to climate change and the ensuing rise of outdoor temperatures, the cooling demand in buildings will increase in the future, as reported by Birol, 2018. Nevertheless, the heating demand in Europe will remain high in wintertime according to Settembrini et al., 2017. In order to achieve the energy turnaround for Europe and to reduce drastically greenhouse gas emissions, innovative, integrated and eco-friendly heating and cooling solutions are required to supply the building stock as well as processes with heating and cooling. On the one hand, the carbon footprint of the energy mix during peak load in winter is high. On the other hand, during summer, large amounts of heat remain unused from waste incineration plants and other industrial processes because of the low heat demand during this season. This heat can be used in summer to power adsorption heat pumps (adHPs) and supply eco-friendly and cost-effective cooling energy to various cooling consumers (e.g. buildings and industries), as reported by Hassan et al., 2020.

District heating networks (DHNs) are a well-known solution to lower the carbon footprint for heating in winter and recover otherwise unused waste heat, as reported by Puschnigg et al., 2021. However, DHNs suffer from two important drawbacks, which limit their energy efficiency and operability: 1) Low efficiency caused by high operating temperatures, especially high return temperatures. 2) Low utilization of the DHN in the summertime, which leads to inefficient operating conditions. The impacts of those two drawbacks are reduced heat distribution capacity for a given pipe diameter (due to limited temperature differences), high heat distribution costs (pumping energy and heat losses) and lower energy efficiency in the heating station (more energy to produce one unit of useful heat).

This work investigates the integration of reversible adsorption heat pumps into DHN to use untapped waste heat and increase the energy efficiency of district heating networks. Two particularly promising integrations of adHPs in DHN have been identified. The DHN return temperature reduction operating mode (Figure 4.1, top) integrates an adHP at substations (SST) providing heat at the building level. The adHP uses the SST return flow as a heat source for the evaporator and thus reduces the temperature of the DHN return flow. This mode of operation increases the temperature difference between the forward and return of the DHN resulting in savings on the pumping energy or in heat delivery capacity increase of a given thermal grid. Additionally, it also reduces heat losses since the return temperatures are lowered. The same adHP and the DHN heat supply can also supply comfort cooling (Figure 4.1, bottom) to the buildings in the summertime. This enables the DHN operators to offer a new energy service to their customers while increasing the sale of heat in summer and thus the profitability of the DHN. Since a major part of the heat is either renewable or waste heat in Swiss DHN, this cold supply will also be renewable in that case. The major challenge for this mode of operation is to dissipate and/or recover condensation and adsorption heat at

Scenario	**Heating Mode**			**Cooling Mode**		
	T_{hot}	T_{con}	T_{eva}	T_{hot}	T_{con}	T_{eva}
min-max	343-383 K	303-338 K	293-323 K	333-363 K	303-338 K	279-288 K

Table 4.1: District heating network temperature requirements in heating and cooling modes.

intermediate temperature without extra cost, with pre-heating of domestic hot water.

These innovative conceptual modes of operation have been evaluated separately with numerical models reflecting the current state of the art of the sorption technology and with experimental work carried out on commercial units by Jobard et al., 2020. It results that the commercial units currently available are not adapted for integration in DHN and do not meet the requirements of DHN operators, especially in terms of temperature drop at the desorber in cooling mode. They suffer also from low power density and low thermal efficiency. Therefore, new adsorption materials are needed as well as a new concept for reversible DHN SSTs for the heating and cooling of buildings. In this work, we move towards the design of such systems. In the first section, we analyze the requirements of the DHN applications based on surveys. Afterwards, we propose a novel sustainable adsorbent material suitable for the application and we analyze its performance by models and simulations. At last, we present the characterization methods to measure the performance of adHP prototypes.

4.2.2 District Heating Networks Implementation Requirements

This section presents the requirements necessary to drive the development and optimization of the adsorption materials for DHN applications. These requirements are the expected operating conditions for both heating and cooling modes. They will define the temperatures driving the adsorption process: the hot source T_{hot}, the condenser/re-cooler T_{con} and the evaporator T_{eva}. T_{hot} is directly set from the supply of the DHN, T_{con} depends on the space heating and domestic hot water distribution system; T_{eva} depends on the space heating return temperature and on the cooling distribution system (radiant ceiling or air conditioning unit), respectively in heating mode and cooling mode. Their ranges were derived from field surveys as well as from discussions with DHN operators and are gathered in Table 4.1.

In the heating mode, the purpose of the substation is to satisfy the building's needs in space heating and domestic hot water. The adHP is implemented in this configuration to reduce the return temperature to the grid. Therefore, the DHN efficiency and capacity are improved. Figure 4.2 presents the simplified hydraulic of the substation. A similar concept was proposed with absorption devices (e.g. Lanser et al., 2016; Stuttgart, n.d.). In this mode, the DHN drives the adHP at a given temperature T_{hot} and supplies heat to the space heating loop via the heat produced at the adsorber and condenser of the adHP. A heat exchanger is present to cool down the heat carrier from the desorber below the condensing temperature. This is possible with low space heating return temperature. For this, to function, the adsorption temperature T_{ads} must be higher than T_{con}.

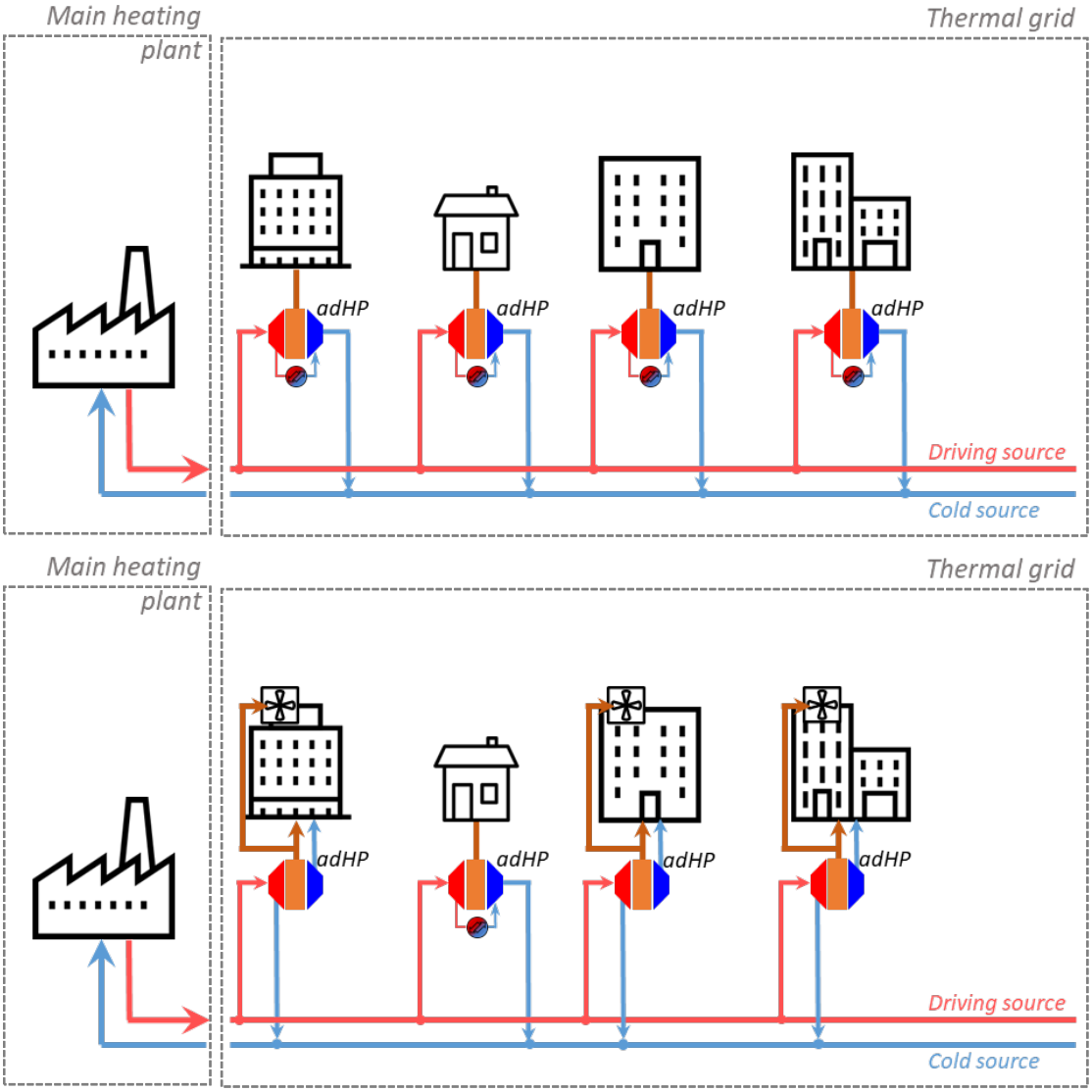

Figure 4.1: Schematic view of the two applications of adHP in DHN targeted. Top: return temperature reduction. Bottom: cooling. The adHP are used in the substations to serve the DHN users.

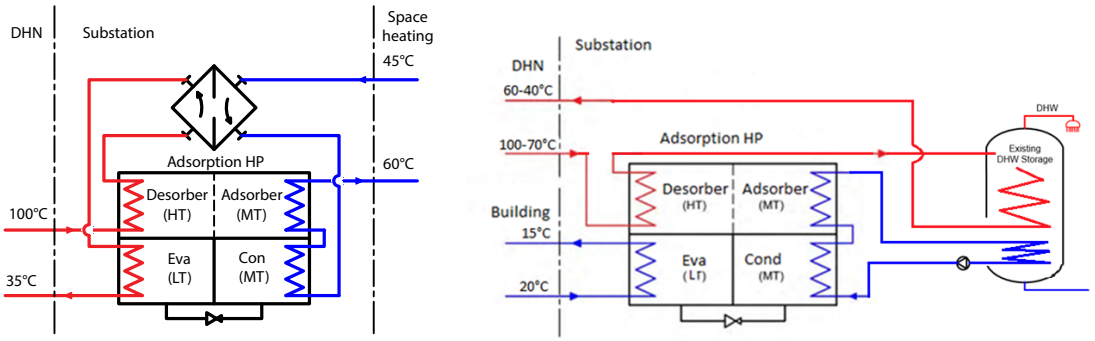

Figure 4.2: Simplified hydraulic diagrams with an example of possible temperature levels of each loop for the heating mode (left) and the cooling mode (right)

For implementation in existing DHN, the substation has to follow the prescription given by the operators of the network that ensure a coherent integration and the supply temperature is fixed. Since DHN must supply a temperature high enough for DHW preparation at 60°C, as reported by Quiquerez, 2017 supplied temperatures are usually above 70°C and smaller than 110°C. Higher temperatures might in general be needed to improve the COP of the machine and cooling power at the evaporator, especially considering that the desorption temperature must be below the hot source temperature to guarantee effective heat transfer. However, selecting the right adsorbent material can guarantee successful desorption. The temperature for the space heating loop is given by the characteristics of the building i.e., its energy standard and heat emission system. High-temperature radiators with temperature needs above 60°C are excluded because the needed temperature is too close to the supply temperature. The supply temperature of the space heating loop can be as low as 30°C for floor heating systems in well-insulated buildings. The evaporating temperature depends on the space heating return temperature and the pinch of the heat exchanger assumed at 5 K. These are estimated with the temperature drop possible in the space heating loop. For radiators with a supply temperature of 65°C, a temperature drop of 10 K and a pinch of 5 K induces a temperature at the evaporator inlet of 50°C. For floor heating, the temperature drop can only be 5 K, resulting in 20°C.

In the cooling mode, the adsorption pump in the substation is used to cool down buildings. In order to be able to operate in the cooling mode without a dry cooler to reject heat, different strategies have to be evaluated in order to valorize the rejection heat locally. One of the most promising local applications for heat rejection valorization is Domestic Hot Water (DHW) preheating. Alternatively, the heat rejected could be used as the cold source for a heat pump for DHW preparation. The challenge with this local heat valorization is that the DHW need consumption affects the amount of cooling which can be produced by the AdHP. In order

to operate successfully AdHP using heat supplied by a DHN, it is necessary to enlarge the temperature difference on the primary side and simultaneously use heat at the lowest possible temperature. This represents a challenge as most of the adsorption chillers commercially available today are operated with a maximum 5°C difference and need heat at a minimum 60-65°C. This application could be interesting for DHN operators. It will intensify the heat demand in the summertime when the DHN infrastructure is underused. Moreover, as most of DHNs today use a large fraction of renewable heat in their energy mix, this new application will make available renewable heat in dense urban areas.

Figure 4.2 shows a possible hydraulic integration of an AdHP in cooling mode in a substation where the heat rejected is valorized to preheat DHW. This configuration is interesting as it eliminates the need for a dry cooler. On the other hand, it has to be operated with an important constraint: there must simultaneous cooling and DWH. A compression HP could be integrated between the heat rejected by the AdHP and the DHW tank to give a bit more operating flexibility. Table 4.1 shows the operating conditions of the AdHP in cooling mode. Those conditions are derived from the exchange with various DHN operators. The cooling is produced between 6 and 15°C. The forward temperature must be at least 60°C in order to reduce too much the cooling COP. In addition, as mentioned above, it is important to ensure a large temperature difference between the DHN forward and return stream to not worsen the DHN distribution losses and pumping energy consumption.

4.2.3 Adsorbent Material Development

Current state-of-the-art activated carbons are synthesized mostly by a bottom-up approach using toxic chemicals such as resorcinol and formaldehyde to form porous networks, as reported by Alshrah et al., 2017, which are then pyrolyzed and activated, as for example by Huber, Ruch, Hauert, Saucke, et al., 2016. The corresponding activated carbons can display a variety of microstructures and properties, making them interesting for different applications – including water sorption (see Civioc et al., 2020; Huber et al., 2019). In the existing literature, green alternatives to petroleum-derived phenolic networks have been thoroughly studied to great avail, as by Nowicki et al., 2010; Prauchner and Rodríguez-Reinoso, 2012. However, none of them displays the array of properties required in our current work (e.g. able to adsorb and desorb in both heating and cooling modes). Therefore, we herein study an alternative starting material: an activated carbon derived from spent coffee grounds (SCG). The properties and microstructure of the corresponding pyrolyzed material, arising from a more sustainable feedstock (thus greatly improving the carbon footprint of the adsorption heat pump) are studied. Its water adsorption characteristic is comparable with the one from more traditional resorcinol-based activated carbons; retaining an optimal performance is crucial for the efficiency of the project overall. However, one of the main advantages of traditional resorcinol-based ACs is their monolithicity; they can be tailored thanks to the bottom-up synthesis approach by pouring the sol into a box of the desired shape. In this regard, SCG are more restrictive because of their granulated nature. Therefore, in this work

Figure 4.3: Spent-Coffee-Ground + Resorcinol and Formaldehyde monoliths before (left) and after (right) pyrolysis.

we opted for minimal usage of resorcinol and formaldehyde as a binder, effectively forming a matrix around SCG. It allows the materials to reach a monolithic state while being mostly sustainable. Importantly, this does not compromise the water adsorption performance of the materials. Our synthesis protocol involves the collection of spent coffee grounds, which are then mixed with a minimal amount of resorcinol and formaldehyde. Typically, 30g of dry SCG and 25 ml of ethanol are mixed with 6g of resorcinol and 12 l of commercial formaldehyde aqueous solution. A catalytic amount of ammonia in the form of an aqueous solution, around 1 $mmol$, is then added to the mixture. It is then poured into polypropylene boxes of the desired shape. The materials are left to cure and dry in a convection oven before being pyrolyzed and physically activated in a one-step heat treatment within a tube furnace – at 800°C for 4 hours under a CO_2 atmosphere. The result is a monolithic activated carbon, depicted in Figure 4.3, which can be characterized as necessary and is ready for water sorption applications.

As a finer particle size of the AC could be beneficial from the mechanical standpoint, it was decided to test the AC obtained from the fraction of the green body with the smaller diameter. Before synthesis, SCG were sieved and only the fraction whose diameter did not exceed 200 μm was used – resulting in a drastic improvement of the adsorption characteristic (60% more water capacity), as visible in Figure 4.4. This result, which surpasses the state-of-the-art carbons, opens very promising applications and should be further investigated, especially given the low desorption temperatures required. However, the material evaluation was performed on the basis of the more complete information available for the AC obtained from the not-sieved SCG.

The ACs are currently sporting a slab shape. Therefore, envelope density ρ_{env} was calculated using a calliper to measure the dimensions of the materials. Subsequently, skeletal density ρ_{skel} was measured by means of helium pycnometry (Accupyc, Micromeritics). This calculation allows for the determination of the entirety of the pore volume within the materials, including their microporosity, mesoporosity, and macroporosity (d > 50 nm) without further quantitative information. The porosity of those materials was further characterized using nitrogen physisorption and carbon dioxide physisorption. For nitrogen sorption, an NLDFT kernel based on the work of Tarazona, 1985 was chosen. For CO_2 sorption, an NLDFT kernel based on the work of Olivier, 1995 was used. The as-obtained isotherms are subsequently

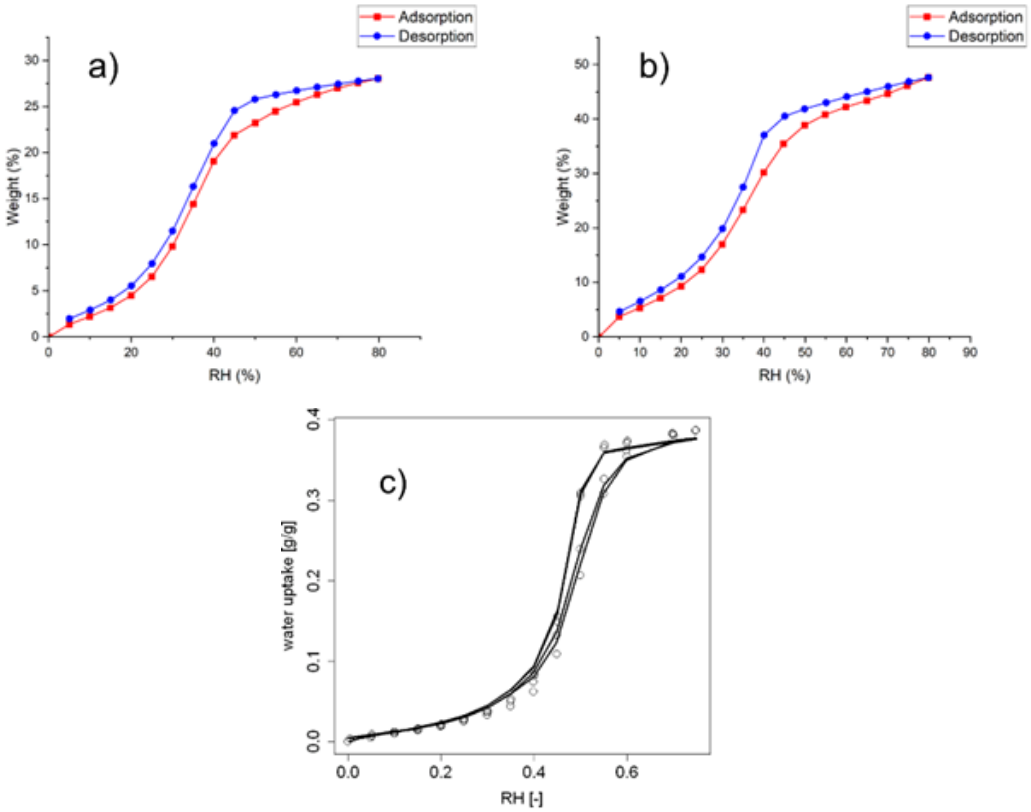

Figure 4.4: Water adsorption isotherms at 30°C of different own activated carbons: not sieved (a) and sieved (b) SCG+RF AC and of RMF AC (c). The SCG+RF carbon shows adsorption at lower relative humidity with respect to the RMF carbon, which is beneficial. Moreover, the pre-sieved carbon shows a very high water adsorption capacity.

Property	ρ_{env}	ρ_{skel}	v_M	v_m	v_μ
Value	0.56 g/cm^3	1.6 g/cm^3	0.83 cm^3/g	0.03cm^3/g	0.30 cm^3/g
Property	ϵ	k_{50}	W	C	N
Value	66%	0.092 $W/m/K$	0.29 g/g	185 J/g	2.6

Table 4.2: Thermophysical properties of the SCG+RF AC monoliths.

merged using the 3Flex software from Micromeritics. Thus, the microporosity v_μ (diameter < 2 nm) and mesoporosity v_m (2 nm < diameter < 50 nm) of the materials were characterized both qualitatively and quantitatively, assuming respectively a slit and a cylindrical geometry. The amount of macroporosity was then determined by subtracting those two values from the total pore volume calculated as in Equation 4.1. The volumetric pore fraction of the material ϵ can be then calculated as in Equation 4.2.

$$v_t = \frac{1}{\rho_{env}} - \frac{1}{\rho_{skel}} \tag{4.1}$$

$$\epsilon = v_t \cdot \rho_{env} \tag{4.2}$$

The wet thermal conductivity k_{50} of the ACs was determined using a custom-made guarded hot plate device (see Stahl et al., 2012) at 30 °C and 50% relative humidity. Finally, dynamic water sorption isotherms were recorded on an isothermal gravimetric device (VTI-SA+ Water Vapor Sorption Analyzer, Porotec) between 5% and 80% relative humidity. For the ACs under analysis, the water adsorption characteristic is well described following the Dubinin-Astakhov model (see Dubinin and Astakhov, 1971):

$$w = W \cdot exp\left(-\left(\frac{F}{C}\right)^N\right) \tag{4.3}$$

$$F = -\frac{R}{M} \cdot T \cdot ln\left(\frac{p}{p_{sat}}\right) \tag{4.4}$$

The results are gathered in Table 4.2. For the sieved SCG+RF AC, the water adsorption parameters were found to be W = 0.48, C = 186, N = 2.4, which means that the total capacity was enhanced without changing the type of adsorption sites.

The thermophysical properties of the AC strongly influence the performance of the adHP. To

estimate the achievable performance of the SCG-based adsorbent monoliths, a dynamic model was used to calculate the energy efficiency and the power that the materials can deliver under the working conditions defined above. The model was developed in OpenModelica, following the lumped-parameter approach described in Section 3.3. Using such an approach assumes that the global adsorption dynamic can be sufficiently well described as if happening in a single effective thermodynamic state (temperature, pressure, loading), instead of simulating all the local thermodynamic states developing within the adsorbent. Such a model includes only the heat and mass transfer within the material itself, therefore can be used as a term of comparison for different materials, boundary conditions and geometries, and not as a reference for the whole adHPs. The model is composed of a temperature boundary condition (representing the HEx fin temperature), a heat transfer resistance (representing the conduction within the AC), a heat and mass balance (representing the adsorption reaction in the pores), a mass transfer resistance (representing the vapour diffusion in the pores), one pressure boundary conditions (representing the evaporator/condenser). All these elements are connected in this order, such that the adsorption dynamics calculated in the heat and mass balance depend on the material's properties and on the boundary conditions.

The temperature and pressure boundary conditions are modelled as square waves oscillating between the adsorption and the desorption heat transfer fluid temperatures and evaporator and condenser pressure, respectively. Moreover, a control mechanism forbids flow reversal for the pressure boundary condition. The model of Section 3.3 for the activated carbon monoliths was used. For the sake of clarity, its main equations are listed below. The heat transfer resistance R_{heat} within the monolith is modelled as transient 1-D conduction:

$$R_{heat} = \frac{(2 \cdot s)^2}{\pi^2 \cdot \alpha \cdot V_t \cdot c \cdot \rho_{env}} \cdot \left(1 - 0.3 \cdot exp\left(-\frac{\tau}{8.9e-4}\right) - 0.7 \cdot exp\left(-\frac{\tau}{1.3e-2}\right)\right) \tag{4.5}$$

The adimensional time τ, determining the transient term, is the equivalent of the Fourier Number in absence of adsorption. However, the adimensional time is stretched due to the additional adsorption energy terms in the heat balance and by its entanglement with the mass transfer. To compensate for this, it is implicitly extracted from the state of the material:

$$\frac{T - T_i}{T_f - T_i} = 1 - 0.82 \cdot exp\left(-\frac{\tau}{0.1}\right) - 0.18 \cdot exp\left(-\frac{\tau}{4.6e-3}\right) \tag{4.6}$$

Similarly, the mass transfer resistance within the monolith is modelled as microscopic surface diffusion and a transient 1-D macroscopic diffusion:

$$R_{mass} = \frac{r_\mu}{3 \cdot D_\mu \cdot s \cdot a_{surf} \cdot \rho_{env} \cdot A_S} + \\ + \frac{s}{D_M \cdot A_S} \cdot \left(1 - 0.3 \cdot exp\left(-\frac{\tau}{8.9e-4}\right) - 0.7 \cdot exp\left(-\frac{\tau}{1.3e-2}\right)\right) \quad (4.7)$$

Equation 4.7 implies that the size of the bigger porosity is not limiting the gas mean free path and therefore no major difference among more or less porous materials should be expected. Furthermore, given the characteristic lengths at play in the microscale and in the macroscale ($r_\mu \approx 1\mu m$ and $s \approx 1mm$) the macroscopic diffusion is by far the limiting mechanism, especially at low values of τ. This is similar to the trends observed for coatings (see Ammann, Michel, and Ruch, 2019).

In Equations 4.5, 4.6 and 4.7 the exponential equations are numerically derived from the analytical solutions of the average thermal resistance and of the average temperature of infinite slabs, respectively (see Carslaw and Jaeger, 1959. It can be noticed how the transient term of the heat and mass transfer resistances are complementary. The reason is that the effective state of the material represents also the position in the monolith in which the adsorption is occurring. At the beginning of each step, the adsorption is temperature driven, so it happens at a minimum distance from the fin surface and at a maximum distance from the vapour interface (R_{heat} is small and R_{mass} is big), while at the end of the step, the opposite will happen. The essence of the heat and mass balance consists of two equations, entangled by the water loading w:

$$\frac{T_f - T}{R_{heat}} + \dot{m}_v \cdot (h_{ext} - h_{int}) = (m_s \cdot c_s + m_a \cdot c_a) \cdot \frac{dT}{dt} - H \cdot m_s \cdot \frac{dw}{dt} + m_v \cdot \frac{dh_{int}}{dt} \quad (4.8)$$

$$\frac{\gamma_{ext} - \gamma_{int}}{R_{mass}} = \gamma_{int} \cdot \frac{dV_v}{dt} + V_v \cdot \frac{d\gamma_{int}}{dt} + V_t \cdot \rho_{env} \cdot \frac{dw}{dt} \quad (4.9)$$

The state of the AC is determined by its properties, namely thermal diffusivity α, specific heat capacity c, envelope density ρ_{env}, thickness s and water adsorption characteristic $w = w(p, T)$. As stated above, one of the advantages of using ACs as adsorbent material is the possibility of tailoring their properties to a given application. In particular, for SCG this can be controlled by changing the pyrolysis process to have more or less microporosity and macroporosity. This will influence the adsorption characteristic, the density and the thermal diffusivity. In order to understand how the different pyrolysis conditions (CO_2 mass flow rate, max temperature and time above the critical temperature of the pyrolysis) affect these properties, a Design of Experiment based on a central composite design was performed on the SCG. Regarding the

Property [Units]	Temp. coeff. a	Time coeff. b	Temp./Time coeff. c	Const. coeff. d
$W[g/g]$	0	-1.30E-03	2.40E-06	0
$C[J/g]$	0.43	1.2	-2.00E-03	0
N	0	0	0	2
$\rho_{skel}[kg/m^3]$	0	-2.10E-03	2.90E-06	1.7
$\rho_{env}[kg/m^3]$	5.60E-04	1.4	2.40E-06	0

Table 4.3: Results of the design of experiment on the spent coffee ground carbons. The coefficients describe SCG AC properties as a function of the pyrolysis parameters.

adsorption characteristic and the density, we established that the flow of CO_2 does not have a significant influence within the range studied, while the maximum temperature and the pyrolysis time have a great influence. The thermal diffusivity, instead, strongly depends on the process of creation of the monolith from the AC powder. As this would add more parameters to the analysis, it was not included and the reference dry thermal conductivity of 0.067 $W/m/K$ (obtained for a highly macroporous RMF AC monolith) was used instead. This means that the thermal resistance might be overestimated for the denser samples. Moreover, the specific heat capacity was assumed to be similar to the one measured for the RMF AC (see Piccoli, Brancato, et al., 2022).

In general, each material property P can be described as a function of the maximum pyrolysis temperature $T \in [632, 968°C]$ and the duration of the pyrolysis above $300°C$ $D \in [244, 429 min]$, as described in Equation 4.10. Table 4.3 summarizes the results obtained for the SCG AC powder.

$$P = a \cdot T + b \cdot D + c \cdot T \cdot D + d \tag{4.10}$$

Given the requirements of DHN for heating and cooling purposes, the performance of the SCG ACs should be tailored accordingly. Therefore, we used the dynamic adsorption model to simulate the Key Performance Indicator (KPI) of the material in a range of process, material and application parameters. The KPI was selected to be a tradeoff between energy efficiency and specific cooling power reached by an adsorption/desorption cycle in a steady state (i.e. after 50 cycles):

$$KPI_{heat} = \frac{(E_{con} + E_{ads})^2}{E_{hot} \cdot t_{cycle}} \tag{4.11}$$

$$KPI_{cool} = \frac{E_{eva}^2}{E_{hot} \cdot t_{cycle}} \tag{4.12}$$

Parameter	Current Demand	Moderate Cooling	High Cooling
T	968°C	968°C	968°C
D	275 min	244 min	244 min

Table 4.4: Optimal pyrolysis parameter for the different application scenarios.

In order to ensure a feasible heat exchange with the heat transfer fluid, the desorption temperature is assumed to be 5 K below T_{hot} and the adsorption temperature is assumed to be 5 K above T_{con}. To minimize the number of simulations required, the working temperatures $T_{eva}, T_{con}, T_{hot}$ were fixed to 293, 308, 368 K for the heating mode and to 288, 303, 363 K for the cooling mode respectively. Firstly, the best pyrolysis conditions for the (improvable) not sieved SCG+RF AC were defined by calculating the KPI for long cycles (reaching full equilibrium). The best material was selected for 3 scenarios, for which the total KPI was calculated as:

$$KPI_t = \left(\frac{\Phi_h}{KPI_{heat}} + \frac{\Phi_c}{KPI_{cool}} \right)^{-1} \tag{4.13}$$

- Current Demand (CD), serving only heating, with Φ_h=1, Φ_c=0
- Moderate Cooling (MC), where the cooling demand is less important than the heating demand, with $\Phi_h = 0.67$, $\Phi_c = 0.33$
- High Cooling (HC), where cooling demand is as important as the heating demand, with $\Phi_h = 0.5$, $\Phi_c = 0.5$

The pyrolysis conditions delivering the ideal materials for the three scenarios are listed in Table 4.4. The material design is clearly limited by the space in which they were investigated: higher temperature and shorter duration of pyrolysis would be beneficial. Moreover, the cooling mode is by far the most constraining and it dominates the choice for MC and HC scenarios.

For the investigation of the optimal material thickness and cycle time, the material for MC and HC was used. When simulating different monolith thicknesses, thinner materials were able to produce much higher power and therefore preferred. For example, a thickness of 1 mm (one order of magnitude higher than conventional coatings), delivered maximum KPI with a full cycle time of about 25 s, which is at the limit of the capacity of conventional heat exchangers (that have important thermal inertia). This means that for thin coatings, work should be done towards fast heat exchanger design. For 2 mm monoliths, however, the ideal cycle time increases to 100 s, as shown in Figure 4.5. The achieved thermal coefficient of performance reached 0.79 and the specific cooling power was 1.4 kW/kg. This means that the monolithicity of the adsorbent offers a great advantage in the design of the heat exchanger.

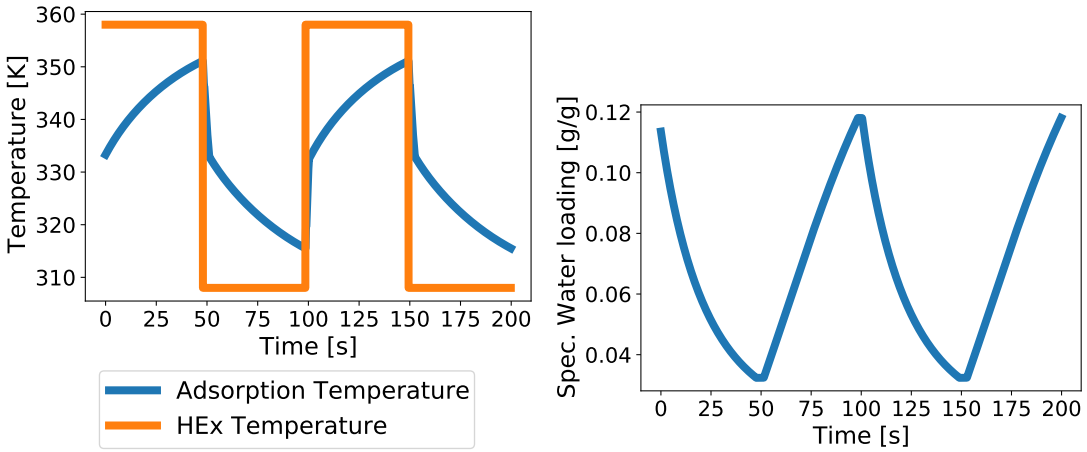

Figure 4.5: Simulation results for a spent coffee ground carbon. In particular. a steady state cooling cycle for a 2 mm monolith. The adsorption temperature (left) increases fast due to the locality of the heat transfer and the idealized boundary condition. The adsorption on the materials (right) happens at a fast rate throughout the cycle.

4.2.4 Adsorption Heat and Mass Exchanger Characterization

For an adHP design in the power range of several kW, small-scale adsorption heat exchanger (AdHEx) cyclic experiments around 1 kW open the possibility to investigate and optimize the HEx design. The design and manufacturing of the AC-based AdHEx unit are some key tasks in the development of an adHP, as highlighted by Mohammadzadeh Kowsari et al., 2018. To characterize the AdHEx efficiency, the sorbate mass is measured dynamically in situ for both half cycles (adsorption and desorption). By knowing the dry mass and the adsorption potential (pressure/temperature conditions), the adsorbed sorbate acts as a reference for the power (i.e. the external heat transfer loop efficiency).

In the adsorber-desorber characterization, the mass uptake $w(t)$ in the adsorption and mass loss in the desorption cycling is measured. The amount of $w(t)$ multiplied by the heat of evaporation L of the sorbate is used as a benchmark for the efficiency of the heat and mass exchanger. L is a function of temperature T and in the case of water $L(20°C) = 2537.5 kJ/kg$ (VDI-Wärmeatlas).

The existing measurement setup of the SNF THRIVE project (see Gantenbein et al., 2017) was modified. The setup features the previously developed adsorbent RMF AC. While the performance will vary with respect to the new and more sustainable SCG AC, the tests are deemed useful to check the equipment, the AdHEx design and the order of magnitude of the different flows. The comprised the modification of the external heat transfer fluid loops and additional sensors – like a new balance beam (HBK Plattformwägezelle 1-SP4MC6MR/7KG-1) of a higher resolution (0.5g). Figure 4.6 shows the graphical user interface (GUI) of the NI LabVIEW data acquisition system. The principle of the setup with heat sources and heat sinks can be seen. Therefore, 3 thermostatic baths are used to perform adsorption and desorption

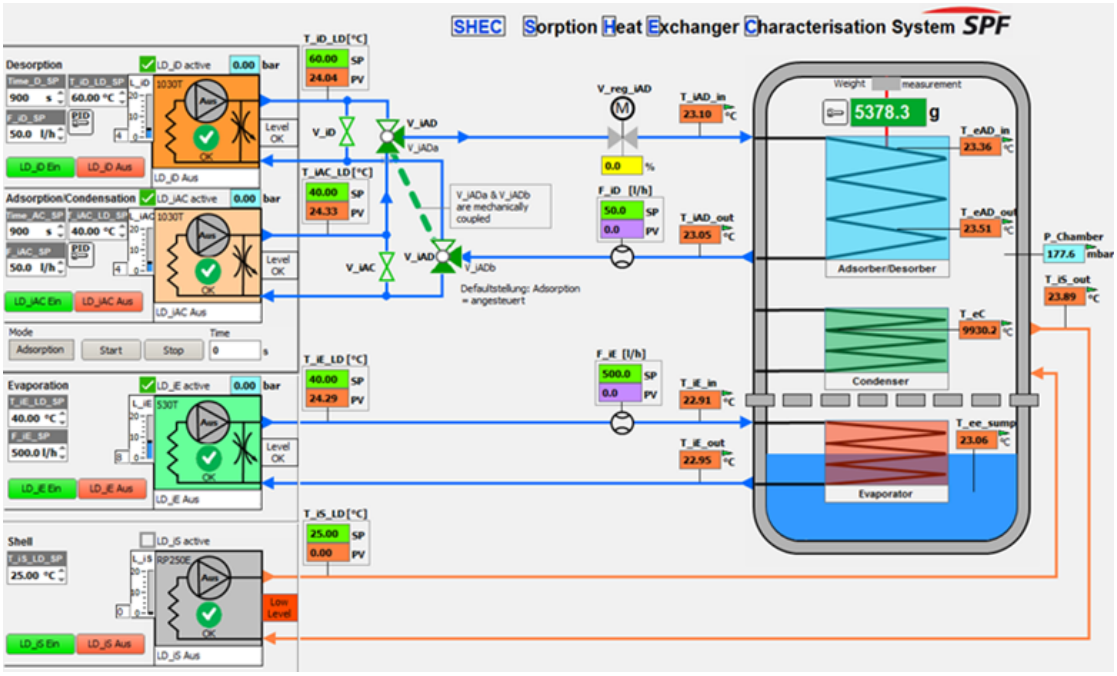

Figure 4.6: The Graphical user interface (GUI) of the NI LabVIEW data acquisition system of the experimental large-scale setup: 4 thermostatic baths as heat sources and heat sinks (left), single chamber setup with double jacket envelope and installed evaporator and adsorber/desorber (right), tubing and sensors. The condenser is not installed – but the evaporator has a double function – evaporation and condensation. Therefore, the evaporator is partly immersed in the liquid sorbate (blue colour and temperature sensor $T_{ee_{sump}}$). While the lower part acts as an evaporator, the upper part acts as a condenser.

(with the AdHEx) as well as evaporation (evaporator) and condensation (condenser) of sorbate in the cycles. With a 4th thermostat, the double jacket is thermostated to avoid heat transfer from and to the environment (the inner vacuum envelope surface) from and to the A/D HEX. In Figure 4.7 part of the open single chamber with the installed A/D HEX (suspended at the beam balance) is shown and the right of this figure shows a section of the activated carbon sorbent disks stack.

Prior to cyclic adsorption and desorption measurements with sorbate, a calibration procedure without sorbate has to be performed for each cycle time t_{cycle}. These calibrations account for all "virtual" mass changes induced by the thermal expansion of the AdHEx, pressure oscillations in the heat transfer fluid and any heat input from the surrounding. Figure 4.8 shows weight measurement data for both adsorption and desorption. At the onset of adsorption (resp. desorption), the behaviour with a high mass uptake (resp. decrease) per time can be seen. In the curve fitting the coefficients have to be determined for each temperature quadruple and cycle time. After this procedure, the functions can be used to parameterise a sorption heat pump model.

After the measurements with the sorbent-sorbate combination, an appropriate data procedure

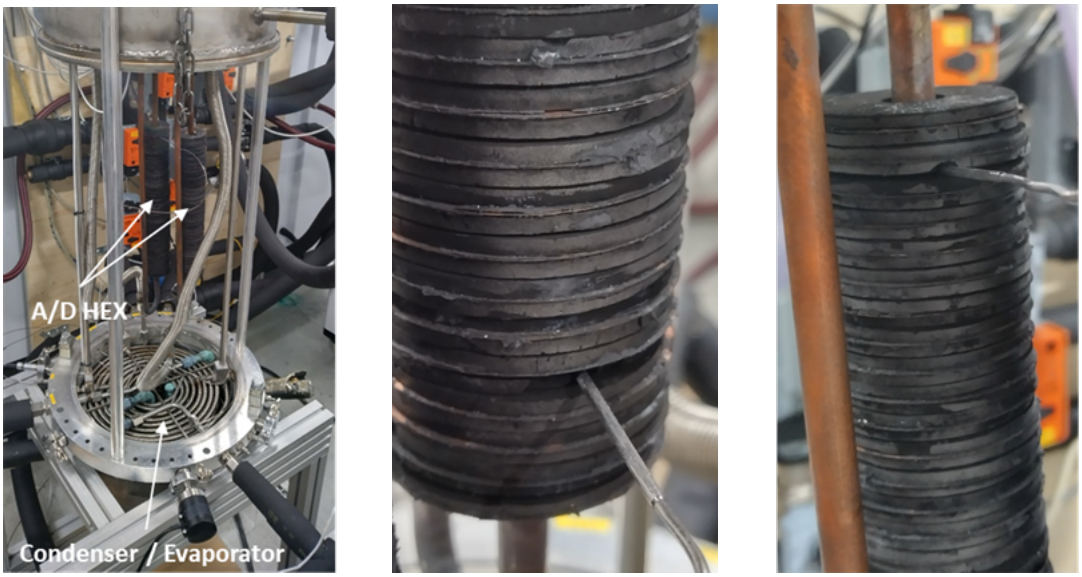

Figure 4.7: Sorption Heat Exchanger Characterization System and installed activated carbon sorbent disks stack: photo of the open single chamber measurement setup (left) and two sections of the AdHEx with clamped Pt 100 temperature sensors (right). The sorbent disks are glued on both sides of the heat-conducting copper fins.

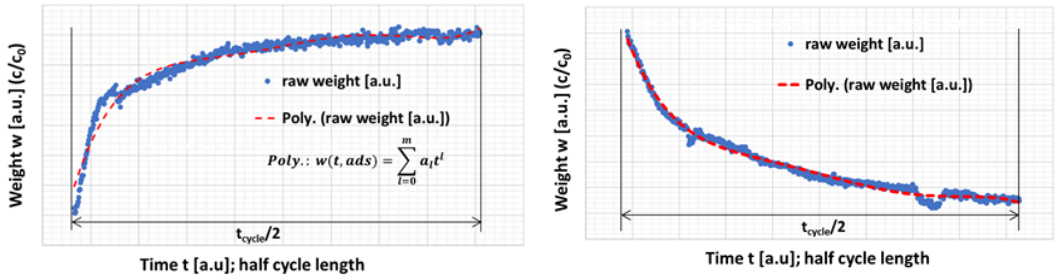

Figure 4.8: Measurement data of the Sorption Heat Exchanger Characterization System: adsorption (left) and desorption (right) curves over the half cycle time (a. u. = arbitrary units) and concept of data curve analysis with peace-wise fit functions.

follows to determine the efficiency parameters. The power of the AdHEx was determined by the sorbate mass uptake $w(t)$ and mass loss through the adsorption-desorption cycles. Although the sorbent shows good kinetic behaviour (a steep increase of the mass uptake at the onset of adsorption) a low power in the range of 100 W was reached (SCP: 300 W/kg) due to a long cycle time t_cycle. A close look at the mass curve $w(t)$ indicates shortening the t_cycle down to at least one half, in agreement with the principle of the findings of the simulations – and therefore nearly a double of the SCP would be reached. An even higher SCP is expected with unaged sorbent material and an unaged AdHEx (no peeling/dissolution of sorbent from the heat-conduction copper fins). In fact, sorbent ageing depends on the interaction with the sorbate and should not occur in normal operating conditions, see Chapter 6. Considering both the cycle time and the ageing variables, an SCP above 1 kW/kg seems at reach.

Based on the defined temperatures of the scenarios, the sorbate vapour pressure is in the range of 17.1 $mbar$ (15°C) and 42.5 $mbar$ (30°C), which are sub-atmospheric pressures. The understanding of the sorption kinetics in the 1 kW power range will allow for the scaling of results to several kW (heating and cooling) power adsorption heat pumps (see Daguenet-Frick et al., 2017).

4.2.5 Conclusions

In this Section, we presented relevant progress obtained towards the design of adsorption heat pumps capable of improving district heating network efficiency in both heating and cooling modes. Firstly, the needs of DHN operators are examined and the most useful applications were selected. Specifically, in the heating mode, the adHP can reduce the return temperature of the network, while in cooling mode the waste heat usage is increased. The adsorbent material developed, an activated carbon (AC) obtained from spent coffee grounds, is a much more sustainable material than state-of-the-art ACs, previously implemented on a first prototype. The obtained adsorbent delivers satisfactory performance for the application studied. In particular, the pyrolysis process gives good control over the adsorption characteristic curve and should be further explored for sieved green bodies and towards higher temperatures and lower durations. Moreover, the models and the simulations of the AC gave useful insight into further development. Thin monoliths (<1mm) can be more performant than thicker ones, but they will be limited by the HEx design. Thicker monoliths are compatible with conventional HEx and are therefore very promising, as they provide a unique solution for effective HEx usage. Lastly, we built and tested a 1 kW prototype characterization setup with increased capacity and accuracy, which will be fundamental for the further development of the adHP. In this setup, we could evaluate the effects of bad material handling and ageing. Future work in this direction should include the validation of the pyrolisis control process to produce optimal adsorbents, the scale-up of its production, its full characterization and its integration onto the AdHEx. The simulations at both material and system levels should guide the design, specifically checking for the robustness of the performance under varying requirements of the DHN substations (e.g. power and temperature regulation). Only after those activities, the

device could be upscaled to commercial size and perfectioned.

4.2.6 Acknowledgments

The author acknowledges the contributions of Juan Antonio Pérez Lopez, Sahana Tavaragondi, Riccardo Torreggiani and Romain Civioc from Empa, Switzerland, Xavier Jobard and Alexis Duret from HEIG-VD, Switzerland, and Xavier Daguenet and Paul Gantenbein from OST, Switzerland. This section was elaborated with the support of the project Characsorb, funded by the Swiss Federal Office of Energy, and presented at EuroSun2022, the ISES and IEA SHC International Conference on Solar Energy for Buildings and Industry, held the 25-29 September 2022 in Kassel, Germany.

4.2.7 Nomenclature

Quantities					
Quantity	**Symbol**	**Unit**	**Quantity**	**Symbol**	**Unit**
Specific heat	c	$J/kg/K$	Area	A	m^2
Thermal conductivity	k	$W/m/K$	Specific area	a	m^2/g
Diffusion coefficient	D	m^2/s	Enthalpy	h	J/kg
Sat. water capacity	W	g/g	Mass	m	kg
Char. ads. energy	C	J/g	Heat	E	J
Thermal diffusivity	α	m^2/s	Mass flow rate	$\dot{m}$	kg/s
Ads. char. shape factor	N		Heat transf. resistance	R_{heat}	K/W
Porosity	ϵ		Heat flow rate	Q	W
Specific pore volume	v	cm^3/g	Mass transf. resistance	R_{mass}	s/m^3
Density	ρ	kg/m^3	Temperature	T	K
Time	t	s	Pressure	p	Pa
Adimensional time	τ		Gas concentration	γ	kg/m^3
Radius	r	m	Volume	V	m^3
Specific ads. loading	w	g/g	Thickness	s	m
Adsorption energy	H	J/kg	Adsorption energy	F	J/g
Evaporation enthalpy	L	J/kg			

Subscripts			
Quantity	**Symbol**	**Quantity**	**Symbol**
Fin	f	Skeletal	$skel$
Saturation	sat	Adsorbate	a
Evaporator	eva	Adsorbent	s
Condenser	con	Vapour	v
Adsorption	ads	Macroscopic	M
Hot source	hot	Microscopic	μ
Internal	int	Mesoscopic	m
External	ext	Initial	i
Envelope	env		

4.3 A Novel Agitated Reactor for Adsorption Heat Transformers

4.3.1 Introduction

The development of adsorption heat transformers is of great interest to the research community for already 50 years, as reported by Meunier, 2013, but for several reasons, its commercial deployment was never extremely successful. The technology faces intrinsic challenges in terms of discontinuous operation due to the need for regeneration, low efficiency dictated by low heat recovery and limiting adsorbent-adsorbate working pairs, and complex designs due to the vacuum requirements, as reported by Demir et al., 2008. Cycle design, working pair selection and heat and mass transfer rates all play a central role in the success of the technology and would be ideally addressed in synergy. Despite the fact that this technology lags with respect to absorption and, especially, mechanical compression systems, there is a great potential interest to solve the mentioned challenges given the compatibility with the abundant waste and renewable heat and the absence of any harmful substance. Pinheiro et al., 2020 point out how adsorption heat pumps can substantially decrease primary energy consumption and increase the share of renewable energy use, therefore decreasing CO_2 emissions. In this work we try to tackle two of the main problems of this technology:

- reducing the energy losses by eliminating the intermittent operation constraint;
- increasing the power density and/or the material usage by mobilizing the transport of the adsorbent material.

The direction in which to advance the adsorption heat transformers design strongly depends on the nature of the adsorbent material and its integration into the adsorption heat exchanger. Initially, the adsorbent materials implemented were mostly granular, as they were easy to handle, and zeolites and silica gel were vastly studied, as reported by Meunier, 2013. However, the fixed-bed configurations used to achieve high energy density inevitably led to poor heat transfer and therefore either low power density or low energy efficiency, as reported by Caprì et al., 2020. The obvious way to cope with this problem was to increase the thermal contact of the adsorbent with coating methods and introduce thermally conductive materials in consolidated beds. Those configurations increase the heat transfer rate leading to faster and better use of the material, as reported by Caprì et al., 2020. However, the mass transfer is not so optimized, given the high density of the material. For example, it was reported by Ammann, Michel, and Ruch, 2019, that the if the coating thickness is not to be too sacrificed, the mass transfer becomes the limiting factor. The natural improvement in the material integration would be to try to balance the benefits of fast heat and mass transfer rates, as for example achieved by Ammann, Ruch, et al., 2019 for coatings and recently by Scherle et al., 2022.

Those developments certainly go in the right direction, as achieving a higher use of the material is fundamental. In fact, Pinheiro et al., 2020 try to formulate minimum requirements for the successful implementation of heat pumps, including high energy efficiency and specific

heating power, short cycle times, and high cycling capacity, and identify in MOF-coated heat exchangers the most promising solution. However, the thermal contact is achieved by immobilizing and densifying the adsorbent, and the chances for heat recovery on the adsorbent side are reduced. Advanced cycles recovering the heat among beds with heat transfer fluids are in any case possible, as reminded by Demir et al., 2008, and should be further investigated. In this work, we reinvestigate the idea of enhancing heat transfer in granular adsorbents. In mechanical compression heat pumps, it would be illogical to use intermittent cycles as the heat transformer media (i.e. the refrigerant) can pass seamlessly from one component to the next without causing parasitic losses (at least if not required by power regulation mechanisms). If the granular adsorbent is mobilized, it can be treated as a refrigerant would be: not only it could go from the adsorber to the desorber seamlessly, but also it could exchange heat in a counter-flow configuration so that the temperature profile (and the material use) is optimized. For open-system heat storage, was experimentally investigated by Nonnen et al., 2016, but without a clear determination of the advantages with respect to fixed bed devices.

In different sectors, such as mining, pharmaceutical, agricultural etc., the transport and agitation of granular materials is common practice. A good example is material drying, as reported by Waje et al., 2006 and Schuitema et al., 2009, where transportation, heat and mass transfers are needed. The vacuum requirements and the fragile nature of the adsorbent materials may pose serious challenges to the application of such agitated reactors to adsorption heat transformers. However, it is an opportunity that should be investigated at least in a preliminary fashion, because its development could be of high interest if successful.

The current trends in the selection of adsorbent materials are using hybrid approaches between advanced material discovery techniques, computer simulations and experiments, as reflected in the works of W. Li et al., 2021, Z. Shi et al., 2021, and also in the present thesis. Of course, the most interesting materials are the ones more tunable, easier to simulate and with the highest cycling capacity. For this reason, among the most commonly presented materials, we find MOFs, as reported for example by AL-Dadah et al., 2020, but also novel zeotypes, as reported by S. K. Henninger et al., 2017, and salt-adsorbent composite materials, as reported by Tan et al., 2019. To the best of our knowledge, the mechanical resistance of the adsorbent was never investigated, as one of the advantages of classical adsorption cycles is the absence of moving parts. Except for coating quality tests, such as those performed by Freni et al., 2013, their mechanical characteristics are largely unknown. Using agitated reactors would undoubtedly open a number of open questions and technical challenges. It is therefore fundamental to investigate the feasibility of such cycles from a thermodynamic point of view. For this reason, we propose to start with purely computational research, although based on experimental data and validated models.

As it was reported in Section 3.1, the literature regarding computational models of adsorption heat transformers is relatively affluent. However, one can notice that in none of the reported works, there are transport phenomena. Modelling the combined heat and mass transfer during

adsorption and transport and mixing is a new challenge. Being a first of a kind, we propose a methodology that draws from both the adsorption community and the agitated reactors community. The existing literature on adsorption heat exchangers was already covered in the previous chapters, so here we will report some relevant works concerning agitated heat exchangers.

The work of Mickley and Fairbanks, 1955 was the foundation of the field of fluidized beds. The heat transfer coefficients are determined as functions of its thermal conductivity, its density, its heat capacity and stirring factor. The latter, in turn, depends on many factors including the particle diameter, the viscosity of the gas, the velocity of the gas, the geometry of the heater and the concentration of the particles. On their shoulders, Martin, 1984 thoroughly investigated the heat transfer mechanisms taking place, applying molecular kinetic theory to the solid particles. The description of the heat transfer is based on adimensional numbers such as Reynolds, Archimedes, Nusselt, Stanton etc, which are specifically derived for fluidised beds. Among the interesting aspects of that work, one could mention the non-dimensional contact time increase with decreasing particle size, but in general, the heat transfer has a maximum between no mobility and infinite velocity. Basu and Nag, 1987 found that the velocity of the particles increases the bed voidage, with a similar effect on the heat transfer. Moreover, denser beds provided higher heat transfer coefficients if the fluidization is maintained.

However, the fluidized bed case is quite different with respect to the adsorption and desorption at subatmospheric pressure. The same applies to the more modern works by Behjat et al., 2008; Chang et al., 2012; Gomez-Garcia et al., 2017; Hamzehei and Rahimzadeh, 2009; Masoumifard et al., 2008; Papadikis et al., 2010. In those works, CFD techniques are used to great avail for acquiring more knowledge on the processes (e.g. local distributions of temperature, pressure and velocity) and for equipment design. In most of the works, an Eulerian method is applied.

Outside the field of fluidised beds, Montante et al., 2001 used CFD simulations to investigate the distribution of solid particles in an agitated tank. Moreno et al., 2016 the heat transfer coefficient during the drying process of biomass particles agitated in a gas phase. This is a relatively similar case to agitated desorption processes. They found that the overall heat transfer coefficient was quite low (i.e. tens of $W/m^2/K$) and related to the Reynolds and Nusselt numbers. They also found that the media behaved as a homogeneous mixture thanks to adequate agitation. Morris et al., 2016 used discrete element simulations to model the heating of solid particles within a solar thermal receiver. They found a strong dependence of the heat transfer coefficient on the particle size, as we also observed comparing the works of A. I. Osman et al., 2021 and Schuitema et al., 2009, with smaller particles being better. Their model, originally developed by Morris et al., 2015, returns quite accurate results, but it is also rather complex as it involves a full-scale simulation of all the different phases and computes the transport with continuity and momentum equations. This is an approach that could be pursued but strongly limits the simulation possibilities as it is computationally intensive.

Based on these findings, we propose an Eulerian heat and mass transfer model based on the

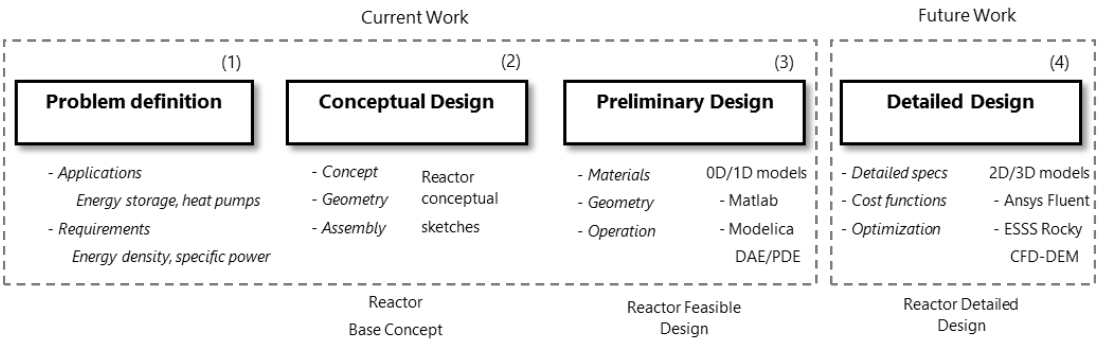

Figure 4.9: Positioning of the present work with respect to the design process for a novel agitated adsorption heat exchanger

use of adimensional numbers. However, given the low density, viscosity and velocity of the gas phase, the heat and mass transfer models were simplified, as it is believed that the gas contributions are probably negligible. The authors are aware that this might be a limitation of the work, but it is believed that without experimental work it would be hard to fully answer this research question. As will be detailed in the next section, we aim to deliver a tool to evaluate the order of magnitude of relevant quantities such as the coefficient of performance, the power density and the energy density for various applications. For this reason, we preferred a discretized model instead of a full-scale CFD analysis. To clarify the positioning of this work with respect to the design process, in Figure 4.9 we propose a schematic representation of the workflow.

In Section 4.3.2 we describe the choice of the reactor concept among the many available in the literature. In Section 4.3.3 we describe the multi-scale model. In Section 4.3.4 we report the results obtained for the preliminary design of the case study and for a sensitivity analysis. In Section 4.3.5, we conclude by summarizing the findings.

4.3.2 Reactor Concept Selection

Potential fluid-like granular reactor concepts were researched and identified. Among the mixers with no agitation and no transportation, static mixers, Ross static mixers, Kenics static mixers, Sulzer static mixers, and Komax static mixers were identified. In the category of mixers with agitation and no transportation the conical screw mixer, rotating drum mixer, paddle blade mixer, vertical bladed mixer, ploughshare mixer, ribbon mixer, double paddle mixer, v-blender mixer, ploughshare mixer, and twin-blade planetary mixer were identified. In the category of mixers with agitation and transportation, screw conveyor-mixer, advanced screw conveyor-mixer, and double screw conveyor were identified.

The reactor conceptual designs are categorized and presented in Figure 4.10. Among these, the screw reactor conceptual design fulfils the required criteria for continuous heat transformation application:

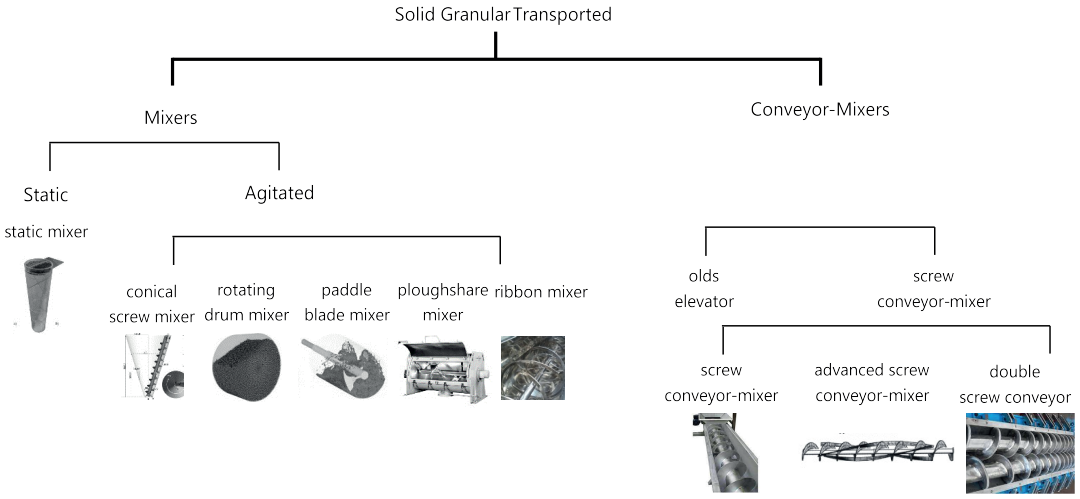

Figure 4.10: Categorization of concepts for agitated reactors

- the system must be closed, such as that low pressures in the range of 1-100 $mbar$ of pure water can be sustained;
- the adsorbent media is to be transported in a continuous fashion so that the parasitic heat losses due to cycling inert mass can be avoided;
- counter-flow heat exchange between the adsorbent media and the heat transfer fluid is to be ensured, such that all available adsorption capacity is fully exploited;
- the reactor ensures good granular mixing so that temperature and pressure stratification are avoided;
- high rates of both heat and mass transfer must be ensured, to keep the reactor size to a minimum;
- the design should be feasibly simple so that the manufacturing costs remain low.

These requirements represent the ideal case in which material handling is not a problem (e.g. abrasion, fracture, fouling etc.). In case the mechanical stress on the adsorbent should be minimized or the moving parts are seen as too costly, they could be reformulated in favour, for example, of static mixers.

In the case of discontinuous processes (such as heat storage), it could be convenient to investigate agitated reactors without material transportation. Such designs could be effective in maximizing heat transfer without creating problems for the storage of the material from one tank to another. However, in this section, we address the continuous operation mode as a starting point.

		Reactor Concept		
Criteria	**Weight**	**A**	**B**	**C**
Heat transfer	3	3	1	3
Mass transfer	2	2	3	3
Insulation	1	3	2	3
Simplicity	2	3	3	1
Evaluation	-	22	17	20

Table 4.5: Qualitative evaluation of screw conveyor reactor concepts. The heat transfer fluid in the inner shaft and the adsorbate diffused by a jacket seem beneficial with a reasonable complexity for manufacturing.

Given the meeting of all the requirements above, the screw reactor sub-conceptual designs were researched (see the works by Mustaffar et al., 2018; Nachenius et al., 2015; H. B. Osman, 2012; Roberts, 1999, 2007), regarding different assembly and operation modes for the sorption material flow, the heat transfer fluid flow, and the adsorbate diffusion design. As a result, three sub-concept designs were analysed.

A. The heat transfer fluid is introduced in the inner shaft, which is thermally connected to the impeller blades that act as extended fins, and the adsorbent material is impelled in the opposite direction to act as a counter-flow *solid-fluid-like* heat exchanger, and the adsorbate is diffused through an external jacket in the outer surface.

B. The adsorbate is circulated in an inner shaft and diffused through a perforated jacket or perforated fins, the heat transfer fluid is circulated in the outer rim, and the adsorbent material is circulated in counter-flow inside the reactor.

C. The principle is the same as the first, but the adsorbate is diffused in an intermediately located jacket to reduce the main average path for interparticle mass diffusion.

The sub-concepts were qualitatively analyzed, based on the design objectives for energy storage and heat pumps, and reduced to four primary weighted criteria: heat transfer, mass transfer, insulation and simplicity. Maximum weights were attributed to heat transfer and mass transfer, given that a high-rate reactor design is pursued, with prevalence considered for the heat transfer since, for solid adsorption of granular media, it is generally the most constraining factor. The results of the analysis are shown in Table 4.5. The analysis showed that the first reactor sub-concept obtains the highest evaluation score, due to the good heat transfer characteristics and its simplicity. Therefore, it was selected and pursued in the present research.

4.3.3 The Model

The concept of a fluid-like, counter-flow adsorption reactor, such as the one proposed here, is well suited for different applications, such as thermochemical energy storage, heat pumping,

drying, or gas separation. The performance of each of these applications depends on different factors, and any attempt to maximize it will evidently lead to different designs. However, it must be noted that given the complexity and novelty of such a concept, an optimal design can be produced only with the support of experimental characterization. In fact, we showed in Section 3.4 that adsorption models are strongly affected by the accuracy of material properties and geometrical parameters. In this section, the aim is to demonstrate the feasibility of modelling such a reactor without excessive computational effort, including multiple scales and non-linear systems, and to prove the advantage of the reactor when compared to traditional ones.

To this aim, a robust modelling solution capturing the most relevant physical phenomena for heat transformation at both reactor and adsorbent material levels is proposed. This methodology is applied to a preliminary design to evaluate the key performance indicators and to analyse the relative importance of the modelled phenomena. Because the advantages of a steady state operation and the high rates of heat and mass transfer expected from the reactor design are highest for continuous processes, the preliminary design is conceived for closed-system heat pumping and cooling. This also eliminates in the first analysis the problem of designing and modelling the material storage during off times, which would be fundamental for discontinuous applications such as heat storage.

The structure of the model capturing multiple scales is represented in Figure 4.11. The model aims to describe the screw-conveyor adsorption heat exchanger and the heat and mass transfer mechanisms associated. The diffusing jacket, the evaporator, the condenser and any other equipment related to the functioning of the system are not included in the analysis.

The model consists of an Eulerian description of the reactor, in which the axial length is discretized and the radial direction is lumped, assuming perfect radial mixing but a certain degree of axial stratification.

The Reactor

The reactor (Figure 4.11) is filled with a large number of particles of adsorbent material, within which the adsorption and desorption process take place and with which it exchanges heat. The number of particles is computed based on the volume of the granular media V_m (calculated assuming a certain filling fraction of the reactor f_p) and the volume of each particle V_p.

$$N_p \approx \frac{V_m}{V_p} \tag{4.14}$$

$$V_m = V_{inner} \cdot f_p \tag{4.15}$$

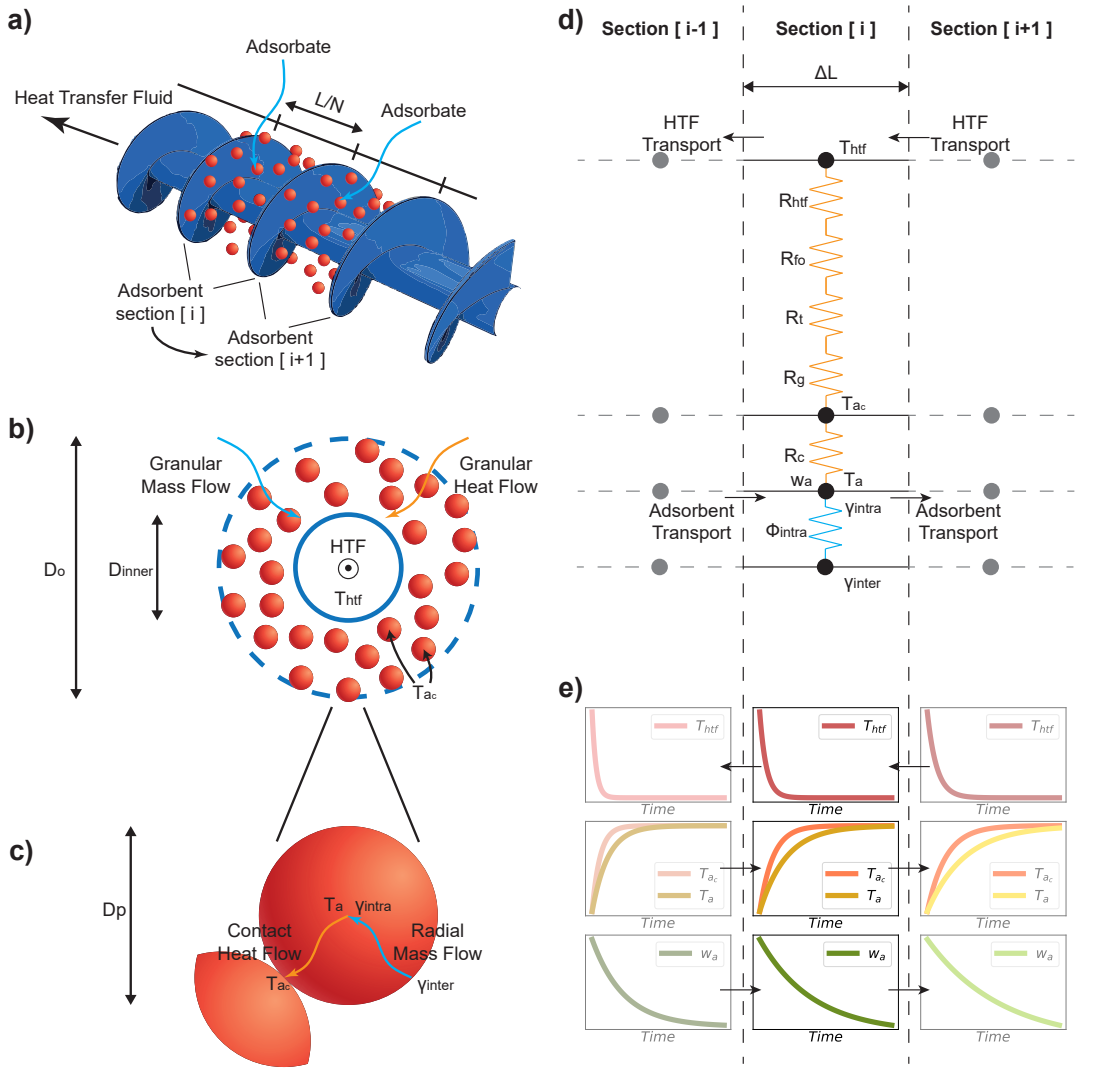

Figure 4.11: The counter-flow fluidized adsorption reactor model, described by a multiscale Eulerian approach. **a)** Reactor scale, describing energy and mass transport and global heat transfer: The reactor length L is discretised into N section of length $\Delta L = L/N$. **b)** Granular media scale, describing the lumped heat and mass transfer in the adsorbent media with perfect mixing: the heat and the vapour travel in the annular region between the fin diameter D_o and the tube diameter D_{inner}, in which the media is perfectly mixed with a homogeneous state. **c)** Adsorbent particle scale, describing the contact-limited heat transfer and the radial mass transfer: the heat and the vapour travel through the adsorbent particle diameter D_p, which is represented by an average state, constant within the section. **d)** Schematic representation of the heat and mass transfer resistive networks: heat and mass are transferred among scales by the resistance R and Φ, respectively. The adjacent sections exchange heat and mass by transport in the direction of the flow. **e)** Representation of the temporal evolution of some state variables in different sections and different scales (the plots are not in scale). The model is continuous in time for each section and discretized using the transport terms of the heat and mass balances. Following the transport arrows at a constant time is equivalent to following the state of a particle or of the heat transfer fluid spatially along the reactor.

$$V_{inner} = \frac{\pi}{4} \cdot (D_o^2 - D_{inner}^2) \cdot L \tag{4.16}$$

$$V_p = \frac{\pi}{6} \cdot D_p^3 \tag{4.17}$$

For a small pitch ($L/p > 10$), the heat transfer area A can be approximated as:

$$A = f_p \cdot \frac{L}{p} \cdot \pi \cdot \left(\frac{D_o^2 - D_{inner}^2}{2} + D_{inner} \cdot (p - t_f) + t_f \cdot (D_o - D_{inner}) \right) \tag{4.18}$$

Given the geometrical features of the reactor, such as the diameter of the shaft D_i and of the fins D_o, the clearance gap g, the blade pitch p, the blade thickness t_f, the volumetric efficiency η_{vol}, and given the rotation frequency ϕ and the media bulk density $\rho_{a_{tap}}$, the adsorbent mass flow rate can be calculated as Roberts, 1999:

$$\dot{m}_a = \frac{1}{8} \cdot \rho_{a_{tap}} \cdot \left(1 + \frac{2 \cdot g}{D_o}\right)^2 - \left(\frac{D_{inner}}{D_o}\right)^2 \cdot \left(\frac{p}{D_o} - \frac{t_f}{D_o}\right) \cdot \phi \cdot D_o^3 \cdot \eta_{vol} \tag{4.19}$$

As it can be convenient to have an internal annulus of diameter D_{an} in the heat transfer fluid tube to increase the fluid velocity, its cross-sectional area has to be corrected for it. The axial velocity of the heat transfer fluid v_{htf} and of the adsorbent media v_a is considered to be constant along the reactor and equal to:

$$v_{htf} = \frac{4 \cdot \dot{m}_{htf}}{\pi \cdot \rho_{htf} \cdot \left(D_{inner}^2 - D_{an}^2\right)} \tag{4.20}$$

$$v_a = \frac{4 \cdot \dot{m}_a}{\pi \cdot \rho_{a_{tap}} \cdot (D_o^2 - D_{inner}^2)} \tag{4.21}$$

The residence time of the adsorbent in the reactor τ can be calculated as:

$$\tau = \frac{L}{v_a} \tag{4.22}$$

The overall heat transfer coefficient U_{tot}, is determined on the basis of the global heat transfer resistance R_{tot}, which is intended as the one standing between the heat transfer fluid and the

surface of the adsorbent material. In this way, the reactor design and the adsorbent material are kept separated in the analysis:

$$U_{tot} = \frac{1}{R_{tot} \cdot A} \tag{4.23}$$

The global heat transfer resistance includes the contributions of the heat transfer fluid convection R_{htf}, the tube fouling R_{fo}, the metal tube R_t, and the fins and the granular media R_g.

$$R_{tot} = R_{htf} + R_{fo} + R_t + R_g \tag{4.24}$$

The fluid thermal resistance in a tube in presence of an annulus is determined based on the fluid properties, the geometry and the flow type, as proposed by Bergman et al., 2019:

$$R_{htf} = \frac{1}{\pi \cdot h_{htf} \cdot D_{inner} \cdot L} \tag{4.25}$$

$$h_{htf} = \frac{\left(1 - 0.14 \cdot (D_{an}/D_{inner})^{0.6}\right) \cdot Nu \cdot k_{htf}}{D_{inner} - D_a} \tag{4.26}$$

$$Nu = \begin{cases} 4.36 & \text{if} Re < 2300 \\ \left(\frac{f_{fr}}{8} \cdot (Re - 1000) \cdot Pr\right) \cdot \left(1 + 12.7 \cdot \left(\left(\frac{f_f}{8}\right)^{0.5}\right) \cdot \left(Pr^{2/3} - 1\right)\right)^{-1} & \text{if} Re \geq 2300 \end{cases} \tag{4.27}$$

$$Re = \frac{v_{htf} \cdot (D_{inner} - D_{an})}{\nu_{htf}} \tag{4.28}$$

Where the thermal conductivity k_{htf}, the dynamic viscosity ν_{htf} and the Prandtl number Pr of the heat transfer fluid can easily be extracted from tables as a function of temperature, while the friction factor f_{fr} can be approximated to 0.02 for simplicity. The thermal resistance due to fouling is assumed constant. The thermal resistance of the tube can be calculated based on the geometry, the tube thickness t_t and its thermal conductivity k_t, as proposed by Bergman et al., 2019:

$$R_t = \frac{ln((D_{inner} + t_t)/D_{inner})}{2 \cdot \pi \cdot L \cdot k_t} \tag{4.29}$$

The fin and granular media resistances are kept together to lump the effect of the mixer/propeller screw. In fact, the fin efficiency η_f, which can be firstly approximated as annular fins if $p < D_o$, and the granular convective global heat transfer coefficient U_g are correlated, as proposed by Bergman et al., 2019:

$$\eta_f = \frac{tanh\left(\left(\frac{2 \cdot U_g}{k_t \cdot A_f}\right)^{0.5} \cdot \left(\frac{D_o}{2} - \frac{D_{inner}}{2} + \frac{t_f}{2}\right)^{3/2}\right)}{\left(\frac{2 \cdot U_g}{k_t \cdot A_f}\right)^{0.5} \cdot \left(\frac{D_o}{2} - \frac{D_{inner}}{2} + \frac{t_f}{2}\right)^{3/2}} \tag{4.30}$$

$$A_f = \left(\frac{D_o}{2} - \frac{D_{inner}}{2} + \frac{t_f}{2}\right) \cdot t_f \tag{4.31}$$

A correlation between the heat transfer coefficient of the granular media U_g, the geometry and the rotational frequency is obtained from the data reported by H. B. Osman, 2012. The maximum heat transfer coefficient was found to be about 600 $W/m^2/K$ for powders of 0.2 mm by Schuitema et al., 2009 and about 100 $W/m^2/K$ for particles of 4 mm. Therefore, we assume a simple linear correlation between particle size and maximum heat transfer coefficient, which should be in the correct order of magnitude in the typical mesh size of adsorbent materials:

$$U_{g_{max}} = 600 - 1.25e5 \cdot D_p \tag{4.32}$$

For simplification, it is assumed there is no interaction between the pitch-to-diameter ratio and the frequency, and that solid sorption has a negligible effect on heat transfer when compared with the heat transport mechanism of granular convection. The granular media heat transfer coefficient calculated below includes the effects of the wall-to-surface heat transfer, the heat penetration in packed beds and the granular convection. In reality, it depends on the flowing, mechanical and thermophysical properties of the granular media (the heat exchanger material is copper) and should be calibrated. However, this correlation is deemed to provide the correct order of magnitude and therefore adequate for the present study.

$$U_g = \left(6.4097 \cdot \phi + 0.376\right) \cdot \left(0.2302 \cdot \left(\frac{p}{D_o}\right)^2 - \frac{0.5755 \cdot p}{D_o} + 1\right) \cdot U_{g_{max}} \tag{4.33}$$

$$R_g = \frac{1}{U_g \cdot A \cdot \eta_f} \tag{4.34}$$

The thermal resistances are calculated globally for the whole reactor as the level of detail of the modelling does not allow for a more precise determination (we avoid using precision without accuracy in this sense). The total heat transfer coefficient U_{tot} (which includes everything except the adsorbent material intraparticle resistance) is then applied to the granular media by calculating the total section heat resistance by calculating the inverse of the total heat transfer coefficient multiplied by the fractional area ΔA (see Equations 4.36, and 4.42 for example).

The Lumped Granular Media

The reactor is discretized in N axial sections, equal in terms of length, heat exchange surface area and the number of adsorbent particles they contain. Each of these sections will be characterised by fractional length, area, the number of particles, and masses (of the heat transfer fluid and adsorbent):

$$\Delta L = \frac{L}{N} \tag{4.35}$$

$$\Delta A = \frac{A}{N} \tag{4.36}$$

$$\Delta N_p = \frac{N_p}{N} \tag{4.37}$$

$$\Delta m = \frac{m_{tot}}{N} \tag{4.38}$$

In each of these sections, the adsorbent media is considered to be perfectly mixed. On average, each particle is subject to the same boundary conditions and will be in the same thermodynamic state. Among sections, no mixing is allowed. Instead, mass and energy are transported from one section to the next. Within each section, five different phases are present,

in five different thermodynamic states

- the adsorbent particles,
- the adsorbed adsorbate,
- the intraparticle vapour phase,
- the interparticle vapour phase,
- the undisturbed vapour phase, exchanged with the evaporator/condenser by the diffusing jacket.

The adsorbent particles share the same properties, thermodynamic state, mass and heat flow rates. The determination of the state and the flow rates within each adsorbent particle will be discussed in detail in the following subsection. However, their energy and mass must be conserved, and the respective transport terms are accounted for at the lumped granular media scale. Considering that the bulk density of the adsorbent is constant, the mass flow rate of the solid adsorbent is conserved. Using the finite difference method (FDM), the average state variables in the axial position $0 \leq x \leq L$ will be represented by the lumped granular media section $i \in \{1...N\} : (i-1) \cdot \frac{L}{N} \leq x \leq (i) \cdot \frac{L}{N}$.:

$$\dot{m}_a(x) = \dot{m}_a \tag{4.39}$$

$$\dot{m}_l(x,t) = \dot{m}_a \cdot w(x,t) \tag{4.40}$$

The conservation of energy applies to the heat transfer fluid, such that:

$$\frac{dm_{htf}}{dx} \cdot c_{htf} \cdot \frac{\partial T_{htf}(x,t)}{\partial t} = U_{tot} \cdot \left(T_{a_c}(x,t) - T_{htf}(x,t)\right) \cdot \frac{dA}{dx} + \dot{m}_{htf} \cdot c_{htf} \cdot \frac{\partial T_{htf}(x,t)}{\partial x} \tag{4.41}$$

Where $T_{htf}(L,t) = T_{htf_{inlet}}$. In the FDM model, instead of a continuous derivative in space, there will be finite differences in the state variables (the temperature, in this case), from one section and the following. In addition, we are using the integral form of the heat balance over the whole segment length. As an example, the FDM equivalent for Equation 4.41 is proposed below. The concept will apply similarly to the rest of the granular media equations.

$$\Delta m_{htf}[i](t) \cdot c_{htf}[i](t) \cdot \frac{\partial T_{htf}[i](t)}{\partial t} = U_{tot} \cdot \left(T_{a_c}[i](t) - T_{htf}[i](t)\right) \cdot \Delta A + \dot{m}_{htf}[i](t) \cdot c_{htf}[i](t) \cdot \left(T_{htf}[i+1](t) - T_{htf}[i](t)\right) \tag{4.42}$$

The time derivative is continuous and solved autonomously by the Modelica solver. The inlet condition is imposed as $T_{htf}[N+1](t) = T_{htf_{inlet}}$. The heat and mass conservation equations for the adsorbent material will differ from this because of the counter-flow configuration. Instead, of computing the spatial derivative $\frac{\partial y(x,t)}{\partial x} = \frac{y[i+1](t)-y[i](t)}{\Delta L}$, it will be $\frac{\partial y(x,t)}{\partial x} = \frac{y[i](t)-y[i-1](t)}{\Delta L}$. For this reason, the inlet condition will be applied as $y[0](t) = y_{inlet}$, instead of as above $y[N+1](t) = y_{inlet}$. In the case of co-flow configuration, the heat transfer fluid equations have the same form as the adsorbent equations.

As it will be evident from the design presented in Section 4.3.4, the thermal mass of the metal (tube and fin) is often negligible with respect to the solid adsorbent, the adsorbed adsorbate and often even with respect to the heat transfer fluid mass. The same applies to the thermal mass of the vapour in all its different states. Therefore, for the sake of simplicity and the saving of computational resources, their heat balance is neglected. The conservation of energy applies to the granular media and all its phases. However, it is known, also from previous sections, that the contribution of the vapour phase to the heat balance is negligible. Therefore, they are omitted for the sake of simplicity.

$$\left(m_{a_p} \cdot c_a(x,t) \cdot \frac{\partial T_a(x,t)}{\partial t} + m_{a_p} \cdot w(x,t) \cdot c_l(x,t) \cdot \frac{\partial T_a(x,t)}{\partial t} - m_{a_p} \cdot H_{ads}(x,t) \cdot \frac{\partial w(x,t)}{\partial t}\right) \cdot \frac{dN_p}{dx} = \left(-\dot{m}_a \cdot c_a(x,t) \cdot \frac{\partial T_a(x,t)}{\partial x} - \dot{m}_a \cdot w(x,t) \cdot c_l(x,t) \cdot \frac{\partial T_a(x,t)}{\partial x} + \dot{m}_a \cdot H_{ads}(x,t) \cdot \frac{\partial w(x,t)}{\partial x}\right) + + U_{tot} \cdot \left(T_{htf}(x,t) - T_{a_c}(x,t)\right) \cdot \frac{dA}{dx} \tag{4.43}$$

Where $T_a(0,t) = T_{a_c}(0,t) = T_{a_{inlet}}$ and $w(0,t) = w_{inlet}$ and m_{a_p} is the dry mass of a single particle. At the same time, the mass in the different phases of the granular media must be conserved (again omitting the contribution to the mass balance of the vapour phase as they are negligible):

$$m_{a_p} \cdot \frac{\partial w(x,t)}{\partial t} \cdot \frac{dN_p}{dx} = -\dot{m}_a \cdot \frac{\partial w(x,t)}{\partial x} + \frac{\gamma_{inter}(x,t) - \gamma_{intra}(x,t)}{\Phi_{intra}(x,t)} \cdot \frac{dN_p}{dx} \tag{4.44}$$

In Equation 4.44, the mass flow rate exchanged between the particle and the media is regulated by the gas concentration in the interparticle vapour phase γ_{inter} and in the intraparticle

volume γ_{intra}, and the intraparticle diffusive resistance Φ_{intra}. In fact, the total diffusive resistance ideally accounts for intraparticle diffusion and interparticle diffusion. However, also in this case it was possible to neglect the interparticle diffusive resistive and capacitive effects due to their negligible contributions in determining the vapour mass flow rate.

Given the low pressures characteristic of the application, the water vapour is considered to behave as an ideal gas, as reported by Adkins, 1983, so the state equations can be written as follows, assuming that the interparticle vapour phase and the undisturbed vapour in the diffusion jacket are in thermal equilibrium:

$$\gamma_{intra}(x,t) = \frac{M \cdot p_{intra}(x,t)}{T_a(x,t)} \tag{4.45}$$

$$\gamma_{inter}(x,t) = \frac{M \cdot p_{inter}(x,t)}{T_e} \tag{4.46}$$

Due to the interparticle diffusion and pressure losses due to viscous effects in the media, the concentration and the pressure of the gas in the interparticle space and in the diffusive jacket could be in general different. However, due to the negligible difference between both, these differences are neglected, and it is assumed that $\gamma_{inter}(x,t) = \gamma_e$ and $p_{inter}(x,t) = p_e$.

More details about all the neglected contributions in the heat and mass balances above can be found in Section 4.3.8. The intraparticle resistances to heat and mass transfer, instead are treated separately below, as they could be changed depending on the nature of the adsorbent material, leaving the rest of the model unmodified.

The Adsorbent Material

The heat and mass transfer taking place within the adsorbent materials particle plays a pivotal role in determining the adsorption and desorption dynamics. In Section 3, we demonstrated how the adsorption dynamics can be correctly captured with a lightweight model based on the material properties. While the heat transfer in an agitated reactor is greatly improved with respect to a fixed-bed configuration, in a counter-flow agitated-bed configuration the temperature difference driving the adsorption process is applied slowly and uniformly over time. This fact represents one of the strengths of the reactor concept, as it allows a good usage of the material, similar to what happens in traditional counter-flow heat exchangers. On the other hand, the initially fast kinetics observed when big temperature jumps are applied are not to be expected, as the initial driving force is smaller. Compared to the transient resistance observed in beads subject to large temperature jumps, we would expect in the present case to observe larger resistance, as the adsorption is expected to take place more uniformly over

the particle volume. For this reason, the heat and mass transfer resistances are conservatively assumed to be the ones occurring in the steady state.

Given the spherical geometry and constraint of heat conduction through contact points, it is still assumed that the heat transfer resistance can be modelled as the contact resistance as by Siu and Lee, 2000. As the resistance of the granular media is already accounted for in Equation 4.34, the intraparticle heat transfer resistance in steady state reduces to:

$$R_c = \frac{f_c(r_p, r_c)}{k_a(x,t) \cdot r_p} \tag{4.47}$$

$$f_c = \frac{0.5788}{3}\left(\frac{r_c}{r_p}^{-1} - \frac{r_c}{r_p}^{-2} \cdot 1.093e-3 + \frac{r_c}{r_p}^{-3} \cdot 3.019e-5 - \frac{r_c}{r_p}^{-4} \cdot 1.202e-7\right) \tag{4.48}$$

The ratio between the contact radius and the bead radius $\psi = r_c/r_b$ is generally unknown. However, in practice, it was found that for packs of spheres, there is a correlation between interparticle porosity and contact area Siu and Lee, 2004. Typical values obtained experimentally range between 0.05 and 0.2.

The mass transfer resistance of a sphere in a steady state, for similarity to the heat conduction case reported by Carslaw and Jaeger, 1959, is:

$$\Phi_{intra} = \frac{r_p^2}{V_{vap_{intra}} \cdot \pi^2 \cdot \delta_{intra}} \tag{4.49}$$

$$V_{vap_{intra}} = V_p \cdot \left(\epsilon_{intra} - \frac{\rho_{a_{env}}}{\rho_l} \cdot w(x,t)\right) \tag{4.50}$$

Depending on the nature of the adsorbent material, several intraparticle mass diffusion mechanisms are possible. For adsorbents presenting mostly porosity of diameter below 3 nm, the main mechanism is the so-called surface diffusion, whose coefficient can be expressed as a function of temperature, as reported by Ruthven, 1984:

$$\delta_{intra} = \delta_0 \cdot \mathrm{e}^{E_a/R/T_a} \tag{4.51}$$

	Adsorption	Desorption
Evaporator/Condenser Temperature	10 °C	38.8 °C
Evaporator/Condenser Pressure	1166 Pa	6283 Pa
HTF Inlet Temperature	25 °C	90 °C
Minimum HTF Temperature Change	10 °C	10 °C

Table 4.6: Boundary conditions used for the case study.

With respect to the original model described in Chapter 3, the heat and mass balances, as discussed above, are completed by the transport term, simplified excluding the vapour phase contributions and solved together with the granular media heat and mass transfer.

4.3.4 Results and Discussion

Case study: a residential heat pump with silica gel

As a proof of concept of the capability of both the reactor and the model, it was decided to investigate the performance of a reactor designed for heat pumping using silica gel beads. The choice of the material is completely arbitrary and motivated by the wide availability of data regarding the material and also heat pump designs integrating it. The working pair is RD Silica Gel from Fuji Davison as adsorbent and water as adsorbate. The fact that the adsorbent is commercially available in different mesh sizes and the fact that the material presents a very broad adsorption peak, make it an ideal candidate for the first exploration of the potential of the heat transformer concept. Moreover, the lumped-parameter modelling concept at the particle level was previously validated for such materials, which minimizes the potential sources of inaccuracies. As for the material properties, the ones reported in Section 3.4 were used.

As for the application, the temperatures of the heat transfer fluids and of the adsorbate during adsorption and desorption were chosen to represent a low-temperature residential heating system, coupled with solar thermal collectors or other low-grade energy sources, and geothermal heat exchangers. The corresponding boundary conditions for the simulations are gathered in Table 4.6. The pressures of the diffusing jacket are chosen on purpose safely below the saturation pressure of the evaporator/condenser, to avoid phase change problems during the simulations that could inadvertently affect the results.

The optimal design of the adsorption reactor depends on the objective function, which is related to the application, and on a very high number of geometrical and operational parameters, even without considering multiple options for the adsorbent material. Given the common limiting factors found in adsorption heat pumps, it was decided to define the objective function OBJ as the product of the thermal Coefficient of Performance COP and the Specific Heating Power SHP:

$$OBJ = COP \cdot SHP \tag{4.52}$$

$$COP = \frac{Q_{con} + Q_{htf_{ads}}}{Q_{htf_{des}}} \tag{4.53}$$

$$Q_{con} = \dot{m}_a \cdot (w_{ads}(L_{ads}, \infty) - w_{des}(L_{des}, \infty)) \cdot H_{con} \tag{4.54}$$

$$Q_{htf_{ads}} = \dot{m}_{htf_{ads}} \cdot c_{htf} \cdot \left(T_{htf_{ads}}(L_{ads}, \infty) - T_{htf_{ads_{inlet}}} \right) \tag{4.55}$$

$$Q_{htf_{des}} = \dot{m}_{htf_{des}} \cdot c_{htf} \cdot \left(T_{htf_{des_{inlet}}} - T_{htf_{des}}(L_{des}, \infty) \right) \tag{4.56}$$

$$SHP = \frac{Q_{con} + Q_{htf_{ads}}}{m_{a_p} \cdot N_p} \tag{4.57}$$

Where the latent heat of condensation is fixed as $H_{con} = 2.413e6 J/kg$. Another performance indicator that can be helpful as a term of comparison with alternative heat transformers is the volumetric heating power VHP of the reactor. It can be calculated based on the SHP:

$$VHP = SHP \cdot \rho_{a_{tap}} \cdot f_p \tag{4.58}$$

The parameters available for the design are many, including the number of discretized sections (influencing the degree of mixing), the length, the pitch, the frequency, the diameters of the annulus, of the tube and of the fins, the thickness of the metallic components, the heat transfer fluid mass flow rate, the diameter of the adsorbent particles, the choice of the heat transfer fluid and of the metallic material. For the case study, most of these parameters were fixed arbitrarily based on experience to simplify the analysis and are gathered in Table 4.7.

The chosen design for the case study was determined by optimizing the length and the heat

Parameter	**Symbol**	**Value**
Number of sections	N	20
Annulus diameter	D_{an}	0 m
Tube diameter	D_{inner}	0.005 m
Fins diameter	D_o	0.025 m
Screw pitch	p	0.02 m
Rotational frequency	ϕ	0.5 Hz
Tube thickness	t_t	0.001 m
Fins thickness	t_f	0.0025 m
Adsorbent diameter	D_p	0.001 m
Heat transfer fluids		Water
Metals		Copper

Table 4.7: Simulation parameters and choices used for the preliminary design of the case study.

transfer fluid mass flow rate for both adsorption and desorption reactors, amounting to four parameters. This is a pretty simple design problem, but it could be easily extended to include more parameters in commercial designs. The results of this design are reactor lengths of 0.274 m and 0.233 m and heat transfer fluid mass flow rates of 2.04 g/s and 2.12 g/s, for the adsorption and desorption stages respectively. The so-obtained profiles of adsorbate loading and of adsorbent and heat transfer fluid temperatures are reported in Figure 4.12.

This design is characterized by a COP of 1.52, an SHP of 807 W/kg and a VHP of 546 kW/m^3. As the power density is more affected than the energy efficiency by the selected design parameters, the best solution tends to be close to the one satisfying the temperature change constraints in the heat transfer fluid with the minimum length. Therefore the reactors are rather short and do not allow for full usage of the material. The reason for this is immediately clear from the comparison between the adsorption rate and the heating and cooling rate in the adsorbent material: while the heat transfer rate is very high, the mass diffusion rate is limiting the speed of the process. This means that the reactor is unbalanced and it is not fully exploiting the potential of the screw conveyor design. This is evident from the low energy efficiency but the high power density achieved. This also means that the power output will be less affected by changes in the heat transfer coefficient, but more affected by changes in the mass transfer dynamics.

The mass flow rate of the adsorbent is 0.505 g/s and its residence time is 338 s, of which 182 s is dedicated to the adsorption reaction. During steady-state operation, all the parasitic energy losses due to the change in temperature of the heat exchanger are eliminated. However, the adsorbent leaves the desorption reactor at a high temperature, and this energy is partly recovered in the adsorption reactor as sensible heat provided to the heat transfer fluid, but partly it is lost due to re-desorption in the first part of the adsorption reactor. The opposite happens between the adsorption and desorption reactor when the material has to re-adsorb vapour at the entrance of the desorption reactor. Except for the difference in the first part of

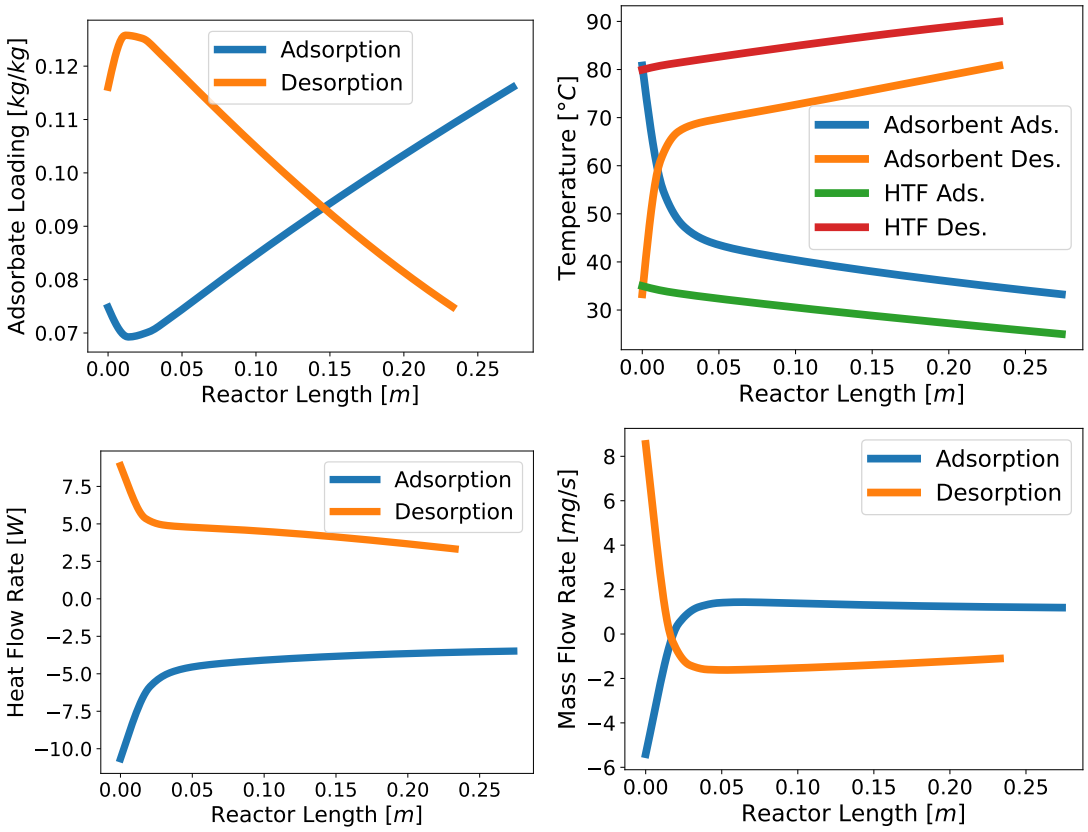

Figure 4.12: Results of the preliminary design for the case study after reaching steady state. On the top left, is the adsorbate loading along the reactor. On the top right, are the temperatures of the adsorbent and of the heat transfer fluid along the reactor. On the bottom left, is the adsorbate heat flow rate along the reactor. On the bottom right, is the adsorbate mass flow rate along the reactor.

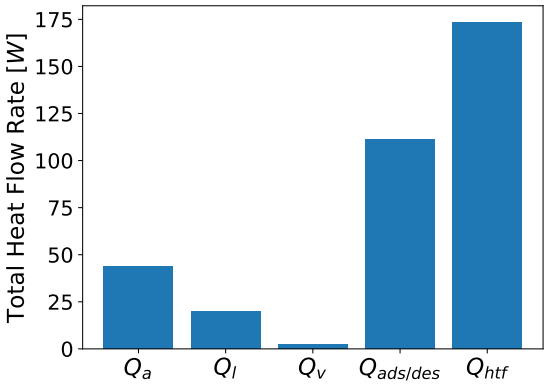

Figure 4.13: Global heat balance of the preliminary design for the case study. Each component is obtained as the sum of the absolute values of the heat flow rates over the whole reactors of both adsorption and desorption. Q_a is the sensible heat of the solid adsorbent, Q_l is the sensible heat of the adsorbed phase, Q_v is the sensible heat of all the vapour phases, $Q_{ads/des}$ is the heat of ad/desorption, and Q_{htf} is the sensible heat of the heat transfer fluid. Most of the heat exchanged by the heat transfer fluid is devoted to the heat of sorption.

the reactor, thanks to the counter-flow configuration the whole length of it is used fairly well, as Figure 4.12 shows.

As for the distribution of the heat flow rates to the different components of the energy balance, Figure 4.13 shows that most of the heat exchanged between the adsorbent and the heat transfer fluid is due to the heat of ad/desorption. The rest is mainly distributed between the sensible heat of the solid phase and of the adsorbed phase. The heat exchanged with the vapour phases (here summed together) is considered negligible, which justifies the simplification of the model proposed above.

The operational parameters

To investigate the importance of the flow configuration, the same design was simulated under co-flow conditions. As reported in Figure 4.14, the temperature change in the heat transfer fluid does not respect the requirements, as they are limited to only about 8 $°C$. The overall performance is also diminished by 19%, as the COP decreases slightly to 1.5 and the SHP decreases greatly to 661 W/kg. From Figure 4.14 it is also evident that the material is used less and that the second half of the reactors contribute only a minor part of the heat transformation.

When the rotational frequency is decreased, we can observe a very strong decrease in the performance, mostly determined by a reduction in power density as shown in Figure 4.15. For increased rotational frequency, only a moderate improvement is observed. However, only solutions with a higher coefficient of performance with respect to the preliminary design can achieve the required temperature lift. These results highlight the relevance of the rotational frequency to modulating the power and optimising the design. For example, if a

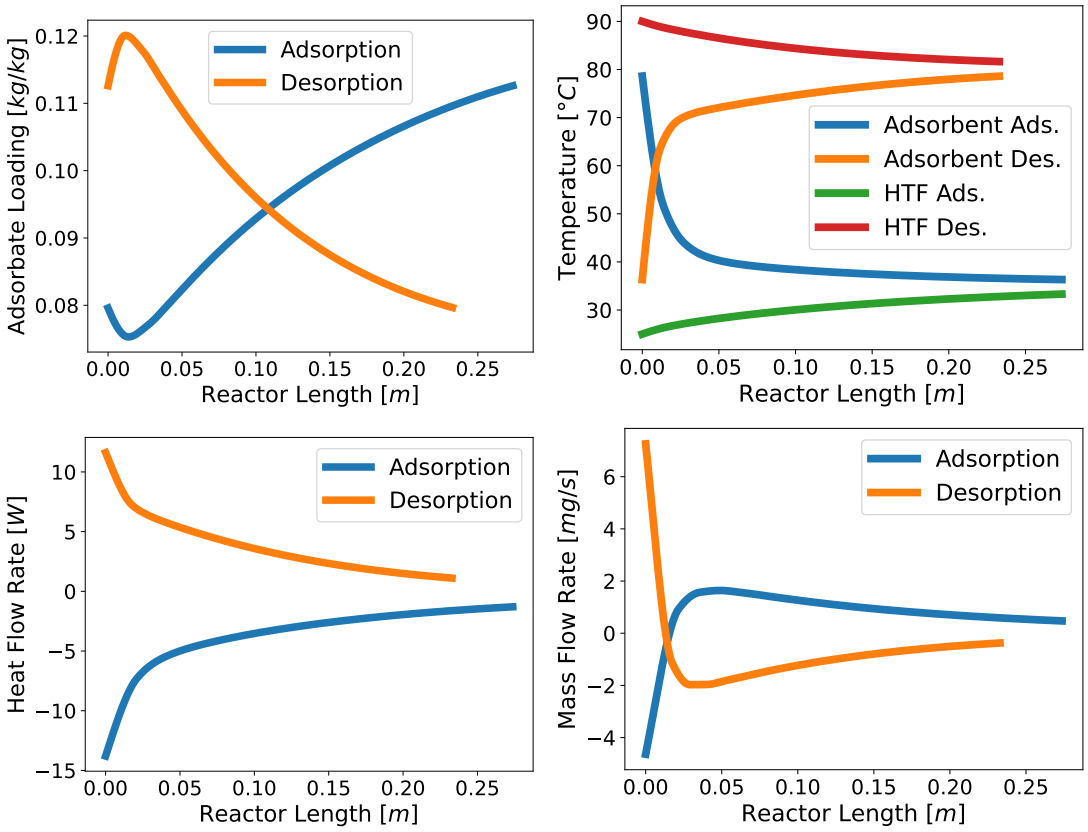

Figure 4.14: Results of the preliminary design in the co-flow configuration after reaching steady state. On the top left, is the adsorbate loading along the reactor. On the top right, are the temperatures of the adsorbent and of the heat transfer fluid along the reactor. On the bottom left, is the adsorbate heat flow rate along the reactor. On the bottom right, is the adsorbate mass flow rate along the reactor. The reactor is used in a less homogeneous way and the material is less exploited.

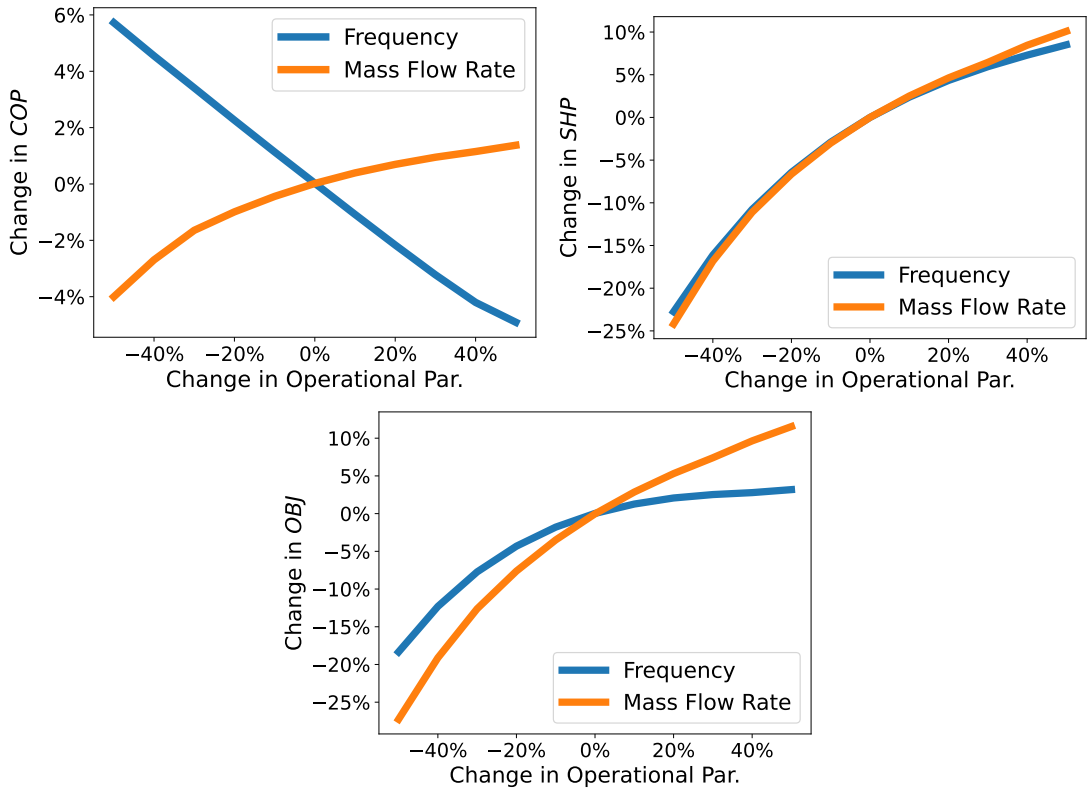

Figure 4.15: Influence of the rotational frequency and heat transfer fluid mass flow rate over the reactor performance. On the top left, is the variation of the COP. In the top right, is the variation of the SHP. On the bottom, is the variation of the OBJ. Both mechanisms offer power regulation capacity below the nominal power requirements, the frequency with a gain of efficiency.

lower temperature lift is required, this could be achieved by decreasing the frequency and gaining something in terms of efficiency. However, an experimental analysis would have to be carried out to evaluate the mechanical stability and power consumption in different cases. The modulation of the mass flow rate of the heat transfer fluid has a similar but stronger effect on the performance, as the energy efficiency, in this case, is (still moderately) influenced in the same direction as the power density. However, also in this case moving toward higher power, and increasing the mass flow rate, violates the constraint on the temperature change of the heat transfer fluid.

The geometrical parameters

To evaluate which geometrical parameters are most likely to influence the performance of the reactor in the vicinity of the preliminary design, a one-at-the-time variation of most of those parameters was simulated. It should be noted how in the adsorption and desorption reactor those parameters should be optimized separately, as demonstrated by the differences found

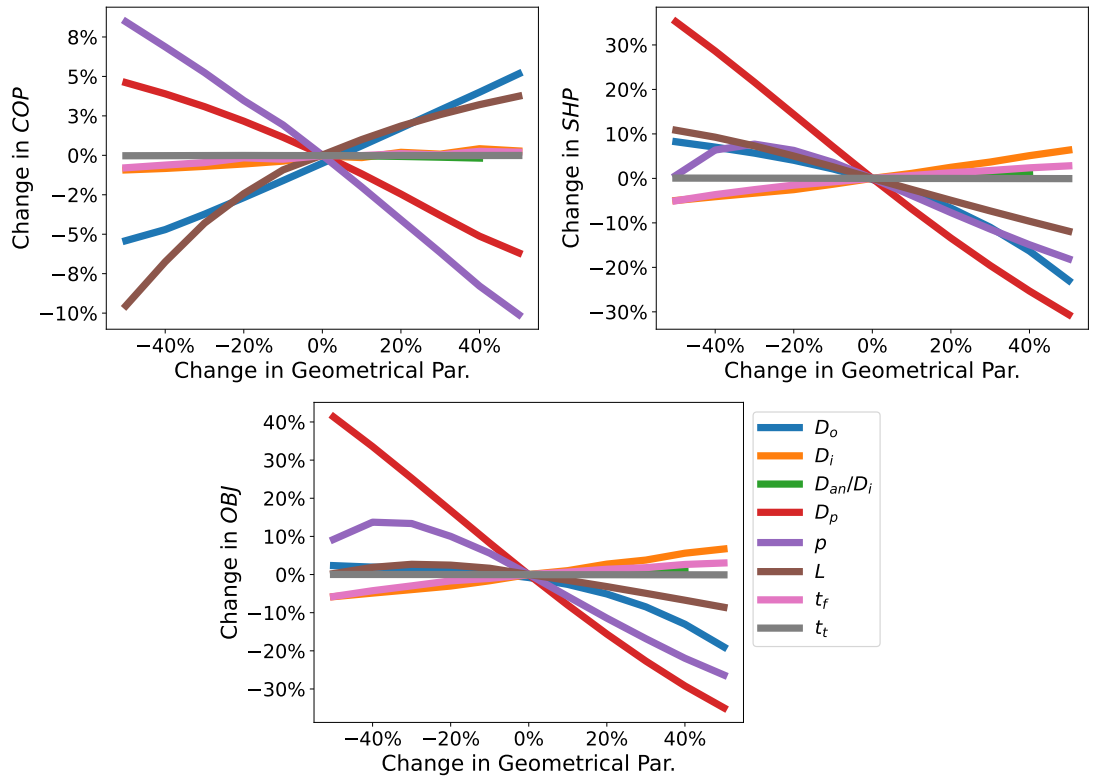

Figure 4.16: Influence of the geometrical parameters over the reactor performance. On the top left, is the variation of the COP. In the top right, is the variation of the SHP. On the bottom, is the variation of the OBJ. The most relevant parameters among the ones fixed a priori are the particle size and the pitch distance, at least in this case study.

in the preliminary design (with the desorption reactor shorter and more powerful than the adsorption one). Nonetheless, even their joint variation guarantees to capture the relative magnitude of the performance variation. The results are gathered in Figure 4.16.

The first thing that can be noticed is that the influence of the geometrical parameters on the COP is three times smaller than the influence on the SHP. This is important and depends on the fact that most of the heat in the energy balance is dedicated to the heat of adsorption. Therefore, within certain limits, the less water is cycled between adsorption and desorption, the smaller the energy requirement (as one can appreciate in Figure 4.13).

The second most evident observation is that the adsorbent particle diameter has the most prominent influence on the reactor performance. This should be expected, as it was already observed from Figure 4.12 that the mass diffusion was limiting the rate of the adsorption. As the mass diffusion rate is inversely proportional to the particle size, it would be expected that by decreasing its diameter great improvements in the kinetics can be achieved.

Other important parameters that should be investigated to achieve an optimal design are the pitch distance and the diameters of the fins and of the shaft. In the current design area, the

presence of an annulus in the shaft does not bring significant advantages, as the heat transfer rate on the fluid side is not limiting the process. The length of the reactor does not seem to be as important as other parameters. One of the reasons behind this is that they were previously optimized, and therefore we probably are in a good range already. An increased fin thickness plays a role in increasing the heat transfer in the granular media by increasing the efficiency of the fins. The thermal resistance of the tube, instead, is so small that its modification does not cause any observable difference.

4.3.5 Conclusions

In this section, we introduced the concept of agitated reactors to the field of adsorption energy transformation as an alternative route to increase material usage, energy efficiency and power density. In particular, for continuous applications such as heat pumping, screw-conveyor heat exchangers are identified as promising for eliminating the majority of the parasitic energy losses.

After introducing the concept and discussing the possible benefits and challenges, a discretized Eulerian heat and mass transfer model was proposed to describe its behaviour. The model described the most relevant heat and mass transfer processes at various scales (i.e. the whole reactor, the granular media and the adsorbent particles) simplifying the analysis wherever possible.

The preliminary design of a heat pump using silica gel beads was used as a case study to demonstrate the capability of the model. Geometrical and operational parameters can be investigated and optimized. In the particular case under examination, it seems to be possible to achieve relatively high energy efficiency and power density, even if the silica gel is not the most thermodynamically attractive material (i.e. limited cycling capacity and quasi-linear adsorption curve).

Our results indicate that the heat transfer is greatly improved with respect to fixed bed configuration, and that particle sizes below 1 mm should be ideally used to reduce the mass diffusion resistance that is limiting the adsorption rate. The possibility of counter-flow configuration increases the performance by ≈20%, and the regulation of the mass flow rates of the heat transfer fluid and of the adsorbent allows for power regulation.

In conclusion, the results seem to confirm the interest in investigating further the reactor concept, possibly also for other applications where heat and mass transfer are both important (e.g. temperature swing gas separation). To continue in that direction, an experimental apparatus would be fundamental. With a dedicated setup, it would be possible to test the model and modify it accordingly. Moreover, it would highlight potential problems related to the practical use of moving parts. The design of this reactor is deemed possible with more detailed simulation techniques, including 2D/3D CFD models, as already done in literature for studies without adsorption.

On the material side, the mechanical resistance of granular adsorbents should be tested and improved if necessary for the relevant application. This would be a new and challenging task for material developers, requiring new characterization methods.

The presence of moving parts undermines one of the main advantages of adsorption systems when compared to absorption systems. However, the advantages of the absence of corrosion and the fast kinetics remain. Further studies should include a detailed comparison of the two alternatives.

4.3.6 Acknowledgments

This section was elaborated together with Ricardo Silva from Empa, Switzerland. Moreover, the authors acknowledge the contributions of Robert Weber by Empa, Switzerland, and Luca Baldini by ZHAW, Switzerland.

4.3.7 Nomenclature

Letters

Symbol	Meaning	Units
A	Area	m^2
c	Specific heat capacity	$J/kg/K$
C	Constant	
D	Diameter	m
d	Sectional	
E_a	Activation Energy	J/mol
f	factor	
g	Gap clearance	m
h	Convective heat transfer coeff.	$W/m^2/K$
H	Specific heat	J/kg
k	Thermal conductivity	$W/m/K$
L	Length	m
M	Molar weight of the adsorbate	g/mol
m	Mass	kg
$\dot{m}$	Mass flow rate	kg/s
N	Number	
p	Pitch length	m
p	Pressure	Pa
Q	Heat flow rate	W
R	Heat transfer resistance	$K/W/m^2$
r	Radius	m
t	Thickness	m
t	Time	s
T	Temperature	K
U	Global heat transfer coeff.	W/K
v	Axial velocity	m/s
V	Volume	m^3
w	Adsorbate loading	kg/kg
x	Position	m

Greek Letters

Symbol	Meaning	Units
δ	Diffusion coefficient	m^2/s
Δ	Difference	
ϵ	Porosity	
η	Efficiency	
γ	Gas concentration	kg/m^3
λ	Mean free path	m
ν	Kinematic viscosity	m^2/s
∂	Partial derivative	
ϕ	Frequency	Hz
Φ	Mass transfer resistance	s/m^3
ρ	Density	$kg/m3$
σ	Molecular diameter	m
τ	Residence time	s

Subscripts

Symbol	Meaning
0	Pre-exponential
a	Adsorbent
ads	Adsorption
an	Annulus
b	Boltzmann
bed	Bed
c	Contact point
con	Condensation
CS	Cross-sectional
des	Desorption
e	External
eff	Effective
eva	Evaporation
f	Fin
fo	Fouling
fr	Friction
g	Granular media
gas	Free gas
htf	Heat transfer fluid
inner	Inner/internal
inlet	Inlet
inter	Interparticle
intra	Intraparticle
l	Adsorbed adsorbate
m	Media
max	Maximum
o	Outer
p	Particle
rms	Root Mean Square
t	Tube
tap	Tap
tor	Tortuosity
tot	Total
vap	Vapour
vol	Volumetric

Acronyms

Symbol	Meaning
COP	Coefficient of Performance
FDM	Finite-Difference-Method
Nu	Nusselt number
OBJ	Objective function
Pr	Prandtl number
Re	Reynolds number
SHP	Specific Heating Power
VHP	Volumetric Heating Power

4.3.8 Neglected Terms in the Heat and Mass Balances

The mass flow rate of the intraparticle vapour and of the interparticle vapour could be calculated as follows:

$$\dot{m}_{vap_{intra}}(x,t) = \dot{m}_a \cdot \frac{m_{vap_p}(x,t)}{m_{a_p}} \tag{4.59}$$

$$\dot{m}_{vap_{inter}}(x,t) = \dot{m}_a \cdot \frac{\gamma_{inter}(x,t)}{\rho_{a_{tap}}} \cdot (1 - f_p) \tag{4.60}$$

The metallic mass of the screw conveyor heat exchanger was neglected in the heat balance of Equation 4.41. It would entail modifying Equation 4.41 in Equation 4.61 and adding Equation 4.62.

$$\frac{dm_{htf}}{dx} \cdot c_{htf} \cdot \frac{\partial T_{htf}(x,t)}{\partial t} = \frac{1}{(R_{htf} + R_{fo}) \cdot A} \cdot \left(T_t(x,t) - T_{htf}(x,t)\right) \cdot \frac{dA}{dx} + \dot{m}_{htf} \cdot c_{htf} \cdot \frac{\partial T_{htf}(x,t)}{\partial x} \tag{4.61}$$

$$\frac{dm_{t+f}}{dx} \cdot c_t(x,t) \cdot \frac{\partial T_t(x,t)}{\partial t} = \left(\frac{1}{(R_t + R_g) \cdot A} \cdot \left(T_{a_c}(x,t) - T_t(x,t)\right) - \frac{1}{(R_{htf} + R_{fo}) \cdot A} \cdot \left(T_t(x,t) - T_{htf}(x,t)\right)\right) \cdot \frac{dA}{dx} \tag{4.62}$$

In addition eq. 4.43 would have to be changed to reflect the heat flow from the screw conveyor rather than directly from the heat transfer fluid. Furthermore, to include the contributions of the vapour phase to the energy balance, some terms would have to be added on both sides:

$$\begin{aligned}
&\ldots \frac{\partial m_{vap_p}(x,t)}{\partial x} \cdot c_{vap_{intra}}(x,t) \cdot \frac{\partial T_a(x,t)}{\partial t} \cdot \frac{dN_p}{dx} = \\
&\ldots - \dot{m}_{vap_p}(x,t) \cdot c_{vap_{intra}}(x,t) \cdot \frac{\partial T_a(x,t)}{\partial x} - \\
&\frac{1}{(R_t + R_g) \cdot A} \cdot \left(T_{a_c}(x,t) - T_t(x,t)\right) \cdot \frac{dA}{dx} - U_{tot} \cdot \left(T_{htf}(x,t) - T_{a_c}(x,t)\right) \cdot \frac{dA}{dx} + \\
&\qquad \frac{\gamma_{inter}(x,t) - \gamma_{intra}(x,t)}{\Phi_{intra}(x,t)} \cdot \left(h_{vap_{inter}}(x,t) - h_{vap_{intra}}(x,t)\right) \cdot \frac{dN_p}{dx}
\end{aligned} \tag{4.63}$$

Moreover, the heat balance of the interparticle vapour phase would have to be added:

$$\begin{aligned}
&\frac{dm_a}{dx} \frac{\gamma_{inter}(x,t)}{\rho_{a_{tap}}} \cdot (1 - f_p) \cdot c_{vap_{inter}}(x,t) \frac{\partial T_e(x,t)}{\partial t} = \\
&- \frac{\dot{m}_a \cdot \gamma_{inter}(x,t)}{\rho_{a_{tap}}} \cdot (1 - f_p) \cdot c_{vap_{inter}}(x,t) \frac{\partial T_e(x,t)}{\partial x} + \dot{m}_{vap_e}(x,t) \cdot \left(h_{vap_e} - h_{vap_{inter}}(x,t)\right)
\end{aligned} \tag{4.64}$$

The mass balance of Equation 4.44, should also include more terms:

$$\begin{aligned}
&\ldots + \left(V_{vap_{intra}}(x,t) \cdot \frac{\partial \gamma_i(x,t)}{\partial t} - \gamma_{intra}(x,t) \cdot V_{a_p} \cdot \frac{\rho_{a_{tap}}}{\rho_l} \cdot \frac{\partial w(x,t)}{\partial t}\right) \cdot \frac{dN_p}{dx} = \\
&\qquad \ldots - \left(\dot{V}_{vap_i}(x,t) \cdot \frac{\partial \gamma_i(x,t)}{\partial x} - \gamma_i(x,t) \cdot \frac{\dot{m}_a}{\rho_l} \cdot \frac{\partial w(x,t)}{\partial x}\right)
\end{aligned} \tag{4.65}$$

Furthermore, the mass balance for the interparticle vapour phase should be added:

$$\frac{dV_{vap_{inter}}}{dx} \cdot \frac{\partial \gamma_{inter}(x,t)}{\partial t} = - \frac{\dot{m}_a \cdot \gamma_{inter}(x,t)}{\rho_{a_{tap}}} \cdot (1 - f_p) \cdot \frac{\partial \gamma_{inter}(x,t)}{\partial x} + \frac{\gamma_{e_{eff}} - \gamma_{inter}(x,t)}{\Phi_{inter}(x,t)} \cdot \frac{dN_p}{dx} \tag{4.66}$$

In this case, two state equations for the vapour phases would exist:

$$\gamma_e = \frac{M \cdot p_e}{T_e} \tag{4.67}$$

$$\gamma_{e_{eff}}(x,t) = \frac{M \cdot p_{e_{eff}}(x,t)}{T_e} \tag{4.68}$$

Due to the viscous fiction of the vapour flow through the adsorbent granular media, there could be a pressure drop with respect to the one provided by the diffusive jacket, which would mean that the effective gas concentration and pressure $\gamma_{e_{eff}}$ and $p_{e_{eff}}$, will be different from the ones provided as boundary condition γ_e and p_e.

The pressure drop due to friction Δp can be calculated as follows:

$$\Delta p(x,t) = |p_e - p_{e_{eff}}(x,t)| = f_{fr}(x,t) \cdot \gamma_{inter} \cdot v_{vap_{inter}}(x,t)^2 \cdot \left(\frac{D_o - D_{inner}}{6}\right) \tag{4.69}$$

$$f_{fr}(x,t) = \frac{172}{Re_{vap}(x,t)} + \frac{4.36}{Re_{vap}(x,t)^{0.12}} \tag{4.70}$$

$$Re_{vap}(x,t) = \frac{2 \cdot \gamma_{inter}(x,t) \cdot v_{vap_{inter}}(x,t) \cdot D_p}{3 \cdot \mu_{vap_{inter}}(x,t) \cdot f_p} \tag{4.71}$$

$$v_{vap_{inter}}(x,t) = \frac{\gamma_e - \gamma_{inter}(x,t)}{\Phi_{inter}(x,t) \cdot \gamma_{inter}(x,t) \cdot A_{CS_{vap}}} \cdot dN_p \tag{4.72}$$

$$A_{CS_{vap}} = \frac{\pi \cdot L \cdot (D_o - D_{inner})}{3 \cdot N} \tag{4.73}$$

To account for the diffusive resistance through the granular media, the following interparticle mass transfer Resistance should be added:

$$\Phi_{inter}(x,t) = \frac{N \cdot ln(D_o/D_{inner}) \cdot f_{tor}}{2 \cdot \pi \cdot L \cdot \delta_{gas}(x,t)} \tag{4.74}$$

The tortuosity factor f_{tor} can be calculated as proposed by Lanfrey et al., 2010.

$$f_{tor} = \frac{1.23 \cdot (1 - \epsilon_{bed})^{0.75}}{\epsilon_{bed}} \tag{4.75}$$

$$\epsilon_{bed} = \left(\frac{1}{\rho_{a_{tap}}} - \frac{1}{\rho_{a_{env}}} \right) \cdot \rho_{a_{tap}} \tag{4.76}$$

$$\delta_{gas}(x,t) = \frac{v_{rms}(x,t) \cdot \lambda(x,t)}{3} \tag{4.77}$$

$$v_{rms}(x,t) = \sqrt{\frac{3 \cdot R \cdot T_e}{M}} \tag{4.78}$$

$$\lambda(x,t) = \frac{C_b \cdot T_e}{\pi \cdot p_{inter} \cdot \sqrt{2} \cdot \sigma^2} \tag{4.79}$$

Where σ is the molecular diameter and M is the molar weight.

As it is possible to appreciate, the contributions of the vapour phases to the heat and mass transfer complicates considerably the formulation of the model. However, on the simulations performed on the design described in Section 4.3.4, their contribution is negligible. Therefore it was decided to exclude them for the sake of computational efficiency.

4.4 Towards the Optimal Integration of Adsorption Transformers in Thermal Processes and Systems

As discussed in Chapter 2, materials and adsorption systems could be designed harmoniously. To go a step forward from the pre-selection of materials from a library towards a more detailed design, more detailed models and tools including the realistic performance of adsorption heat transformers under different operational scenarios are required. In this section we propose an approach to move towards this direction, covering the main gaps to be addressed.

The characterization methods used in Chapter 3, or similar, could be used to provide the dynamically relevant properties, including heat conductivity and mass diffusivity, or their impedances.

As discussed amply in the literature, the model of adsorption heat transformers is a complex task, and researchers struggle to provide a modular description of the device. An approach similar to the one of Bau et al., 2017; Lanzerath et al., 2015 and Palomba et al., 2021 would allow the separate sizing and optimization of the various components. Currently, those models include the possibility of choosing adsorbers from a library. Even better would be to have a material-based description of the adsorber performance (on the line with what is described in this chapter). One key challenge to be overcome is the connection of such models to a wider library of material properties so that a wider exploration would be possible. Furthermore, ideally, the development of fully open-source libraries would be beneficial for the wider usability of the model. In particular, of great interest would be the integration with the adsorption equilibrium equations open databases (such as the ones by Engelpracht et al., 2020; Siderius, 2020).

One of the key decision-supporting information is the cost of a system. This topic is largely under-investigated and little information is known about the cost of adsorption systems. One interesting approach proposed by AL-Hasni et al., 2022 consists in decomposing the cost factors in manufacturing, adsorbent materials, and the rest of the materials (e.g. tubing etc.). They also propose to extrapolate the cost of manufacturing towards higher production scales, to explore the system feasibility under different scenarios. This would also make a more fair comparison between materials with different performances but also different production costs.

For a complete and significant system design, an objective function including capital and operational costs, as well as key performance indicators (energetic and exergetic performance, robustness under varying conditions, power density) should be defined.

A framework in which integrating different modelling environments for process design and optimization based on physical modelling already exists (see Palazzi et al., 2010). These tools are constantly improved and expanded to enhance their capability (e.g. by Yoo et al., 2015) and used to great avail. One gap preventing the use of such a framework for system optimization is the creation of a functional interface between the mentioned models (developed in Modelica) and a framework like the cited Osmose. Given the nonlinearity of the performance (and therefore of the cost) of adsorption systems, specific methods might have to be adopted, including performance mapping or dedicated master-slave computational architectures. Inspiration could be taken from the work of Wallerand et al., 2017.

4.4.1 Acknowledgments

The research pathway proposed in this section was imagined thanks to the fruitful discussions with Shihab Al-Hasni and Giulio Santori from the University of Edinburgh, United Kingdom, and with Eduardo Pina from EPFL, Switzerland.

4.5 Conclusions and Outlook

In this chapter, we presented two relevant examples of how a lumped-parameter approach to material modelling can be useful to develop improved adsorption heat transformation applications.

Despite the promising results, these are both examples of preliminary efforts supporting the early stages of material and heat exchanger development. More advanced stages would require additional modelling and simulation efforts and experimental activity for the validation of the results.

Tailored activated carbon for district heating and cooling could be produced, as the results show promising performance in reversible operation, including satisfactory energy efficiency and power density. However, its experimental performance should be compared with the predictions. Material integration issues such as shaping, glueing and thermal interfaces should be addressed. The tests should cover different operation modes comparable with the requirements of the substation operators.

The novel agitated reactor for adsorption heat transformation could be modelled and showed promising results in terms of material use and power density. Further developments include a more refined model accounting for the particle dynamics, mechanical characterization of promising adsorbents and the construction of an experimental setup.

Lastly, we proposed a pathway to the development of more attractive adsorption processes based on a full-scale integration of modelling and characterization techniques, which has the potential to decrease the impact of energy systems and produce energy and cost savings.

5 Post-Combustion Carbon Capture by Rapid Thermal Swing Adsorption: a Knowledge Transfer Opportunity

5.1 Introduction

The utilization of fossil fuels for energy conversion, clearing of forests, and manufacturing of products such as cement increased atmospheric CO_2 concentration and average global temperature. CO_2 sequestration or carbon capture and storage (CCS) addresses this challenge by storing captured CO_2 at the Gt-scale in geological formations, as described by Raza et al., 2019. Removal of CO_2 from ambient air, called direct air capture (DAC), contributes to "negative carbon emission", as reported by X. Shi et al., 2020. However, entropically DAC consumes five times more resources than the capture from 5-15% CO_2 point sources which are responsible for 60-80% CO_2 emissions. For this reason, it is important to reduce energy demand and the cost of point source CO_2 capture to attract industrial investment. Capture differs for thermal power plant CCS among oxy-combustion, chemical looping combustion, post-combustion and pre-combustion CO_2 capture (see Sifat and Haseli, 2019; Wilberforce et al., 2021. Among gas separation solutions, chemical and physisorption are prominent, thanks to their low energy consumption, as reported by Hussin and Aroua, 2020. For amine-based chemical absorption, a lot of progress was made in decreasing the regeneration energy for modulated amines, as reported by A. I. Osman et al., 2021, with this innovation extended to physisorption processes as well.

The efficiency of primary energy use is very low such that two-thirds are lost to waste heat. CO_2 point sources are mostly co-located with the rejection of low-grade waste heat but current gas separation technologies cannot use this abundant resource. Capture from point sources addresses >60% CO_2 emissions and when extended to renewable fuel power stations enables better and cheaper "negative carbon emission" scenarios. Rapid thermal swing adsorption (RTSA) in heat-driven heat pumps has focused on the use of data centre lowest-grade waste heat (see Ammann, Ruch, et al., 2019; Brunschwiler et al., 2009). Shorter regeneration times are enabled by the lowest thermal and mass transport resistances, developed as part of high-performance computer cooling and adsorption heat pumps. RTSA is thus the best technology to tap into this "free" resource and eliminate two weaknesses of the energy system at once:

emission of CO_2 and waste of heat.

Temperature swing adsorption (TSA) gas purification differs from separation because it removes diluted components («1%), leaving packed bed columns in production for a long i.e. the time for 100-10'000x of the column volume to pass, matches with regeneration time. For externally heated TSA the number of columns is large which renders capital cost high because the large thermal resistance of nanoporous adsorbents and the large column dimensions require hours to days for regeneration heat introduction. Steam heating introduces heat faster but "contaminates" adsorbed gas and corrodes water-sensitive sorbents. An additional TSA disadvantage is a large resistance to the flue gas flow caused by the bed of beads requiring additional energy for air movers. All these problems cause TSA systems to require a large column inventory and trigger too large a capital cost.

Another technology for gas purification is pressure swing adsorption (PSA) where the regeneration is triggered with a pressure reduction, but gas flow limitations also apply. PSA was revolutionized by the introduction of rapid pressure swing adsorption (RPSA) that massively reduces sorption and regeneration times. RPSA improves column capacity making it competitive in new applications including medical oxygen concentrators, but fast pressure changes need a lot of electrical energy. RPSA also triggered hierarchically structured sorbents that improve mass transport to cope with larger gas flows. The key is preferential paths for gas to move fast into the sorbents, minimizing slow diffusion. Because sorption energy is mostly small, efforts focused on increasing mass transport while thermal transport was neglected. Developments as in RPSA are needed to implement RTSA but with a much stronger focus on reducing thermal resistance. While this was successfully proven in the application of data centre cooling, the development of rapid materials and RTSA separation columns for CO_2 capture is still lacking. In this chapter, the basis for the advancement of RTSA CO_2 capture is laid down by characterizing better materials and structuring methods, for dynamic performance, and integration into CO_2 separation columns for post-combustion and other applications.

5.2 Materials

In the last decades, extensive efforts were taken to develop and characterize many classes of nanoporous materials for the separation of CO_2 through physical adsorption, due to faster kinetics when compared with traditional separation columns, as reported by Hedin et al., 2013. Microporous materials (pore size $\leq 2nm$) have been used because of their high specific surface area and pore volume. Among the amorphous materials, functionalized silica gels, polymers and activated carbons are promising at different CO_2 partial pressures (e.g. see Raganati et al., 2020; M. Saleh et al., 2015; Wurzbacher et al., 2011). Among the crystalline materials, the main research focus ranged from zeolites (e.g. see Merel et al., 2008) to MOFs and ZIFs (e.g. see Bahamon et al., 2018; Ben-Mansour and Qasem, 2018; R. Li et al., 2014; Subramanian Balashankar and Rajendran, 2019). Mesoporous materials (pore sizes up to 50 nm) were extensively investigated due to their capacity of hosting CO_2-capturing molecules.

A special effort was devoted to mesoporous silicas doped with amines (e.g. see Chen et al., 2017; Dhoke et al., 2020; W. Zhang et al., 2016). For this special class, the main interest is given by the high cycling capacity and selectivity of the amine groups hosted by the porous matrix, while the major challenge is given by anchoring high amounts of nitrogen per surface area in a hydrothermally stable way, able to resist thousands of cycles, as reported by Jacobs et al., 2021; L. Liu et al., 2020. A review of CO_2 adsorbing materials by Zeng et al., 2022 highlights how more material understanding and development are needed to ensure a successful industrial application of physisorption-based CO_2 capture. While selecting materials with the highest capacity and fast sorption kinetics is essential, it is not sufficient: additional efforts are needed on material integration into TSA systems to efficiently utilize the adsorbents. In a related field, DeWitt et al., 2018 found that structured sorbent contractors helped to improve kinetics including pressure drop, and external heat integration.

In this section, representatives of these material classes have been selected for investigation and comparison of their characteristics for RTSA. Key requisites were: small powder size to ensure good mechanical properties of coatings for AdHEX surfaces, market or in-house availability for fast industrial deployment, and promising performance of CO_2 capture in industrially relevant conditions. The materials analyzed include:

- Molecular sieve 13X (zeolite 13X) and Molecular sieve 5A (zeolite 5A) from Sigma-Aldrich
- Purmol 4ST (zeolite 4A) from Zeochem
- Zeobeads 50 NH2 from Zeochem (surface-modified amorphous silica)
- AQSOA-ZO2 (SAPO-34) and AQSOA-ZO1 (FAPO-5) from Mitsubishi Plastics
- Resorcinol-melamine-formaldehyde activated carbon (RMF AC) from Empa
- Spent coffee ground activated carbon (SCG AC)
- Chemically activated SCG AC counterparts SCG AC $ZnCl_2$ and SCG AC $CaCO_3$ from Empa
- Mesoporous silicas MCM-41 and SBA-15 from ACS Materials

The zeolites (13X, 5A and 4A and SAPO-34 and FAPO-5) and the functionalized silica were coated on the aluminium (Al) substrates following the 2-hydroxyethyl ether binder-based procedure reported by Ammann, Michel, and Ruch, 2019. SAPO-34 and Zeolite 13X samples were diced following the procedure by Ammann, Michel, Studart, et al., 2019, with 30 μm channels at 200 μm pitch. Mass and heat transport in zeolite 13X was co-optimized for thicknesses of 0.1-1 mm using magnetically aligned structures and neck formation between sorbent particles, as reported by Ammann, Ruch, et al., 2019. The adsorption rate enhancement was for the first time applied to Zeolite 13X coatings for CO_2. Depending on the stirring frequency used during the slurry preparation, the samples were named 13X M XX, where XX is the stirring

frequency (in rpm) divided by 100. The adhesion properties of zeolite 13X on Al were worse than for SAPO-34. To improve the mechanical stability of the coating, the magnetic alignment of the structuring process was performed at 313 K, so that the binder effect increased.

Resorcinol-melamine-formaldehyde activated carbons (RMF AC) were prepared following the procedure reported by Huber, Ruch, Hauert, Matam, et al., 2016. The so-obtained 3.1 mm thick monolith was glued to the Al substrate using Thermal Glue by EC360. After crushing RMF AC monoliths into a fine powder with particle size ≤ 200 μm, it was coated on the substrate following the approach described by Ammann, Michel, and Ruch, 2019. In one of the RMF AC coatings, 10% in mass of graphite nanoplatelets (Sigma-Aldrich) was added to the slurry to increase the thermal conductivity of the sample.

Spent coffee ground activated carbons (SCG AC) were prepared by pyrolysis and activation of the green body under CO_2 at 800 $^\circ C$. Given the coarse nature of the green body, the particle size of the AC worsened the coating uniformity and cohesion compared to other finer powders. When only its finer fraction – with a particle size ≤ 200 μm was used for activation, it showed better mechanical properties. As an alternative to physical activation, SCG AC was prepared by chemical activation under N_2. In one case, the SCG was impregnated with a solution of $ZnCl_2$ in water. In the second case, the SCG was thoroughly mixed with $CaCO_3$ powder, and the solid mixture was pyrolyzed as is. As for the rest of the coatings, the powder was integrated on the metallic substrates following the approach described by Ammann, Michel, and Ruch, 2019.

Mesoporous silicas MCM-41 and SBA-15 were impregnated with polyethyleneimine (PEI) (nb20=1.5240, d=1.050, Mw=800, Mn=600, Sigma-Aldrich) following the methods reported by Sanz et al., 2010; Xu et al., 2002. Depending on their composition, the impregnated powders are named adding the ending PEI-XX, where XX is the PEI mass percentage over the sum of the masses. Successively, the adsorbent coatings have been prepared following the 2-hydroxyethyl ether binder-based procedure described by Ammann, Michel, and Ruch, 2019. However, due to the variable density of the adsorbent powders, variations in the amount of binder were necessary, resulting in a binder content of 5- 25%.

For the magnetically aligned 13X coatings, the observed adhesion properties of the slurry were worst with respect to the ones observed for the SAPO-34 slurry. While for certain recipes the adhesion was guaranteed, the results were unreliable. For this reason, an improved coating methodology was implemented:

- The Al substrates were sandblasted using silicon carbide (120 mesh, TdK, Germany) with a Glastar tool (pressure 3.5 bar, nozzle 3 mm, distance 10 cm, time 3 s).
- After the degreasing step and before the application of the slurry, the substrate surface was activated by exposition to oxygen plasma for 60 s

After a first experience-based formulation of the 13X + ferrofluid slurry (10 g of 5% binder-

water solution, 6 g of adsorbent, 1.85 g of ferrofluid, 1.5 g of 5% PVA solution), a design of experiment over the coating parameters was attempted. In particular, a 2^{14-10} fractional factorial design including change in the composition of the slurry, time and strategy of mixing, thickness and magnetical alignment process parameters was defined and carried out to determine the most relevant factors. However, the adhesion properties were insufficient to correlate the factors to the coating performance. It is believed that the amount optimal of ferrofluid should be carefully investigated, as it strongly affects the adhesion properties of slurries of different viscosity. Mixing rotational frequency of 1000-1300 rpm produced the best pore formation performance. Also, further characterization and optimization are needed.

5.3 Experimental

Material research for carbon capture is hampered by the need for large amounts (kg) of adsorbents to build a gas separation column and the long duration of experiments. The most relevant material-related RTSA parameters are: (1) cycled mass, (2) mass transport resistance and kinetics for sorption and desorption, (3) thermal resistance, and (4) static and dynamic selectivity, parameters which have to be recorded for beads and 0.05-1 mm thick layers. Mass transport and thermal resistance increase with layer thickness, but thick layers maximize the active-to-dead mass ratio, reducing the sensible heat demand. In this work, two instruments were used to analyze small amounts of sorbents (1) dynamic vapour sorption (DVS) to assess equilibrium sorption (cycled mass) and sorption isotherms for pure gasses and gas mixtures, and (2) the Temperature Jump System (TJS) to assess cycled mass and sorption kinetics for the RTSA geometry. Established research tools for porous materials cannot accurately predict the performance in a PSA, TSA, or RTSA system and are not useful for directed material optimization research. DVS is a gravimetric technique to determine the gas loading on an adsorbent, in particular the adsorption capacity for pure gases, including H_2O and CO_2, as illustrated in the work by Thompson and Zones, 2020. In this work, a DVS Vacuum system (SMS, London, UK) was modified with a CO_2 source in addition to the water source so that it could be used to measure adsorption data of H_2O, CO_2, and their mixtures. The pressure ranges for CO_2 and H_2O were 25-800 $mbar$ and 5-70 $mbar$, respectively and the temperature was 298-368 K. By dosing CO_2 and H_2O in the adsorption chamber, many compositions were created but the change in composition during adsorption and desorption is not monitored, which means that exact adsorption capacities were not measured in case of displacement of one gas in favour of another. However, the different kinetics of H_2O and CO_2 can help in determining its scope. Due to the high reactivity of water with the adsorption sites, co-adsorption data were measured as follows: first, a water background pressure is established until equilibrium is reached; second, carbon dioxide is injected until a new equilibrium is reached. When the injection of CO_2 provokes a quick weight decrease and afterwards a slow increase, water might be displaced from the adsorption sites by CO_2. Figure 5.1 shows RMF AC losing some of the water adsorbed at 25 mbar, possibly being gradually replaced by CO_2 as its partial pressure increases. In case no fast desorption is observed, the CO_2 finds empty

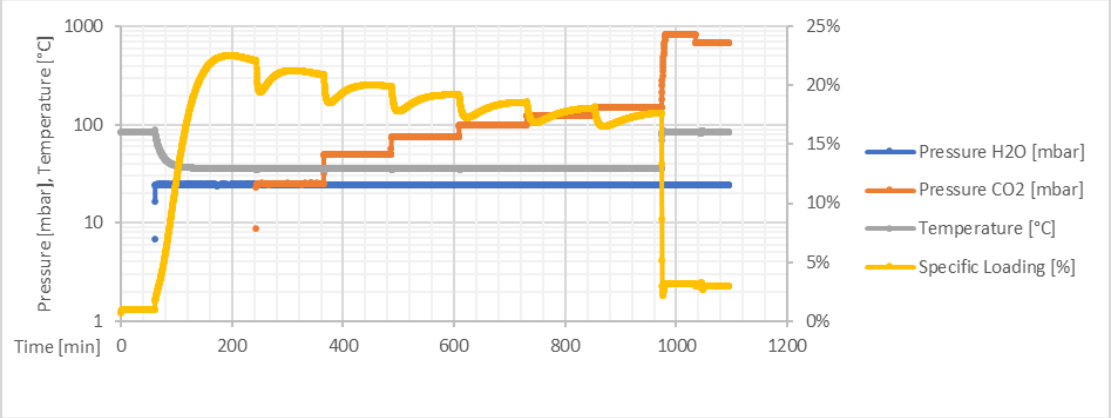

Figure 5.1: Example of co-adsorption experiment for RMF AC. Possible H_2O displacement in favour of CO_2 is visible after CO_2 pressure increments.

adsorption sites.

Single gas adsorption isotherms were measured separately to investigate more about the material characteristics. The isotherms were either interpolated or fitted, to feed multi-gas adsorption predictions obtained using the Ideal Adsorption Solution Theory, as explained by Simon et al., 2016. The so-obtained co-adsorption prediction is then compared to the multi-gas adsorption data.

The low speed of TSA is caused by "bad" heat and mass transport in large beds filled with 1-3 mm diameter sorbent beads. The increasing interest in efficient adsorption heat pumps (AdHP) and carbon capture (CC) triggered RTSA systems that reduce cycle duration from hours to minutes. Structured sorbents coated on adsorption heat exchangers (AdHEX) further reduce column inventories and capital costs. Knowledge of how to reduce thermal and mass transport resistances increases the use of low-grade waste or renewable heat for regeneration and accelerates RTSA development, as done by Ammann, Ruch, et al., 2019. Mass transport is characterized by gas diffusivity and permeability while heat transport is characterized by thermal diffusivity. For the characterization of co-joined mass and heat transport properties, large temperature jump (LTJ) systems trigger sorption cycles by temperature steps, as for example done by Graf et al., 2016. The resulting transient mass uptake and adsorbent temperature are fitted to a lumped-parameter model. Transport Impedance Analysis (TIA) can distinguish heat and mass transfer in fixed-bed configurations, but little is known about transport in adsorbent coatings.

Isochoric temperature step measurements were conducted in the TJS system having a 1.93 dm^3 chamber, CO_2, N_2, $H2_O$ sources, infrared (IR) camera and 6/2-way valve. The TJS implements an RTSA unit cell - a coated Al layer with 1 cm^2 sorbent coating placed on the microchannel heat exchanger (μHEX) using a thermal interface material resulting in a total fluid-adsorbent thermal resistance of 0.8 $K \cdot cm^2/W$. The interface resistance between the adsorbent and Al substrate is included as part of CC systems. The TJS temperature stability

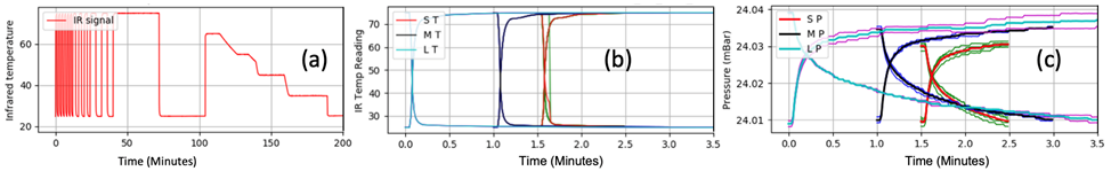

Figure 5.2: The TJS experimental procedure: (a) calibration; (b) data acquisition of temperature; (c) data acquisition of pressure.

Material	13X	5A	4A	13X aligned	AQSOA-ZO2	AQSOA-ZO1
Density (g/cm3)	0.8	0.8	0.8	0.9	0.9	0.9
Material	SCG AC	SCG AC ZnCl2	SCG AC CaCO3	MCM-41 PEI25	MCM-41 PEI40	SBA-15 PEI35
Density (g/cm3)	0.3	0.3	0.3	0.4	0.4	0.3
Material	RMF AC monolithic	RMF AC	SCG AC coarse	SBA-15 PEI40	MOF-303	Zeobeads
Density (g/cm3)	0.4	0.6	0.4	0.3	0.7	0.6

Table 5.1: Measured density for the coatings characterized in the TJS.

was improved by thermally decoupling the μHEX from the chamber and the accuracy of IR thermography was improved by an aperture that blocks stray radiation. A vacuum-tight chamber with three precision pressure sensor gauges (Ceravac Transmitter CTR100N, 20 and 100 Torr, CTR 1000N 1000 Torr, Balzers) was used to determine adsorbed and free gas mass at respective pressure ranges. The IR signal was periodically calibrated using equilibrium measurements at 65, 55, 45, 35 and 25 $^{\circ}C$ (see Figure 5.2a). Upon reaching equilibrium the adsorbent surface IR signal was associated with $T_{\mu HEX}$. A calibration for T_{max} and T_{min} after each measurement was necessary since the IR signal includes reflected radiation. The maximum 75 $^{\circ}C$ and minimum 25 $^{\circ}C$ temperatures were calibrated during consecutive 2x32 minutes. The accuracy is improved by averaging five 1-minute, three 2-minute, and two 4-minute swings (see Figure 5.2b) while recording the IR signal and pressure at 1-second intervals. The Al substrates coated with the adsorbent were characterized in terms of covered surface and thickness to calculate the coating volume, and their weight was recorded before and after removing the coating from the substrate to calculate the mass. Coating densities varied between 0.3 and 0.9 g/cm^3, as reported in Table 5.1.

5.4 Results

5.4.1 Equilibrium Adsorption

Adsorbent coatings were evaluated for post-combustion CC from flue gases through RTSA with a majority composition of ≈ 800 $mbar\ N_2$, 100 $mbar\ CO_2$, 50 $mbar\ H_2O$ and 50 $mbar\ O_2$, and a minimum temperature of 308-313 K. While high N_2 concentration reduces CO_2 capture capacity, the presence of water is more detrimental, as reported by Thompson and Zones, 2020. For this reason, DVS experiments focused on measuring CO_2 working capacity (CO_2 loading at adsorption conditions – CO_2 loading at desorption conditions) and purity (CO_2 fraction of all the desorbed gas) for adsorption conditions of 100 $mbar\ CO_2$ + 50 $mbar\ H_2O$

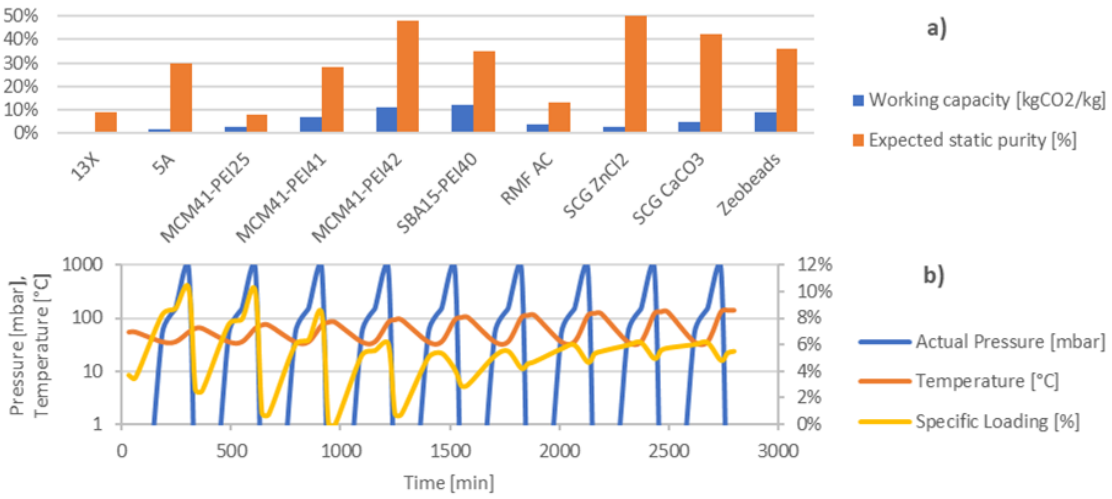

Figure 5.3: (a) Working Capacity and expected gas purity from DVS equilibrium measurements for several materials for realistic conditions (adsorption at 100 $mbar$ CO_2+50 $mbar$ H_2O and desorption at 800 $mbar$). (b) Pure CO_2 adsorption after regeneration at increasingly higher temperatures for MCM41-PEI40. After the water (initially about 4% in weight) is completely displaced, the CO_2 is chemically adsorbed on the impregnated material and the cycling cap.

at 313 K and desorption conditions of 750 $mbar$ CO2 + 50 $mbar$ H2O at 368K. (Figure 5.3a). Under static conditions, no material showed sufficient selectivity, and the expected gas purity obtained using the maximum working capacity is 10 to 50%. Cycled mass was interesting only for impregnated materials (>10%) and less so for functionalized silica and activated carbons (>5%). Zeolites performed poorly.

As part of a measurement campaign, it was noticed that the main driver for capacity and selectivity is the strength of the bonds with water and the adsorbate competition. In zeolites the sites are preferentially occupied by H_2O, therefore limiting the CO_2 cycling capacity. For materials with a smaller water affinity, water enhances the CO_2 adsorption properties while compromising purity, as reported in Table 5.2. However, the mixture formed between H_2O and CO_2 in the pore space makes estimates of the desorbed gas purity less reliable, requiring further research. In the pores of activated carbons and functionalized silica, water seems to be similarly displaced by CO_2. Interestingly, these materials capture CO_2 better from a humid stream than zeolites, even though the total capacity of pure CO_2 of the former is inferior, as visible from adsorption isotherms in Figure 5.4. Given that the desorption of water requires higher regeneration temperatures, the purity of the degassed stream can be optimized by lowering regeneration temperatures to <90°C. This also offers advantages as more waste heat could be used. Therefore, a moderate CO_2 affinity might be beneficial for future material development. For impregnated materials, especially for MCM41, hydrothermal stability over multiple cycles seems problematic (see Figure 5.3b).

From DVS measurements it seems that the adsorption capacity is seriously compromised by the presence of water, while for the other materials, the situation is slightly better, and

p water	SBA15-PEI40	RMF AC	Zeobeads	MCM41-PEI40	SCG $ZnCl_2$	SCG $CaCO_3$
			Carbon dioxide cycled mass			
0 mbar	1-3%	0-3%	1-3%		0-1%	0-1%
6 mbar	2-3%	0-2%	2-3%		0-1%	0-1%
12 mbar	4-6%	1-3%	2-3%	1-3%	0-1%	0-1%
25 mbar	5-10%	2-6 %	2-4%		0-2%	0-2%
50 mbar		1-6%	4-11%	4-7%	2-7%	2-12%
			Carbon dioxide purity			
0 mbar	100%	100%	100%		0-100%	0-100%
6 mbar	100%	100%	67-75%		0-50%	0-50%
12 mbar	100%	50-75%	50-67%	100%	0-33%	0-33%
25 mbar	50-100%	11-40%	33-50%		0-50%	0-40%
50 mbar		3-16%	18-48%	20-35%	20-87%	20-100%

Table 5.2: CO_2 performance for moderately hydrophilic materials under adsorption conditions 25-150 $mbar$ CO_2 at 35 $^{\circ}C$ and desorption at 90 $^{\circ}C$ as deduced by DVS. Variations for each H_2O background pressure are mainly due to water displacement.

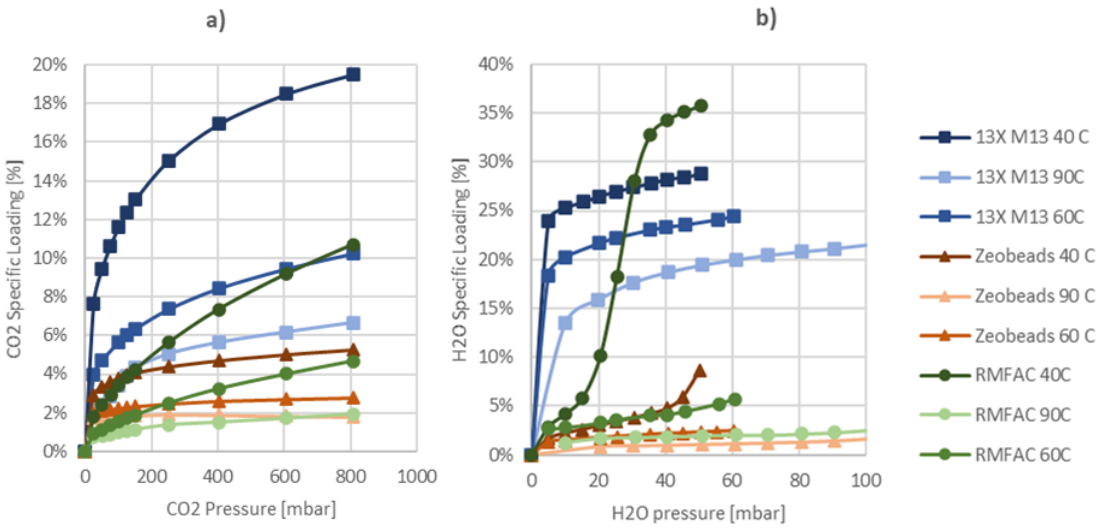

Figure 5.4: CO_2 and H_2O isotherms at 40, 60 and 90 $^{\circ}C$ for selected materials: Zeolite 13X M13, Zeobeads, and RMF AC.

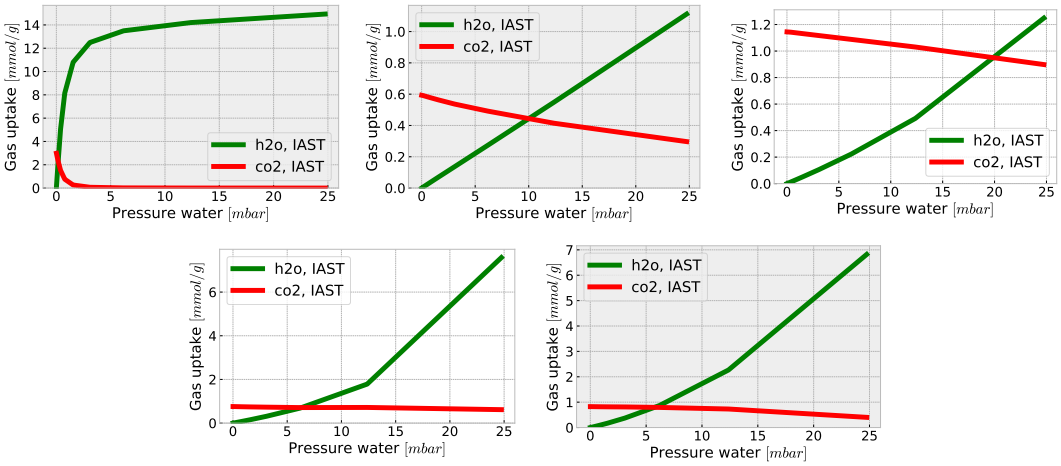

Figure 5.5: Co-adsorption of CO_2 and H_2O as it would be predicted by the IAST model. The temperature and the CO_2 pressure are constant and equal to 313 K and 150 $mbar$. In order, from top to bottom and from left to right: Zeoite 13X; Zeobeads, SBA15-PEI40, RMF AC, SCG AC. Moderately hydrophilic materials would require a less stringent dehumidification stage.

some water displacement might occur. The single-gas isotherms were also used to predict the multi-gas adsorption isotherms according to the IAST model for a better interpretation of the DVS results, as shown in Figure 5.5. Of course, better models to describe multi-component adsorption exist (see Yun et al., 1996), but the simple application of IAST is of great advantage for the scope of the work. The interpolation and the predictions were performed using the Python library *pyiast* developed by Simon et al., 2016. In particular, the co-adsorption results were obtained by interpolation of the isotherms at 313K, to avoid biases deriving from the fitting model. It is important to remember that the IAST model can correctly be applied only in the case of physisorption. The predictions made for Zeobeads and, especially, for SBA15-PEI40 should not be considered accurate. They can rather be used to visualize the CO_2/H_2O selectivity of the materials. From these results, we can appreciate that, at low water pressures, the moderately hydrophilic materials could be used for CC with moderate energy expenditure. In particular, for a carbon dioxide pressure of 150 $mbar$, the activated carbons could accept water pressures above 5 $mbar$, while Zeobeads and SBA15-PEI40 up to 10-20 $mbar$, respectively. Getting to such low water pressures is still a challenge, but it gives at least a margin for engineering optimization.

It is interesting to compare the prediction of IAST to the results obtained from DVS, at least for the activated carbons, for which the model should be more accurate. To do so, the IAST predictions for RMF AC and SCG AC are plotted respectively in Figure 5.6 and 5.7, with the correction of the first point to eliminate noise for the sake of comparison. Analysing the results, the first conclusion is that the agreement between the experiments and IAST is quite good. However, at 25 $mbar$ of water pressure, IAST does a H_2O displacement in favour of CO_2 so high as observed indirectly in the DVS. There are several possible reasons to explain such a difference, including:

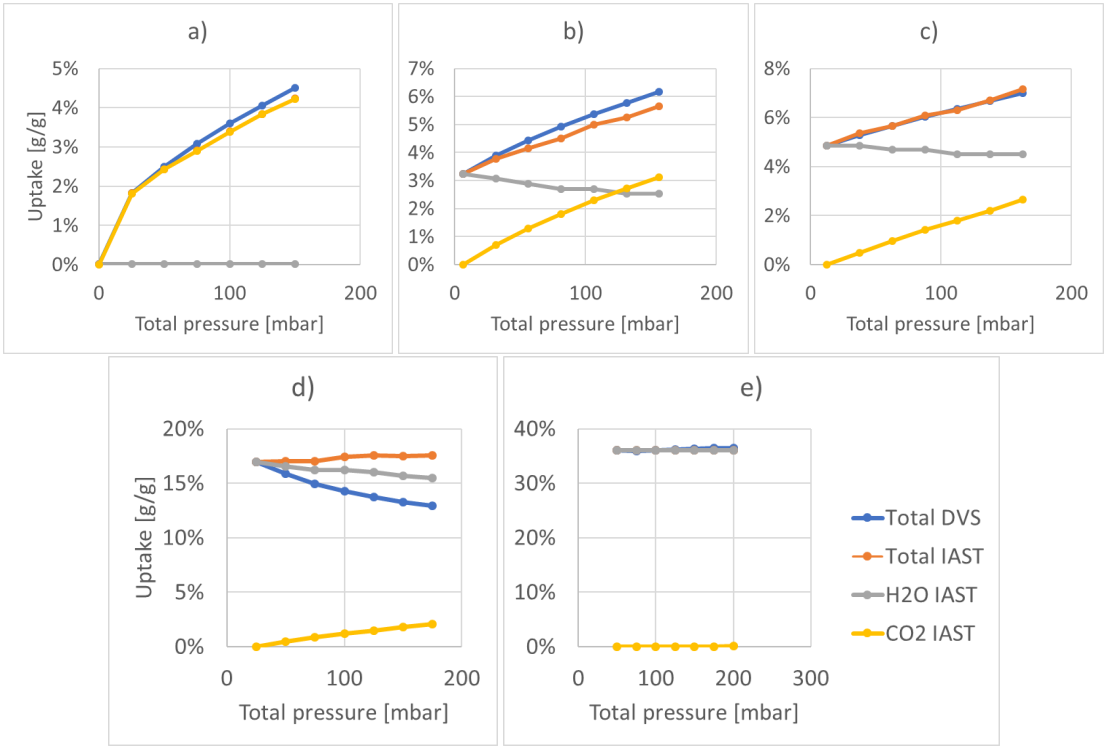

Figure 5.6: $CO_2 + H_2O$ adsorption equilibria obtained with DVS compared to IAST predictions for RMF AC. The background water pressure is: a) ≈0 $mbar$, b) 6.25 $mbar$, c) 12.5 $mbar$, d) 25 $mbar$, e) 50 $mbar$. The agreement is fairly good, but some of the observed water displacement could have been misinterpreted.

- inadequacy of IAST to the situation;
- experimental gravimetric inaccuracies;
- deviation between theoretical gas composition and real gas composition.

All the explanations are possible, and further experimental work, including monitoring of the gas composition, would be necessary to achieve a better understanding of the phenomenon. One option is to move away from purely gravimetric approaches to the characterization altogether, so that mass spectrometry is allowed. For example, breakthrough curves can be measured as reported by Gebald et al., 2013; G. Li et al., 2009, even though achieving a fine temperature control is still an issue.

5.4.2 Dynamic Adsorption

Measurements were conducted to evaluate materials with good properties for dry and wet flue gas conditions. The TJS system described by Ammann, Michel, and Ruch, 2019 was upgraded for better accuracy and fast material screening with a simplified process needing only 5,3,2

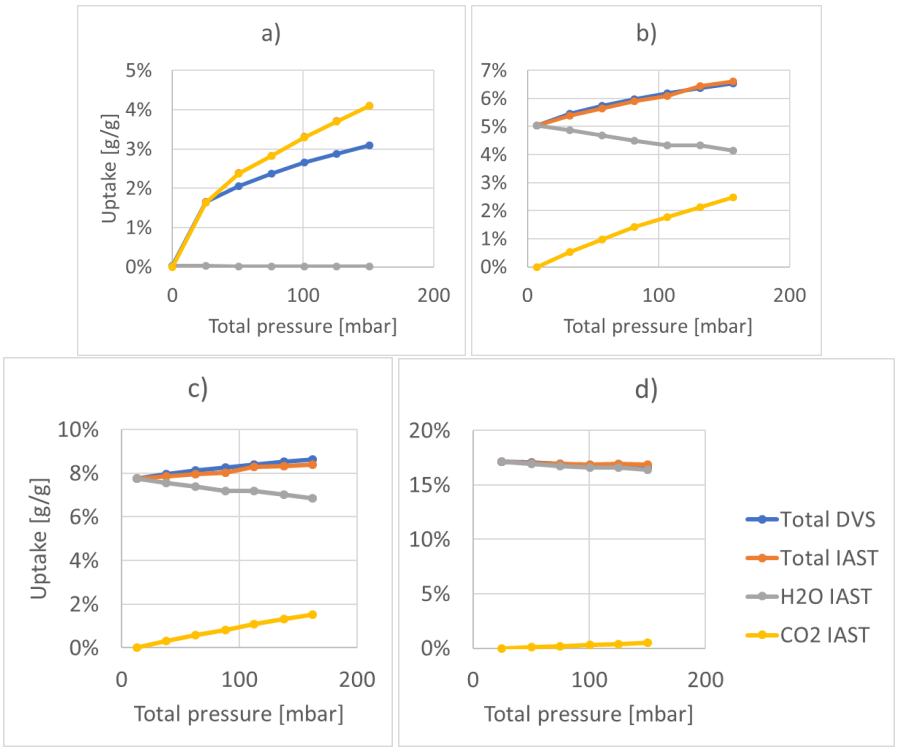

Figure 5.7: $CO_2 + H_2O$ adsorption equilibria obtained with DVS compared to IAST predictions for SCG AC. The background water pressure is: a) 0 $mbar$, b) 6.25 $mbar$, c) 12.5 $mbar$, d) 25 $mbar$.The agreement is fairly good, but only calibrating the mass such that there is a deviation on the pure CO_2 adsorption (at the limit of the experimental accuracy).

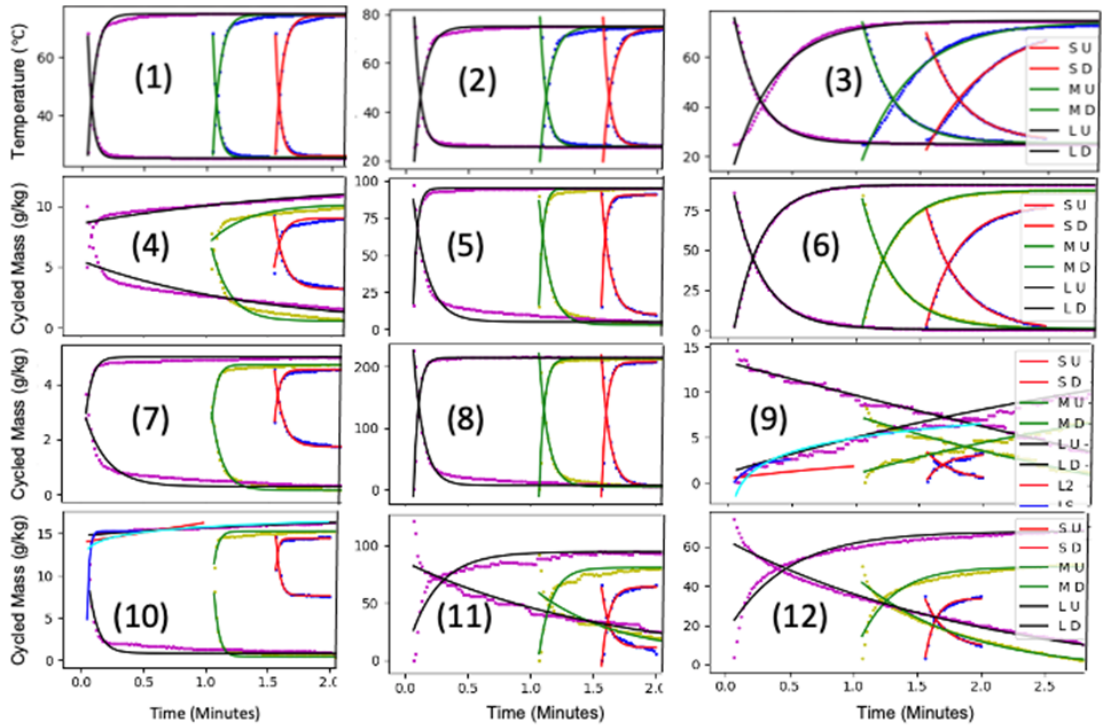

Figure 5.8: TJS temperature transients (1-3) and mass transients (4-12) with 1st order fits for 1 (red), 2 (green), and 4 (black) minute transients for the adsorption (falling t/p, rising adsorbed mass) and desorption (rising t/p, falling adsorbed mass). Materials measured are Zeolite X13 (1-9) with and without aligned pores, a carbonaceous material RMF AC (10), amine-impregnated silica carriers SBA15-PEI40 (11), and chemically-activated carbonaceous materials SCG AC $CaCO_3$. Cycled gas: 20 $mbar\ CO_2$ (4,5,10-12), 100 $mbar\ CO_2$ (7,8), 20 $mbar\ H_2O$ (3,6), and 100 $mbar\ N_2$ (9).

swings at 1,2,4 minute followed by 32-minute maximum and minimum steady states (see Figure 5.2). Mass and heat transfer on adsorbent coatings are characterized by the fitting of 1st order exponents to the averaged pressure and temperature transients. This allows a quantitative comparison of mass and heat transfer and reveals the limiting transport mode within <2 hours for one sample condition. Typically, pure gas properties were measured at 20, 100 $mbar\ CO_2$, 100 $mbar\ N_2$, and 20 $mbar\ H_2O$, as well as a first mixed gas result, was acquired for 100 $mbar\ N_2$ and 20 $mbar\ CO_2$. With this setup, one sample can be well characterized for one swing configuration during one day. Figure 5.8 shows twelve examples of measurements and 1st order fitting: for Zeolite 13X, 20 $mbar\ CO_2$ temperature (1), mass (4) and 100 $mbar\ CO_2$ mass (7); 100 $mbar\ N_2$, mass (9); 20 $mbar\ H_2O$ temperature (3), mass (6); Zeolite 13X with magnetically aligned pores 20 $mbar\ CO_2$, temperature (2), mass (5); 100 $mbar\ CO_2$, mass (8); RMF AC at 100 $mbar\ CO_2$ mass (10); SBA15-PEI40 at 100 $mbar\ CO_2$ mass (11); SCG AC $CaCO_3$ at 20 $mbar\ CO_2$ (12).

For Zeolite 13X at 20 $mbar$ we see a fast thermal transient that matches well with a 1st-order fit for 1-,2- and 4-minute swings for CO_2 sorption experiments (Figure 5.8 1, 2) but less for

water sorption experiments (Figure 5.8 3). The mass transients are more complex with a good 1st order fit for the short swing but more 2nd order components for the longer swings (Figure 5.8 4-12). This is in agreement with the general findings in the characterization of water adsorption dynamics reported by Y. I. Aristov, 2020. Since all analyses were done on short swings, the 2nd order components were neglected. Comparing zeolite 13X without (Figure 5.8 4) and with aligned pores (Figure 5.8 5) we see the faster kinetics and that the cycled mass is much larger for the 2 min cycle compared to longer cycles. This is due to better material usage in the latter thanks to improved kinetics. The water experiment shows the larger latent heat effect on the thermal transient (Figure 5.8 3) and the slower sorption (Figure 5.8 6) but larger cycled mass. This is also expected given the information gathered by DVS. Carbon dioxide adsorption experiments at 100 $mbar$ typically show twice larger cycled mass compared to the 20 $mbar$ experiments for both Zeolite 13X and Zeolite 13X M with aligned pores (Figure 5.8 7 and 8). Once again, this is in agreement with the expected adsorption capacity measured with DVS. Nitrogen adsorption at 100 $mbar$ is much smaller (coherently with literature data, e.g. by Merel et al., 2008) and not far away from the resolution limit of the pressure sensor (Figure 5.8 9) but the temperature transient is the same as for CO_2 sorption (Figure 5.8 1,2, not shown). This is expected as the heat of sorption plays a marginal contribution to the total thermal inertia of the system.

Figure 5.9 shows cycled mass per hour for different adsorbents: SAPO-34/FAPO-05/Silica gel (left), zeolites (second from left), carbonaceous materials (middle) and PEI-coated carrier materials (right) with CO_2 at 20 and 100 $mbar$, H_2O, and N_2. The vertical axis shows grams of cycled mass per hour and kilograms of adsorbent which is the relevant parameter for RTSA systems since it combines sorption capacity and speed. To display all gasses on the same graph, stretching factors were applied to 100 $mbar$ CO_2 (0.5), 20 $mbar$ H_2O (0.25), and 100 $mbar$ N_2 (50). Zeolite 13X with magnetically aligned pores shows very good performance (2235 $g_{CO_2}/kg/h$). A similar performance is reached by RMF (1978 $g_{CO_2}/kg/h$). SAPO-34 and other zeolites perform worse <100 $g_{CO_2}/kg/h$. Other carbonaceous materials also show low values <135 $g_{CO_2}/kg/h$. Nitrogen adsorption is low for all materials except for SCG which reaches 37 $g_{CO_2}/kg/h$. While Zeolite performs very well for pure CO_2, it shows lower values in presence of water because water competes for the sorption sites. This is different for carbonaceous materials and coated carrier materials. They show slightly lower pure gas CO_2 performance, but this performance is maintained in presence of water. The functionality that improves CO_2 sorption in presence of water is the PEI modification applied onto mesoporous carrier materials like MCM-41 and SBA-15.

Figure 5.9 shows a combined result of material properties and coating geometry (thickness, density and effective heat and mass transfer paths length). The thickness of the coatings is similar for all samples (0.5 - 0.6 mm), but changes in the rate of adsorption may affect effective adsorbent usage. Most of the adsorbents are limited by the mass transfer rate, but some of the magnetically aligned zeolites 13X M and the SBA15-based samples make an exception. In both cases, the reason is the presence of wider porosity in the coating, by structuring in the first case and by the intrinsic mesoporosity (up to 11 nm) in the latter. For samples

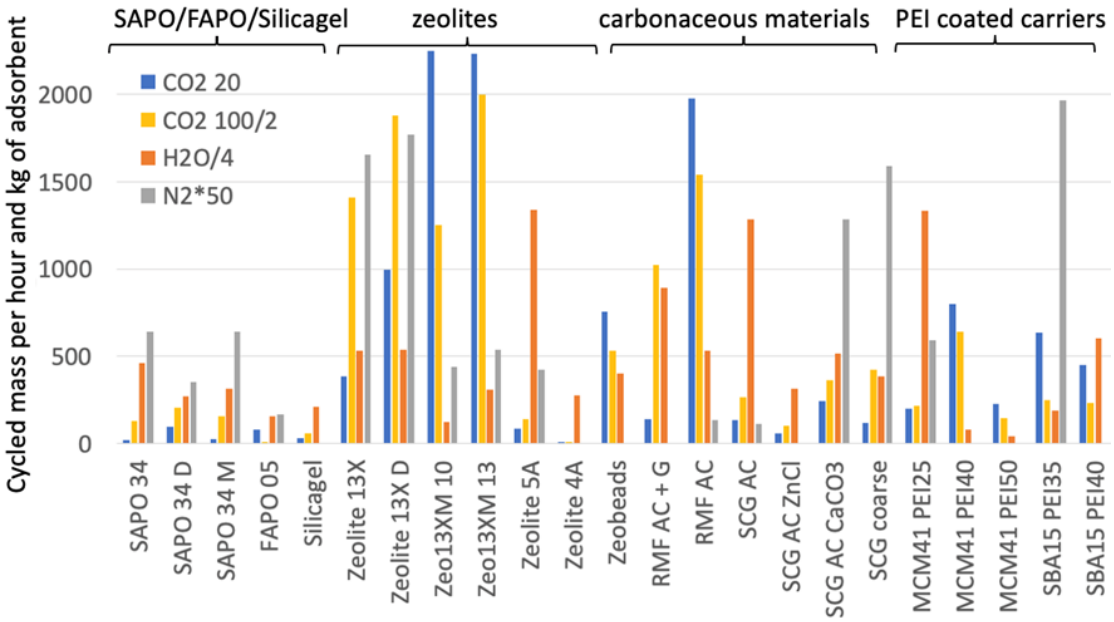

Figure 5.9: Ranking by TJS results on CO2, H2O, and N2 pure gas rapid cycling with 1-minute desorption and 1-minute adsorption. The vertical axis shows grams of cycled mass per hour and a kilogram of sorbent (g/kg*h), thus combining static and kinetic properties into one selection parameter.

limited by mass transfer, a smaller thickness was increasing the cycled mass per sorbent mass but decreasing the thickness also decreases the active-to-dead-mass ratio; this increases the effective material usage but reduces energy efficiency since less gas is cycled. When heat and mass transfer resistances are more balanced and pore formation is effective, the thickness can be enlarged without reducing material usage. Another interesting limit case is given by zeolite 4A, where the mass transfer resistance is very high probably due to the narrow size of the micropores (0.4 nm) showing the physical limit for the diffusion of CO_2 molecules. As expected, CO_2-related performance is bad for SAPO-34, FAPO-5 and silica gel but the latter can act as carriers for N-doping. Zeolite 5A also fits into this category having higher water sorption than CO_2 sorption.

Specific observation for PEI-modified samples was that the cycled masses for a 25-75°C temperature swing were not larger for 100 $mbar$ than for 20 $mbar$ CO_2. In fact, for some samples, the cycled mass was larger for 20 or even 5 $mbar$ than for 100 $mbar$ CO_2. This indicates that PEI modifications provide means for the chemisorption of CO_2 as opposed to physisorption on unmodified mesoporous carriers like MCM41 and on zeolites. With PEI-modified samples cycled masses more than doubled for 45-95°C and tripled for 25-95°C temperature swings confirming the above conclusion. When analyzing equilibrium and dynamic results the following conclusions can be taken.

- Magnetically aligned zeolite 13X is an excellent material for CO_2 capture from dry

streams, with good capacity and high adsorption rates. However, the preferential H_2O sorption adds the cost of an efficient drying column, which rises the overall system cost.

- Nitrogen-rich carbonaceous materials show moderate to good performance in presence of water but should be optimized to increase the overall capacity. An increase in mass transfer by structuring would be beneficial.

- Amine-impregnated materials offer also moderate performance, but the low stability of physisorbed coatings hinders industrial application. Higher regeneration temperatures strongly improve capacity but can only be applied for N-containing polymers with higher molecular masses or when they are chemisorbed. SBA15 offers a better hosting of PEI than MCM41 but also shows a higher heat transfer resistance. Different molecules and treatment methods for N-doping should be investigated to accelerate progress.

5.5 Towards Rapid Thermal Swing Adsorption

5.5.1 An experimental separation column

TSA, PSA and combinations thereof have recently received a lot of attention triggering the commercially successful RPSA and an intensive research effort to accelerate TSA. Using TSA models S. Li et al., 2019 found that entropy increases with adsorbed CO_2 and temperature variations, and that mass transfer dominates entropy generation, while sensible heat dominates heat consumption. With tuned regeneration time 663.8kWh/t_{CO_2} were reached for separation from N_2 by Ben-Mansour and Qasem, 2018. A TSA analysis for wet flue gas by Hefti and Mazzotti, 2018 reached 90% CO2 recovery and 95% purity (see Hefti and Mazzotti, 2018) and a model was developed for adsorbent screening (see J. Wang et al., 2021). TSA Cycle times were reduced with added metal wires and regeneration energy with added pressure swing (see Parkar et al., 2022; combined with self-regeneration, RTSA consumed 80% less energy (see Jung et al., 2022). The advantages of structured adsorption materials are important for the industrial impact of VPSA (see Tian et al., 2021) and fast cyclic ad/desorption (see Verougstraete et al., 2020). Coal-fired power plant VTSA runs with 2.41 MJ_{th}/kg_{CO2} waste heat (see Plaza and Rubiera, 2019) and the cement industry can be decarbonized via the retrofittable swing adsorption reactor cluster (SARC) with avoidance costs of 52 £/t (see Cloete et al., 2020). Solar-assisted PTSA (see Zhao et al., 2018) and TSA can reach second-law efficiencies of 3.24-9.23% (see Z. Liu et al., 2011 and TSA can also be applied for the separation of CO2, H2 and CH4 (see Streb and Mazzotti, 2021).

RTSA systems depend on the excellent mass and thermal transport and on handling a large stream of flue gas at low pressure drop using large cross sections. Since columns filled with 1-4 mm beads have tortuous gas flow paths, the RTSA system uses a finned heat exchanger with fins oriented parallel to the gas flow path. Figure 5.10a shows a short column setup to test the AdHEX. The setup is equipped with the inlet and outlet flange metrology to determine partial pressures, CO_2 concentrations, temperatures, and gas flow. Thermal baths with a heat transfer

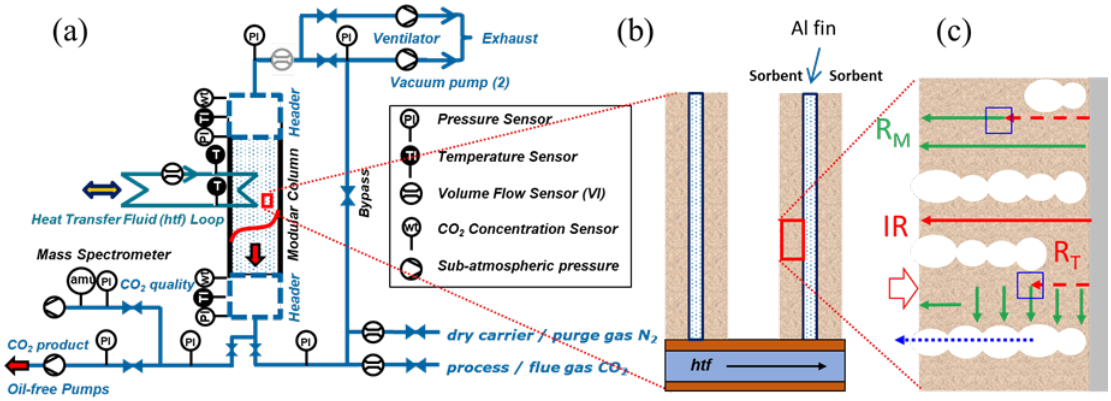

Figure 5.10: RTSA Experimental system with gas separation column and sensors (a). Simplified schematic of an Al fin coated with sorbent on both sides (b) and qualitative sorbent layer morphology (c). Sorbent coating resistances are indicated by RM (mass transfer, green) and RT (heat transfer, red).

fluid (HTF) switch like in the TJS are used to provide fast temperature swings for the AdHEX. From there the heat is conducted via a ≈0.2 mm thick Al fin into the 0.3-1 mm thick layer of sorbent (Figure 5.10b). The unit cell of the RTSA system is thus an Al fin coated with sorbent on both sides that can make use of aligned pores for mass and "necking" at particle contact points for thermal transport enhancement (Figure 5.10 b,c). Concentrations of CO_2 are measured at the inlet and outlet and along elongated separation columns to accurately characterize loading and breakthrough CO_2 capacity. The cyclic process starts with the column adsorbing CO_2 from a flue gas stream until CO_2 breaks through to the outlet. Then, the outlet valve closes and while switching to high desorption temperature to push the low concentration CO_2 towards the inlet until the purity threshold is reached to deliver CO_2 to the product port. Together with product quality control sensors key parameters are determined: capture yield, product purity, capacity, and energy/exergy efficiency. With the known characteristics of the adsorbent and the column, a scale-up path is defined from the gram, via kilogram to ton scale building on the previous expertise from the scale-up of the AdHP RTSA process [49].

Considering the promising results obtained with process optimization with water-sensitive materials by Hefti and Mazzotti, 2018; Joss et al., 2017, the experimental test and material optimization in a scaled-up column could give new and encouraging support to the technology. In fact, the column design must be such that the advantage of the enhanced heat and mass transfer is harvested under realistic operation conditions. The use of less hydrophilic materials could be an additional advantage in terms of energy efficiency and cost of the drying column. However, to have an effective design, two key aspects should be fulfilled: realistic dynamic modelling of the TSA process and an upscale of the coating process.

5.5.2 Modelling approaches

As discussed above and widely reported in the literature, dynamic models are crucial to evaluate the performance of sorption systems for gas separation (e.g. see Plaza and Rubiera, 2019. While thermodynamic models could give some rough indications regarding the maximum achievable cycling capacity and energy consumption, all the fundamental indicators (such as productivity, capture efficiency, purity of the CO_2, and real energy consumption) cannot be calculated. In general, the kinetics parameters of the separation columns are obtained experimentally (e.g. by Casas et al., 2012). Whenever the material and the operating window are fixed prior, this is a valid and effective approach, for example for process design purposes. When the material selection and integration have to be performed at the same time, however, this approach is limiting. In fact, the heat and mass transfer coefficients more correctly depend on the geometry and on the thermodynamic state of the material.

It appears that also in this case, a computationally efficient approach to the material modelling would be ideally integrated with process modelling. In fact, it would correspond to using the approach proposed by Bau et al., 2014 to the carbon capture TSA system. In fact, a similar approach is already under development by Postweiler et al., 2022. The challenge would be to substitute classical kinetics models such as the linear driving force to include the material properties. Moreover, it is foreseen that the competitive adsorption of different gases will alter the adsorption dynamics as well.

Similarly to what was done in Section 4.2, material and process parameters could be tuned simultaneously. An experimental design of experiment could map the influence of the coating parameters over the single gas heat and mass transfer resistances. The relation between single gas and multi-component heat and mass transfer resistances, instead, should be evaluated by separate experiments. Ideally, a dedicated small-scale setup would be used, to isolate the microscopic kinetics from the macroscopic flow. Those relations are likely to be unaffected by the coating process as will depend on the microscopic properties of the material. Finally, the coating can be optimized for a real column design, computing the macroscopic gradients of temperature and pressure.

5.5.3 Coating methods

While the manual coating method proposed above is well suited for small-scale characterization of a limited number of samples, the upscale in both size and quantity of adsorbent will require different approaches.

The first issue is replicability. The slurry formulation, the doctor-blading, and the alignment and drying procedures involved a great deal of manual operation. A more consistent and machine-based formulation, coating and characterization procedure must be set in place for industrial up-scaling. Viscosity and ferrofluid droplet size should be characterized for all experiments.

The coating method for complex surfaces cannot be doctor-blading. Dip coating would be a feasible option if the required thickness would be below 0.5 mm. However, the thermal mass of the RTSA is likely to be such that cycle times below 4 minutes are not sufficiently efficient. For this reason, fast and thick coatings will allow a high active/dead mass ratio and high material usage (high cycling capacity). For this reason, simple 3D printing techniques might be adequate, as the viscosity of the slurry (in this case, ink) is compatible with commercial equipment. The first tests with 13X proved that the method is fast and reliable. However, the effect of the printing (including degassing by planetary speed-mixing) over the pore formation is to be investigated. Another similar but more flexible and fast method could be jet-dispensing (see Go et al., 2019; Serizawa et al., 2014. This technique seems to be faster and more economic, and able to coat more complex surfaces. However, some first feasibility tests should be performed.

The magnetic alignment performed with permanent magnets has the limitation of the size or the latter. Either a homogeneous magnetic field is created by an array of magnets, or an electrically induced field should be created such that could host multiple heat exchanger fins in parallel. In fact, alignment and drying require several hours and are likely to be the most time-consuming steps.

5.6 Conclusions

The RTSA gas separation system draws a lot of know-how from the innovations done as part of the AdHP projects and thus has a large technological advantage compared to classical TSA gas separation. But understanding and developing materials and structuring processes is a key factor to expand the RTSA advantage such that it can prevail against state-of-the-art technologies. Building on top of the material innovation developed as part of RPSA, numerous adsorbent candidates have been tested under realistic conditions to measure their applicability in industrial RTSA applications. Specifically, both the equilibrium properties of the materials and the dynamic performance of coatings derived thereof were characterized with specifically developed DVS and TJS measurements using only a few grams of materials required. The measurements allowed us to quantify the factors limiting the applicability of the materials, clearly distinguishing their causes (working capacity, competition with water, thickness of the coating, heat conduction, and mass diffusion). None of the tested materials could solve all the challenges related to post-combustion CO_2 capture, but they offer interesting insights on which to base further material development. In particular, the currently available materials would need a dehumidification stage to process real humid flue gas and/or an increase in the adsorption capacity. For this reason, the co-development of material and process design is desirable to valorize all the possible synergies among them. When it comes to the kinetics (crucial for RTSA), it was confirmed that coatings suffer from high resistance to CO_2 gas diffusion and that tailoring the coatings (i.e. magnetic alignment of macro-porosity) can balance the heat-to-mass diffusion path length and enhance the use of the material for very short cycle times. These findings allow the development of effective column designs and manufacturing

processes that consider the specific constraints of the CO_2 adsorption/desorption process on the adsorbents.

Future research should address at the same time materials and processes. From one side, improved adsorbents should be integrated into the heat exchanger stably and effectively, and the separation column should be designed to provide maximum benefits. Specifically, the characterization methods should be improved to better quantify the effects of the co-adsorption of diverse gas mixtures and to evaluate the effect of the column design and control on the performance. A dedicated experimental setup could empower such an analysis and the design of an industrial-scale prototype for specific use cases. Dynamic models and optimization algorithms could be powerful allies in such developments. An additional effort is needed to study the long-term effects of particulate, SO_x and NO_x on the sorption capacity. The identification of the optimal material among the thousands of possibilities is a challenge probably even beyond the capacity of human intelligence. In this respect, it is envisioned that novel computational tools are developed to assist the experimental efforts by proposing new candidates and carrying out pre-evaluations in silico so that the number of required experiments is reduced and the incremental progress per research cycle is improved. State-of-the-art deep search and natural language processing have been successfully applied in many fields but still fall short of making an impact on materials research in general.

As this decade will decide whether we can keep the planet habitable or we lose control of the climate, fast development and deployment of RTSA can be crucial. RTSA could bring new edges in the fight against climate change, especially when combined with energy efficiency and the combustion of renewable fuels to enable carbon-neutral or even carbon-negative energy systems, as it uniquely combines abundant heat waste with carbon capture.

5.7 Acknowledgments

This section was elaborated in collaboration with Stephan Paredes, Patrick Ruch and Bruno Michel from IBM-Research Zürich, Switzerland, Romain Civioc from Empa, Switzerland, and Paul Gantenbein from OST, Switzerland. Moreover, the author thanks Tingting Wu and Shanyu Zhao from Empa, Switzerland, and Patrik Postweiler from RWTH Aachen, Germany, for the fruitful discussions. Part of the content was published by Piccoli, Gantenbein, et al., 2022.

6 Long-Term Effects of Use and Storage of Adsorbent Materials

6.1 Introduction

Despite the abundant literature concerning adsorbent materials, little is known about the long-term effects of their storage and use. A specific sub-category of this field does exist and concerns the stability of Metal-Organic-Frameworks (MOFs) under operational conditions. As mentioned numerous times in this chapter, these crystalline synthetic materials are of great interest as they are almost infinitely tunable to our needs, from catalysis to drug delivery and from heat transformation to gas separation. However, to cite Lee et al., 2018, *"A primary shortcoming of early MOFs is their low structural stability upon exposure to water (or steam), which significantly limits their practical use with water"*. Considering that the most frequent adsorbate in heat transformation is water and that water is present in large quantities in carbon capture, one can see the concern when related to the applications evaluated in this thesis. For this reason, research on water-stable MOFs is a well-established field, and one not without success, as reported for example by Burtch et al., 2014; Lee et al., 2018.

Another emerging field is the degradation of CO2-adsorbing materials for carbon capture application. Particular effort is dedicated to aminosilicates materials, as discussed in Section 5, with a relevant example in the work performed by Bollini et al., 2011 on their oxidative degradation.

In the field of adsorption heat transformers, two main research groups addressed the topic. The Fraunhofer-ISE group (see e.g. S. K. Henninger et al., 2015) tested the cycling stability under various conditions for many materials, representative of different applications (i.e. thermal energy storage and heat pumping). They found that above certain temperatures (generally above 150°C or higher) the degradation is significantly faster. S. Henninger et al., 2011 also find that short tests are essential to exclude the most problematic adsorbents at the early stages of the investigation.

The CNR-ITAE group developed methods to evaluate the hydrothermal and mechanical stability of adsorbents too, see Frazzica and Brancato, 2019; Freni et al., 2013. In this thesis, we

Designation	Producer	Type	Type of ageing
Siogel	Oker-Chemie GmbH	Silica Gels	cyclic / on-shelf / intensive
SAPO-34	Fahrenheit GmbH	Zeolites	on-shelf / intensive
RMF-AC	Empa	Activated Carbons	cyclic / on-shelf / intensive
SiO2+LiCl	CNR-ITAE/ Boreskov Inst. of Catalysis	Composite	cyclic

Table 6.1: Overview of different materials aged under different conditions

build on those methods and test different categories of adsorbents under different conditions. Furthermore, we test also on-shelf and severe ageing conditions.

6.2 Materials and Methods

6.2.1 Materials

Four different adsorbent materials have been considered for ageing experimental tests (see Table 6.1). In particular, materials (Oker Siogel, Fahrenheit SAPO34, RMF-AC, SiO2+LiCl composite) belonging to 4 different classes of materials (silica gel, zeolite, activated carbon and salt-in-porous-matrix composite) were tested for ageing during cyclic adsorption/desorption at CNR-ITAE lab. Nevertheless, during the experimental campaign, the testing of the Fahrenheit SAPO34 sample resulted to be impossible in the experimental test rig CNR-ITAE due to the low density of this material, causing elutriation of the sample during the cycling activity. Therefore, a total of three adsorbent materials were tested successfully for cyclic ageing at CNR-ITAE. Three of the materials considered for cyclic ageing at CNR-ITAE (Oker Siogel, Fahrenheit SAPO-34 and RMF-AC from Empa) were also aged under different conditions at Empa. Both on-shelf ageing under different relative humidity and severe ageing under high water pressure / high temperature were considered.

6.2.2 Cycling ageing

The schematic layout and a picture of the cycling test rig are reported in Figure 6.1. The main components of the experimental rig, shown in Figure 6.2, are:

- A large vacuum testing chamber, equipped with three plate heat exchangers (HEX) to carry out cycles and shelf tests at desorption and adsorption conditions. This chamber represents the core of the system. It was realized in stainless steel AISI 316, to guarantee high vacuum tightness and corrosion resistance. The evaporator, the vacuum circuit, the venting valve, and pressure and temperature sensors are connected to the chamber by means of flanges welded on the wall of the chamber. Also, six threaded tubes are welded across the chamber in order to permit the flux of the heat transfer fluid to each installed flat plate HEX. The flat plate HExs, designed and realized ad hoc, are situated inside the testing chamber. They were realized in aluminium to guarantee a high thermal conductivity, thus allowing fast cycling of the adsorbent material. The

adsorbent material that has to be aged is positioned upon the HEXs.

- A smaller vacuum chamber, used as an evaporator/condenser, maintains constant water vapour pressure inside the system. This chamber consists of a glass evaporator/condenser horizontal cylinder specifically designed and realized. Inside the cylinder a spiral is inserted, in order to let the external fluid flow through it, thus maintaining the liquid water contained inside the chamber at a constant temperature.
- A vacuum valve that connects the two chambers.
- Three thermostatic baths: one to provide high temperature for the desorption, one to provide medium temperature for adsorption and one to keep constant the temperature inside the evaporator.
- A fully automatic hydraulic system, equipped with electrically activated valves, allows replicating the defined cycle and shelf conditions.
- Several temperatures and pressure sensors are needed to monitor the system under operation. The management and acquisition system is based on National Instrument Compact Field Point hardware and on the LabView control panel, which can permit both automatic and manual management of the testing rig as well as the acquisition of all the relevant parameters (i.e., temperature and pressure). Particular attention was paid to the selection of proper sensors for the monitoring of the main thermophysical parameters affecting the cycling tests, namely, pressure and temperature. The pressure sensors were selected considering the need to monitor the pressure in the absolute range between vacuum and ambient pressure. Accordingly, a sensor from Thyracont company (model MT-VSC43MA4) was selected. Its absolute pressure measuring range varies from 1 to 1400 absolute $mbar$. As temperature sensors, standard thermocouples type T were selected, thanks to their good accuracy ($\pm 0.5K$) and high reliability in the range of measurement between 73 K up to 673 K.
- A properly designed thermostatic box was designed to keep constant the temperature of the ambient surrounding the system, avoiding possible condensation of the water vapour on the surfaces of the vacuum chamber, thanks to an electric heater and an external thermoregulator.

6.2.3 On-shelf ageing

Three climatic rooms with controlled and constant temperature and relative humidity were used to store the adsorbents over a prolonged time. The humidity was kept at 37%, 50% and 80% respectively, while the temperature was kept at $20°C$ in all of them. The samples were kept in those rooms exposed to the air so that the conditions on the sample were exactly the same as in the room. In addition, other samples of the same materials were kept in a closed box, with limited exchange with the surrounding atmosphere, to have a benchmark.

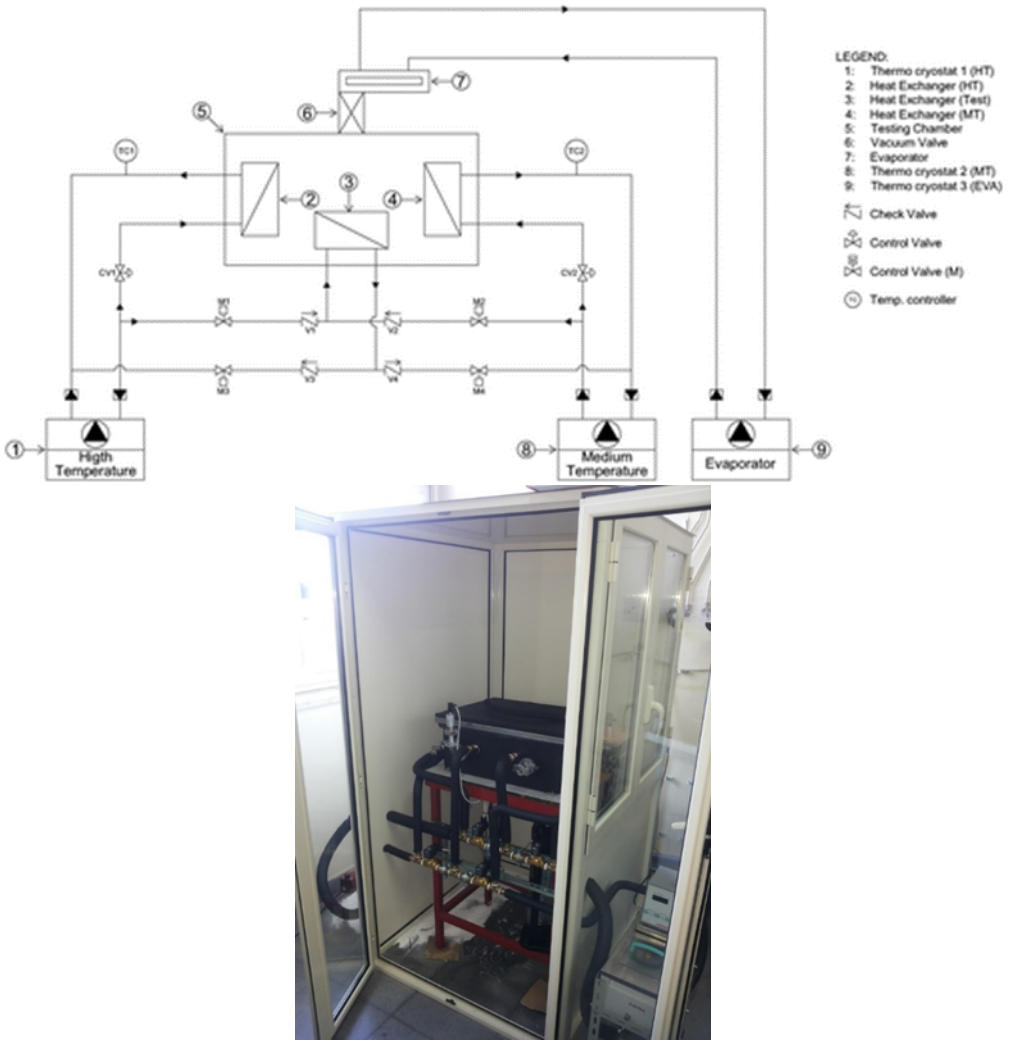

Figure 6.1: Top: schematic layout of the realized ageing setup. Bottom: the ageing test rig at CNR-ITAE

Figure 6.2: Components of the experimental cyclic ageing setup. Two views of the vacuum testing chamber, the flat plate heat exchanger upon which the material is positioned, the glass evaporator/condenser chamber, and the Labview management and acquisition panel.

6.2.4 Intensive ageing

For the intensive ageing, the samples underwent iteratively a wetting and drying process.

A. The samples were placed in a domestic pressure cooker with a layer of water at its bottom. The sample was put in a petri dish over a raised stand, and protected by a glass cap so that water droplets condensing on the cooker cap would not wet the sample. The vapour access is granted by the space between the dish and the cap.

B. The pressure cooker is brought twice to a pressure of 2 bar, corresponding to a temperature of 120°C and kept under this condition for at least 2-3 hours. At the end of the first cycle, the cooker was refilled with water to operate during the second cycle.

C. A fraction of the sample was separated and tested in the DVS instrument (VTI TA+).

D. The rest of the sample was dried at 140°C and vacuumed (between 50-100 $mbar$) overnight.

E. The procedure was repeated from point 1.

After ageing, the water sorption, envelope and skeletal density, thermal-gravimetric analysis and physisorption were characterized again.

6.3 Results

6.3.1 Cycling ageing

The ageing process was carried out by cycling the samples between desorption at 90°C and adsorption at °C, maintaining the evaporator/condenser temperature at 15°C. These cycle conditions are more extreme than a typical adsorption process of the adsorbent materials since the amount of water exchanged per cycle is much higher than the one occurring during the operation of an adsorption chiller. Accordingly, it can be considered an accelerated ageing procedure compared with standard operation.

About 2000 ageing cycles have been performed on each sample. During the ageing process of the Oker Siogel, an early withdrawal stage has been done at 320 cycles, in order to verify if any degradation process of the adsorbent material occurred. While, only a single withdrawal has been done for the samples RMF-AC and SiO2+LiCl composite, at 2273 and 1916 cycles, respectively.

The adsorbent samples were tested before and after the ageing process by means of DVS Vacuum, Surface Measurement Systems Ltd, in order to evaluate water adsorption isobars or isotherms. To characterize the equilibrium properties of the adsorbent materials, around 10 – 15 mg of the sample was put inside the DVS apparatus. The material was degassed

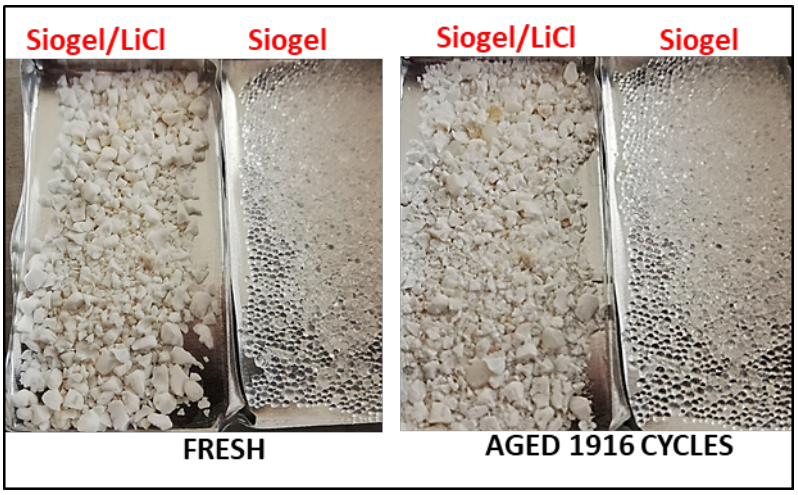

Figure 6.3: Comparison of the fresh and aged Siogel/LiCl and Oker Siogel

under continuous evacuation for 12 h at 160°C. The adsorption properties of the composite material (SiO2+LiCl) and of Oker Siogel were evaluated by measuring the equilibrium curve following the isobaric route, at a constant pressure of 8.7 $mbar$ (5°C in the evaporator) and at the equilibrium points were taken at 150°C, 100°C, 90°C, 85°C, 80°C, 75°C, 70°C, 65°C, 60°C, 55°C, 50°C, 40°C and 35°C. While, the adsorption curves of the RMF-AC, before and after the ageing process, have been evaluated by measuring the equilibrium isotherm at 35°C. Figure 6.3 conveys the degradation process that is produced by the ageing cycles on the Oker Siogel sample and on the composite sorbent material. The images of the Siogel/LiCl sample reveal that the material is partially destroyed from the mechanical point of view during the ageing process, indeed the silica gel grains size is reduced due to the ageing process. On the contrary, the morphology of the Oker Siogel remained unchanged.

From the adsorption capacity point of view, Figure 6.4 shows the adsorption curves of the three tested adsorbent materials, before, during and after the ageing process. As evident, the maximum uptake and the shape of the curves remain almost unaffected for all the investigated samples. Therefore, even though Figure 6.3 displays that the composite sorbent is partially destroyed, it was demonstrated that the adsorption features of the sample are not affected by the morphology degradation.

6.3.2 On-shelf ageing

After more than a year of on-shelf ageing in a closed box and in the climatic rooms respectively, the samples of SAPO-34 from Fahrenheit, Siogel from Oker and RMF Activated Carbon from Empa were characterized with DVS to check for any change in the water cycling capacity. The results are shown in Figure 6.5. One year of storage in a closed box did not bring any relevant change in the adsorption characteristic of the adsorbent materials. Exposition to humid air brought different effects depending on the material. The SAPO-34 from Fahrenheit was the

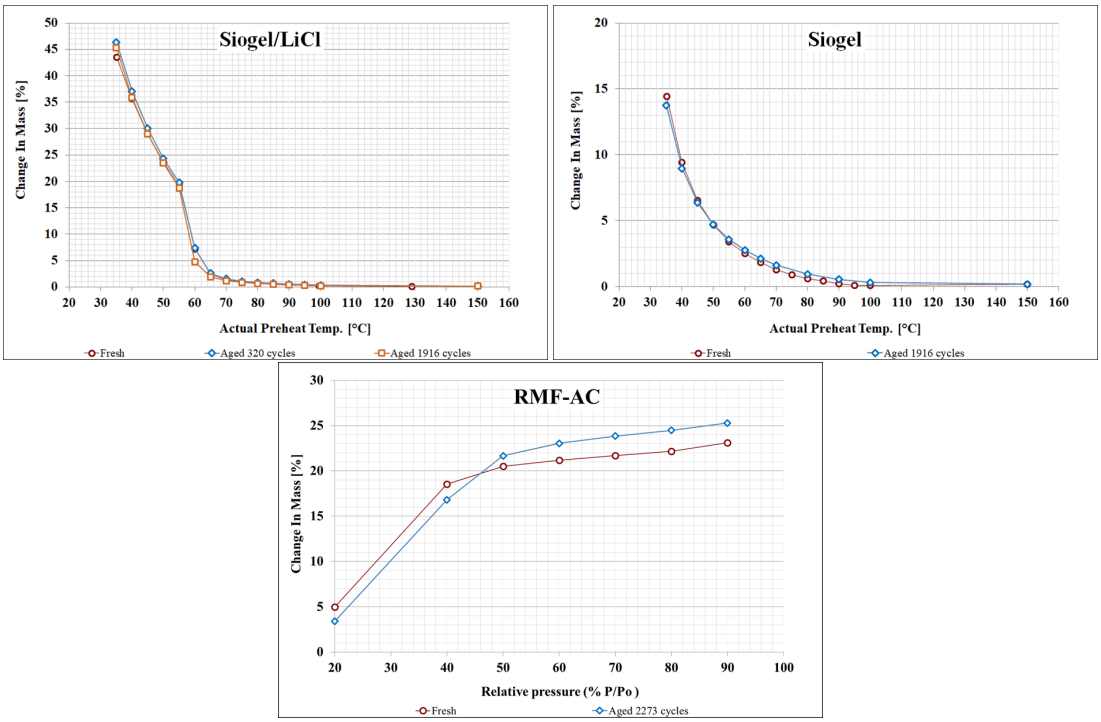

Figure 6.4: Isobars of Siogel/LiCl composite adsorbent before and after the ageing process, Isobars of Oker Siogel before and after the ageing process, Isotherms at 35°C of RMF-AC, before and after the ageing process

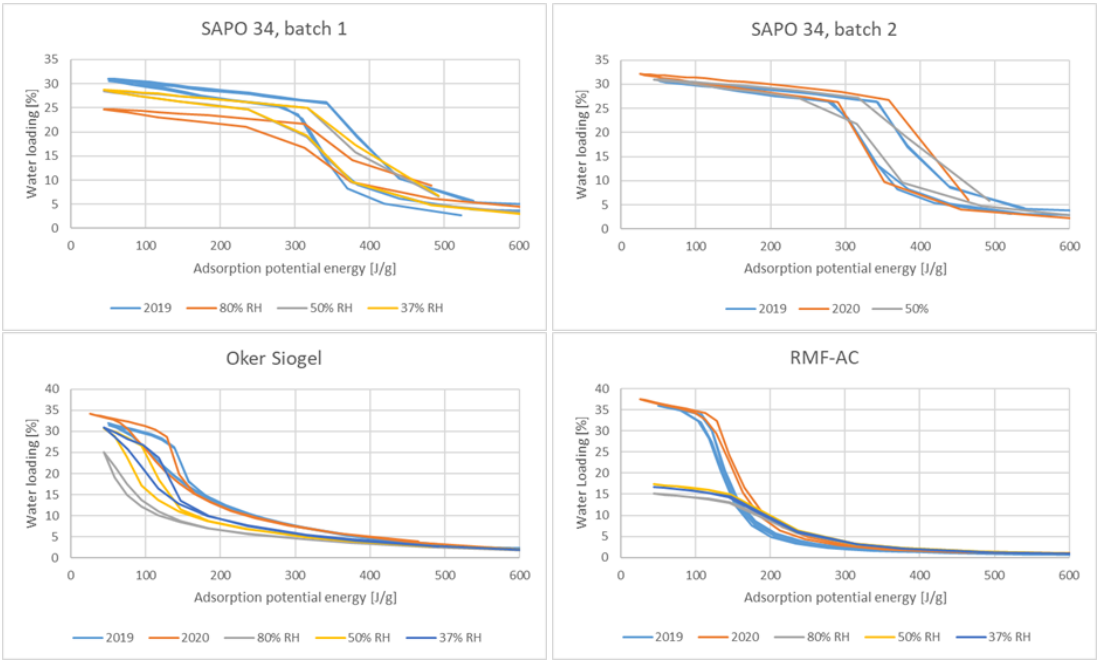

Figure 6.5: DVS isotherms measured at 50°*C* of selected samples as received (2019), after one year stored in a closed box (2020), after at least two years stored in a climatic room at constant relative humidity (80%, 50% or 37%)

least affected among the three. For 37% and 50% relative humidity (RH), little to no change was observed. For the batch stored at 80% RH, a reduction of about 16% in saturation capacity (from 30% maximum water loading to 25%) was registered. The Siogel from Oker was gradually more affected as the humidity of the storage room increased. The adsorption capacity at higher adsorption potential energy decreased, especially for the sample stored at 80% relative humidity, where more than 28% of the water sorption capacity was lost (maximum adsorption decreasing from 35% to 20%). Adsorption at lower potential energy (bigger pores) seemed to be less affected. The adsorption capacity of the RMF activated carbon from Empa was drastically reduced by about 50% (maximum water sorption dropping from 35-37% to 15-17%) for all the exposed samples. The decrease comes mainly from a drop in adsorption at low adsorption potential (bigger pores), showing an inverse trend compared to Oker Siogel.

6.3.3 Intensive ageing

Intensive ageing of the adsorbent samples under high temperature and water pressure showed similar results as longer ageing under high relative humidity, atmospheric pressure and 20°*C*. SAPO-34 showed good stability even in these harsh conditions, showing little to no change in its adsorption characteristic whereas both Oker Siogel and RMF-AC show deterioration of the sorption properties with increased ageing. However contrary to the on-shelf ageing, with high pressure and temperature ageing the deterioration is more severe for Oker Siogel than for RMF-AC. The Siogel showed a gradual decrease in adsorption capacity of up to 50%

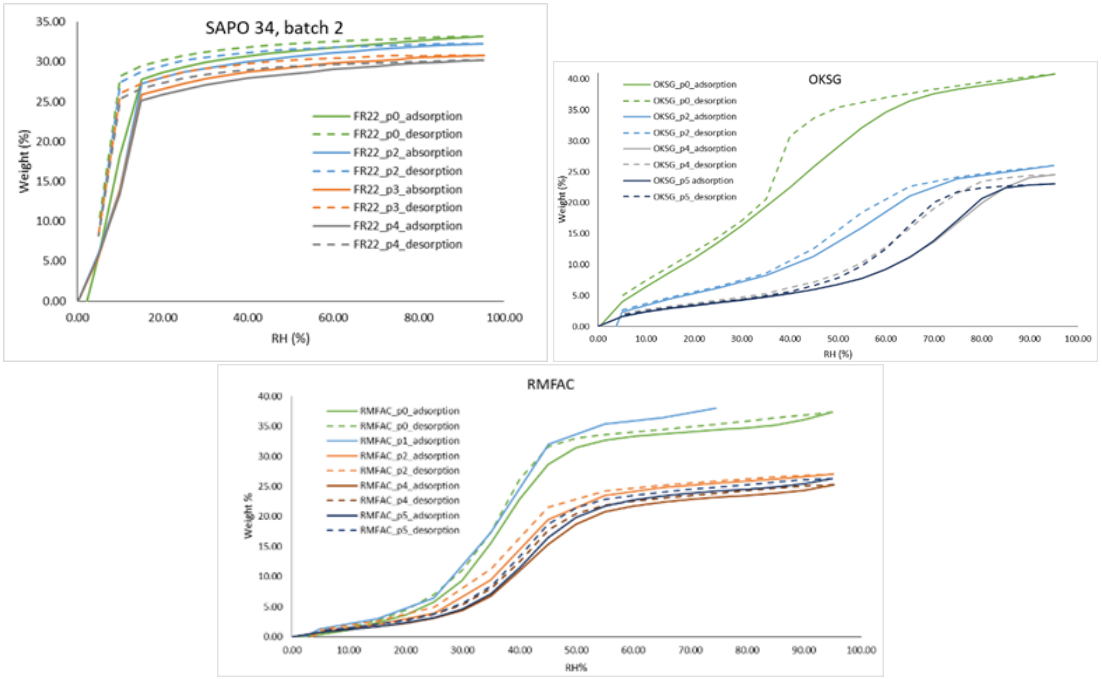

Figure 6.6: DVS results of isotherms at 40°C of SAPO-34, Siogel and RMF AC as received (p0) and after a certain amount of intensive ageing cycles (p1...p5)

(maximum sorption capacity dropping from 40% to 20%). The deterioration seems more pronounced at the low-pressure range (smallest porosity). The activated carbon showed a reduction of about 30% of the total adsorption capacity (from 37% to 25%) already from the second cycle, after which it seems stable during additional cycles. The shape of the adsorption isotherms is similar before and after ageing, indicating a loss of all types of sorption-relevant pores. The results are gathered in Figure 6.6.

Further characterization was done to understand the observed ageing mechanism and see if the aged materials can be regenerated. The results of skeletal and envelope density of the adsorbent materials before and after ageing on-shelf is gathered in Table 6.2. From the results from RMF (decreased skeletal density and increased envelope density), a possible explanation is the formation of a low-density phase (possibly a hydrate) forming within the pore space of the adsorbents. For the other two samples, where the envelope density could not be measured directly, the envelope density remains similar within the measurement accuracy.

Exposure to high vacuum (<0.1 $mbar$) did not lead to the recuperation of the porosity. To explore the possibility of thermal decomposition of the component blocking the porosity, thermal-gravimetric analysis (TGA) were done, where such a decomposition should show as a weight loss peak. Up to 800°C the TGA showed little to no change for SAPO-34, as visible in Figure 6.7, and only a minor change, due to lower water content, for Siogel, as visible in Figure 6.8. In the case of RMF activated carbon, instead, the lower water content is also accompanied by two clear mass loss peaks at high temperatures in presence of oxygen, as shown in Figure

Material	**Orig. skeletal density** $[g/cm^3]$	**80% RH aged skeletal density** $[g/cm^3]$
Fahrenheit SAPO-34	2.2	2.2
Oker Chemie Siogel	2.1	1.7
Empa RMF-AC	2	1.7
Material	**Orig. envelope density** $[g/cm^3]$	**80% RH aged envelope density** $[g/cm^3]$
Fahrenheit SAPO-34	1.3*	1.4*
Oker Chemie Siogel	1.1*	1.0*
Empa RMF-AC	0.43	0.55

Table 6.2: Density measurements. * Calculated from skeletal density and pore volume from physisorption.

6.9. The weight loss peak at high temperatures under air is expected due to the oxidation of the carbon. However, the initial mass loss during around $100°C$ was larger than expected, almost double that under nitrogen, even if the initial water loading was presumably the same. Consequently, we tested whether partial regeneration of the RMF-AC was possible by thermal treatment at $150°C$ overnight under air. However, the thermal treatment did not result in any change in the water sorption capacity.

Physisorption measurements on the samples aged in the most humid conditions (80% RH) confirmed the impressions deriving from density measurements and provided some interesting insight into the relationship between the porosity and the water adsorption characteristic. The SAPO-34 crystalline structure of the original sample showed two characteristic pore sizes: one at 0.3-0.4 nm and one at 0.7-0.8 nm, well-fitting the theoretical structure. After ageing, while the total pore volume remains very similar, additional pore size appears, between 0.4 and 0.5 nm, compensated by a pore volume decrease at 0.7-0.8 nm. When comparing this with the DVS results shown above, it appears that the larger population of pores was partly blocked, decreasing their size and reducing water sorption capacity slightly. In Figure 6.10 it is possible to see the NLDFT results.

The Siogel and RMF activated carbon are, instead, amorphous materials. For Siogel the existence of two types of pores contributing to water adsorption was previously observed: one happening at higher adsorption potential (with stronger bonds) that could be attributed to micropores, and one happening at lower adsorption potential that could be attributed to mesopores. When looking at the DVS and BET results for the aged samples (Figure 6.5 and Figure 6.11), it is possible to notice how the disappearance of the S-shaped peak at high adsorption potential energy corresponds to the drastic decrease of the porosity between 0.6 and 2 nm, which is indeed microporosity.

In the case of the RMF activated carbon, the DVS curve shape did not change after ageing. However, the water capacity decreased greatly after the on-shelf period of two years. In this case, only one porosity type seemed responsible for the water adsorption. From the BET results

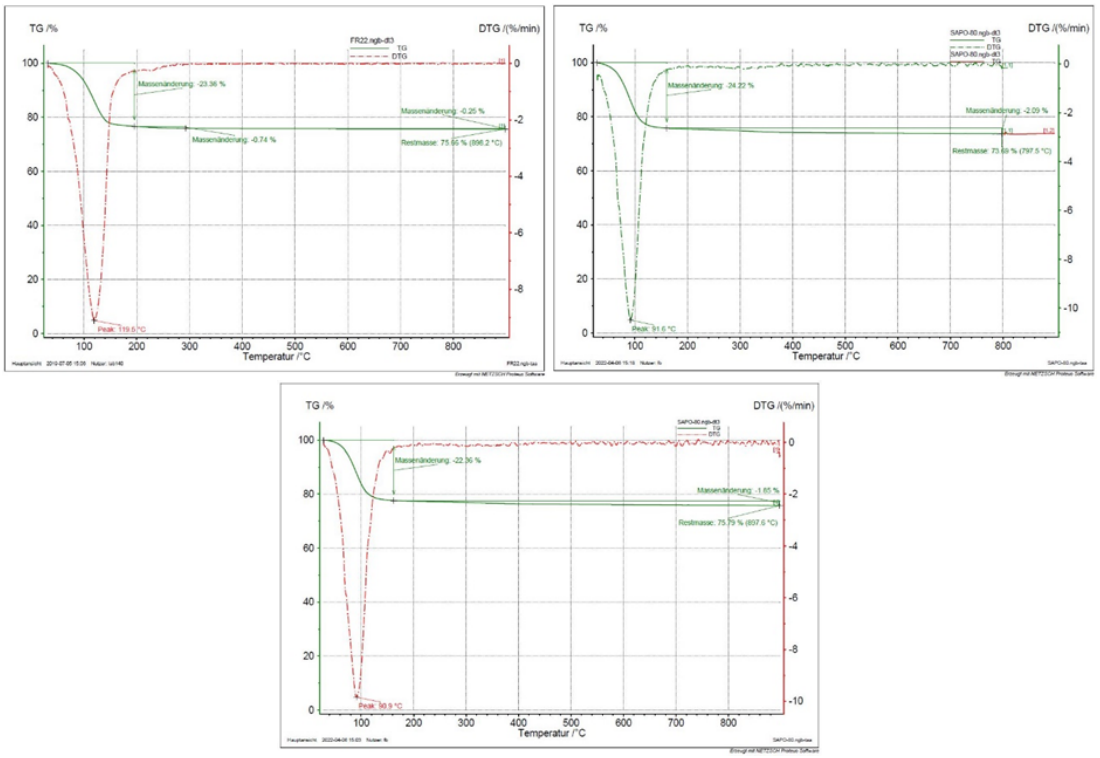

Figure 6.7: TGA on SAPO-34. Top-left: original, nitrogen atmosphere. Top right: aged at 80% relative humidity, nitrogen atmosphere. Bottom: aged at 80% relative humidity, air atmosphere.

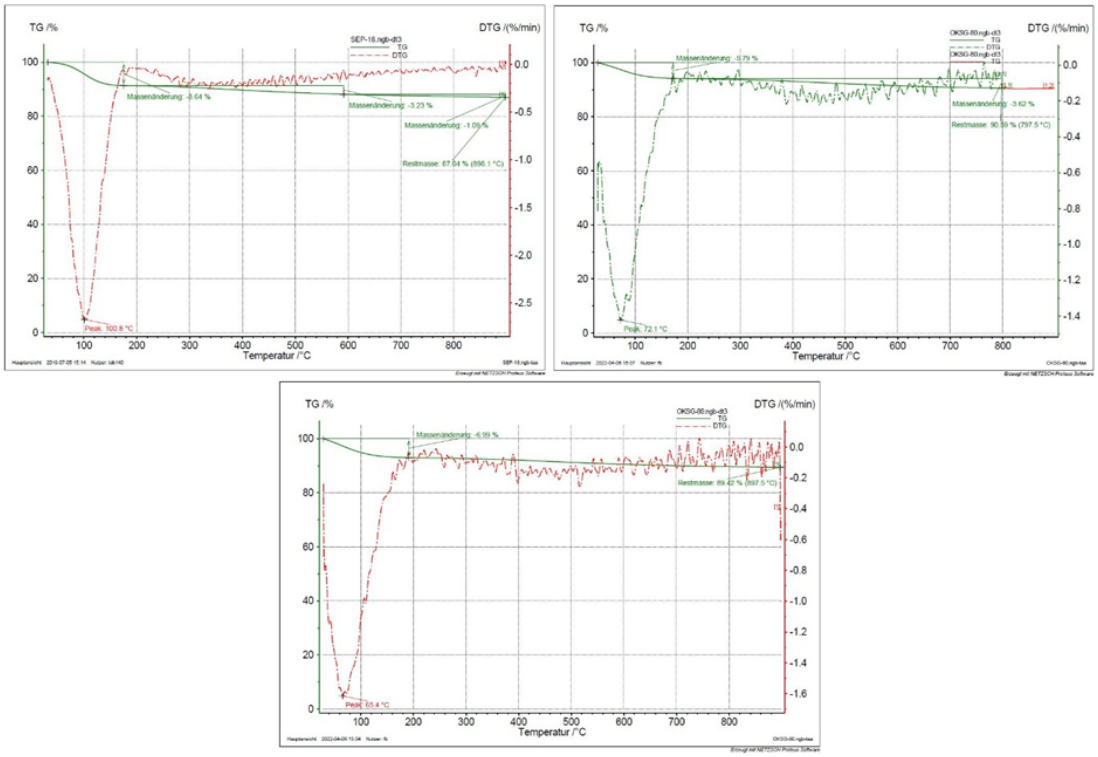

Figure 6.8: TGA on Siogel. Top-left: original, nitrogen atmosphere. Top right: aged at 80% relative humidity, nitrogen atmosphere. Bottom: aged at 80% relative humidity, air atmosphere.

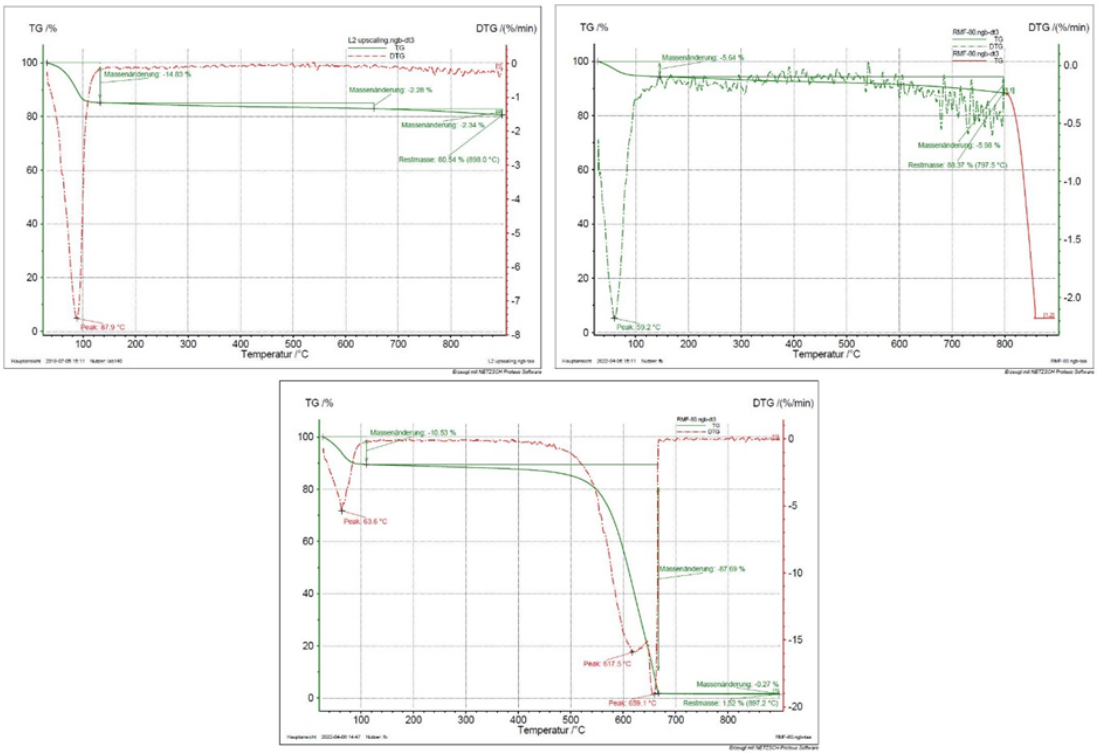

Figure 6.9: TGA on RMF AC. Top-left: original, nitrogen atmosphere. Top right: aged at 80% relative humidity, nitrogen atmosphere. Bottom: aged at 80% relative humidity, air atmosphere.

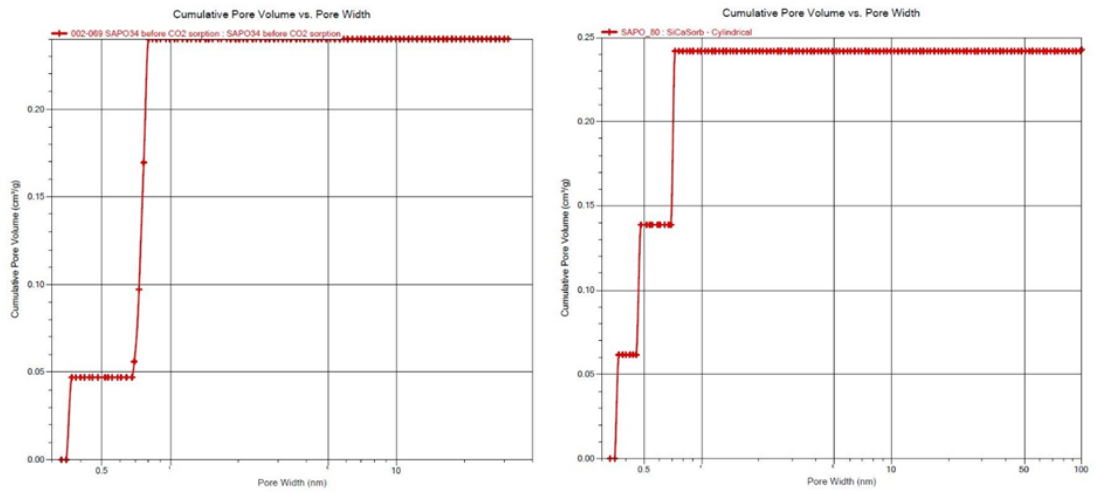

Figure 6.10: Cumulative pore volume results for SAPO-34 from Fahrenheit. On the left, is the original sample; on the right is the sample after ageing for 2 years at 80% relative humidity.

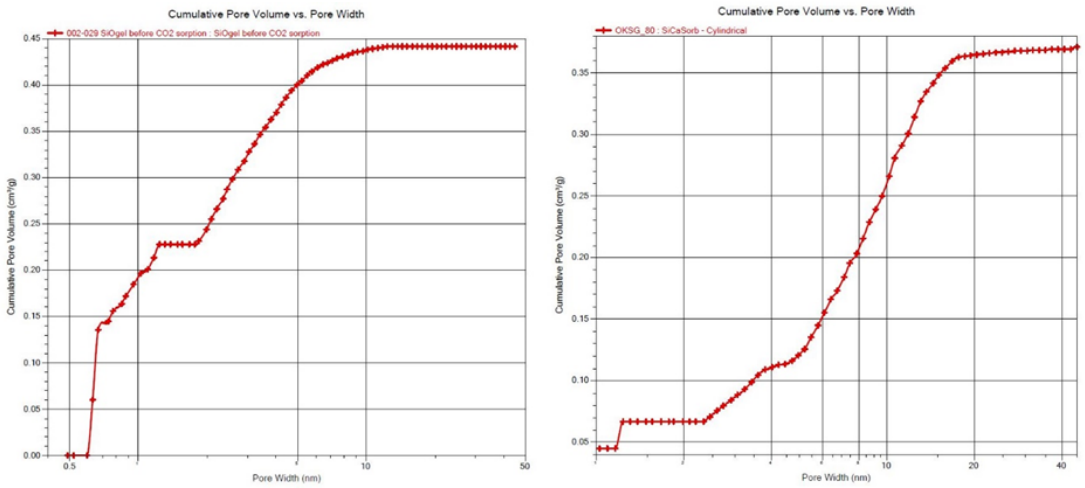

Figure 6.11: Cumulative pore volume results for Siogel from OKerChemie. On the left, is the original sample; on the right is the sample after ageing for 2 years at 80% relative humidity.

of Figure 6.12, it is possible to appreciate how the smallest "graphitic pores" (0.3-0.4 nm) were not subject to any change. However, the bigger microporosity (0.7-1.1 nm) greatly decreased in volume, reducing the size of some of the pores, but mostly decreasing the available pore volume.

In conclusion, for all the materials, even if in different measures, some of the bigger microporosity (0.5-2 nm) was lost, probably due to a low-density phase forming. From one side, this led to a partial reduction of the pore size and an overall loss of available pore volume which affected the water adsorption performance of the material negatively, also resulting in bigger average pore size, as bigger porosity (>2 nm) was not much affected by the phenomenon.

6.4 Conclusions

In summary, our results indicated that ageing can occur under humid storage conditions, especially for the amorphous sorbents and in the pore size range of 0.5-2 nm. The detrimental effect does seem to come from the exchange with a water vapour reservoir and can be accelerated by exposing the samples to high water pressure and temperature. The latter procedure seems to be a good way to check for this type of ageing in the laboratory. While ageing can be avoided by appropriate storage conditions, no regeneration strategy for aged samples could be identified. This ageing directly affected the adsorption heat exchanger prototype characterized in Section 4.2, considerably reducing the measured performance.

The cyclic accelerated ageing, one of the most important when considering the industrial cooling application, did not show important degradation effects. This means that, at least from a water adsorption point of view, adsorption chillers can be run in normal operation for a long time without expecting any need for maintenance. As for the storage condition, a

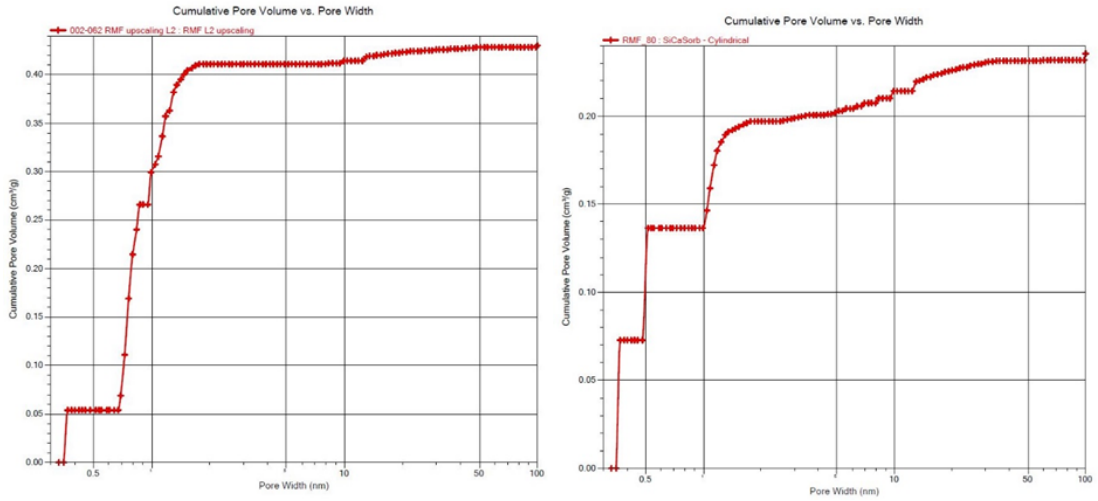

Figure 6.12: Cumulative pore volume results for RMF activated carbon from Empa. On the left, is the original sample; on the right is the sample after ageing for 2 years at 80% relative humidity.

potential risk was highlighted. When the adsorbent material is not stored correctly under a dry environment (vacuum or nitrogen), some adsorbents can experience degradation and the adsorption chillers may suffer from a decrease in power and energy efficiency, without an easy regeneration procedure to inverse the ageing. The reason appears to be the formation of a low-density phase in the adsorbent porosity. This was recorded also for Oker Siogel adsorbent, which is commercially implemented in adsorption chillers (e.g. from Fahrenheit GmbH). In general, this type of ageing should not be an issue, as the adsorber is degassed before powering off the chiller, but it is a confirmation of the importance of this degassing step as an ageing mitigation strategy, even before and after shipping the components, in case of long storage times. An adapted accelerated test procedure to test for ageing under humid conditions (exposure of the samples to high water pressure and high temperature for a few cycles of a couple of hours) has been identified.

6.5 Acknowledgments

This section was elaborated in collaboration with Yael Maulaz, Foteini Zafeiri, and Sahana Tavaragondi from Empa, Switzerland, and Vincenza Brancato, Angela Caprì and Andrea Frazzica from CNR-ITAE, Italy, with the support of the project *HyCool: Industrial Cooling through Hybrid system based on Solar Heat*, funded by the European Commission H2020 Programme under Grant Agreement No. 792073.

7 Conclusions

7.1 Key findings

In this thesis, some scientific challenges to the development of adsorption energy technology have been addressed. They include:

- the characterization and pre-selection of the adsorbent materials according to the process energy requirements,
- the development of a scalable modelling approach to describe heat and mass transfer in the adsorbent material during adsorption,
- the application of lightweight modelling approach to novel and more performing applications,
- the application of material's research to develop rapid thermal swing adsorption carbon capture,
- the effects of long-term usage and storage on the adsorbent materials.

The *fil rouge* connecting these relevant, but different research topics is the use of material characterization techniques to trigger performance improvements (or to prevent its degradation).

In fact, the first and most relevant finding of the research is the confirmation that material characterization and development are powerful tools that can be used at every scale of technological development.

More specifically, we demonstrated the following:

- The traditional method for characterizing adsorption curves is not efficient. Either faster screening techniques or more detailed models should be used instead.

- The integration of material selection and process design is a low-hanging fruit in system optimization. It requires further development for more accurate designs, but the tool can improve considerably the overall performance of adsorption systems.
- The localized lumped-parameter modelling approach is a convenient method to describe adsorption dynamics in the adsorbent materials. It works for different material classes and geometries, and it should be further extended for more complex simulations.
- The tailoring of sustainable activated carbons is a concrete opportunity to make our energy systems more efficient. We set up all the methods to design efficient equipment for reversible use (heating and cooling) and we identified the direction of further research (pyrolysis parameters, thickness, process temperature and working schemes).
- The agitated screw-conveyor adsorption heat exchanger concept can deliver increased energy and power performance, due to its intrinsic steady-state operation possibility. We developed a modelling tool that can be used for further research. This concept could be a game changer in the field if the relative design challenges (e.g. moving parts, wear, vacuum) are solved.
- Post-combustion carbon capture by rapid thermal swing adsorption is possible. We proved that adsorbent materials can be selected by virtue of their properties and can be tailored to cycle from adsorption to desorption in the span of a few minutes with minimal parasitic losses. The technology development still faces key challenges such as the evaluation of the key performance parameters under realistic scenarios and the upscale of the coating process.
- Material degradation is relevant to technological development and we provided methods to identify it.

7.2 Lessons Learned

In almost exactly four years of research, discussions with colleagues, and industrial and academic partners, the more important finding was that such a time is barely enough to scratch the surface of this interesting, multidisciplinary, and challenging field. To approach the right research questions with confidence and effectiveness, a great deal of knowledge and understanding of the scientific and technological frameworks is necessary. My own perspective and perception of the relative importance of different aspects of the research inevitably changed as well.

Among the lessons learned, I would surely list the few below.

As a fundamental source of data, the accuracy in the characterization of the adsorbent materials is of paramount importance. The difficulties related to such accuracy should not be underestimated by the users of such data (e.g. modelling at a higher scale). There is room for

improvement in the characterization techniques for sure, but the correct management of the basics provides a very solid foundation.

The material characterization can benefit not only from more accuracy but also from more effectiveness. Many resources can be wasted due to poor planning or because we do not make full use of pre-existing knowledge. One example is the adsorption equilibrium curves, illustrated in this thesis.

There is a missing link in the characterization from the material scale to the heat exchanger/prototype scale. Many things can change during the integration of the material on the heat exchanger, which threatens to jeopardize all the characterization efforts of the material developers. Experimental techniques to completely characterize the material as is, in situ, or even during real operation would help understand what are the limiting factors in this higher scale.

Because of the combination of the first and of the latter points, there is sometimes not much added value deriving from a very sophisticated heat and mass transfer knowledge. While it can be useful to describe the heat exchangers to evaluate macroscopic variations of temperature and pressure, observing it within the adsorbent materials is very challenging. For this reason, the localized lumped-parameter approach described in this thesis could be a good compromise to have a properties-based description of the adsorption and feasible simulation times. It does require more effort than fully lumped models, but it should ensure more flexibility.

Defining the conditions for application development is a challenging task. It is not simple, to develop a material before identifying a specific application, and vice-versa. This can generate a dangerous loop where the decision taking ball is metaphorically passed among different actors. A circular approach, in which decisions are taken by different actors in sequence with constant increments of required effort is a possible solution. For the activated carbon development for the district heating and cooling application, multiple rounds of decisions helped (and still help in further development) to narrow down the pyrolisis process parameters, as well as the requirements for the testing rig.

In the case of the preliminary design of the agitated adsorption heat exchanger, it was not easy to draw a line to which detail the model should go to have a credible estimate of the potential of the concept. It took a lot of discussions and quite some trials before settling on the approach presented. When research feels like a step in the dark, it is easy to give in to temptation and try to construct a whole map of the room in your head. But also in this case, the incremental effort approach should be applied, and the level of analysis reported gives ample room for the first experimental tests. We showed that the concept is promising and we developed a preliminary tool to play with to check for interesting applications.

The application of heat transformer coatings to rapid thermal swing adsorption of carbon dioxide from combustion flue gas was probably one of the more difficult and exciting challenges. In fact, in such a field, a consistent amount of additional knowledge regarding chemistry,

material science and the engineering of adsorption processes is required. It was interesting and exciting to reproduce research in the literature to create the coatings, adapting their formulations to our needs. Having to deal with methods and instruments that were not originally designed for the present scope: the restructuring of both software and hardware and the collection of the results showed how much the interaction among separated fields can give, but also its limitations. From our research, we set the foundations for more sophisticated material research and optimization, but we had to realize that the tools and the knowledge internally available were not sufficient. State-of-the-art methods will serve as inspiration in the future and external collaborations are envisaged for the success of the technology. Multi-gas adsorption dynamics play such a fundamental role, that dedicated tools are likely to be necessary for this peculiar application.

Handling different adsorbents for an extended period of time made it possible to have a first-hand experience of what the degradation of their performance means. As an energy engineer I would have carelessly assumed that once you have a material characterized, you can rely on it. It turns out that even what is considered "stable", is not really so. Driven by the observation of the change in adsorption capacity in our own activated carbons, we developed methods to assess what are the risks associated with the long-term use and storage of the adsorbents. This was industrially relevant, as also silica gels are not immune to degradation under certain circumstances.

The quality of the research requires time. It can be cumulated over various people and projects, but there is no escape from this fact. A team of experts, with long and consistent history in the field, allows for getting much quicker at the roots of the problems, and their subsequent solutions. Diversity within the team is also of great value. In fact, the topic is highly interdisciplinary (and even more so for gas separation processes), and it is surely challenging to have a complete background. Having chemists, material scientists, and chemical and mechanical engineers in the team would be undoubtedly beneficial. One of the limitations to more profound and more accurate scientific findings is the availability of such resources: time, experience and diversity. The synthesis of knowledge through writing, teaching and discussing is of paramount importance to mastering a field. Solo work, though highly efficient and necessary (especially in times of pandemics), can become a time-wasting trap if excessive. The risk is to miss very important facts while following the flow of your own work.

7.3 A look towards the future

Unfortunately, looking into the adsorbent materials and adsorption heat transformers did not provide answers regarding the future of our energy system and of humanity.

However, it did shed a feeble beam of light on some of the things that can be done to make adsorption energy technology penetrate the market. After many years passed wondering whether -to cite Uli Jakob- this is a sleeping giant or simply wishful thinking, the growing interest in adsorption carbon capture might change things rapidly.

The conjuncture of investor interest and scientific progress may as well be a turning point. Artificial intelligence and the unprecedented computational power of material researchers open fascinating possibilities, the affluence of experts from different domains promises a refreshing view, and the experimental and computational tools seem fit to bridge many of the existing gaps. As carbon capture becomes more prevalent, the demand for adsorbents and adsorption technology is likely to increase, which could lead to further research and development in this field and the creation of new business opportunities. Furthermore, the discovery of a new material, or a new method of material functionalization, could rapidly change the pace of deployment.

There is a chance something good will come out of this field. The potential of waste heat harvesting, exergetically efficient heating, cooling and carbon capture, and use of solar heat is incredible. The future awaits, maybe with a different society, maybe with a more sustainable energy system, and maybe with efficient and reliable adsorption energy technology used for that.

Bibliography

Abbasi, I. (2022). New Approach to CO2 Adsorption Could Improve Carbon Capture. *AZo Nano*. https://www.azonano.com/news.aspx?newsID=38534

Adkins, C. J. (1983). *Equilibrium thermodynamics* (3rd ed). Cambridge University Press.

Alahmer, A., Ajib, S., & Wang, X. (2019). Comprehensive strategies for performance improvement of adsorption air conditioning systems: A review. *Renewable and Sustainable Energy Reviews*, *99*, 138–158. https://doi.org/10.1016/j.rser.2018.10.004

AL-Dadah, R., Mahmoud, S., Elsayed, E., Youssef, P., & Al-Mousawi, F. (2020). Metal-organic framework materials for adsorption heat pumps. *Energy*, *190*, 116356. https://doi.org/10.1016/j.energy.2019.116356

AL-Hasni, S., Grant, R., & Santori, G. (2022). The cost of manufacturing adsorption chillers. *Heat Powered Cycles 2021*, 138–148.

AL-Hasni, S., & Santori, G. (2020). 3D printing of vacuum and pressure tight polymer vessels for thermally driven chillers and heat pumps. *Vacuum*, *171*, 109017. https://doi.org/10.1016/j.vacuum.2019.109017

Alshrah, M., Tran, M.-P., Gong, P., Naguib, H. E., & Park, C. B. (2017). Development of high-porosity resorcinol formaldehyde aerogels with enhanced mechanical properties through improved particle necking under CO 2 supercritical conditions. *Journal of Colloid and Interface Science*, *485*, 65–74. https://doi.org/10.1016/j.jcis.2016.09.030

Altintas, C., Avci, G., Daglar, H., Nemati Vesali Azar, A., Velioglu, S., Erucar, I., & Keskin, S. (2018). Database for CO $_2$ Separation Performances of MOFs Based on Computational Materials Screening. *ACS Applied Materials & Interfaces*, *10*(20), 17257–17268. https://doi.org/10.1021/acsami.8b04600

Ammann, J., Michel, B., & Ruch, P. W. (2019). Characterization of transport limitations in SAPO-34 adsorbent coatings for adsorption heat pumps. *International Journal of Heat and Mass Transfer*, *129*, 18–27. https://doi.org/10.1016/j.ijheatmasstransfer.2018.09.053

Ammann, J., Michel, B., Studart, A. R., & Ruch, P. W. (2019). Sorption rate enhancement in SAPO-34 zeolite by directed mass transfer channels. *International Journal of Heat and Mass Transfer*, *130*, 25–32. https://doi.org/10.1016/j.ijheatmasstransfer.2018.10.065

Ammann, J., Ruch, P., Michel, B., & Studart, A. R. (2018). Quantification of heat and mass transport limitations in adsorption heat exchangers: Application to the silica gel/water working pair. *International Journal of Heat and Mass Transfer*, *123*, 331–341. https://doi.org/10.1016/j.ijheatmasstransfer.2018.02.076

Ammann, J., Ruch, P., Michel, B., & Studart, A. R. (2019). High-Power Adsorption Heat Pumps Using Magnetically Aligned Zeolite Structures. *ACS Applied Materials & Interfaces*, *11*(27), 24037–24046. https://doi.org/10.1021/acsami.9b04692

Andreas Ruckstuhl, C. S. (2005). *Robust fitting of nonlinear regression models*.

Aristov, Y., Sapienza, A., Ovoshchnikov, D., Freni, A., & Restuccia, G. (2012). Reallocation of adsorption and desorption times for optimisation of cooling cycles. *International Journal of Refrigeration*, *35*(3), 525–531. https://doi.org/10.1016/j.ijrefrig.2010.07.019

Aristov, Y. (2014). Concept of adsorbent optimal for adsorptive cooling/heating. *Applied Thermal Engineering*, *72*(2), 166–175. https://doi.org/10.1016/j.applthermaleng.2014.04.077

Aristov, Y. I. (2017). Adsorptive transformation and storage of renewable heat: Review of current trends in adsorption dynamics. *Renewable Energy*, *110*, 105–114. https://doi.org/10.1016/j.renene.2016.06.055

Aristov, Y. I. (2020). Dynamics of adsorptive heat conversion systems: Review of basics and recent advances. *Energy*, *205*, 117998. https://doi.org/10.1016/j.energy.2020.117998

Aristov, Y. I. (2009). Optimal adsorbent for adsorptive heat transformers: Dynamic considerations. *International Journal of Refrigeration*, *32*(4), 675–686. https://doi.org/10.1016/j.ijrefrig.2009.01.022

Aristov, Y. I. (2012). Adsorptive transformation of heat: Principles of construction of adsorbents database. *Applied Thermal Engineering*, *42*, 18–24. https://doi.org/10.1016/j.applthermaleng.2011.02.024

Aristov, Y. I. (2013). Challenging offers of material science for adsorption heat transformation: A review. *Applied Thermal Engineering*, *50*(2), 1610–1618. https://doi.org/10.1016/j.applthermaleng.2011.09.003

Aristov, Y. I., Glaznev, I. S., & Girnik, I. S. (2012). Optimization of adsorption dynamics in adsorptive chillers: Loose grains configuration. *Energy*, *46*(1), 484–492. https://doi.org/10.1016/j.energy.2012.08.001

Aristov, Y. I. (2007). Novel Materials for Adsorptive Heat Pumping and Storage: Screening and Nanotailoring of Sorption Properties. *JOURNAL OF CHEMICAL ENGINEERING OF JAPAN*, *40*(13), 1242–1251. https://doi.org/10.1252/jcej.07WE228

Askalany, A. A., Salem, M., Ismael, I., Ali, A., Morsy, M., & Saha, B. B. (2013). An overview on adsorption pairs for cooling. *Renewable and Sustainable Energy Reviews*, *19*, 565–572. https://doi.org/10.1016/j.rser.2012.11.037

Bahamon, D., Díaz-Márquez, A., Gamallo, P., & Vega, L. F. (2018). Energetic evaluation of swing adsorption processes for CO 2 capture in selected MOFs and zeolites: Effect of impurities. *Chemical Engineering Journal*, *342*, 458–473. https://doi.org/10.1016/j.cej.2018.02.094

Banerjee, D., Simon, C. M., Plonka, A. M., Motkuri, R. K., Liu, J., Chen, X., Smit, B., Parise, J. B., Haranczyk, M., & Thallapally, P. K. (2016). Metal–organic framework with optimally selective xenon adsorption and separation. *Nature Communications*, *7*(1), ncomms11831. https://doi.org/10.1038/ncomms11831

Basu, P., & Nag, P. (1987). An investigation into heat transfer in circulating fluidized beds. *International Journal of Heat and Mass Transfer*, *30*(11), 2399–2409. https://doi.org/10.1016/0017-9310(87)90230-4

Bau, U., Hoseinpoori, P., Graf, S., Schreiber, H., Lanzerath, F., Kirches, C., & Bardow, A. (2017). Dynamic optimisation of adsorber-bed designs ensuring optimal control. *Applied Thermal Engineering*, *125*, 1565–1576. https://doi.org/10.1016/j.applthermaleng.2017.07.073

Bau, U., Lanzerath, F., Gräber, M., Graf, S., Schreiber, H., Thielen, N., & Bardow, A. (2014). Adsorption energy systems library - Modeling adsorption based chillers, heat pumps, thermal storages and desiccant systems, 875–883. https://doi.org/10.3384/ecp14096875

Behjat, Y., Shahhosseini, S., & Hashemabadi, S. H. (2008). CFD modeling of hydrodynamic and heat transfer in fluidized bed reactors. *International Communications in Heat and Mass Transfer*, *35*(3), 357–368. https://doi.org/10.1016/j.icheatmasstransfer.2007.09.011

Ben-Mansour, R., & Qasem, N. A. (2018). An efficient temperature swing adsorption (TSA) process for separating CO2 from CO2/N2 mixture using Mg-MOF-74. *Energy Conversion and Management*, *156*, 10–24. https://doi.org/10.1016/j.enconman.2017.11.010

Bergman, T. L., Lavine, A., & Incropera, F. P. (2019). *Fundamentals of heat and mass transfer* (Eighth edition. Wiley abridged print companion) [OCLC: 1111712337]. John Wiley & Sons, Inc.

Birol, D. F. (2018). The Future of Cooling, 92.

Bollini, P., Choi, S., Drese, J. H., & Jones, C. W. (2011). Oxidative Degradation of Aminosilica Adsorbents Relevant to Postcombustion CO $_2$ Capture. *Energy & Fuels*, *25*(5), 2416–2425. https://doi.org/10.1021/ef200140z

Boman, D. B., Hoysall, D. C., Pahinkar, D. G., Ponkala, M. J., & Garimella, S. (2017). Screening of working pairs for adsorption heat pumps based on thermodynamic and transport characteristics. *Applied Thermal Engineering*, *123*, 422–434. https://doi.org/10.1016/j.applthermaleng.2017.04.153

Brancato, V., & Frazzica, A. (2018). Characterisation and comparative analysis of zeotype water adsorbents for heat transformation applications. *Solar Energy Materials and Solar Cells*, *180*, 91–102. https://doi.org/10.1016/j.solmat.2018.02.035

Brunauer, S., Emmett, P. H., & Teller, E. (1938). Adsorption of Gases in Multimolecular Layers. *Journal of the American Chemical Society*, *60*(2), 309–319. https://doi.org/10.1021/ja01269a023

Brunschwiler, T., Smith, B., Ruetsche, E., & Michel, B. (2009). Toward zero-emission data centers through direct reuse of thermal energy. *IBM Journal of Research and Development*, *53*(3), 11:1–11:13. https://doi.org/10.1147/JRD.2009.5429024

Builes, S., Sandler, S. I., & Xiong, R. (2013). Isosteric Heats of Gas and Liquid Adsorption. *Langmuir*, *29*(33), 10416–10422. https://doi.org/10.1021/la401035p

Burtch, N. C., Jasuja, H., & Walton, K. S. (2014). Water Stability and Adsorption in Metal–Organic Frameworks. *Chemical Reviews*, *114*(20), 10575–10612. https://doi.org/10.1021/cr5002589

Butler, K. T., Davies, D. W., Cartwright, H., Isayev, O., & Walsh, A. (2018). Machine learning for molecular and materials science. *Nature*, *559*(7715), 547–555. https://doi.org/10.1038/s41586-018-0337-2

Çağlar, A. (2016). The effect of fin design parameters on the heat transfer enhancement in the adsorbent bed of a thermal wave cycle. *Applied Thermal Engineering*, *104*, 386–393. https://doi.org/10.1016/j.applthermaleng.2016.05.092

Calabrese, L., Bonaccorsi, L., Bruzzaniti, P., Frazzica, A., Freni, A., & Proverbio, E. (2018). Adsorption performance and thermodynamic analysis of SAPO-34 silicone composite foams for adsorption heat pump applications. *Materials for Renewable and Sustainable Energy*, *7*(4), 24. https://doi.org/10.1007/s40243-018-0131-y

Calise, F., Figaj, R. D., & Vanoli, L. (2017). A novel polygeneration system integrating photovoltaic/thermal collectors, solar assisted heat pump, adsorption chiller and electrical energy storage: Dynamic and energy-economic analysis. *Energy Conversion and Management*, *149*, 798–814. https://doi.org/10.1016/j.enconman.2017.03.027

Caprì, A., Frazzica, A., & Calabrese, L. (2020). Recent Developments in Coating Technologies for Adsorption Heat Pumps: A Review. *Coatings*, *10*(9), 855. https://doi.org/10.3390/coatings10090855

Carslaw, H., & Jaeger, J. (1959). *Conduction of Heat in Solids* (2nd). Oxford University Press.

Casas, N., Schell, J., Pini, R., & Mazzotti, M. (2012). Fixed bed adsorption of CO2/H2 mixtures on activated carbon: experiments and modeling. *Adsorption*, *18*(2), 143–161. https://doi.org/10.1007/s10450-012-9389-z

Ceballos, G., Ehrlich, P. R., Barnosky, A. D., García, A., Pringle, R. M., & Palmer, T. M. (2015). Accelerated modern human–induced species losses: Entering the sixth mass extinction. *Science Advances*, *1*(5), e1400253. https://doi.org/10.1126/sciadv.1400253

Chakraborty, A., Saha, B. B., Koyama, S., Ng, K. C., & Srinivasan, K. (2009). Adsorption Thermodynamics of Silica GelWater Systems. *Journal of Chemical & Engineering Data*, *54*(2), 448–452. https://doi.org/10.1021/je800458k

Chang, J., Wang, G., Gao, J., Zhang, K., Chen, H., & Yang, Y. (2012). CFD modeling of particle–particle heat transfer in dense gas-solid fluidized beds of binary mixture. *Powder Technology*, *217*, 50–60. https://doi.org/10.1016/j.powtec.2011.10.008

Chao, C., Deng, Y., Dewil, R., Baeyens, J., & Fan, X. (2021). Post-combustion carbon capture. *Renewable and Sustainable Energy Reviews*, *138*, 110490. https://doi.org/10.1016/j.rser.2020.110490

Chen, C., Zhang, S., Row, K. H., & Ahn, W.-S. (2017). Amine–silica composites for CO2 capture: A short review. *Journal of Energy Chemistry*, *26*(5), 868–880. https://doi.org/10.1016/j.jechem.2017.07.001

Cheng, D., Peters, E. (, & Kuipers, J. ((2016). Numerical modelling of flow and coupled mass and heat transfer in an adsorption process. *Chemical Engineering Science*, *152*, 413–425. https://doi.org/10.1016/j.ces.2016.06.036

Chun, J., Kang, S., Park, N., Park, E. J., Jin, X., Kim, K.-D., Seo, H. O., Lee, S. M., Kim, H. J., Kwon, W. H., Park, Y.-K., Kim, J. M., Kim, Y. D., & Son, S. U. (2014). Metal–Organic Framework@Microporous Organic Network: Hydrophobic Adsorbents with a Crys-

talline Inner Porosity. *Journal of the American Chemical Society*, *136*(19), 6786–6789. https://doi.org/10.1021/ja500362w

Civioc, R., Lattuada, M., Koebel, M. M., & Galmarini, S. (2020). Monolithic resorcinol–formaldehyde alcogels and their corresponding nitrogen-doped activated carbons. *Journal of Sol-Gel Science and Technology*, *95*(3), 719–732. https://doi.org/10.1007/s10971-020-05288-x

Cloete, S., Giuffrida, A., Romano, M. C., & Zaabout, A. (2020). Economic assessment of the swing adsorption reactor cluster for CO2 capture from cement production. *Journal of Cleaner Production*, *275*, 123024. https://doi.org/10.1016/j.jclepro.2020.123024

community, T. S. (n.d.). PCHIP 1-D monotonic cupic interpolation.

Cowie, R. H., Bouchet, P., & Fontaine, B. (2022). The Sixth Mass Extinction: fact, fiction or speculation? *Biological Reviews*, *97*(2), 640–663. https://doi.org/10.1111/brv.12816

Crawford, C. B., & Quinn, B. (2017). The interactions of microplastics and chemical pollutants. In *Microplastic Pollutants* (pp. 131–157). Elsevier. https://doi.org/10.1016/B978-0-12-809406-8.00006-2

Curry, P. (2011). *Ecological ethics: an introduction* (2nd ed., fully rev. and expanded) [OCLC: ocn707263814]. Polity Press.

Daguenet-Frick, X., Moullet, Y., Gantenbein, P., Persdorf, P., & Notter, D. (2017). Adsorption Heat Pump Upscaling from 1 KW to 10 KW of Cooling Power: Experimental Based Modelling. *International Sorption Heat Pump Conference 2017*.

D'Alessandro, D. M., Smit, B., & Long, J. R. (2010). Carbon Dioxide Capture: Prospects for New Materials. *Angewandte Chemie International Edition*, *49*(35), 6058–6082. https://doi.org/10.1002/anie.201000431

Daly, H. E. (1997). *Beyond growth: the economics of sustainable development* (Nachdr.). Beacon Press.

de Lange, M. F., van Velzen, B. L., Ottevanger, C. P., Verouden, K. J. F. M., Lin, L.-C., Vlugt, T. J. H., Gascon, J., & Kapteijn, F. (2015). Metal–Organic Frameworks in Adsorption-Driven Heat Pumps: The Potential of Alcohols as Working Fluids. *Langmuir*, *31*(46), 12783–12796. https://doi.org/10.1021/acs.langmuir.5b03272

de Lange, M. F., Verouden, K. J. F. M., Vlugt, T. J. H., Gascon, J., & Kapteijn, F. (2015). Adsorption-Driven Heat Pumps: The Potential of Metal–Organic Frameworks. *Chemical Reviews*, *115*(22), 12205–12250. https://doi.org/10.1021/acs.chemrev.5b00059

Demir, H., Mobedi, M., & Ülkü, S. (2008). A review on adsorption heat pump: Problems and solutions. *Renewable and Sustainable Energy Reviews*, *12*(9), 2381–2403. https://doi.org/10.1016/j.rser.2007.06.005

DeWitt, S. J., Sinha, A., Kalyanaraman, J., Zhang, F., Realff, M. J., & Lively, R. P. (2018). Critical Comparison of Structured Contactors for Adsorption-Based Gas Separations. *Annual Review of Chemical and Biomolecular Engineering*, *9*(1), 129–152. https://doi.org/10.1146/annurev-chembioeng-060817-084120

Dhoke, C., Cloete, S., Krishnamurthy, S., Seo, H., Luz, I., Soukri, M., Park, Y.-k., Blom, R., Amini, S., & Zaabout, A. (2020). Sorbents screening for post-combustion CO2 capture via combined temperature and pressure swing adsorption. *Chemical Engineering Journal*, *380*, 122201. https://doi.org/10.1016/j.cej.2019.122201

Dias, J. M., & Costa, V. A. (2019). Which dimensional model for the analysis of a coated tube adsorber for adsorption heat pumps? *Energy*, *174*, 1110–1120. https://doi.org/10.1016/j.energy.2019.03.028

Dino, G. E., Palomba, V., Nowak, E., & Frazzica, A. (2021). Experimental characterization of an innovative hybrid thermal-electric chiller for industrial cooling and refrigeration application. *Applied Energy*, *281*, 116098. https://doi.org/10.1016/j.apenergy.2020.116098

Do, D., & Do, H. (2000). A model for water adsorption in activated carbon. *Carbon*, *38*(5), 767–773. https://doi.org/10.1016/S0008-6223(99)00159-1

Drage, T. C., Snape, C. E., Stevens, L. A., Wood, J., Wang, J., Cooper, A. I., Dawson, R., Guo, X., Satterley, C., & Irons, R. (2012). Materials challenges for the development of solid sorbents for post-combustion carbon capture. *J. Mater. Chem.*, *22*(7), 2815–2823. https://doi.org/10.1039/C2JM12592G

Dubbeldam, D., Calero, S., Ellis, D. E., & Snurr, R. Q. (2016). RASPA: molecular simulation software for adsorption and diffusion in flexible nanoporous materials. *Molecular Simulation*, *42*(2), 81–101. https://doi.org/10.1080/08927022.2015.1010082

Dubinin, M., & Astakhov, V. (1971). Development of the concepts of volume filling of micropores in the adsorption of gases and vapors by microporous adsorbents, 5.

Düren, T., Bae, Y.-S., & Snurr, R. Q. (2009). Using molecular simulation to characterise metal–organic frameworks for adsorption applications. *Chemical Society Reviews*, *38*(5), 1237. https://doi.org/10.1039/b803498m

El-Sharkawy, I. I. (2011). On the linear driving force approximation for adsorption cooling applications. *International Journal of Refrigeration*, *34*(3), 667–673. https://doi.org/10.1016/j.ijrefrig.2010.12.006

El-Sharkawy, I. I., Pal, A., Miyazaki, T., Saha, B. B., & Koyama, S. (2016). A study on consolidated composite adsorbents for cooling application. *Applied Thermal Engineering*, *98*, 1214–1220. https://doi.org/10.1016/j.applthermaleng.2015.12.105

Engelpracht, M., Yang, Z., Gluesenkamp, K. R., Turnaoglu, T., Seiler, J. M., & Bardow, A. (2020). SorpPropLib : An Open-Source Database for Sorption Equilibrium Properties [Artwork Size: pages 33-36 Publisher: RWTH Aachen University]. *ISHPC 2021 proceedings – online pre-conference 2020 : August 17th, 2020*, pages 33–36. https://doi.org/10.18154/RWTH-2020-09119

Eun, T.-H., Song, H.-K., Han, J. H., Lee, K.-H., & Kim, J.-N. (2000). Enhancement of heat and mass transfer in silica-expanded graphite composite blocks for adsorption heat pumps. Part II. Cooling system using the composite blocks. *International Journal of Refrigeration*, *23*(1), 74–81. https://doi.org/10.1016/S0140-7007(99)00036-5

Fernandes, M., Brites, G., Costa, J., Gaspar, A., & Costa, V. (2014). Review and future trends of solar adsorption refrigeration systems. *Renewable and Sustainable Energy Reviews*, *39*, 102–123. https://doi.org/10.1016/j.rser.2014.07.081

Fischer-Kowalski, M., Krausmann, F., & Pallua, I. (2014). A sociometabolic reading of the Anthropocene: Modes of subsistence, population size and human impact on Earth. *The Anthropocene Review*, *1*(1), 8–33. https://doi.org/10.1177/2053019613518033

Frazzica, A., Palomba, V., Dawoud, B., Gullì, G., Brancato, V., Sapienza, A., Vasta, S., Freni, A., Costa, F., & Restuccia, G. (2016). Design, realization and testing of an adsorption refrigerator based on activated carbon/ethanol working pair. *Applied Energy, 174*, 15–24. https://doi.org/10.1016/j.apenergy.2016.04.080

Frazzica, A., & Brancato, V. (2019). Verification of hydrothermal stability of adsorbent materials for thermal energy storage. *International Journal of Energy Research, 43*(12), 6161–6170. https://doi.org/10.1002/er.4270

Frazzica, A., Decorme, R., Calderoni, M., Cuneo, A., Ťaťáková, Z., Scoccia, R., Jakob, U., Carbonell, D., Karellas, S., Spijker, E., Cioni, G., Varga, S., Mahkamov, K., Gracia, A. D., Zsembinszki, G., Cabeza, L. F., Ciccolanti, L., Vuillerme, V., & Fabiani, C. (2020). Renewable Heating and Cooling Solutions for Buildings and Industry. *The 8th Annual International Sustainable Places Conference (SP2020) Proceedings*, 16. https://doi.org/10.3390/proceedings2020065016

Frazzica, A., & Freni, A. (2017). Adsorbent working pairs for solar thermal energy storage in buildings. *Renewable Energy, 110*, 87–94. https://doi.org/10.1016/j.renene.2016.09.047

Frazzica, A., Palomba, V., & Dawoud, B. (2021). Thermodynamic Performance of Adsorption Working Pairs for Low-Temperature Waste Heat Upgrading in Industrial Applications. *Applied Sciences, 11*(8), 3389. https://doi.org/10.3390/app11083389

Frazzica, A., Sapienza, A., & Freni, A. (2014). Novel experimental methodology for the characterization of thermodynamic performance of advanced working pairs for adsorptive heat transformers. *Applied Thermal Engineering, 72*(2), 229–236. https://doi.org/10.1016/j.applthermaleng.2014.07.005

Freni, A., Calabrese, L., Malara, A., Frontera, P., & Bonaccorsi, L. (2019). Silica gel microfibres by electrospinning for adsorption chillers. *Energy, 187*, 115971. https://doi.org/10.1016/j.energy.2019.115971

Freni, A., Bonaccorsi, L., Calabrese, L., Caprì, A., Frazzica, A., & Sapienza, A. (2015). SAPO-34 coated adsorbent heat exchanger for adsorption chillers. *Applied Thermal Engineering, 82*, 1–7. https://doi.org/10.1016/j.applthermaleng.2015.02.052

Freni, A., Frazzica, A., Dawoud, B., Chmielewski, S., Calabrese, L., & Bonaccorsi, L. (2013). Adsorbent coatings for heat pumping applications: Verification of hydrothermal and mechanical stabilities. *Applied Thermal Engineering, 50*(2), 1658–1663. https://doi.org/10.1016/j.applthermaleng.2011.07.010

Freni, A., Maggio, G., Sapienza, A., Frazzica, A., Restuccia, G., & Vasta, S. (2016). Comparative analysis of promising adsorbent/adsorbate pairs for adsorptive heat pumping, air conditioning and refrigeration. *Applied Thermal Engineering, 104*, 85–95. https://doi.org/10.1016/j.applthermaleng.2016.05.036

Fritsch, F. N., & Butland, J. (1984). A Method for Constructing Local Monotone Piecewise Cubic Interpolants. *SIAM Journal on Scientific and Statistical Computing, 5*(2), 300–304. https://doi.org/10.1137/0905021

Froestad, J., & Shearing, C. (2017). Energy and the Anthropocene: security challenges and solutions. *Crime, Law and Social Change, 68*(5), 515–528. https://doi.org/10.1007/s10611-017-9700-8

Fu, Q., Yan, H., Shen, Y., Qin, Y., Zhang, D., & Zhou, Y. (2018). Optimal design and control of pressure swing adsorption process for N2/CH4 separation. *Journal of Cleaner Production*, *170*, 704–714. https://doi.org/10.1016/j.jclepro.2017.09.169

Galmarini, S., Piccoli, E., & Civioc, R. (2019). D4.1 Measuring protocol for the characterization of adsorber materials [Publisher: Zenodo Version Number: 5]. https://doi.org/10.5281/ZENODO.7224978

Gantenbein, P., Daguenet-Frick, X., Bont, F., Persdorf, P., & Notter, D. (2017). Cooling power determination by measuring the adsorbed vapor mass variations: comparison of mass adsorption cooling power correlation and external fluid loop power measurement. *International Sorption Heat Pump Conference 2017*.

Gebald, C., Wurzbacher, J. A., Tingaut, P., & Steinfeld, A. (2013). Stability of Amine-Functionalized Cellulose during Temperature-Vacuum-Swing Cycling for CO_2 Capture from Air. *Environmental Science & Technology*, *47*(17), 10063–10070. https://doi.org/10.1021/es401731p

Glass, S. V., Boardman, C. R., Thybring, E. E., & Zelinka, S. L. (2018). Quantifying and reducing errors in equilibrium moisture content measurements with dynamic vapor sorption (DVS) experiments. *Wood Science and Technology*, *52*(4), 909–927. https://doi.org/10.1007/s00226-018-1007-0

Glaznev, I., Ovoshchnikov, D., & Aristov, Y. (2010). Effect of Residual Gas on Water Adsorption Dynamics Under Typical Conditions of an Adsorption Chiller. *Heat Transfer Engineering*, *31*(11), 924–930. https://doi.org/10.1080/01457631003604335

Go, M., Hwang, B., & Lim, S. (2019). Highly reliable mulberry paper (Hanji)-based electrode with printed silver nanowire/zinc oxide hybrid for soft electronics. *Materials and Manufacturing Processes*, *34*(14), 1605–1611. https://doi.org/10.1080/10426914.2019.1594266

Gomez-Garcia, F., Gauthier, D., & Flamant, G. (2017). Design and performance of a multistage fluidised bed heat exchanger for particle-receiver solar power plants with storage. *Applied Energy*, *190*, 510–523. https://doi.org/10.1016/j.apenergy.2016.12.140

Gordeeva, L., & Aristov, Y. (2014). Dynamic study of methanol adsorption on activated carbon ACM-35.4 for enhancing the specific cooling power of adsorptive chillers. *Applied Energy*, *117*, 127–133. https://doi.org/10.1016/j.apenergy.2013.11.073

Gordeeva, L., & Aristov, Y. (2019). Adsorptive heat storage and amplification: New cycles and adsorbents. *Energy*, *167*, 440–453. https://doi.org/10.1016/j.energy.2018.10.132

Graf, S., Lanzerath, F., & Bardow, A. (2017). The IR-Large-Temperature-Jump method: Determining heat and mass transfer coefficients for adsorptive heat transformers. *Applied Thermal Engineering*, *126*, 630–642. https://doi.org/10.1016/j.applthermaleng.2017.06.054

Graf, S., Lanzerath, F., Sapienza, A., Frazzica, A., Freni, A., & Bardow, A. (2016). Prediction of SCP and COP for adsorption heat pumps and chillers by combining the large-temperature-jump method and dynamic modeling. *Applied Thermal Engineering*, *98*, 900–909. https://doi.org/10.1016/j.applthermaleng.2015.12.002

Greenhouse gas emissions from energy: overview (tech. rep.). (2021). IEA. Paris. Retrieved February 25, 2022, from https://www.iea.org/reports/greenhouse-gas-emissions-from-energy-overview

Gulledge, J. (2013). Anthropocene. https://editors.eol.org/eoearth/wiki/Anthropocene

Hamzehei, M., & Rahimzadeh, H. (2009). Experimental and Numerical Study of Hydrodynamics with Heat Transfer in a GasSolid Fluidized-Bed Reactor at Different Particle Sizes. *Industrial & Engineering Chemistry Research*, *48*(6), 3177–3186. https://doi.org/10.1021/ie801413q

Han, B., & Chakraborty, A. (2020). Adsorption characteristics of methyl-functional ligand MOF-801 and water systems: Adsorption chiller modelling and performances. *Applied Thermal Engineering*, *175*, 115393. https://doi.org/10.1016/j.applthermaleng.2020.115393

Hassan, A. A., Elwardany, A. E., Ookawara, S., Ahmed, M., & El-Sharkawy, I. I. (2020). Integrated adsorption-based multigeneration systems: A critical review and future trends. *International Journal of Refrigeration*, *116*, 129–145. https://doi.org/10.1016/j.ijrefrig.2020.04.001

Hedin, N., Andersson, L., Bergström, L., & Yan, J. (2013). Adsorbents for the post-combustion capture of CO2 using rapid temperature swing or vacuum swing adsorption. *Applied Energy*, *104*, 418–433. https://doi.org/10.1016/j.apenergy.2012.11.034

Hefti, M., & Mazzotti, M. (2018). Postcombustion CO $_2$ Capture from Wet Flue Gas by Temperature Swing Adsorption. *Industrial & Engineering Chemistry Research*, acs.iecr.8b03580. https://doi.org/10.1021/acs.iecr.8b03580

Henninger, S. K., Hügenell, P., Munz, G., Baumgartner, M., Kummer, H., & Jeremias, F. (2015). Untersuchung des Degradationsverhaltens von Sorptionsmaterialien und Verbundsystemen zur Wärmespeicherung und -transformation.

Henninger, S., Munz, G., Ratzsch, K.-F., & Schossig, P. (2011). Cycle stability of sorption materials and composites for the use in heat pumps and cooling machines. *Renewable Energy*, *36*(11), 3043–3049. https://doi.org/10.1016/j.renene.2011.03.032

Henninger, S., Schmidt, F., & Henning, H.-M. (2010). Water adsorption characteristics of novel materials for heat transformation applications. *Applied Thermal Engineering*, *30*(13), 1692–1702. https://doi.org/10.1016/j.applthermaleng.2010.03.028

Henninger, S. K., Ernst, S.-J., Gordeeva, L., Bendix, P., Fröhlich, D., Grekova, A. D., Bonaccorsi, L., Aristov, Y., & Jaenchen, J. (2017). New materials for adsorption heat transformation and storage. *Renewable Energy*, *110*, 59–68. https://doi.org/10.1016/j.renene.2016.08.041

Henninger, S. K., Jeremias, F., Kummer, H., & Janiak, C. (2012). MOFs for Use in Adsorption Heat Pump Processes. *European Journal of Inorganic Chemistry*, *2012*(16), 2625–2634. https://doi.org/10.1002/ejic.201101056

Hickel, J. (2021). *Less Is More: How Degrowth Will Save the World*. Windmill Books.

Hickel, J. (2019). Is it possible to achieve a good life for all within planetary boundaries? *Third World Quarterly*, *40*(1), 18–35. https://doi.org/10.1080/01436597.2018.1535895

Hogan, M. (2012). Holocene Climate. https://editors.eol.org/eoearth/wiki/Holocene_Climate

Hong, S. W., Ahn, S. H., Kwon, O. K., & Chung, J. D. (2014). Validity of intra-particle models of mass transfer kinetics in the analysis of a fin-tube type adsorption bed. *Journal of Mechanical Science and Technology*, *28*(5), 1985–1993. https://doi.org/10.1007/s12206-014-0347-4

Hou, D., Qiao, G., & Wang, P. (2021). Molecular dynamics study on water and ions transport mechanism in nanometer channel of 13X zeolite. *Chemical Engineering Journal*, *420*, 129975. https://doi.org/10.1016/j.cej.2021.129975

Huber, L., Hauser, S. B., Brendlé, E., Ruch, P., Ammann, J., Hauert, R., Widmer, R. N., Ubert, C. J., Matam, S. K., Yoon, S., Zhang, Y., & Koebel, M. M. (2019). The effect of activation time on water sorption behavior of nitrogen-doped, physically activated, monolithic carbon for adsorption cooling. *Microporous and Mesoporous Materials*, *276*, 239–250. https://doi.org/10.1016/j.micromeso.2018.09.025

Huber, L., Ruch, P., Hauert, R., Matam, S. K., Saucke, G., Yoon, S., Zhang, Y., & Koebel, M. M. (2016). Water sorption behavior of physically and chemically activated monolithic nitrogen doped carbon for adsorption cooling. *RSC Advances*, *6*(84), 80729–80738. https://doi.org/10.1039/C6RA18660B

Huber, L., Ruch, P., Hauert, R., Saucke, G., Matam, S. K., Michel, B., & Koebel, M. M. (2016). Monolithic nitrogen-doped carbon as a water sorbent for high-performance adsorption cooling. *RSC Advances*, *6*(30), 25267–25278. https://doi.org/10.1039/C6RA00548A

Hussin, F., & Aroua, M. K. (2020). Recent trends in the development of adsorption technologies for carbon dioxide capture: A brief literature and patent reviews (2014–2018). *Journal of Cleaner Production*, *253*, 119707. https://doi.org/10.1016/j.jclepro.2019.119707

IEA. (2019). World Energy Balances 2019 Edition.

IEA. (2020). Energy Technology Perspectives 2020. *Energy Technology Perspectives*, 400.

IEA. (2021). Net Zero by 2050 - A Roadmap for the Global Energy Sector, 224.

Institute, G. C. (2021). Global Status of CCS 2021.

IPCC. (2014). *Climate Change 2014: Synthesis Report* (tech. rep.). IPCC. Geneva, Switzerland.

Jacobs, J. H., Deering, C. E., Lesage, K. L., Stashick, M. J., & Marriott, R. A. (2021). Rapid Cycling Thermal Swing Adsorption Apparatus: Commissioning and Data Analyses for Water Adsorption of Zeolites 4A and 13X Over 2000 Cycles. *Industrial & Engineering Chemistry Research*, *60*(19), 7487–7494. https://doi.org/10.1021/acs.iecr.1c00469

Jahan, I., Islam, M. A., Palash, M. L., Rocky, K. A., Rupam, T. H., & Saha, B. B. (2020). Experimental Study on the Influence of Metal Doping on Thermophysical Properties of Porous Aluminum Fumarate. *Heat Transfer Engineering*, 1–10. https://doi.org/10.1080/01457632.2020.1777005

Jahan, I., Rupam, T. H., Palash, M., Rocky, K. A., & Saha, B. B. (2022). Energy efficient green synthesized MOF-801 for adsorption cooling applications. *Journal of Molecular Liquids*, *345*, 117760. https://doi.org/10.1016/j.molliq.2021.117760

Jeremias, F., Fröhlich, D., Janiak, C., & Henninger, S. K. (2014). Advancement of sorption-based heat transformation by a metal coating of highly-stable, hydrophilic aluminium fumarate MOF. *RSC Adv.*, *4*(46), 24073–24082. https://doi.org/10.1039/C4RA03794D

Jeremias, F., Lozan, V., Henninger, S. K., & Janiak, C. (2013). Programming MOFs for water sorption: amino-functionalized MIL-125 and UiO-66 for heat transformation and heat storage applications. *Dalton Transactions*, *42*(45), 15967. https://doi.org/10.1039/c3dt51471d

Jiang, L., Wang, R., Gonzalez-Diaz, A., Smallbone, A., Lamidi, R., & Roskilly, A. (2020). Comparative analysis on temperature swing adsorption cycle for carbon capture by using internal heat/mass recovery. *Applied Thermal Engineering*, *169*, 114973. https://doi.org/10.1016/j.applthermaleng.2020.114973

Jiang, L., Fox, V. G., & Biegler, L. T. (2004). Simulation and optimal design of multiple-bed pressure swing adsorption systems. *AIChE Journal*, *50*(11), 2904–2917. https://doi.org/10.1002/aic.10223

Jobard, X., Padey, P., Guillaume, M., Duret, A., & Pahud, D. (2020). Development and Testing of Novel Applications for Adsorption Heat Pumps and Chillers. *Energies*, *13*(3), 615. https://doi.org/10.3390/en13030615

Joss, L., Gazzani, M., & Mazzotti, M. (2017). Rational design of temperature swing adsorption cycles for post-combustion CO 2 capture. *Chemical Engineering Science*, *158*, 381–394. https://doi.org/10.1016/j.ces.2016.10.013

Jung, W., An, H., Lee, J., & Lee, J. S. (2022). Self-regenerative rapid thermal swing adsorption process using structured fiber sorbents for energy-efficient H2O removal. *Chemical Engineering Journal*, *446*, 137219. https://doi.org/10.1016/j.cej.2022.137219

Jungell-Michelsson, J., & Heikkurinen, P. (2022). Sufficiency: A systematic literature review. *Ecological Economics*, *195*, 107380. https://doi.org/10.1016/j.ecolecon.2022.107380

Kayal, S., Baichuan, S., & Saha, B. B. (2016). Adsorption characteristics of AQSOA zeolites and water for adsorption chillers. *International Journal of Heat and Mass Transfer*, *92*, 1120–1127. https://doi.org/10.1016/j.ijheatmasstransfer.2015.09.060

Kayal, S., Chakraborty, A., & Teo, H. W. B. (2018). Green synthesis and characterization of aluminium fumarate metal-organic framework for heat transformation applications. *Materials Letters*, *221*, 165–167. https://doi.org/10.1016/j.matlet.2018.03.099

Khutia, A., Rammelberg, H. U., Schmidt, T., Henninger, S., & Janiak, C. (2013). Water Sorption Cycle Measurements on Functionalized MIL-101Cr for Heat Transformation Application. *Chemistry of Materials*, *25*(5), 790–798. https://doi.org/10.1021/cm304055k

Kocka, J. (2018). *Capitalism: a short history* (J. M. Riemer, Trans.; Third printing, and first paperback printing). Princeton University Press.

Kohler, T., Hinze, M., Müller, K., & Schwieger, W. (2017). Temperature independent description of water adsorption on zeotypes showing a type V adsorption isotherm. *Energy*, *135*, 227–236. https://doi.org/10.1016/j.energy.2017.06.115

Krzywanski, J., Grabowska, K., Herman, F., Pyrka, P., Sosnowski, M., Prauzner, T., & Nowak, W. (2017). Optimization of a three-bed adsorption chiller by genetic algorithms and neural networks. *Energy Conversion and Management*, *153*, 313–322. https://doi.org/10.1016/j.enconman.2017.09.069

Kutarov, V. V., Robens, E., Tarasevich, Y. I., & Aksenenko, E. V. (2011). Adsorption hysteresis at low relative pressures. *Theoretical and Experimental Chemistry*, *47*(3), 163–168. https://doi.org/10.1007/s11237-011-9198-6

Lambert, M. A., & Jones, B. J. (2005). Review of Regenerative Adsorption Heat Pumps. *Journal of Thermophysics and Heat Transfer*, *19*(4), 471–485. https://doi.org/10.2514/1.8075

Lanfrey, P.-Y., Kuzeljevic, Z., & Dudukovic, M. (2010). Tortuosity model for fixed beds randomly packed with identical particles. *Chemical Engineering Science*, *65*(5), 1891–1896. https://doi.org/10.1016/j.ces.2009.11.011

Langmuir, I. (1918). THE ADSORPTION OF GASES ON PLANE SURFACES OF GLASS, MICA AND PLATINUM. *Journal of the American Chemical Society*, *40*(9), 1361–1403. https://doi.org/10.1021/ja02242a004

Lanser, W., Albers, J., Hüls, W., Paitazoglou, C., Hunt, S., & Petersen, S. (2016). Systemintegration von Absorptionskälte: Erste Betriebserfahrungen aus einem Feldtest für KWKK-Systeme. *Kälte Luft Klimatechnik*.

Lanzerath, F., Bau, U., Seiler, J., & Bardow, A. (2015). Optimal design of adsorption chillers based on a validated dynamic object-oriented model. *Science and Technology for the Built Environment*, *21*(3), 248–257. https://doi.org/10.1080/10789669.2014.990337

Lanzerath, F., Seiler, J., Erdogan, M., Schreiber, H., Steinhilber, M., & Bardow, A. (2016). The impact of filling level resolved: Capillary-assisted evaporation of water for adsorption heat pumps. *Applied Thermal Engineering*, *102*, 513–519. https://doi.org/10.1016/j.applthermaleng.2016.03.052

Laurenz, E. (2021). Frequency response analysis for the determination of thermal conductivity and water transport in MOF adsorbent coatings for heat transformation. *International Journal of Heat and Mass Transfer*, 13.

Lee, Y.-J., Chang, Y.-J., Lee, D.-J., & Hsu, J.-P. (2018). Water stable metal-organic framework as adsorbent from aqueous solution: A mini-review. *Journal of the Taiwan Institute of Chemical Engineers*, *93*, 176–183. https://doi.org/10.1016/j.jtice.2018.06.035

Lefebvre, D., & Tezel, F. H. (2017). A review of energy storage technologies with a focus on adsorption thermal energy storage processes for heating applications. *Renewable and Sustainable Energy Reviews*, *67*, 116–125. https://doi.org/10.1016/j.rser.2016.08.019

Li, G., Xiao, P., & Webley, P. (2009). Binary Adsorption Equilibrium of Carbon Dioxide and Water Vapor on Activated Alumina. *Langmuir*, *25*(18), 10666–10675. https://doi.org/10.1021/la901107s

Li, R., Dai, Y., & Cui, G. (2019). Multi-objective optimization of solar powered adsorption chiller combined with river water heat pump system for air conditioning and space heating application. *Energy*, *189*, 116141. https://doi.org/10.1016/j.energy.2019.116141

Li, R., Ren, X., Feng, X., Li, X., Hu, C., & Wang, B. (2014). A highly stable metal- and nitrogen-doped nanocomposite derived from Zn/Ni-ZIF-8 capable of CO2 capture and separation. *Chemical Communications*, *50*(52), 6894. https://doi.org/10.1039/c4cc01087f

Li, S., Deng, S., Zhao, L., Xu, W., Yuan, X., Guo, Z., & Du, Z. (2019). Energy dissipation evaluation of temperature swing adsorption (TSA) cycle based on thermodynamic entropy insights. *Scientific Reports*, *9*(1), 16599. https://doi.org/10.1038/s41598-019-53398-6

Li, W., Liu, Z., & Li, S. (2021). The optimal step locations for high-performance adsorption heat pumps under various working conditions. *Thermal Science and Engineering Progress*, *25*, 101033. https://doi.org/10.1016/j.tsep.2021.101033

Li, X., Hou, X., Zhang, X., & Yuan, Z. (2015). A review on development of adsorption cooling—Novel beds and advanced cycles. *Energy Conversion and Management*, *94*, 221–232. https://doi.org/10.1016/j.enconman.2015.01.076

Lima, É. C., Adebayo, M. A., & Machado, F. M. (2015). Kinetic and Equilibrium Models of Adsorption [Series Title: Carbon Nanostructures]. In C. P. Bergmann & F. M. Machado (Eds.), *Carbon Nanomaterials as Adsorbents for Environmental and Biological Applications* (pp. 33–69). Springer International Publishing. https://doi.org/10.1007/978-3-319-18875-1_3

Liu, H., Nagano, K., Sugiyama, D., Togawa, J., & Nakamura, M. (2013). Honeycomb filters made from mesoporous composite material for an open sorption thermal energy storage system to store low-temperature industrial waste heat. *International Journal of Heat and Mass Transfer*, *65*, 471–480. https://doi.org/10.1016/j.ijheatmasstransfer.2013.06.021

Liu, L., Jin, S., Ko, K., Kim, H., Ahn, I.-S., & Lee, C.-H. (2020). Alkyl-functionalization of (3-Aminopropyl)triethoxysilane-grafted zeolite beta for carbon dioxide capture in temperature swing adsorption. *Chemical Engineering Journal*, *382*, 122834. https://doi.org/10.1016/j.cej.2019.122834

Liu, Z., Grande, C. A., Li, P., Yu, J., & Rodrigues, A. E. (2011). Adsorption and Desorption of Carbon Dioxide and Nitrogen on Zeolite 5A. *Separation Science and Technology*, *46*(3), 434–451. https://doi.org/10.1080/01496395.2010.513360

Liu, Z., Li, W., Moghadam, P. Z., & Li, S. (2021). Screening adsorbent–water adsorption heat pumps based on an experimental water adsorption isotherm database. *Sustainable Energy & Fuels*, *5*(4), 1075–1084. https://doi.org/10.1039/D0SE01824D

Llano-Restrepo, M., & Mosquera, M. A. (2009). Accurate correlation, thermochemistry, and structural interpretation of equilibrium adsorption isotherms of water vapor in zeolite 3A by means of a generalized statistical thermodynamic adsorption model. *Fluid Phase Equilibria*, *283*(1-2), 73–88. https://doi.org/10.1016/j.fluid.2009.06.003

Lombardo, W., Ottaviano, S., Branchini, L., Vasta, S., De Pascale, A., & Sapienza, A. (2019). A dynamic model of a solar driven trigeneration system based on micro-ORC and adsorption chiller prototypes, 020098. https://doi.org/10.1063/1.5138831

Lu, Z., & Wang, R. (2013). Performance improvement by mass-heat recovery of an innovative adsorption air-conditioner driven by 50–80 °C hot water. *Applied Thermal Engineering*, *55*(1-2), 113–120. https://doi.org/10.1016/j.applthermaleng.2013.03.001

Maggio, G., Freni, A., & Restuccia, G. (2006). A dynamic model of heat and mass transfer in a double-bed adsorption machine with internal heat recovery. *International Journal of Refrigeration*, *29*(4), 589–600. https://doi.org/10.1016/j.ijrefrig.2005.10.005

Mahmoodi, F., Darvishi, P., & Vaferi, B. (2018). Prediction of coefficients of the Langmuir adsorption isotherm using various artificial intelligence (AI) techniques. *Journal of*

the Iranian Chemical Society, *15*(12), 2747–2757. https://doi.org/10.1007/s13738-018-1462-4

Mapping and analysis of the current and future (2020-2030) heating/cooling fuel deployment (fossil/renewables) (tech. rep. N°ENER/C2/2014-641). (2016). European Commission Directorate-General for Energy. Retrieved February 25, 2022, from https://energy.ec.europa.eu/studies/final-studies-old/mapping-and-analyses-current-and-future-2020-2030-heatingcooling-fuel-deployment-fossilrenewables_en

Maraver, D., Sin, A., Royo, J., & Sebastián, F. (2013). Assessment of CCHP systems based on biomass combustion for small-scale applications through a review of the technology and analysis of energy efficiency parameters. *Applied Energy*, *102*, 1303–1313. https://doi.org/10.1016/j.apenergy.2012.07.012

Marletta, L., Maggio, G., Freni, A., Ingrasciotta, M., & Restuccia, G. (2002). A non-uniform temperature non-uniform pressure dynamic model of heat and mass transfer in compact adsorbent beds. *International Journal of Heat and Mass Transfer*, *45*(16), 3321–3330. https://doi.org/10.1016/S0017-9310(02)00045-5

Martin, H. (1984). Heat transfer between gas fluidized beds of solid particles and the surfaces of immersed heat exchanger elements, part I. *Chemical Engineering and Processing: Process Intensification*, *18*(3), 157–169. https://doi.org/10.1016/0255-2701(84)80005-7

Masoumifard, N., Mostoufi, N., Hamidi, A.-A., & Sotudeh-Gharebagh, R. (2008). Investigation of heat transfer between a horizontal tube and gas–solid fluidized bed. *International Journal of Heat and Fluid Flow*, *29*(5), 1504–1511. https://doi.org/10.1016/j.ijheatfluidflow.2008.06.004

McBain, J. W., & Bakr, A. M. (1926). A NEW SORPTION BALANCE [1]. *Journal of the American Chemical Society*, *48*(3), 690–695. https://doi.org/10.1021/ja01414a021

McCallum, C. L., Bandosz, T. J., McGrother, S. C., Müller, E. A., & Gubbins, K. E. (1999). A Molecular Model for Adsorption of Water on Activated Carbon: Comparison of Simulation and Experiment. *Langmuir*, *15*(2), 533–544. https://doi.org/10.1021/la9805950

McDonough, J. R., Law, R., Reay, D. A., & Zivkovic, V. (2018). Intensified carbon capture using adsorption: Heat transfer challenges and potential solutions. *Thermal Science and Engineering Progress*, *8*, 17–30. https://doi.org/10.1016/j.tsep.2018.07.012

Mehio, N., Dai, S., & Jiang, D.-e. (2014). Quantum Mechanical Basis for Kinetic Diameters of Small Gaseous Molecules. *The Journal of Physical Chemistry A*, *118*(6), 1150–1154. https://doi.org/10.1021/jp412588f

Merel, J., Clausse, M., & Meunier, F. (2008). Experimental Investigation on CO $_2$ PostCombustion Capture by Indirect Thermal Swing Adsorption Using 13X and 5A Zeolites. *Industrial & Engineering Chemistry Research*, *47*(1), 209–215. https://doi.org/10.1021/ie071012x

Meunier, F. (2001). Adsorptive cooling: a clean technology. *Clean Products and Processes*, *3*(1), 0008–0020. https://doi.org/10.1007/s100980000096

Meunier, F. (2013). Adsorption heat powered heat pumps. *Applied Thermal Engineering*, *61*(2), 830–836. https://doi.org/10.1016/j.applthermaleng.2013.04.050

Mickley, H. S., & Fairbanks, D. F. (1955). Mechanism of heat transfer to fluidized beds. *AIChE Journal*, *1*(3), 374–384. https://doi.org/10.1002/aic.690010317

Minx, J. C., & Nemet, G. (2018). The inconvenient truth about carbon capture. *The Washington Post*.

Moghadam, P. Z., Islamoglu, T., Goswami, S., Exley, J., Fantham, M., Kaminski, C. F., Snurr, R. Q., Farha, O. K., & Fairen-Jimenez, D. (2018). Computer-aided discovery of a metal–organic framework with superior oxygen uptake. *Nature Communications*, *9*(1), 1378. https://doi.org/10.1038/s41467-018-03892-8

Mohammadzadeh Kowsari, M., Niazmand, H., & Tokarev, M. M. (2018). Bed configuration effects on the finned flat-tube adsorption heat exchanger performance: Numerical modeling and experimental validation. *Applied Energy*, *213*, 540–554. https://doi.org/10.1016/j.apenergy.2017.11.019

Mohammed, R. H., Mesalhy, O., Elsayed, M. L., & Chow, L. C. (2019). Assessment of numerical models in the evaluation of adsorption cooling system performance. *International Journal of Refrigeration*, *99*, 166–175. https://doi.org/10.1016/j.ijrefrig.2018.12.017

Monpezat, A., Topin, S., Deliere, L., Farrusseng, D., & Coasne, B. (2019). Evaluation Methods of Adsorbents for Air Purification and Gas Separation at Low Concentration: Case Studies on Xenon and Krypton. *Industrial & Engineering Chemistry Research*, *58*(11), 4560–4571. https://doi.org/10.1021/acs.iecr.8b04866

Montante, G., Micale, G., Magelli, F., & Brucato, A. (2001). Experiments and CFD Predictions of Solid Particle Distribution in a Vessel Agitated with Four Pitched Blade Turbines. *Chemical Engineering Research and Design*, *79*(8), 1005–1010. https://doi.org/10.1205/02638760152721253

Moreno, R. M., Antolín, G., & Reyes, A. E. (2016). Heat transfer during forest biomass particles drying in an agitated fluidised bed. *Biosystems Engineering*, *151*, 65–71. https://doi.org/10.1016/j.biosystemseng.2016.08.002

Morris, A., Ma, Z., Pannala, S., & Hrenya, C. (2016). Simulations of heat transfer to solid particles flowing through an array of heated tubes. *Solar Energy*, *130*, 101–115. https://doi.org/10.1016/j.solener.2016.01.033

Morris, A., Pannala, S., Ma, Z., & Hrenya, C. (2015). A conductive heat transfer model for particle flows over immersed surfaces. *International Journal of Heat and Mass Transfer*, *89*, 1277–1289. https://doi.org/10.1016/j.ijheatmasstransfer.2015.06.004

Mustaffar, A., Phan, A., & Boodhoo, K. (2018). Hybrid heat pipe screw dryer: A novel, continuous and highly energy-efficient drying technology. *Chemical Engineering and Processing - Process Intensification*, *128*, 199–215. https://doi.org/10.1016/j.cep.2018.04.035

Nachenius, R., van de Wardt, T., Ronsse, F., & Prins, W. (2015). Residence time distributions of coarse biomass particles in a screw conveyor reactor. *Fuel Processing Technology*, *130*, 87–95. https://doi.org/10.1016/j.fuproc.2014.09.039

Nelder, J. A., & Mead, R. (1965). A Simplex Method for Function Minimization. *The Computer Journal*, *7*(4), 308–313. https://doi.org/10.1093/comjnl/7.4.308

Nelson, K., & Nelson, R. R. (2003). The cumulative advance of human know-how (A. G. J. MacFarlane, Ed.). *Philosophical Transactions of the Royal Society of London. Series*

A: Mathematical, Physical and Engineering Sciences, *361*(1809), 1635–1653. https://doi.org/10.1098/rsta.2003.1229

Ng, K., Chua, H., Chung, C., Loke, C., Kashiwagi, T., Akisawa, A., & Saha, B. (2001). Experimental investigation of the silica gel–water adsorption isotherm characteristics. *Applied Thermal Engineering*, *21*(16), 1631–1642. https://doi.org/10.1016/S1359-4311(01)00039-4

Ng, K. C., Burhan, M., Shahzad, M. W., & Ismail, A. B. (2017). A Universal Isotherm Model to Capture Adsorption Uptake and Energy Distribution of Porous Heterogeneous Surface. *Scientific Reports*, *7*(1), 10634. https://doi.org/10.1038/s41598-017-11156-6

Nienborg, B., Gschwander, S., Munz, G., Fröhlich, D., Helling, T., Horn, R., Weinläder, H., Klinker, F., & Schossig, P. (2018). Life Cycle Assessment of thermal energy storage materials and components. *Energy Procedia*, *155*, 111–120. https://doi.org/10.1016/j.egypro.2018.11.063

Nonnen, T., Beckert, S., Gleichmann, K., Brandt, A., Unger, B., Kerskes, H., Mette, B., Bonk, S., Badenhop, T., Salg, F., & Gläser, R. (2016). A Thermochemical Long-Term Heat Storage System Based on a Salt/Zeolite Composite. *Chemical Engineering & Technology*, *39*(12), 2427–2434. https://doi.org/10.1002/ceat.201600301

Nowicki, P., Pietrzak, R., & Wachowska, H. (2010). Sorption properties of active carbons obtained from walnut shells by chemical and physical activation. *Catalysis Today*, *150*(1-2), 107–114. https://doi.org/10.1016/j.cattod.2009.11.009

Ntiamoah, A., Ling, J., Xiao, P., Webley, P. A., & Zhai, Y. (2016). CO_2 Capture by Temperature Swing Adsorption: Use of Hot CO_2 -Rich Gas for Regeneration. *Industrial & Engineering Chemistry Research*, *55*(3), 703–713. https://doi.org/10.1021/acs.iecr.5b01384

Odoh, S. O., Cramer, C. J., Truhlar, D. G., & Gagliardi, L. (2015). Quantum-Chemical Characterization of the Properties and Reactivities of Metal–Organic Frameworks. *Chemical Reviews*, *115*(12), 6051–6111. https://doi.org/10.1021/cr500551h

Ohba, T., & Kaneko, K. (2007). Cluster-associated filling of water molecules in slit-shaped graphitic nanopores. *Molecular Physics*, *105*(2-3), 139–145. https://doi.org/10.1080/00268970701192081

Olivier, J. (1995). Modeling physical adsorption on porous and nonporous solids using density functional theory. *J. Porous Mater.*, *2*(1), 9–17.

O'Neill, D. W., Fanning, A. L., Lamb, W. F., & Steinberger, J. K. (2018). A good life for all within planetary boundaries. *Nature Sustainability*, *1*(2), 88–95. https://doi.org/10.1038/s41893-018-0021-4

Ongari, D., Yakutovich, A. V., Talirz, L., & Smit, B. (2019). Building a Consistent and Reproducible Database for Adsorption Evaluation in Covalent–Organic Frameworks. *ACS Central Science*, *5*(10), 1663–1675. https://doi.org/10.1021/acscentsci.9b00619

on Renewable Heating and Cooling, E. T. P. (2012). Strategic Research Priorities for Renewable Heating and Cooling Cross-Cutting Technology.

Osman, A. I., Hefny, M., Abdel Maksoud, M. I. A., Elgarahy, A. M., & Rooney, D. W. (2021). Recent advances in carbon capture storage and utilisation technologies: a review. *Environmental Chemistry Letters*, *19*(2), 797–849. https://doi.org/10.1007/s10311-020-01133-3

Osman, H. B. (2012). *Granular Flow and Heat Transfer in a Screw Conveyor Heater: A Discrete Element Modeling Study* (Master's thesis). National University of Singapore. Singapore. Retrieved December 31, 2022, from https://scholarbank.nus.edu.sg/handle/10635/36355

Pal, A., Thu, K., Mitra, S., El-Sharkawy, I. I., Saha, B. B., Kil, H.-S., Yoon, S.-H., & Miyawaki, J. (2017). Study on biomass derived activated carbons for adsorptive heat pump application. *International Journal of Heat and Mass Transfer*, *110*, 7–19. https://doi.org/10.1016/j.ijheatmasstransfer.2017.02.081

Palazzi, F., Périn-Lavasseur, Z., Bolliger, R., & Gassner, M. (2010). OSMOSE. https://infoscience.epfl.ch/record/227388

Palomba, V., Nowak, S., Dawoud, B., & Frazzica, A. (2021). Dynamic modelling of Adsorption systems: a comprehensive calibrateddataset for heat pump and storage applications. *Journal of Energy Storage*, *33*, 102148. https://doi.org/10.1016/j.est.2020.102148

Palomba, V., Ferraro, M., Frazzica, A., Vasta, S., Sergi, F., & Antonucci, V. (2018). Experimental and numerical analysis of a SOFC-CHP system with adsorption and hybrid chillers for telecommunication applications. *Applied Energy*, *216*, 620–633. https://doi.org/10.1016/j.apenergy.2018.02.063

Pan, Q., Shan, H., Tamainot-Telto, Z., & Wang, R. (2022). Heat Recovery for Adsorption Refrigeration System via Pinch Technology. *Journal of Thermal Science*, *31*(2), 379–389. https://doi.org/10.1007/s11630-022-1535-7

Pan, Q., & Wang, R. (2017). Experimental study on operating features of heat and mass recovery processes in adsorption refrigeration. *Energy*, *135*, 361–369. https://doi.org/10.1016/j.energy.2017.06.131

Pan, Q., Wang, R., & Wang, L. (2015). Comparison of different kinds of heat recoveries applied in adsorption refrigeration system. *International Journal of Refrigeration*, *55*, 37–48. https://doi.org/10.1016/j.ijrefrig.2015.03.022

Pan, Q., Wang, R., Wang, L., & Liu, D. (2016). Design and experimental study of a silica gel-water adsorption chiller with modular adsorbers. *International Journal of Refrigeration*, *67*, 336–344. https://doi.org/10.1016/j.ijrefrig.2016.03.001

Papadikis, K., Gu, S., & Bridgwater, A. (2010). Computational modelling of the impact of particle size to the heat transfer coefficient between biomass particles and a fluidised bed. *Fuel Processing Technology*, *91*(1), 68–79. https://doi.org/10.1016/j.fuproc.2009.08.016

Parkar, S., Mulukh, R., Narhari, G., & Kulkarni, S. a. (2022). Intensification of Temperature Swing Adsorption. *Journal of Sustainable Materials Processing and Management*, *2*(1). https://doi.org/10.30880/jsmpm.2022.02.01.009

Pedregosa, F., Varoquaux, G., Gramfort, A., Michel, V., Thirion, B., Grisel, O., Blondel, M., Prettenhofer, P., Weiss, R., Dubourg, V., Vanderplas, J., Passos, A., & Cournapeau, D. (n.d.). Scikit-learn: Machine Learning in Python. *MACHINE LEARNING IN PYTHON*, 6.

Peoples, H. C., Duda, P., & Marlowe, F. W. (2016). Hunter-Gatherers and the Origins of Religion. *Human Nature*, *27*(3), 261–282. https://doi.org/10.1007/s12110-016-9260-0

Pesaran, A., Lee, H., Hwang, Y., Radermacher, R., & Chun, H.-H. (2016). Review article: Numerical simulation of adsorption heat pumps. *Energy*, *100*, 310–320. https://doi.org/10.1016/j.energy.2016.01.103

Piccoli, E., Brancato, V., Frazzica, A., Maréchal, F., & Galmarini, S. (2022). Adsorption Energy System Design and Material Selection: Towards a Holistic Approach. *Thermal Science and Engineering Progress*.

Piccoli, E. (2022). Water Isotherms of Adsorbent Materials Evaluated in the Hycool Project [Type: dataset]. https://doi.org/10.5281/ZENODO.7093134

Piccoli, E., Gantenbein, P., Galmarini, S., Ruch, P., & Michel, B. (2022). Low-Grade Heat Driven Rapid Thermal Swing Adsorption Gas Separation. *SSRN Electronic Journal*. https://doi.org/10.2139/ssrn.4274156

Piccoli, E., Torreggiani, R., & Galmarini, S. (2023). D4.4 Validation of the developed model for lab-scale experiments [Publisher: Zenodo Version Number: Final]. https://doi.org/10.5281/ZENODO.7543626

Pinheiro, J. M., Salústio, S., Rocha, J., Valente, A. A., & Silva, C. M. (2020). Adsorption heat pumps for heating applications. *Renewable and Sustainable Energy Reviews*, *119*, 109528. https://doi.org/10.1016/j.rser.2019.109528

Plaza, M., & Rubiera, F. (2019). Evaluation of a novel multibed heat-integrated vacuum and temperature swing adsorption post-combustion CO2 capture process. *Applied Energy*, *250*, 916–925. https://doi.org/10.1016/j.apenergy.2019.05.079

Polanyi, M. (1963). The Potential Theory of Adsorption: Authority in science has its uses and its dangers. *Science*, *141*(3585), 1010–1013. https://doi.org/10.1126/science.141.3585.1010

Pole, J. (2022). 'Mammoth' new air capture plant will suck up 36,000 tonnes of CO2 per year in Iceland. *euronews*. https://www.euronews.com/green/2022/06/28/mammoth-new-air-capture-plant-will-suck-up-36000-tonnes-of-co2-per-year-in-iceland

Postweiler, P., Engelpracht, M., Gibelhaus, A., & von der Assen, N. V. (2022). Environmental Process Optimisation of Adsorption-based Direct Air Capture of CO2. *Heat Powered Cycles 2021*.

Prauchner, M. J., & Rodríguez-Reinoso, F. (2012). Chemical versus physical activation of coconut shell: A comparative study. *Microporous and Mesoporous Materials*, *152*, 163–171. https://doi.org/10.1016/j.micromeso.2011.11.040

Pulido, A., Chen, L., Kaczorowski, T., Holden, D., Little, M. A., Chong, S. Y., Slater, B. J., McMahon, D. P., Bonillo, B., Stackhouse, C. J., Stephenson, A., Kane, C. M., Clowes, R., Hasell, T., Cooper, A. I., & Day, G. M. (2017). Functional materials discovery using energy–structure–function maps. *Nature*, *543*(7647), 657–664. https://doi.org/10.1038/nature21419

Puschnigg, S., Jauschnik, G., Moser, S., Volkova, A., & Linhart, M. (2021). A review of low-temperature sub-networks in existing district heating networks: examples, conditions, replicability. *Energy Reports*, *7*, 18–26. https://doi.org/10.1016/j.egyr.2021.09.044

Qian, S., Ling, J., Muehlbauer, J., Hwang, Y., & Radermacher, R. (2015). Study on high efficient heat recovery cycle for solid-state cooling. *International Journal of Refrigeration*, *55*, 102–119. https://doi.org/10.1016/j.ijrefrig.2015.03.023

Quiquerez, L. (2017). Décarboner le système énergétique à l'aide des réseaux de chaleur: état des lieux et scénarios prospectifs pour le canton de Genève [Publisher: Université de Genève]. https://doi.org/10.13097/ARCHIVE-OUVERTE/UNIGE:93380

Radu, A. I. (2017). Insights from modeling dynamics of water sorption in spherical particles for adsorption heat pumps. *International Journal of Heat and Mass Transfer*, 12.

Raganati, F., Chirone, R., & Ammendola, P. (2020). CO $_2$ Capture by Temperature Swing Adsorption: Working Capacity As Affected by Temperature and CO $_2$ Partial Pressure. *Industrial & Engineering Chemistry Research*, *59*(8), 3593–3605. https://doi.org/10.1021/acs.iecr.9b04901

Raworth, K. (2017). *Doughnut Economics: Seven Ways to Think Like a 21st-Century Economist*. Random House Business.

Raza, A., Gholami, R., Rezaee, R., Rasouli, V., & Rabiei, M. (2019). Significant aspects of carbon capture and storage – A review. *Petroleum*, *5*(4), 335–340. https://doi.org/10.1016/j.petlm.2018.12.007

The reality of carbon capture utilisation technology. (2022). *Open Access Government*.

Restuccia, G., Freni, A., & Maggio, G. (2002). A zeolite-coated bed for air conditioning adsorption systems: parametric study of heat and mass transfer by dynamic simulation. *Applied Thermal Engineering*, *22*(6), 619–630. https://doi.org/10.1016/S1359-4311(01)00114-4

Restuccia, G., Freni, A., Vasta, S., & Aristov, Y. (2004). Selective water sorbent for solid sorption chiller: experimental results and modelling. *International Journal of Refrigeration*, *27*(3), 284–293. https://doi.org/10.1016/j.ijrefrig.2003.09.003

Rezk, A., Al-Dadah, R., Mahmoud, S., & Elsayed, A. (2013a). Experimental investigation of metal organic frameworks characteristics for water adsorption chillers. *Proceedings of the Institution of Mechanical Engineers, Part C: Journal of Mechanical Engineering Science*, *227*(5), 992–1005. https://doi.org/10.1177/0954406212456469

Rezk, A., Al-Dadah, R., Mahmoud, S., & Elsayed, A. (2013b). Effects of contact resistance and metal additives in finned-tube adsorbent beds on the performance of silica gel/water adsorption chiller. *Applied Thermal Engineering*, *53*(2), 278–284. https://doi.org/10.1016/j.applthermaleng.2012.04.008

Robens, E., & Jayaweera, S. A. A. (2014). Early History of Adsorption Measurements. *Adsorption Science & Technology*, *32*(6), 425–442. https://doi.org/10.1260/0263-6174.32.6.425

Roberts, A. (1999). The influence of granular vortex motion on the volumetric performance of enclosed screw conveyors. *Powder Technology*, *104*(1), 56–67. https://doi.org/10.1016/S0032-5910(99)00039-X

Roberts, A. (2007). DESIGN CONSIDERATIONS AND PERFORMANCE EVALUATION OF SCREW CONVEYORS.

Roque-Malherbe, R. M. A. (2018). *Adsorption and Diffusion in Nanoporous Materials, Second Edition*. CRC Press. https://doi.org/10.1201/b22379

Ruthven, D. M. (1984). *Principles of adsorption and adsorption processes*. Wiley.

Sah, R. P., Choudhury, B., Das, R. K., & Sur, A. (2017). An overview of modelling techniques employed for performance simulation of low–grade heat operated adsorption cooling systems. *Renewable and Sustainable Energy Reviews*, *74*, 364–376. https://doi.org/10.1016/j.rser.2017.02.062

Saleh, M. M., Al-Dadah, R., Mahmoud, S., Elsayed, E., & El-Samni, O. (2020). Wire fin heat exchanger using aluminium fumarate for adsorption heat pumps. *Applied Thermal Engineering*, *164*, 114426. https://doi.org/10.1016/j.applthermaleng.2019.114426

Saleh, M., Baek, S. B., Lee, H. M., & Kim, K. S. (2015). Triazine-Based Microporous Polymers for Selective Adsorption of CO $_2$. *The Journal of Physical Chemistry C*, *119*(10), 5395–5402. https://doi.org/10.1021/jp509188h

Sami, S., & Tribes, C. (1996). An improved model for predicting the dynamic behaviour of adsorption systems. *Applied Thermal Engineering*, *16*(2), 149–161. https://doi.org/10.1016/1359-4311(95)00054-H

Samsatli, S., & Samsatli, N. J. (2018). A general mixed integer linear programming model for the design and operation of integrated urban energy systems. *Journal of Cleaner Production*, *191*, 458–479. https://doi.org/10.1016/j.jclepro.2018.04.198

San, J.-Y., & Tsai, F.-K. (2014). Testing of a lab-scale four-bed adsorption heat pump. *Applied Thermal Engineering*, *70*(1), 274–281. https://doi.org/10.1016/j.applthermaleng.2014.05.014

Santamaria, S., Sapienza, A., Frazzica, A., Freni, A., Girnik, I. S., & Aristov, Y. I. (2014). Water adsorption dynamics on representative pieces of real adsorbers for adsorptive chillers. *Applied Energy*, *134*, 11–19. https://doi.org/10.1016/j.apenergy.2014.07.053

Santori, G., Frazzica, A., Freni, A., Galieni, M., Bonaccorsi, L., Polonara, F., & Restuccia, G. (2013). Optimization and testing on an adsorption dishwasher. *Energy*, *50*, 170–176. https://doi.org/10.1016/j.energy.2012.11.031

Santori, G., & Di Santis, C. (2017). Optimal fluids for adsorptive cooling and heating. *Sustainable Materials and Technologies*, *12*, 52–61. https://doi.org/10.1016/j.susmat.2017.04.005

Santos, H. G., & Toffolo, T. A. M. (2020). Python - MIP. https://pypi.org/project/mip/

Sanz, R., Calleja, G., Arencibia, A., & Sanz-Pérez, E. (2010). CO2 adsorption on branched polyethyleneimine-impregnated mesoporous silica SBA-15. *Applied Surface Science*, *256*(17), 5323–5328. https://doi.org/10.1016/j.apsusc.2009.12.070

Sapienza, A., Brancato, V., Aristov, Y., & Vasta, S. (2021). Plastic heat exchangers for adsorption cooling: Thermodynamic and dynamic performance. *Applied Thermal Engineering*, *188*, 116622. https://doi.org/10.1016/j.applthermaleng.2021.116622

Sapienza, A., Frazzica, A., Freni, A., & Aristov, Y. (2018). Measurement of Adsorption Dynamics: An Overview [Series Title: SpringerBriefs in Applied Sciences and Technology]. In *Dynamics of Adsorptive Systems for Heat Transformation* (pp. 19–29). Springer International Publishing. https://doi.org/10.1007/978-3-319-51287-7_2

Sapienza, A., Palomba, V., Gullì, G., Frazzica, A., & Vasta, S. (2017). A new management strategy based on the reallocation of ads-/desorption times: Experimental operation of a full-

scale 3 beds adsorption chiller. *Applied Energy*, *205*, 1081–1090. https://doi.org/10.1016/j.apenergy.2017.08.036

Scarre, C. (Ed.). (2018). *The human past: world prehistory and the development of human societies* (Fourth edition) [OCLC: on1004247869]. Thames & Hudson.

Scherle, M., Nowak, T. A., Welzel, S., Etzold, B. J., & Nieken, U. (2022). Experimental study of 3D – structured adsorbent composites with improved heat and mass transfer for adsorption heat pumps. *Chemical Engineering Journal*, *431*, 133365. https://doi.org/10.1016/j.cej.2021.133365

Schlüsener, C., Xhinovci, M., Ernst, S.-J., Schmitz, A., Tannert, N., & Janiak, C. (2019). Solid-Solution Mixed-Linker Synthesis of Isoreticular Al-Based MOFs for an Easy Hydrophilicity Tuning in Water-Sorption Heat Transformations. *Chemistry of Materials*, *31*(11), 4051–4062. https://doi.org/10.1021/acs.chemmater.9b00617

Schnabel, L., Füldner, G., Velte, A., Laurenz, E., Bendix, P., Kummer, H., & Wittstadt, U. (2018). Innovative Adsorbent Heat Exchangers: Design and Evaluation. In H.-J. Bart & S. Scholl (Eds.), *Innovative Heat Exchangers* (pp. 363–394). Springer International Publishing. https://doi.org/10.1007/978-3-319-71641-1_12

Schreiber, H., Graf, S., Lanzerath, F., & Bardow, A. (2015). Adsorption thermal energy storage for cogeneration in industrial batch processes: Experiment, dynamic modeling and system analysis. *Applied Thermal Engineering*, *89*, 485–493. https://doi.org/10.1016/j.applthermaleng.2015.06.016

Schuitema, R., van Helden, W., Zondag, H. A., Krosse, L., van Essen, M., Bleijendaal, L., & Kalbasenka, A. (2009). First studies in reactor concepts for Thermochemical Storage.

Scotton, S., Decorme, R., Calderoni, M., Costa, S. V., Cuneo, A., Frazzica, A., Barberis, S., Fuligni, F., Martinelli, F., & Magrassi, F. (2019). Sun and Thermal Energy: Europe's Precious Energy Sources for Efficient Industries and Buildings. *Sustainable Places 2019*, 3. https://doi.org/10.3390/proceedings2019020003

Seol, S.-H., Nagano, K., & Togawa, J. (2020). Modeling of adsorption heat pump system based on experimental estimation of heat and mass transfer coefficients. *Applied Thermal Engineering*, *171*, 115089. https://doi.org/10.1016/j.applthermaleng.2020.115089

Serizawa, R., Shitara, M., Gong, J., Makino, M., Kabir, M. H., & Furukawa, H. (2014). 3D jet printer of edible gels for food creation. In N. C. Goulbourne & H. E. Naguib (Eds.). https://doi.org/10.1117/12.2045082

Settembrini, G., Domingo-Irigoyen, S., Heim, T., Jurt, D., Zakovorotnyi, A., Seerig, A., Zweifel, G., & Menti, U. (2017). *ClimaBau - Planen angesichts des Klimawandels* (tech. rep.). Lucerne University of Applied Sciences and Arts.

Shalizi, C. R. (2006). Methods and Techniques of Complex Systems Science: An Overview [Series Title: Topics in Biomedical Engineering International Book Series]. In T. S. Deisboeck & J. Y. Kresh (Eds.), *Complex Systems Science in Biomedicine* (pp. 33–114). Springer US. https://doi.org/10.1007/978-0-387-33532-2_2

Sharafian, A., & Bahrami, M. (2014). Assessment of adsorber bed designs in waste-heat driven adsorption cooling systems for vehicle air conditioning and refrigeration. *Renewable*

and Sustainable Energy Reviews, *30*, 440–451. https://doi.org/10.1016/j.rser.2013.10.031

Shi, X., Xiao, H., Azarabadi, H., Song, J., Wu, X., Chen, X., & Lackner, K. S. (2020). Sorbents for the Direct Capture of CO $_2$ from Ambient Air. *Angewandte Chemie International Edition*, *59*(18), 6984–7006. https://doi.org/10.1002/anie.201906756

Shi, Z., Yuan, X., Yan, Y., Tang, Y., Li, J., Liang, H., Tong, L., & Qiao, Z. (2021). Techno-economic analysis of metal–organic frameworks for adsorption heat pumps/chillers: from directional computational screening, machine learning to experiment. *Journal of Materials Chemistry A*, *9*(12), 7656–7666. https://doi.org/10.1039/D0TA11747A

Siderius, D. (2020). NIST/ARPA-E Database of Novel and Emerging Adsorbent Materials [Version Number: 1.0.4 Type: dataset]. https://doi.org/10.18434/T43882

Siegelman, R. L., Milner, P. J., Kim, E. J., Weston, S. C., & Long, J. R. (2019). Challenges and opportunities for adsorption-based CO $_2$ capture from natural gas combined cycle emissions. *Energy & Environmental Science*, *12*(7), 2161–2173. https://doi.org/10.1039/C9EE00505F

Sifat, N. S., & Haseli, Y. (2019). A Critical Review of CO2 Capture Technologies and Prospects for Clean Power Generation. *Energies*, *12*(21), 4143. https://doi.org/10.3390/en12214143

Simon, C. M., Smit, B., & Haranczyk, M. (2016). pyIAST: Ideal adsorbed solution theory (IAST) Python package. *Computer Physics Communications*, *200*, 364–380. https://doi.org/10.1016/j.cpc.2015.11.016

Siu, W. W. M., & Lee, S. H.-K. (2000). Transient effect on the constriction resistance between spheres. *Computational Mechanics*, *25*(1), 59–65. https://doi.org/10.1007/s004660050015

Siu, W., & Lee, S.-K. (2004). Transient temperature computation of spheres in three-dimensional random packings. *International Journal of Heat and Mass Transfer*, *47*(5), 887–898. https://doi.org/10.1016/j.ijheatmasstransfer.2003.08.022

Smith, O. J., & Westerberg, A. W. (1991). The optimal design of pressure swing adsorption systems. *Chemical Engineering Science*, *46*(12), 2967–2976. https://doi.org/10.1016/0009-2509(91)85001-E

Solovyeva, M. V., Aristov, Y. I., & Gordeeva, L. G. (2017). NH 2 -MIL-125 as promising adsorbent for adsorptive cooling: Water adsorption dynamics. *Applied Thermal Engineering*, *116*, 541–548. https://doi.org/10.1016/j.applthermaleng.2017.01.080

Sonar, D., Soni, S., & Sharma, D. (2014). Micro-trigeneration for energy sustainability: Technologies, tools and trends. *Applied Thermal Engineering*, *71*(2), 790–796. https://doi.org/10.1016/j.applthermaleng.2013.11.037

Spier, F. (2015). *Big history and the future of humanity* (Second edition). Wiley Blackwell.

Stahl, T., Brunner, S., Zimmermann, M., & Ghazi Wakili, K. (2012). Thermo-hygric properties of a newly developed aerogel based insulation rendering for both exterior and interior applications. *Energy and Buildings*, *44*, 114–117. https://doi.org/10.1016/j.enbuild.2011.09.041

Stoeckli, F. (2002). Water adsorption in activated carbons of various degrees of oxidation described by the Dubinin equation. *Carbon*, *40*(6), 969–971. https://doi.org/10.1016/S0008-6223(02)00087-8

Stoeckli, F., Jakubov, T., & Lavanchy, A. (1994). Water adsorption in active carbons described by the Dubinin–Astakhov equation. *J. Chem. Soc., Faraday Trans.*, *90*(5), 783–786. https://doi.org/10.1039/FT9949000783

Streb, A., & Mazzotti, M. (2021). Adsorption for efficient low carbon hydrogen production: part 1—adsorption equilibrium and breakthrough studies for H2/CO2/CH4 on zeolite 13X. *Adsorption*, *27*(4), 541–558. https://doi.org/10.1007/s10450-021-00306-y

Stuttgart, U. (n.d.). Optimierung von Absorptionswärmepumpen zum Einsatz im Wärmenetz 4.0. https://www.igte.uni-stuttgart.de/forschung/aktuelle/optawew/

Subramanian Balashankar, V., & Rajendran, A. (2019). Process Optimization-Based Screening of Zeolites for Post-Combustion CO $_2$ Capture by Vacuum Swing Adsorption. *ACS Sustainable Chemistry & Engineering*, *7*(21), 17747–17755. https://doi.org/10.1021/acssuschemeng.9b04124

Sung, E., Han, C. D., & Rhee, H.-K. (1979). Optimal design of multistage adsorption-bed systems. *AIChE Journal*, *25*(1), 87–100. https://doi.org/10.1002/aic.690250110

Syvitski, J., Waters, C. N., Day, J., Milliman, J. D., Summerhayes, C., Steffen, W., Zalasiewicz, J., Cearreta, A., Gałuszka, A., Hajdas, I., Head, M. J., Leinfelder, R., McNeill, J. R., Poirier, C., Rose, N. L., Shotyk, W., Wagreich, M., & Williams, M. (2020). Extraordinary human energy consumption and resultant geological impacts beginning around 1950 CE initiated the proposed Anthropocene Epoch. *Communications Earth & Environment*, *1*(1), 32. https://doi.org/10.1038/s43247-020-00029-y

Tan, B., Luo, Y., Liang, X., Wang, S., Gao, X., Zhang, Z., & Fang, Y. (2019). Composite salt in MIL-101(Cr) with high water uptake and fast adsorption kinetics for adsorption heat pumps. *Microporous and Mesoporous Materials*, *286*, 141–148. https://doi.org/10.1016/j.micromeso.2019.05.039

Tarazona, P. (1985). Free-energy density functional for hard spheres. *Physical Review A, 31*(4), 2672.

Teng, W., Leong, K., & Chakraborty, A. (2016). Revisiting adsorption cooling cycle from mathematical modelling to system development. *Renewable and Sustainable Energy Reviews*, *63*, 315–332. https://doi.org/10.1016/j.rser.2016.05.059

Thomas, W. J., & Crittenden, B. (1998). The development of adsorption technology. In *Adsorption Technology & Design* (pp. 1–7). Elsevier. https://doi.org/10.1016/B978-075061959-2/50002-1

Thompson, J. A., & Zones, S. I. (2020). Binary- and Pure-Component Adsorption of CO $_2$, H $_2$ O, and C $_6$ H $_{14}$ on SSZ-13. *Industrial & Engineering Chemistry Research*, *59*(40), 18151–18159. https://doi.org/10.1021/acs.iecr.0c03480

Thorpe, D. (2021). What's the truth about carbon capture and storage? *The Fifth Estate*. https://thefifthestate.com.au/urbanism/climate-change-news/whats-the-truth-about-carbon-capture-and-storage/

Tian, J., Shen, Y., Zhang, D., & Tang, Z. (2021). CO2 capture by vacuum pressure swing adsorption from dry flue gas with a structured composite adsorption medium. *Journal of Environmental Chemical Engineering*, *9*(5), 106037. https://doi.org/10.1016/j.jece.2021.106037

Tierney, M., Ketteringham, L., & Azri Mohd Nor, M. (2017). Performance of a finned activated carbon cloth-ethanol adsorption chiller. *Applied Thermal Engineering*, *110*, 949–961. https://doi.org/10.1016/j.applthermaleng.2016.08.102

Tomarelli, F. (2019). *Mathematical analysis tools for engineering* [OCLC: 1312624421]. Esculapio.

Toolbox, E. (2004). Water - Specific Heat (online). https://www.engineeringtoolbox.com/specific-heat-capacity-water-d_660.html

Tovbin, I. K. (2018). *The molecular theory of adsorption in porous solids* [OCLC: 1007048477]. CRC Press.

Towsif Abtab, S. M., Alezi, D., Bhatt, P. M., Shkurenko, A., Belmabkhout, Y., Aggarwal, H., Weseliński, Ł. J., Alsadun, N., Samin, U., Hedhili, M. N., & Eddaoudi, M. (2018). Reticular Chemistry in Action: A Hydrolytically Stable MOF Capturing Twice Its Weight in Adsorbed Water. *Chem*, *4*(1), 94–105. https://doi.org/10.1016/j.chempr.2017.11.005

Uddin, K. (2018). Specific heat capacities of carbon-based adsorbents for adsorption heat pump application. *Applied Thermal Engineering*, 10.

van Benthem, G., Cacciola, G., & Restuccia, G. (1995). Regenerative adsorption heat pumps: Optimization of the design. *Heat Recovery Systems and CHP*, *15*(6), 531–544. https://doi.org/10.1016/0890-4332(95)90063-2

Velasco, L. F., Guillet-Nicolas, R., Dobos, G., Thommes, M., & Lodewyckx, P. (2016). Towards a better understanding of water adsorption hysteresis in activated carbons by scanning isotherms. *Carbon*, *96*, 753–758. https://doi.org/10.1016/j.carbon.2015.10.017

Velte, A., Füldner, G., Laurenz, E., & Schnabel, L. (2017). Advanced Measurement and Simulation Procedure for the Identification of Heat and Mass Transfer Parameters in Dynamic Adsorption Experiments. *Energies*, *10*(8), 1130. https://doi.org/10.3390/en10081130

Verougstraete, B., Martín-Calvo, A., Van der Perre, S., Baron, G., Finsy, V., & Denayer, J. F. (2020). A new honeycomb carbon monolith for CO2 capture by rapid temperature swing adsorption using steam regeneration. *Chemical Engineering Journal*, *383*, 123075. https://doi.org/10.1016/j.cej.2019.123075

von der Leyen, U. (2022). Statement by President von der Leyen on energy.

Wagner, W., & Pruß, A. (2002). The IAPWS Formulation 1995 for the Thermodynamic Properties of Ordinary Water Substance for General and Scientific Use. *Journal of Physical and Chemical Reference Data*, *31*(2), 387–535. https://doi.org/10.1063/1.1461829

Waje, S. S., Thorat, B. N., & Mujumdar, A. S. (2006). An Experimental Study of the Thermal Performance of a Screw Conveyor Dryer. *Drying Technology*, *24*(3), 293–301. https://doi.org/10.1080/07373930600564506

Wallerand, A. S., Kermani, M., Kantor, I. D., & Maréchal, F. (2017). General Superstructure Synthesis and Bi-level Solution Strategy for Industrial Heat Pumping. In *Computer*

Aided Chemical Engineering (pp. 1159–1164). Elsevier. https://doi.org/10.1016/B978-0-444-63965-3.50195-1

Wang, D., Li, Y., Li, D., Xia, Y., & Zhang, J. (2010). A review on adsorption refrigeration technology and adsorption deterioration in physical adsorption systems. *Renewable and Sustainable Energy Reviews*, *14*(1), 344–353. https://doi.org/10.1016/j.rser.2009.08.001

Wang, D., & Zhang, J. (2009). Design and performance prediction of an adsorption heat pump with multi-cooling tubes. *Energy Conversion and Management*, *50*(5), 1157–1162. https://doi.org/10.1016/j.enconman.2009.01.028

Wang, H.-J., Kleinhammes, A., McNicholas, T. P., Liu, J., & Wu, Y. (2014). Water Adsorption in Nanoporous Carbon Characterized by in Situ NMR: Measurements of Pore Size and Pore Size Distribution. *The Journal of Physical Chemistry C*, *118*(16), 8474–8480. https://doi.org/10.1021/jp501518f

Wang, J., Guo, Z., Deng, S., Zhao, R., Chen, L., & Xue, J. (2021). A rapid multi-objective optimization of pressure and temperature swing adsorption for CO2 capture based on simplified equilibrium model. *Separation and Purification Technology*, *279*, 119663. https://doi.org/10.1016/j.seppur.2021.119663

Wang, L., Zhu, D., & Tan, Y. (1999). Heat Transfer Enhancement on the Adsorber of Adsorption Heat Pump. *Adsorption*, *5*(3), 279–286. https://doi.org/10.1023/A:1008964013879

Wang, L., Wang, R., & Oliveira, R. (2009). A review on adsorption working pairs for refrigeration. *Renewable and Sustainable Energy Reviews*, *13*(3), 518–534. https://doi.org/10.1016/j.rser.2007.12.002

Wilberforce, T., Olabi, A., Sayed, E. T., Elsaid, K., & Abdelkareem, M. A. (2021). Progress in carbon capture technologies. *Science of The Total Environment*, *761*, 143203. https://doi.org/10.1016/j.scitotenv.2020.143203

Wright, A. (2022). 'Breakthrough' carbon capture tech slashes costs. *gasworld*. https://www.gasworld.com/breakthrough-carbon-capture-tech-slashes-costs/2022928.article

Wu, J., Wang, R., & Xu, Y. (2002). Dynamic analysis of heat recovery process for a continuous heat recovery adsorption heat pump. *Energy Conversion and Management*, *43*(16), 2201–2211. https://doi.org/10.1016/S0196-8904(01)00158-3

Wurzbacher, J. A., Gebald, C., & Steinfeld, A. (2011). Separation of CO2 from air by temperature-vacuum swing adsorption using diamine-functionalized silica gel. *Energy & Environmental Science*, *4*(9), 3584. https://doi.org/10.1039/c1ee01681d

WWF. (2022). Living Planet Report 2022 – Building a nature positive society.

Xebec Announces MOU for CO2 Capture and Sequestration Equipment with Summit Carbon Solutions. (2022). *Businesswire*. https://www.businesswire.com/news/home/20220328005939/en/Xebec-Announces-MOU-for-CO2-Capture-and-Sequestration-Equipment-with-Summit-Carbon-Solutions

Xu, X., Song, C., Andresen, J. M., Miller, B. G., & Scaroni, A. W. (2002). Novel Polyethylenimine-Modified Mesoporous Molecular Sieve of MCM-41 Type as High-Capacity Adsorbent for CO $_2$ Capture. *Energy & Fuels*, *16*(6), 1463–1469. https://doi.org/10.1021/ef020058u

Yaïci, W., & Entchev, E. (2019). Coupled unsteady computational fluid dynamics with heat and mass transfer analysis of a solar/heat-powered adsorption cooling system for

use in buildings. *International Journal of Heat and Mass Transfer*, *144*, 118648. https://doi.org/10.1016/j.ijheatmasstransfer.2019.118648

Yin, Y., Shao, J., Zhang, L., Cui, Q., & Wang, H. (2021). Study on heat conduction and adsorption/desorption characteristic of MIL-101/few layer graphene composite. *Journal of Porous Materials*, *28*(4), 1197–1213. https://doi.org/10.1007/s10934-021-01074-4

Yong, L., & Sumathy, K. (2002). Review of mathematical investigation on the closed adsorption heat pump and cooling systems. *Renewable and Sustainable Energy Reviews*, *6*(4), 305–338. https://doi.org/10.1016/S1364-0321(02)00010-2

Yoo, M.-J., Lessard, L., Kermani, M., & Maréchal, F. (2015). OsmoseLua – An Integrated Approach to Energy Systems Integration with LCIA and GIS. In *Computer Aided Chemical Engineering* (pp. 587–592). Elsevier. https://doi.org/10.1016/B978-0-444-63578-5.50093-1

Younes, M. M., El-Sharkawy, I. I., Kabeel, A., & Saha, B. B. (2017). A review on adsorbent-adsorbate pairs for cooling applications. *Applied Thermal Engineering*, *114*, 394–414. https://doi.org/10.1016/j.applthermaleng.2016.11.138

Yu, D., Yazaydin, A. O., Lane, J. R., Dietzel, P. D. C., & Snurr, R. Q. (2013). A combined experimental and quantum chemical study of CO2 adsorption in the metal–organic framework CPO-27 with different metals. *Chemical Science*, *4*(9), 3544. https://doi.org/10.1039/c3sc51319j

Yu, X., Choi, S., Tang, D., Medford, A. J., & Sholl, D. S. (2021). Efficient Models for Predicting Temperature-Dependent Henry's Constants and Adsorption Selectivities for Diverse Collections of Molecules in Metal–Organic Frameworks. *The Journal of Physical Chemistry C*, *125*(32), 18046–18057. https://doi.org/10.1021/acs.jpcc.1c05266

Yun, J. H., Park, H. C., & Moon, H. (1996). Multicomponent adsorption calculations based on adsorbed solution theory. *Korean Journal of Chemical Engineering*, *13*(3), 246–254. https://doi.org/10.1007/BF02705946

Zeng, H., Qu, X., Xu, D., & Luo, Y. (2022). Porous Adsorption Materials for Carbon Dioxide Capture in Industrial Flue Gas. *Frontiers in Chemistry*, *10*, 939701. https://doi.org/10.3389/fchem.2022.939701

Zhai, X., & Wang, R. (2009). A review for absorbtion and adsorbtion solar cooling systems in China. *Renewable and Sustainable Energy Reviews*, *13*(6-7), 1523–1531. https://doi.org/10.1016/j.rser.2008.09.022

Zhang, C., Xie, Y., Xie, C., Dong, H., Zhang, L., & Lin, J. (2022). Accelerated discovery of porous materials for carbon capture by machine learning: A review. *MRS Bulletin*, *47*(4), 432–439. https://doi.org/10.1557/s43577-022-00317-2

Zhang, L. (2000). Design and testing of an automobile waste heat adsorption cooling system. *Applied Thermal Engineering*, *20*(1), 103–114. https://doi.org/10.1016/S1359-4311(99)00009-5

Zhang, W., Liu, H., Sun, Y., Cakstins, J., Sun, C., & Snape, C. E. (2016). Parametric study on the regeneration heat requirement of an amine-based solid adsorbent process for post-combustion carbon capture. *Applied Energy*, *168*, 394–405. https://doi.org/10.1016/j.apenergy.2016.01.049

Zhao, H., Luo, X., Zhang, H., Sun, N., Wei, W., & Sun, Y. (2018). Carbon-based adsorbents for post-combustion capture: a review: Review: Carbon-based adsorbents for post-combustion capture: a review. *Greenhouse Gases: Science and Technology*, *8*(1), 11–36. https://doi.org/10.1002/ghg.1758

Emanuele Piccoli

piccoli.emanuele@gmail.com emanuelepiccoli
https://orcid.org/0000-0002-2496-626X

Employment History

feb 2019 – ongoing	**Pre-doctoral Researcher,** Empa, Building Energy Materials and Components.
jan 2021 – ongoing	**Pre-doctoral Researcher,** IBM-Research Zürich.
nov 2017 – jan 2019	**Research Fellow,** Politecnico di Milano, Energy Department.
sep 2014 – dec 2014	**Technical Consultant,** Sertec Engineering.

Education

2019 – ongoing — **Ph.D., Ecole Polytechnique Fédéral de Lausanne** Energy.
Thesis title: *Selection and Optimal Use of Nanoporous Materials in Adsorption Energy Technologies*

2015 – 2017 — **M.Sc. Energy Engineering, Universitat Politécnica de Catalunya** in Renewable Energy.
Thesis title: *Modelling an innovative shading system integrating PV.*

2011 – 2015 — **B.Sc. Energy Engineering, Politecnico di Torino**

Research Publications

Journal Articles

1. E. Piccoli, V. Brancato, A. Frazzica, F. Maréchal, and S. Galmarini, "Adsorption energy system design and material selection: Towards a holistic approach," en, *Thermal Science and Engineering Progress*, p. 101 572, Nov. 2022, ISSN: 24519049. DOI: 10.1016/j.tsep.2022.101572.
2. E. Piccoli, A. Dama, A. Dolara, and S. Leva, "Experimental validation of a model for PV systems under partial shading for building integrated applications," en, *Solar Energy*, vol. 183, pp. 356–370, May 2019, ISSN: 0038092X. DOI: 10.1016/j.solener.2019.03.015.

Conference Proceedings

1. E. Piccoli, R. Civioc, S. Galmarini, *et al.*, "Optimized Adsorption Heat Pump for Efficiency Increase of District Heating Networks," in *press in Proceedings of EuroSun 2022*, Kassel, DE, 2022.
2. E. Piccoli, V. Brancato, A. Frazzica, F. Maréchal, and S. Galmarini, "Early-Stage Adsorber Material Selection for Adsorption Heat Transformers," in *Heat Powered Cycles 2021*, Bilbao, ES, 2022, ISBN: 978-0-9563329-7-4.
3. E. Piccoli, P. Gantenbein, S. Galmarini, P. Ruch, and B. Michel, "Low-Grade Heat Driven Rapid Thermal Swing Adsorption Gas Separation," en, in *Proceedings of the 16th Greenhouse Gas Control Technologies Conference*, 2022. DOI: 10.2139/ssrn.4274156.
4. E. Piccoli and A. Dama, "Modelling The Performances Of An Innovative Shading Device Integrating PV," en, in *Building Simulation 2019*, Rome, Italy, 2019, pp. 4879–4886. DOI: 10.26868/25222708.2019.210564.

5. E. Piccoli and A. Dama, "Shading device with extensible louvres for BIPV and daylight control," en, in *Advanced Building Skins*, Bern, CH, Oct. 2018, p. 11, ISBN: 978-3-9524883-4-8.

In Submission

1. E. Piccoli, F. Maréchal, and S. Galmarini, *Effective Strategies for Characterizing and Modelling Water Adsorption Equilibrium Curves*, 2023.
2. E. Piccoli, R. Silva, R. Weber, S. Galmarini, and L. Baldini, *A Novel Agitated Adsorption Heat Exchanger*, 2023.
3. E. Piccoli, R. Torreggiani, R. Civioc, F. Maréchal, and S. Galmarini, *Modelling Transient Heat and Mass Transfer During Adsorption with a Lightweight Approach*, 2023.

Skills

Experimental	Thermophysical characterization of water and carbon dioxide adsorbing materials; Adsorption Dynamics; Photovoltaic modules characterization
Modelling	Heat and mass transfer in porous media, Adsorption equilibrium, Building simulations, Photovoltaic systems
Programming Languages	Modelica, Python, R, Matlab
Organizational	Management of projects both internally and within a consortium; International representation of teams and projects; Establishment of external collaborations; Project proposals ideation and writing

References

Prof. François Maréchal
Adjunct Professor
EPFL
francois.marechal@epfl.ch

Dr. Sandra Galmarini
Team Leader
Empa
sandra.galmarini@empa.ch

Dr. Bruno Michel
IBM Academic and Inventor
IBM Research
bmi@zurich.ibm.com

Dr. Alessandro Dama
Researcher
Politecnico di Milano
alessandro.dama@polimi.it